R-13-19

Hydrology and near-surface hydrogeology at Forsmark – synthesis for the SR-PSU project

SR-PSU Biosphere

Kent Werner, EmpTec

Mona Sassner, DHI Sverige AB

Emma Johansson, SKB

December 2013

Svensk Kärnbränslehantering AB
Swedish Nuclear Fuel
and Waste Management Co

Box 250, SE-101 24 Stockholm
Phone +46 8 459 84 00

ISSN 1402-3091
SKB R-13-19
ID 1429794

Hydrology and near-surface hydrogeology at Forsmark – synthesis for the SR-PSU project

SR-PSU Biosphere

Kent Werner, EmpTec

Mona Sassner, DHI Sverige AB

Emma Johansson, SKB

December 2013

Summary

The Swedish final repository for short-lived low and intermediate level radioactive waste, SFR 1, is located in rock beneath the sea floor at Forsmark in the Municipality of Östhammar, northern Uppland. In order to be able to store also decommissioning waste from the Swedish nuclear power plants, an extension of the repository, referred to as SFR 3, is planned. As a part of the license application for this extension, the Swedish Nuclear Fuel and Waste Management Company (SKB) has performed the SR-PSU project to assess the long-term radiological safety of the entire future SFR repository.

The present report, which is one of the background reports for the biosphere part of SR-PSU, provides modelling results and descriptions of present and future hydrological and near-surface hydrogeological conditions at Forsmark. The modelling includes data evaluations and numerical water-flow modelling, primarily using the modelling tool MIKE SHE. Descriptions are presented both on landscape scale and for specific subareas (biosphere objects), including water-flux parameters required for the modelling of radionuclide transport in the biosphere. Moreover, the report recommends how potential future land- and water-resources management at Forsmark shall be handled in the SR-PSU project, including near-surface drainage of agricultural land, surface-water supplies and water-supply wells in regolith and rock.

As a basis for models of the future, a MIKE SHE model was developed to represent present-day hydrological and near-surface hydrogeological conditions at Forsmark. The model setup is based on MIKE SHE models produced for SDM-Site and SR-Site, i.e. the site description and the safety assessment, respectively, for the planned final repository for spent nuclear fuel. The setup takes into account recently updated, underlying site models of topography and bathymetry, regolith (surface distribution, depth and stratigraphy), and hydrogeological properties of the rock.

As part of the model development, the MIKE SHE model was calibrated using long-term monitoring data on groundwater levels in regolith and rock, surface-water levels and stream discharges. Only minor model adjustments of the initial setup were made during the calibration process. Adjustments made include, for instance, adaptation of the unsaturated-zone classification in the model and increase of the hydraulic conductivity of glacial clay below lakes. The resulting present-day MIKE SHE model setup is judged to be reasonable. Specifically, it reproduces monitoring data with an accuracy that is sufficient as a basis for models of the future. The model-calculated accumulated stream discharge downstream one of the lakes, Lake Eckarfjärden, is only 80% of the measured accumulated discharge. However, it is judged that this deficit in calculated stream discharge has minor or no effects on the modelling of future conditions at SFR and downstream areas.

The MIKE SHE modelling of future conditions considers two temperate climate cases, present-day climate, referred to as the normal year, and a possible wet and warm future climate. MIKE SHE models were established for the future times 3000, 5000 and 11,000 AD, using results from modelling of sea-shoreline displacement and other landscape development. As a result of these processes new lakes will be formed, gradually filled with gyttja and peat and transformed to mires. At 3000 AD, the coastline is located immediately downstream of SFR. The year 5000 AD represents an intermediate stage, with co-existing lakes and mires within the considered model area. At 11,000 AD, all previous lakes within the model area are infilled.

Regional MIKE SHE models were established for the mentioned future times to provide external boundary conditions for local models, which were used in the analysis of biosphere objects. These objects represent subareas in the future landscape that may be affected by a potential release of radionuclides from SFR. One main input for the biosphere-object delineations is discharge locations at the interface between rock and regolith, which were calculated for particles released from SFR in the DarcyTools modelling of rock hydrogeology. The local MIKE SHE models were used to produce various types of modelling results, representative for the normal year at each future time and its associated shoreline location and landscape setting. Moreover, the influence of a wet and warm climate on hydrology and near-surface hydrogeology was analysed using the 5000 AD model setup.

The modelling results show that for a given land area, infilling of lakes and other landscape-development processes have a larger, but not dramatic, influence on evapotranspiration and runoff than the effects of shoreline displacement. At 11,000 AD, when all previous lakes in the considered area are infilled and transformed to mires, evapotranspiration is 5–10% less and the runoff is slightly larger compared to 5000 AD. In comparison, the wet and warm climate case has much larger influence of the water balance than shoreline displacement and other landscape development. In the vicinity of the shoreline during its passage, shoreline displacement influences the directions of hydraulic gradients in the upper part of the rock. Similar to present land areas, groundwater recharge and discharge patterns in the regolith are governed by the ground-surface topography in new land areas, whereas the topography has less influence on vertical hydraulic gradients in the rock in such areas.

The distance to the shoreline has some minor influence on the depth to the groundwater table in new land areas, and according to the MIKE SHE modelling results the influence decreases with this distance. Moreover, the report demonstrates that landscape development influences stream-discharge characteristics. Due to the absence of lakes, the 11,000 AD landscape is characterised by less evapotranspiration and higher runoff compared to the landscape at 5000 AD. Lakes present at 5000 AD reduce and prolong high-discharge peaks and provide base flow during low-discharge periods. Hence, discharge peaks are generally most pronounced in the 11,000 AD landscape, when the former lakes are infilled and transformed to mires.

The report summarises residence times and inter-basin exchanges for marine basins, calculated using the MIKE 3 FM modelling tool. Moreover, totally 27 types of water-flux components for temperate conditions are derived and delivered for each of the seven delineated biosphere objects, using the water-balance tool in MIKE SHE. These components represent water fluxes into and out from objects, and fluxes between compartments of the radionuclide-transport model. At 3000 AD, all objects are submerged and net vertical groundwater fluxes are small. It is shown that the influence of shoreline displacement on net groundwater fluxes depends on the distance to the shoreline. Hence, biosphere objects demonstrate different net-flux changes due to shoreline displacement during the 3000–5000 AD and 5000–11,000 AD periods, during which all objects emerge from the sea and previous lakes are infilled, respectively.

Periglacial conditions with permafrost have a large influence on hydrology and near-surface hydrogeology. Such conditions are characterised by a relatively short, hydrologically active period during snowmelt. During this period water is redistributed on the ground surface and in the above-permafrost active layer, which is a relatively thin layer subject to cyclic freeze and thaw. Through taliks, i.e. unfrozen “windows” in the permafrost, connect the unfrozen groundwater flow system at depth with the surface system, and are therefore important hydrogeological features in a permafrost landscape. Water-flux components are derived and delivered to the radionuclide-transport modelling for two potential taliks in a future permafrost landscape at Forsmark. These two taliks represent a lake and a wetland, and they coincide with discharge locations calculated for a permafrost landscape using DarcyTools.

Extended hydrological analyses for temperate climate conditions are presented for one of the biosphere objects, 157_2, which is a future mire that does not pass a lake stage subsequent to its separation from the sea. According to DarcyTools particle-tracking simulations, this object will likely receive most of the radionuclide-containing groundwater in case of a future release from SFR. One analysis concerns the influence of the object delineation on fluxes used in the radionuclide transport modelling. Using MIKE SHE, the smallest upward groundwater flux is obtained if the delineated object only contain potential arable land with low-permeable regolith. The largest net vertical flux is noted if the object delineation follows subareas with upward hydraulic gradients and a high density of DarcyTools-calculated discharge locations. Moreover, MIKE SHE was used to investigate the influence of the surface-flow characteristics in the area between object 157_2 and the downstream object 157_1. It was found that the water balance of object 157_2 is rather insensitive to whether surface flow occurs in the form of overland or stream flow.

The report considers water-resources management of different types of future, self-sufficient communities in Forsmark. Specifically, it presents analyses of hydrological issues related to agriculture and water uses for humans, cattle and irrigation. The analyses of future agriculture are focused on conceptual descriptions and parameterisations of percolation and groundwater uptake, respectively, in the radionuclide-model compartment for a biologically active layer above the groundwater table.

Moreover, the report discusses drainage of agricultural land in terms of drainage depth, drainage-caused subsidence, and effects of drainage on groundwater recharge-discharge and runoff.

Based on literature data, the report presents estimates of future water uses for humans, cattle and irrigation, and it analyses the quantity and quality of potential surface- and groundwater supplies in the future Forsmark landscape. It is shown that there likely will be access to both surface water and groundwater of sufficient quantity and quality for self-sufficient inhabitants. It cannot be ruled out that wells in regolith or wells drilled in rock will be used by future Forsmark inhabitants. Based on MIKE SHE and DarcyTools analyses, the report presents methodologies for calculation of radionuclide concentrations in water-supply wells. It also provides recommendations for identification of a representative of the most exposed group, in terms of water uses for the community types considered in the SR-PSU safety assessment.

Sammanfattning

Det svenska slutförvaret för kortlivat låg- och medelaktivt radioaktivt avfall, SFR 1, är beläget i berg under havsbotten i Forsmark, i Östhammars kommun i norra Uppland. En utbyggnad av förvaret, benämnd SFR 3, är planerad för att även möjliggöra lagring av rivningsavfall från de svenska kärnkraftverken. Som en del av tillståndsansökan för utbyggnaden har Svensk Kärnbränslehantering AB (SKB) genomfört projektet SR-PSU för att analysera den långsiktiga radiologiska säkerheten för hela den framtida SFR-anläggningen.

Denna rapport, som är en av bakgrundsrapporterna för biosfärsdelen av SR-PSU-projektet, tillhandahåller modelleringsresultat och beskrivningar av nuvarande och framtida hydrologiska och ytnära hydrogeologiska förhållanden i Forsmark. Modelleringen inkluderar datautvärdering samt numerisk flödesmodellering, främst med modelleringsverktyget MIKE SHE. Beskrivningarna presenteras både på landskapsskala och för specifika delområden (biosfärsobjekt), inklusive vattenflödesparametrar som behövs för modellering av radionuklidtransport i biosfären. Rapporten ger också rekommendationer för hur potentiell framtida mark- och vattenhushållning i Forsmark ska hanteras i SR-PSU-projektet, inklusive dikning av jordbruksmark, ytvattentäkter och vattenförsörjningsbrunnar i jord och berg.

Som en utgångspunkt för modeller för framtida förhållanden har en MIKE SHE-modell utvecklats för att representera dagens hydrologiska och ytnära hydrogeologiska förhållanden i Forsmark. Modellen baseras på de MIKE SHE-modeller som tagits fram för SDM-Site och SR-Site, det vill säga platsbeskrivningen respektive säkerhetsanalysen för det planerade slutförvaret för använt kärnbränsle. I modellen beaktas nyligen uppdaterade, underliggande modeller av platsens topografi och batymetri, jordförhållanden (ytfördelning, djup och stratigrafi) samt hydrogeologiska egenskaper i berg.

Som del av modellutvecklingen kalibrerades MIKE SHE-modellen med data från långtidsmonitering av grundvattennivåer i jord och berg, ytvattennivåer och vattenföring i bäckar. Under kalibreringsprocessen gjordes endast mindre justeringar i modellen. Exempel på sådana justeringar är anpassningar i modellen av klassindelningen av den omättade zonen samt att den hydrauliska konduktiviteten för glaciallera under sjöar ökades. Den framtagna MIKE SHE-modellen bedöms som rimlig. Specifikt återskapar modellen moniteringsdata med tillräcklig noggrannhet som utgångspunkt för modeller för framtida förhållanden. Den modellberäknade kumulativa vattenföringen nedströms en av sjöarna i området, Eckarfjärden, utgör endast 80 % den av uppmätta ackumulerade vattenföringen. Bedömningen är att detta modellberäknade underskott har liten eller ingen inverkan på modelleringen av framtida förhållanden vid SFR eller nedströms belägna områden.

I MIKE SHE-modelleringen av framtida förhållanden beaktas två tempererade klimatfall, nämligen dagens klimat, som benämns som normalåret, och ett potentiellt blött och varmt framtida klimat. MIKE SHE-modeller etablerades för de framtida tidpunkterna år 3000, 5000 och 11 000, genom att nyttja modelleringsresultat för förskjutning av strandlinjen mot havet och annan landskapsutveckling. Sådana processer innebär att nya sjöar kommer att bildas, gradvis fyllas igen med gyttja och torv och övergå till att bli myrar. År 3000 är strandlinjen belägen direkt nedströms SFR. År 5000 representerar ett mellanliggande steg, då det finns både sjöar och myrar i modellområdet. År 11 000 är alla tidigare sjöar igenfyllda.

Regionala MIKE SHE-modeller etablerades för de nämnda tidpunkterna för att erhålla externa randvillkor för lokala modeller, som i sin tur användes i analyser av biosfärsobjekt. Dessa objekt representerar delområden i det framtida landskapet som kan påverkas av potentiella radionuklidutsläpp från SFR. Ett huvudsakligt underlag för biosfärsobjektens avgränsningar är utströmningsområden vid övergången mellan berg och jord, och som beräknats för partiklar som släppts från SFR i DarcyTools-modelleringen av bergets hydrogeologi. De lokala MIKE SHE-modellerna användes för att ta fram olika typer av modelleringsresultat som representerar normalåret vid varje framtida tidpunkt, med tillhörande strandlinje och landskapsbeskrivning. Inverkan av ett blött och varmt klimat på hydrologi och ytnära hydrogeologi analyserades med modellen för år 5000.

Modelleringsresultaten visar att för ett visst landområde har igenfyllnad av sjöar och andra landskapsutvecklingsprocesser större, men ändå inte dramatiska, effekter på evapotranspiration och avrinning jämfört med själva strandlinjeförskjutningen. År 11 000, när alla tidigare sjöar i det betraktade området

är igenfyllda och har övergått till att bli myrar, är evapotranspirationen 5–10 % lägre och avrinningen är något högre jämfört med år 5000. Jämfört med strandlinjeförskjutning och annan landskapsutveckling har det blöta och varma klimatfallet mycket större inverkan på vattenbalansen. Nära strandlinjen, då den passerar, ändrar strandlinjeförskjutningen riktningar på hydrauliska gradienter i den övre delen av berget. På motsvarande sätt som i dagens landområden, styr markytans topografi fördelningen av in- och utströmningsområden i jord i nytillkommande landområden. I nytillkommande landområden har däremot topografin mindre betydelse för de vertikala hydrauliska gradienterna i berget.

Avståndet till strandlinjen har en liten inverkan på djupet till grundvattenytan i nytillkommande landområden, och enligt resultat från MIKE SHE-modelleringen minskar betydelsen med avståndet. I rapporten visas hur landskapsutvecklingen påverkar vattenföringen i bäckarna. Frånvaron av sjöar innebär att landskapet år 11 000 karaktäriseras av mindre evapotranspiration och mer avrinning jämfört med landskapet år 5000. År 5000 reducerar och förlänger sjöarna flödestopparna och ger basflöde under lågflödesperioder. Detta innebär att bäckarna generellt har tydligare flödestoppar år 11 000, då de tidigare sjöarna är igenfyllda och övergått till att bli myrar.

Rapporten sammanfattar uppehållstider och flöden mellan marina bassänger, som beräknats med modelleringsverktyget MIKE 3 FM. Vidare har totalt 27 typer av vattenflödeskomponenter härletts för tempererade förhållanden med vattenbalansverktyget i MIKE SHE och levererats för sju avgränsade biosfärsobjekt. Dessa komponenter representerar vattenflöden in till och ut från objekt samt flöden mellan olika delar av radionuklidtransportmodellen. År 3000 är alla objekt belägna under havet och grundvattnets nettoflöden är små. I rapporten visas att strandlinjeförskjutningens inverkan på grundvattnets nettoflöden beror på avståndet till strandlinjen. Detta innebär att strandlinjeförskjutningen ger olika förändringar av nettoflödena för olika biosfärsobjekt under perioderna år 3000–5000, då objekten stiger upp ur havet, och år 5000–11 000, då tidigare sjöar fylls igen.

Periglaciala förhållanden med permafrost har stor inverkan på hydrologi och ytnära hydrogeologi. Sådana förhållanden karaktäriseras av relativt korta, hydrologiskt aktiva perioder i samband med snösmältning. Under denna period sker en omfördelning av vatten på markytan och i det ovan permafrosten belägna aktiva lagret, vilket är ett relativt tunt lager som omväxlande utsätts för frysning och upptining. Genomgående talikar, det vill säga ofrusna ”fönster” i permafrosten, utgör en koppling mellan det djupa, ofrusna grundvattenflödessystemet och ytsystemet, och är därför hydrogeologiskt viktiga i ett permafrostlandskap. Vattenflödeskomponenter har härletts och levererats till modelleringen av radionuklidtransport för två potentiella talikar i ett framtida permafrostlandskap i Forsmark. Dessa två talikar representerar en sjö och en våtmark, som sammanfaller med DarcyTools-beräknade utströmningsområden i ett permafrostlandskap.

Utökade hydrologiska analyser har genomförts för tempererade klimatförhållanden för ett av biosfärsobjekten, 157_2, som är en framtida myr som inte genomgår ett sjöstadium efter det avskiljts från havet. Enligt partikelspårning som utförts med DarcyTools kommer detta objekt, i händelse av ett framtida utsläpp från SFR, sannolikt att ta emot den största delen av det radionuklidinnehållande grundvattnet. En av analyserna behandlar betydelsen av objektets avgränsning för de flöden som används i modelleringen av radionuklidtransport. Det lägsta MIKE SHE-beräknade, uppåtriktade grundvattenflödet erhålls om det avgränsade objektet endast innehåller potentiell jordbruksmark med lågpermeabla jordarter. Det största nettoflödet erhålls om objektsavgränsningen följer delområden med uppåtriktade hydrauliska gradienter och en hög densitet av DarcyTools-beräknade utströmningspunkter. Vidare användes MIKE SHE för att undersöka inverkan av hur ytvattenflöden i området mellan objekt 157_2 och det nedströms belägna objektet 157_1 hanteras i modellen. Analysen visar att vattenbalansen för objekt 157_2 är ganska okänslig för huruvida ytvattenflödena antas ske genom ytavrinning eller via en bäck.

I rapporten hanteras vattenhushållning för olika typer av framtida, självförsörjande samhällen. Specifikt presenteras analyser av hydrologiska frågeställningar som är relaterade till jordbruk och vattenanvändning för människor, boskap och bevattning. Analyserna av framtida jordbruk fokuserar på konceptuella beskrivningar samt parameteriseringar av perkolation respektive grundvattenupptag i den del av radionuklidtransportmodellen som representerar ett biologiskt aktivt lager ovanför grundvattenytan. Rapporten diskuterar även dikning av jordbruksmark, i termer av dikningsdjup, marksättningar till följd av dikning samt dikningens effekter på in- och utströmning av grundvatten och avrinning.

Baserat på litteraturdata presenterar rapporten uppskattningar av framtida vattenanvändning för människor, boskap och bevattning, och den analyserar kvantitet och kvalitet för potentiella yt- och grundvattentäkter i det framtida landskapet i Forsmark. Enligt rapporten kommer det sannolikt att finnas tillräckligt med yt- och grundvatten av tillfredsställande kvalitet för självförsörjande invånare. Det kan inte uteslutas att jordbrunnar eller bergborrade brunnar kommer att användas av framtida Forsmarksinvånare. Baserat på MIKE SHE- och DarcyTools-analyser presenteras metodik för att beräkna radionuklidkoncentration i vattenförsörjningsbrunnar. Det ges också rekommendationer rörande identifiering av en representant för den mest exponerade gruppen, i termer av vatten-användning för de samhällstyper som beaktas i säkerhetsanalysen SR-PSU.

Contents

1 Introduction

1.1 Background and setting

The final repository for short-lived low and intermediate level radioactive waste, SFR 1, is located in Forsmark in northern Uppland, in the immediate vicinity of the Forsmark nuclear power plant (Figures 1-1 and 1-2). The SFR 1 repository consists of a set of disposal rooms situated in rock at c 60 m depth beneath the sea floor, and is built to receive and after closure serve as a passive repository for the low- and intermediate-level, short-lived radioactive waste. The radioactive waste stored in SFR includes operational waste from Swedish nuclear power plants and from the interim storage facility for spent nuclear fuel, Clab, as well as radioactive waste from other industry, research institutions and medical care. In order to be able to store also decommissioning waste from the Swedish nuclear power plants in SFR, an extension of the repository, referred to as SFR 3, is planned.

As a part of the license application for the extension of SFR, the Swedish Nuclear Fuel and Waste Management Company (SKB) has performed the SR-PSU project. The objective of this project is to assess the long-term radiological safety of the entire future SFR repository, i.e. both the existing SFR 1 and the planned SFR 3. The SR-PSU project is reported in a series of SKB reports, which includes a main report (SKB 2014f) and a set of primary references. These include, among others, the reports denoted as Biosphere synthesis report (summary and synthesis of the biosphere assessment) (SKB 2014a), Climate report (climate and climate-related issues) (SKB 2014b), Radionuclide transport report (radionuclide transport and dose calculations) (SKB 2014e), FEP report (features, events and processes) (SKB 2014c) and FHA report (future human actions) (SKB 2014d). In addition to these primary references, the safety assessment is based on a large number of background reports (such as the present report) and other references.

The biosphere is a key part of the system considered in a safety assessment of a nuclear waste repository. This is where the main consequences of potential future radionuclide releases from the repository could arise, and hence radionuclide transport and dose calculations are performed within the framework of the biosphere assessment. This report belongs to the biosphere part of the SR-PSU project, SR-PSU Biosphere. SR-PSU Biosphere mainly describes the information needed to calculate effects on humans and the environment in case of a radionuclide release from SFR. The calculated effects are then used to show compliance with regulations related to the future repository performance for time spans up to 100,000 years after closure. Because of the uncertainties associated with the prediction of future development of the site in this time frame, a number of calculation cases are analysed to describe a range of possible site developments. For further details of the biosphere assessment and associated tasks, methodology, organisation and report structure of SR-PSU Biosphere, see SKB (2014a).

1.2 Objectives and scope

The present report is a background report for SR-PSU Biosphere, providing modelling results and descriptions of hydrology and near-surface hydrogeology at Forsmark. The report is primarily a background report for the Biosphere synthesis report (SKB 2014a). Specifically, the report presents results of conceptual and numerical modelling of present hydrological and near-surface hydrogeological conditions and their future development at Forsmark, on time scales of interest for SR-PSU Biosphere. Descriptions of groundwater flow in rock and analyses of hydrological and hydrogeological effects of construction and operation of SFR are reported elsewhere (Öhman 2010, Öhman and Follin 2010a, b, Öhman et al. 2012, 2013, Odén et al. 2014, SKBdoc 1346469).

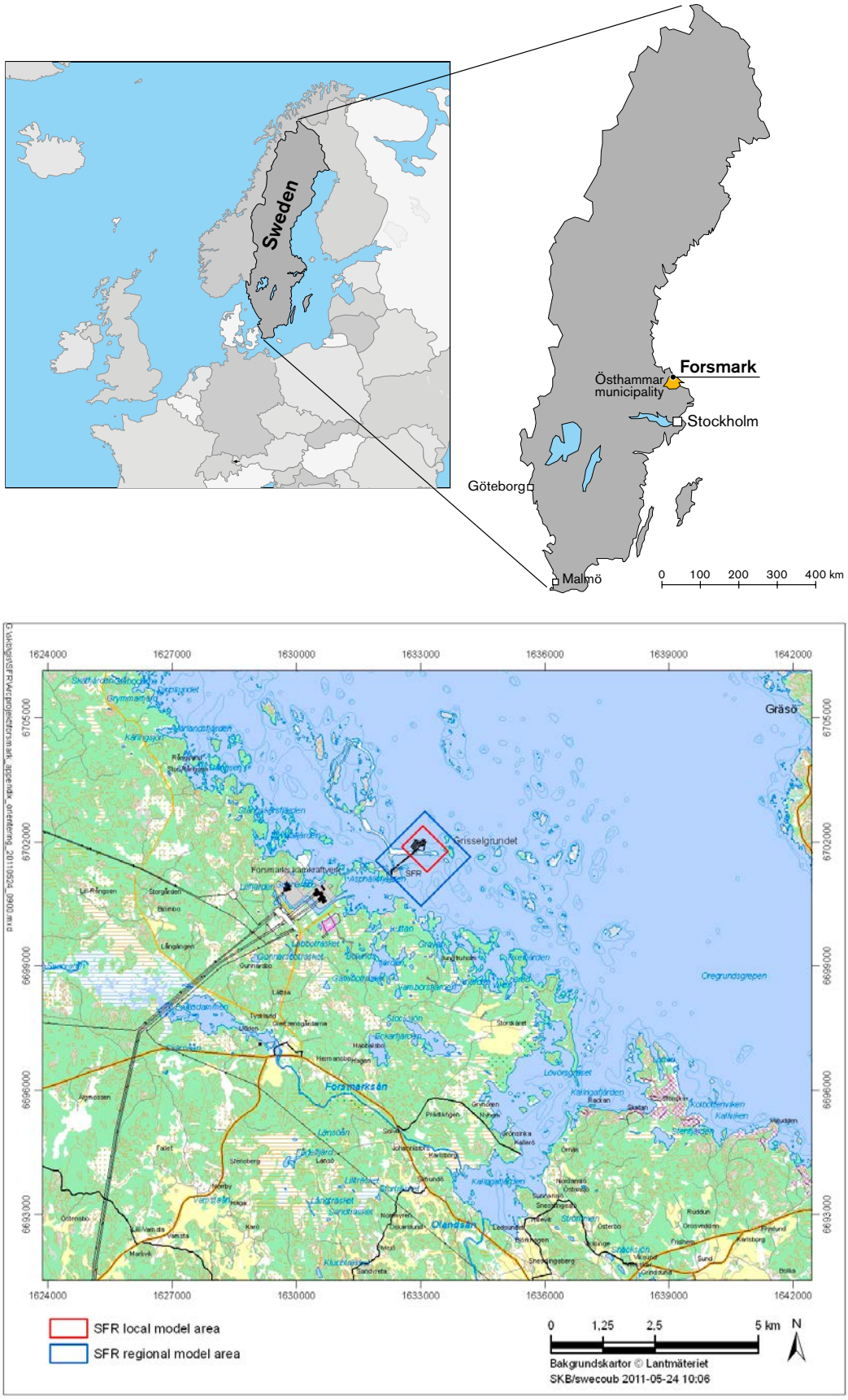

Figure 1-1. *Location of Forsmark in norther Uppland. The lower map shows the boundaries of the SFR local and regional model area, respectively, and the location of the SFR 1 facility. The local model area (or domain) covers the volume that hosts SFR 1 and SFR 3, whereas the regional model domain places the description of the local domain in a larger context (SKB 2013).*

Figure 1-2. *The surface faclities of SFR 1 in the Forsmark harbour.*

The modelling includes data evaluations and numerical analyses, primarily using the water-flow modelling tool MIKE SHE. In contexts of groundwater flow and transport in rock, the report utilises results from DarcyTools, which is a modelling tool specifically developed to analyse groundwater flow and transport in fractured rock. Descriptions are presented both on landscape scale and for specific subareas (biosphere objects), including flow parameters required for radionuclide transport and dose calculations. Moreover, the report recommends how potential future land and water-resources management at Forsmark shall be handled in the SR-PSU project, including near-surface drainage of agricultural land, surface-water supplies and water-supply wells in regolith and rock.

The modelling and results presented in this report build on previous safety assessments for existing and planned nuclear waste repositories in Sweden. The SFR repository has been in operation since 1988 and a number of safety assessments have been performed for the repository since SKB received permission to start building SFR 1 in 1983. These include the previous SFR safety assessments SAFE (Kautsky 2001, Lindgren et al. 2001) and SAR-08 (SKB 2008a). Moreover, the site description SDM-Site (Bosson et al. 2008, Johansson 2008, SKB 2008b) and the safety assessment SR-Site (Bosson et al. 2010, SKB 2011) were produced for the planned repository for spent nuclear fuel in Forsmark. The description of present hydrological and near-surface hydrogeological conditions at Forsmark presented in the site description SDM-PSU (SKB 2008c, 2013) is mainly based on SDM-Site. The present report considers longer time-series datasets and models developed subsequent to SDM-Site, as well as models of e.g. future landscape development that have been updated subsequent to SR-Site.

Section 1.3 summarises modelling methodology and tools, whereas **Chapter 2** describes data and models used for the conceptual and numerical modelling. **Chapter 3** presents the MIKE SHE model setups representing present and future conditions at Forsmark. **Chapter 4** and **Chapter 5** present conceptual and numerical modelling results and associated descriptions of present (**Chapter 4**) and future (**Chapter 5**) conditions at Forsmark on a landscape scale. **Chapter 6** analyses impacts on hydrology and near-surface hydrogeology of drainage and wells, whereas **Chapter 7** presents numerical modelling results for biosphere objects, i.e. areas that may be affected by a potential future release of radionuclides from SFR. For readability, many figures are assembled in appendices at the end of the report.

This report uses the coordinate systems RT 90 2.5 gon V/0:15 (X, Y) and RHB 70 (Z), i.e. vertical (Z) coordinates are expressed in terms of elevation (m) above the RHB 70 datum (0 m elevation). Moreover, some parameters and properties, e.g. depth to the groundwater table, are commonly expressed in terms of depth below the ground surface. Accordingly, the abbreviation mbgs used in this report means metres below the ground surface.

1.3 Modelling methodology and tools

Descriptions of present and future conditions presented in this report are based on data evaluations and numerical analyses, primarily using the water-flow modelling tool MIKE SHE. Evaluations of meteorological, hydrological and hydrogeological monitoring data are presented in a separate report (Werner et al. 2013). The MIKE SHE modelling tool (Graham and Butts 2005, DHI Software 2012) is used in the SR-PSU project for numerical modelling of surface and near-surface water flow and solute transport. MIKE SHE is a dynamic, physically based modelling tool that describes main processes in the land phase of the hydrological cycle, including precipitation (rain or snow), evapotranspiration (ET), overland flow (OL), water flow in the unsaturated zone (UZ), and groundwater flow in the saturated zone (SZ).

MIKE SHE is fully integrated with a channel-flow modelling tool, MIKE 11. The exchange of water-flow data between these two models takes place during simulation. In the present study initial and boundary conditions from regional MIKE SHE models, established for present (2000 AD) and future conditions (3000, 5000 and 11,000 AD), are used to set up local models for the area in the vicinity of SFR.

In the SR-PSU project, advective solute transport is modelled using the particle-tracking module of MIKE SHE. In such simulations, inert "water parcels" are tracked as they are advected in the three-dimensional groundwater flow field in the model volume. The resulting groundwater flow paths connect starting and exit locations and can be used for calculation of associated particle travel times. In MIKE SHE, particles can only be tracked in the saturated zone (SZ). For further details regarding modelling of water flow and solute transport in MIKE SHE, see DHI Software (2012) and Bosson et al. (2010).

The MIKE SHE water-balance tool is used to produce all water-balance results presented in this study. Specifically, this is a post-processing tool for generating water-balance summaries from MIKE SHE simulations. Water-balance outputs include area-normalised flows (storage depths), storage changes, and model errors for individual model components (e.g. unsaturated-zone evapotranspiration components). A water balance can be generated at a variety of spatial and temporal scales. For further details regarding the MIKE SHE water balance utility, see DHI Software (2012).

2 Data and models

This chapter describes data and models used in the SR-PSU project for description of present (Section 2.1) and future (Section 2.2) hydrological and near-surface hydrogeological conditions at Forsmark, with emphasis on data and models updated subsequent to SDM-Site and SR-Site (cf Section 1.2).

2.1 Data and models representing present conditions

2.1.1 Topography and bathymetry

The DEM (digital elevation model) used in the SR-PSU project is presented in Strömgren and Brydsten (2013), see Figure 2-1. In terrestrial areas, the DEM is based on field inspections and aerial photographs taken from an altitude of 2,300 m. In marine areas, the DEM is constructed using a combination of nautical charts, supplementary depth probing and marine-geological surveys (Elhammer and Sandkvist 2005, Nyberg et al. 2011).

In land areas of the Forsmark area, elevation differences are usually less than 20 m. Prominent topographical features of the landscape are the relatively small glacial landforms like eskers. The highest observed point is at 50 m elevation and is located in the south-western part of the DEM area. The marine areas have a gentle slope towards the northwest. A deep trough (Gräsörännan) runs in the north-south direction in the eastern part of the embayment, and the lowest point (–55 m elevation) is located in the northern part of this trough.

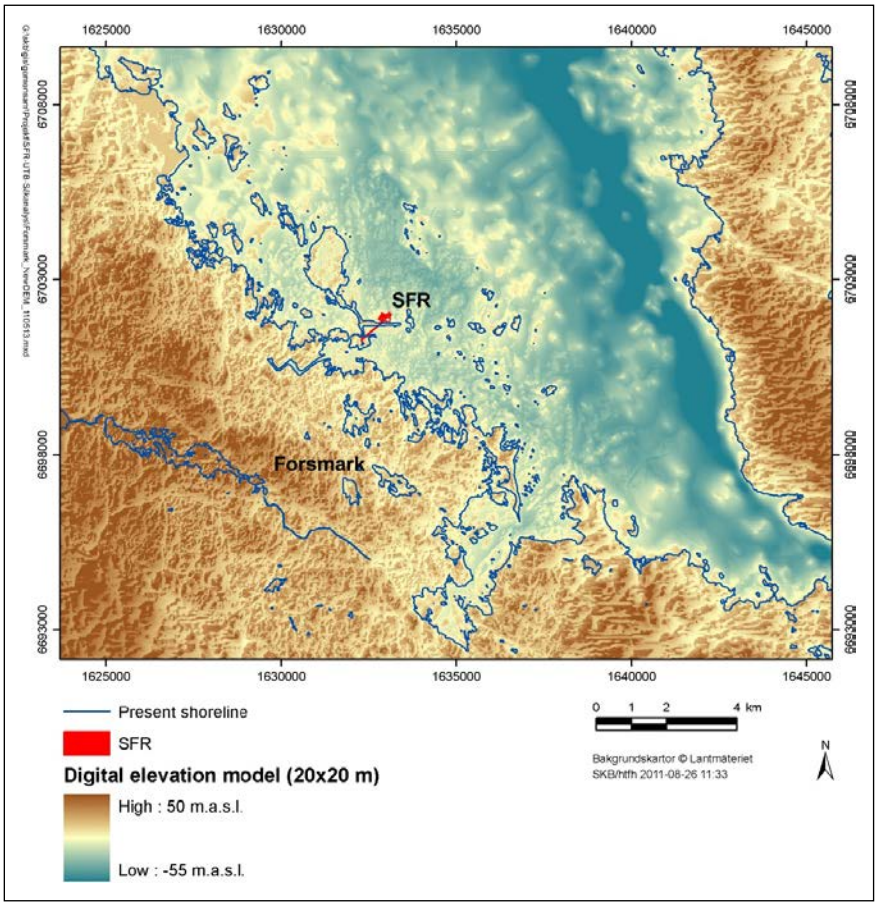

Figure 2-1. *DEM (digital elevation model) of the Forsmark area, including the bathymetry (bottom level) of lakes and the near-coastal sea. The map shows present lake shorelines, the present shoreline towards the sea, and the location of the existing SFR facility.*

2.1.2 Surface distribution, depth and stratigraphy of regolith

In the Forsmark area, as in other parts of Sweden, most regolith, i.e. unconsolidated deposits above the rock, was formed during or after the final phase of the latest glaciation (c 8800 BC). The regolith can therefore also be referred to as Quaternary deposits. The surface distribution of regolith in Forsmark is typical for areas located below the highest postglacial coastline. The description of the surface distribution of regolith is presented in Sohlenius et al. (2013a), see Figure 2-2. This description is based on Hedenström and Sohlenius (2008) and recent, supplementary depth probing and marine-geological surveys of the sea floor outside Forsmark (Nyberg et al. 2011).

In the highest topographical areas till is the dominant type of regolith. Till occupies some 65% of the surface in terrestrial areas and 30% of the sea floor outside Forsmark. As indicated in Figure 2-2, the shallowest areas and islands have a high proportion of exposed rock. The glaciofluvial deposit Börstilåsen has N–S and NW–SE directions along the coast of the mainland, and continues at the sea floor east of SFR. Glacial clay, which is often covered by postglacial sand, primarily occurs in sea-floor depressions and below present lakes. Postglacial clay gyttja, which is rich in organic material, is predominantly found and is presently deposited in shallow bays and at the deepest parts of the sea floor. Gyttja, which mainly consists of organic material, is currently deposited in the lakes. Peat is accumulating in fens and along lake shores. As shown in Figure 2-2, till dominates the sea floor around the pier of the SFR facility, whereas sand-covered glacial clay occurs in the lower topographical areas of the sea floor.

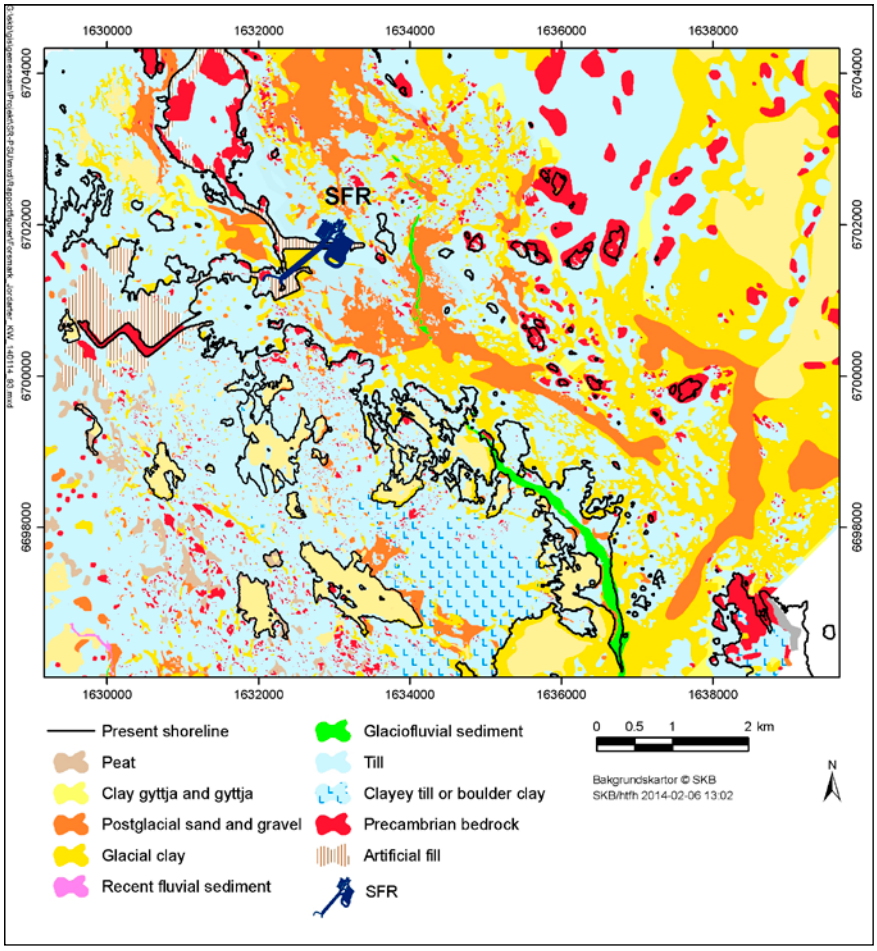

Figure 2-2. *Surface distribution (at the mapping depth 0.5 m) of regolith and areas with exposed rock in the Forsmark area. Note that lakes and the sea are shown without surface water.*

An RDM (regolith depth and stratigraphy model) has been developed to provide a geometric model of regolith depths and layers at landscape level (Sohlenius et al. 2013a). The RDM is based on Hedenström et al. (2008) and supplementary probing and geological surveys in marine (cf above) and terrestrial areas (e.g. Sohlenius and Hedenström 2009, Werner et al. 2009). In the RDM, the regolith is subdivided into a number of layers, denoted Z2–Z6 (see Table 2-1). As shown in Figure 2-3, the general top-down stratigraphical distribution of regolith in Forsmark is bog peat (layer Z2, youngest), gyttja (present below lakes), clay gyttja (present in coastal areas and below lakes), postglacial sand and gravel, glacial clay, glaciofluvial sediments, and till (layer Z5, oldest). Note that all these layers are not present everywhere.

The total regolith depth in the RDM area (Figure 2-4) varies between 0.1 and 47 m. The coastal zone and the islands (including the coastal zone of the island of Gräsö) are characterised by thin regolith and frequent rock outcrops. Generally, the regolith is deeper in the marine area (average depth c 8 m), whereas the average depth in the land area is c 4 m. The regolith thickness is 1–4 m on the sea floor around the SFR pier.

2.1.3 Hydrogeological description of the rock

Modelling of groundwater flow in rock at SFR was previously performed within the SAFE and SAR-08 safety assessments (Holmén 2005, 2007, Holmén and Stigsson 2001a, b), whereas the SDM-PSU/SR-PSU modelling is presented in Öhman (2010), Öhman and Follin (2010a, b), Öhman et al. (2012, 2013), and Odén et al. (2014). Figure 2-5 shows the boundaries of the flow-modelling domain (red line) defined for the SR-PSU project (Odén et al. 2014). This domain has its bottom boundary at –1,100 m elevation, whereas its lateral boundaries take into account present and future water divides set by the DEM and the subsea trough Gräsörännan (cf above).

Table 2-1. Layers in the RDM (Sohlenius et al. 2013a).

Layer	Description	Comments
Z1	Surface layer	Upper 0.6 m of the regolith and modelled as the upper 0.1 m of rock outcrops; represents regolith affected by soil-forming processes
Z2	Fen peat, bog peat	
Z3a	Postglacial sand and gravel	
Z3b	Glaciofluvial sediments	
Z3c	Artificial fill	
Z4a	Gyttja/clay gyttja	
Z4b	Glacial clay	
Z5	Till	
Z6	Uppermost rock	Upper 0.5 m of rock outcrops, upper 0.6 m of rock in other areas

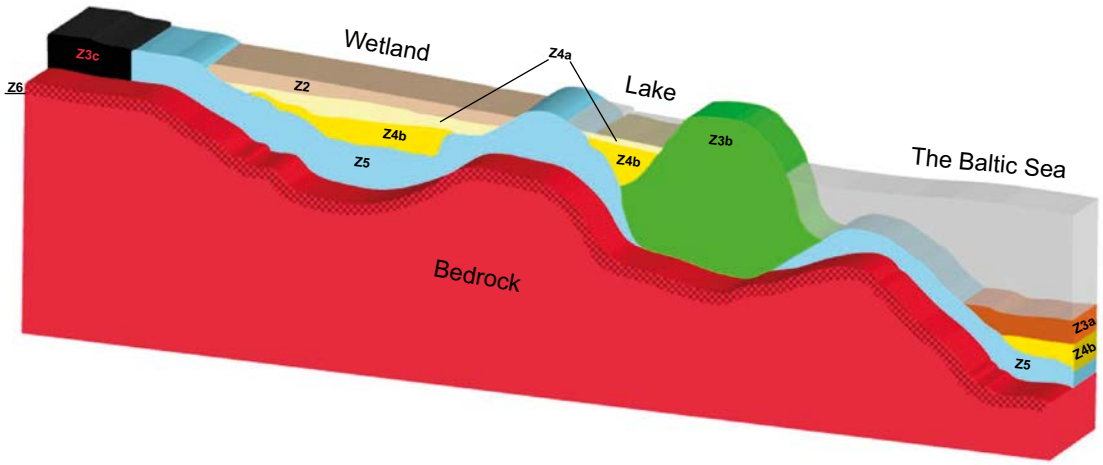

Figure 2-3. General stratigraphy of the RDM (Sohlenius et al. 2013a).

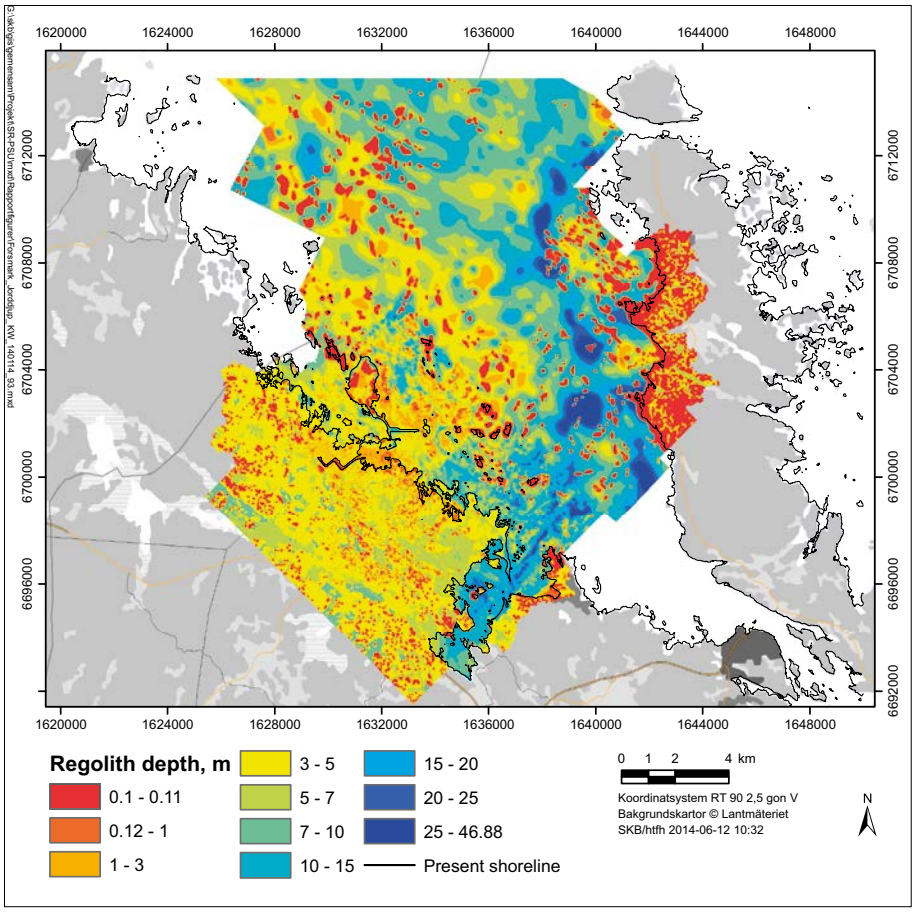

Figure 2-4. *Modelled total regolith depth at Forsmark (Sohlenius et al. 2013a).*

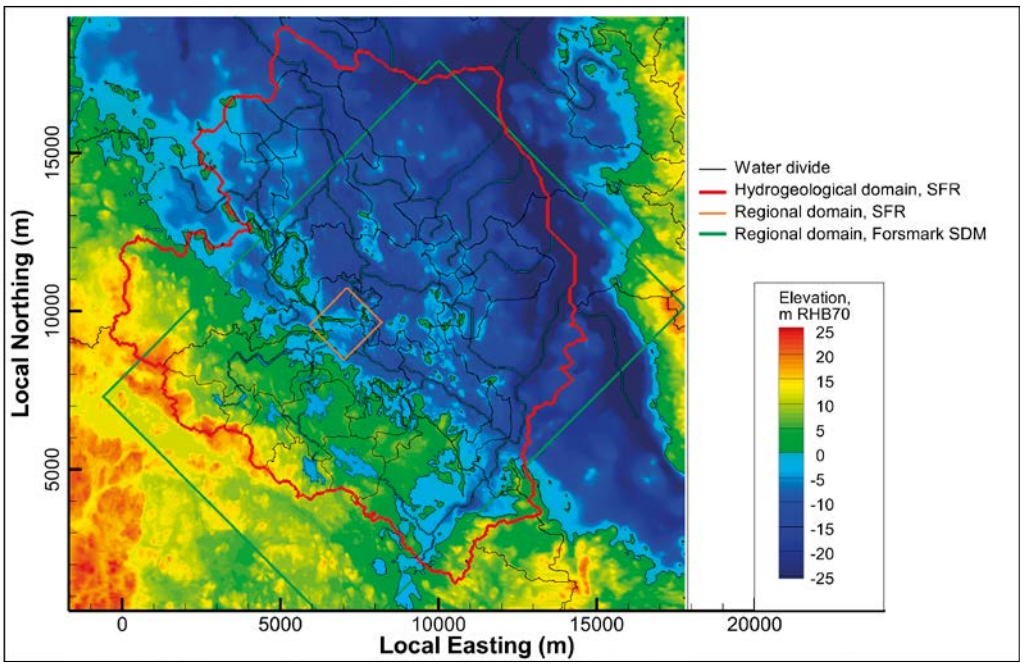

Figure 2-5. *Boundaries of the SFR regional model domain (Regional domain, SFR) (SKB 2013), the SDM-Site regional model domain (Regional domain, Forsmark SDM; site investigations for a final repository for spent nuclear fuel) (SKB 2008b) and the domain for modelling of groundwater flow in the rock in the SR-PSU project (Hydrogeological domain, SFR) (Odén et al. 2014).*

The MIKE SHE model has its bottom boundary at –634 m elevation, and hence requires input data describing the hydrogeological properties of the rock. The hydrogeological modelling of the rock divides the rock into HCD (Hydraulic Conductor Domain, representing deterministic deformation zones), HRD (Hydraulic Rock-mass Domain, which involves a stochastic representation of less fractured rock between deformation zones), and SBA structures, which represent a network of predominantly sub-horizontal fractures of elevated transmissivity (e.g. Odén et al. 2014).

Figure 2-5 displays the boundaries of the regional model domain defined for the PSU project (Regional domain, SFR). The PSU site investigations (SKB 2013) mainly involved investigations of the rock in a local model domain (cf Figure 1-1). Moreover, the geological and hydrogeological descriptions of the rock performed within SDM-PSU concern the regional model domain, whereas the descriptions of the rock outside this domain are taken from SDM-Site/SR-Site (e.g. Stephens et al. 2007, Joyce et al. 2010).

The groundwater-flow modelling comprises data evaluations (Öhman and Follin 2010a, Öhman et al. 2012), within the context of the SDM-PSU geological model (Curtis et al. 2011), and groundwater-flow modelling, using the numerical water-flow modelling tool DarcyTools (Svensson et al. 2010) within the SDM-PSU (Öhman et al. 2013) and SR-PSU projects (Odén et al. 2014). DarcyTools is a modelling tool specifically developed to analyse groundwater flow and transport in fractured rock. Data evaluations comprise the site investigations performed prior to (1980–1983) and during (1984–1986) the construction of the SFR 1 facility, site investigations related to construction of the discharge tunnels from the Forsmark nuclear power plant, relevant data from site investigations for a final repository for spent nuclear fuel (2002–2007), and site investigations for the planned SFR 3 facility (2008–2009).

For the regional model area, a number of model variants were investigated and evaluated as part of the DarcyTools modelling, including HCD, HRD, flow resistance (skin) at the tunnel walls of SFR 1, and the hydraulic contact between the sea and the rock above SFR across sea-floor sediments (Öhman et al. 2013, Odén et al. 2014). For instance, model variants were evaluated by comparing flow-modelling results to measured inflow to SFR 1 and groundwater levels in surface and tunnel boreholes, including transient developments of inflow and heads after completion of SFR 1.

As a result of these above evaluations, a base case model (denoted BASE_CASE1_DFN_R85) of the hydrogeological properties of the rock was delivered from the DarcyTools model to be used in the MIKE SHE modelling in the SR-PSU project. Specifically, the delivered model considers homogeneous transmissivity, coupled with a depth trend, for HCD (BASE_CASE1), whereas the HRD (DFN_R85) is represented by a DFN realisation with large fractures connecting rock vaults in the SFR 1 facility (Odén et al. 2014). Note that hydrogeological properties of the rock were delivered from another modelling tool (ConnectFlow) in the MIKE SHE modelling in SR-Site (Bosson et al. 2010).

The DarcyTools delivery to MIKE SHE contains the parameters K_x and K_y (hydraulic conductivity in two horizontal directions), K_z (vertical hydraulic conductivity) and porosity. The delivered data have a horizontal spatial resolution of 40 by 40 m from the rock surface to –634 m elevation, whereas the vertical spatial resolution is 4 m down to –170 m elevation and 16 m below this level. Spatial averaging of the delivered data was required, due to the vertical discretization of the MIKE SHE model and its limited capability to represent anisotropic hydrogeological properties in the horizontal plane (see Section 3.1.4). Figures 2-6 and 2-7 show examples of resulting horizontal and vertical hydraulic conductivities of the rock (c –40 m elevation). In these figures, one can see the extensions of fracture zones and also the high horizontal hydraulic conductivity of structures recognised as sheet joints (cf Follin 2008). The post-processed (averaged) hydrogeological-properties data of the rock were used directly in the MIKE SHE model, and no further data adjustments were hence made during the MIKE SHE modelling process.

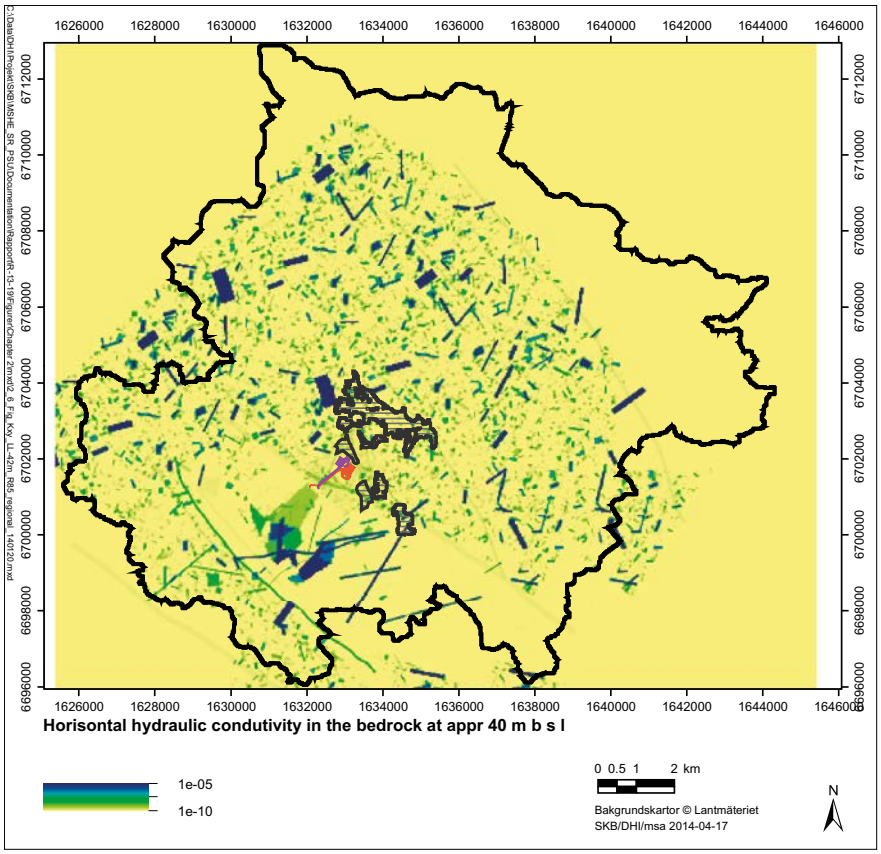

Figure 2-6. *Horizontal hydraulic conductivity (K_h) of the rock at c –40 m elevation.*

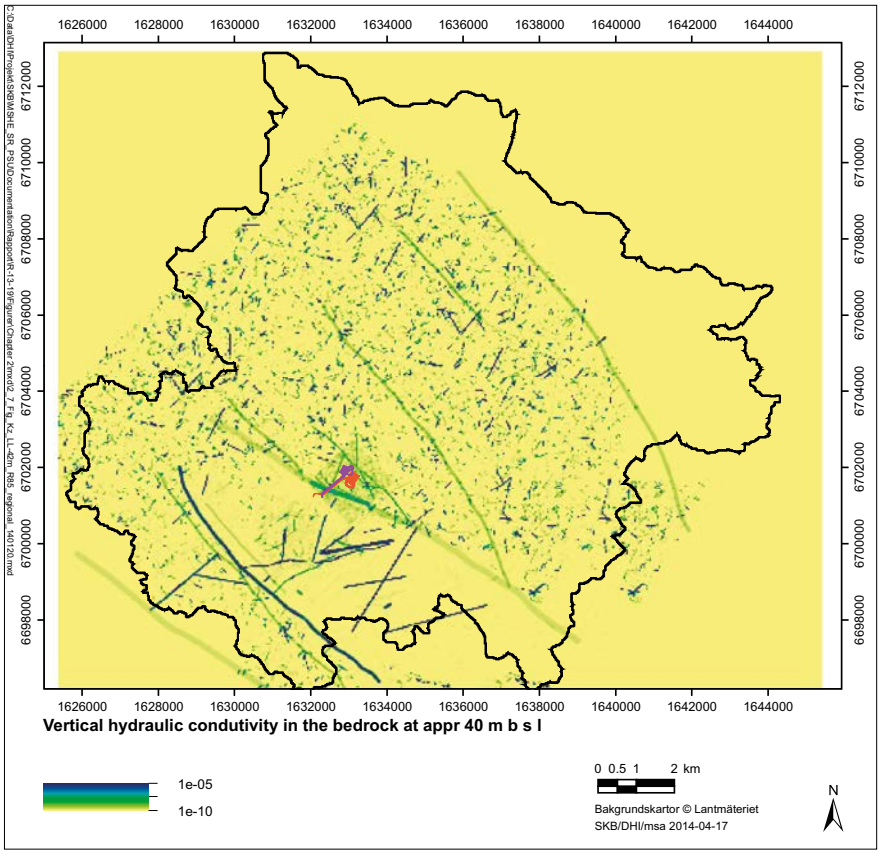

Figure 2-7. *Vertical hydraulic conductivity (K_v) of the rock at c –40 m elevation.*

2.1.4 Hydrogeological properties of regolith

Table 2-2 summarises values of K_h (horizontal hydraulic conductivity), K_v (vertical hydraulic conductivity), S_y (specific yield) and S_s (specific storage coefficient) assigned to each regolith type. These values are identical to those assigned by Bosson et al. (2010).

2.1.5 Geometries of lakes and streams

Figure 2-8 shows the present stream network represented in MIKE 11. Geometrical data for present lakes and streams are obtained from Bosson et al. (2010). These data include measured lake thresholds and bathymetries, and measured cross sections and bottom elevations (Brydsten and Strömgren 2004). In MIKE 11, it was required to adjust some local stream stretches and cross-section elevations to obtain a numerically stable match between stream sections and the local ground-surface topography as specified by the DEM (see Section 3.1.2).

2.1.6 Monitoring data for description of boundary conditions and for model calibration

As described further below, in MIKE SHE the upper boundary condition is represented as daily time series of precipitation and potential evapotranspiration (PET), whereas near-surface air temperature is required to calculate snow accumulation and snow melt during simulation. Moreover, in offshore (sea) areas of the model domain, the sea is represented by a geological layer of highly permeable material and a time-varying head equal to sea-level time series.

The MIKE SHE modelling of present conditions is conducted using the meteorological and sea-level data sets presented in Werner et al. (2013). Specifically, Werner et al. (2013) compile and analyse data sets up to the end of 2010, thereby extending the corresponding SDM-Site data sets (that extend up to March 31, 2007) by more than three years. Figures 2-9 to 2-12 show time-series plots of daily precipitation (Figure 2-9), PET (Figure 2-10), near-surface air temperature (Figure 2-11; measured 2 m above ground) and sea level (Figure 2-12; SKB gauging station PFM010038), which represent the upper boundary condition, input for calculation of snow accumulation/snow melt and the sea-level boundary condition in the present-day MIKE SHE model setup. The two highest sea-level peaks seen in Figure 2-12 were caused by the two storms named Gudrun and Per, which occurred in January 2005 and January 2007, respectively.

Table 2-2. Hydrogeological properties of layers of the RDM. As also done in Bosson et al. (2010), K_h is multiplied by a factor of 2 in the catchment area of Lake Eckarfjärden.

QD type		K_h ($m \cdot s^{-1}$)	K_v ($m \cdot s^{-1}$)	S_y (–)	Ss (m^{-1})
Z1: Surface layer					
	Till	$1.5 \cdot 10^{-4}$	$1.5 \cdot 10^{-5}$	0.15	0.001
	Gyttja	$3.0 \cdot 10^{-7}$	$3.0 \cdot 10^{-7}$	0.03	0.006
	Clay	$5.0 \cdot 10^{-6}$	$5.0 \cdot 10^{-7}$	0.05	0.006
	Sand	$7.5 \cdot 10^{-4}$	$7.5 \cdot 10^{-5}$	0.20	0.004
	Peat	$5.0 \cdot 10^{-6}$	$5.0 \cdot 10^{-7}$	0.20	0.020
	Rock	$1.0 \cdot 10^{-7}$	$1.0 \cdot 10^{-7}$	0.15	0.001
Z2: Fen peat, bog peat		$3.0 \cdot 10^{-7}$	$3.0 \cdot 10^{-7}$	0.05	0.005
Z3a: Postglacial sand and gravel		$1.0 \cdot 10^{-4}$	$1.0 \cdot 10^{-4}$	0.20	0.350
Z3b: Glaciofluvial sediments		$1.0 \cdot 10^{-4}$	$1.0 \cdot 10^{-4}$	0.20	0.350
Z3c: Artificial fill		$1.0 \cdot 10^{-4}$	$1.0 \cdot 10^{-4}$	0.20	0.350
Z4a: Gyttja/clay gyttja		$1.5 \cdot 10^{-8}$	$1.5 \cdot 10^{-8}$	0.03	0.006
Z4b: Glacial clay		$1.5 \cdot 10^{-8}$	$1.5 \cdot 10^{-8}$	0.03	0.006
	Z5: Till				
	Fine till	$5.0 \cdot 10^{-7}$	$5.0 \cdot 10^{-8}$	0.05	0.001
	Coarse till	$7.5 \cdot 10^{-6}$	$7.5 \cdot 10^{-7}$	0.03	0.001
Z6: Uppermost rock		$1.5 \cdot 10^{-6}$	$1.5 \cdot 10^{-6}$	0.15	0.001

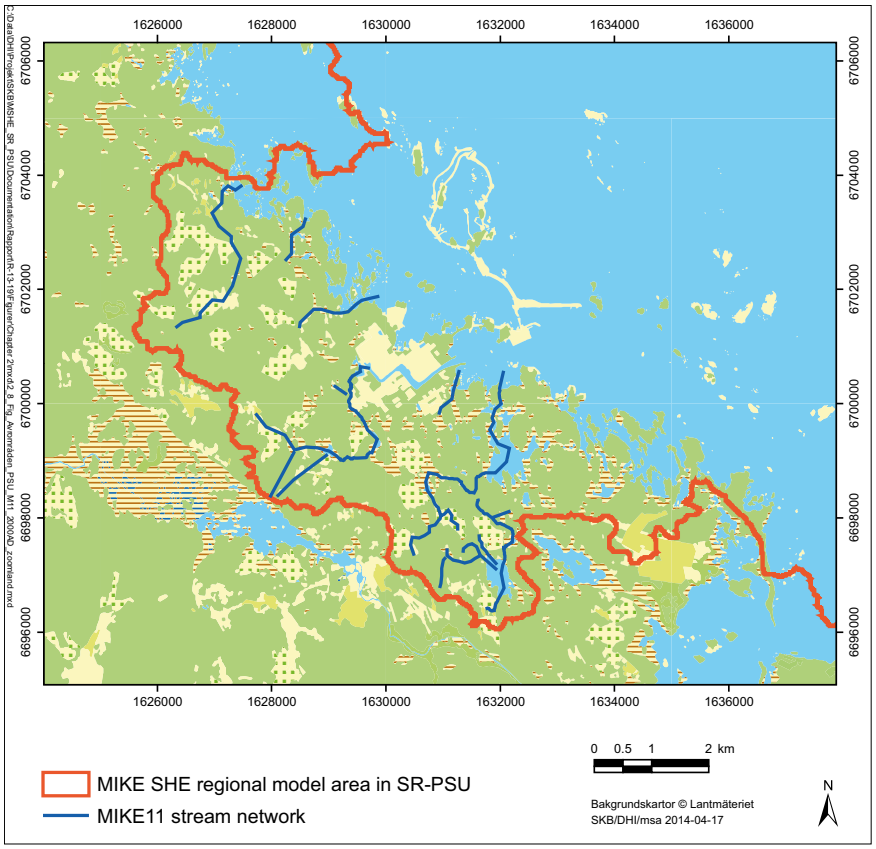

Figure 2-8. *MIKE 11 stream network in the MIKE SHE regional model area (2000 AD), cf Section 3.1.1.*

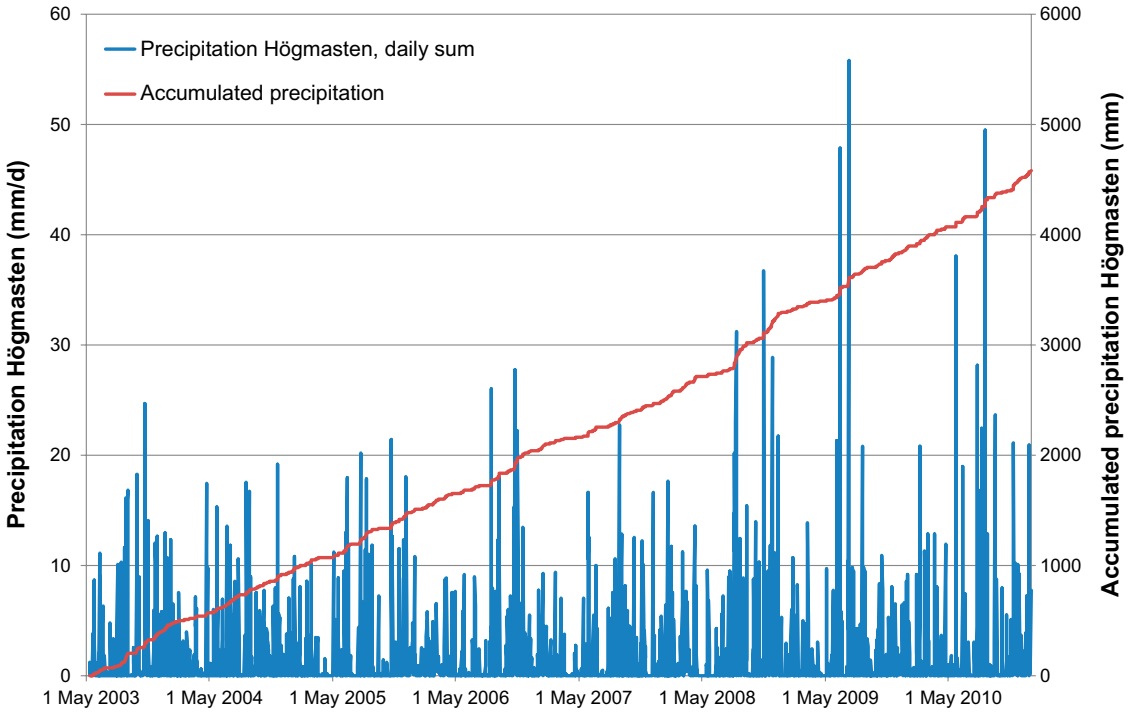

Figure 2-9. *Time-series plot of daily and totally accumulated precipitation for the period 2003–2010 (Högmasten meteorological station).*

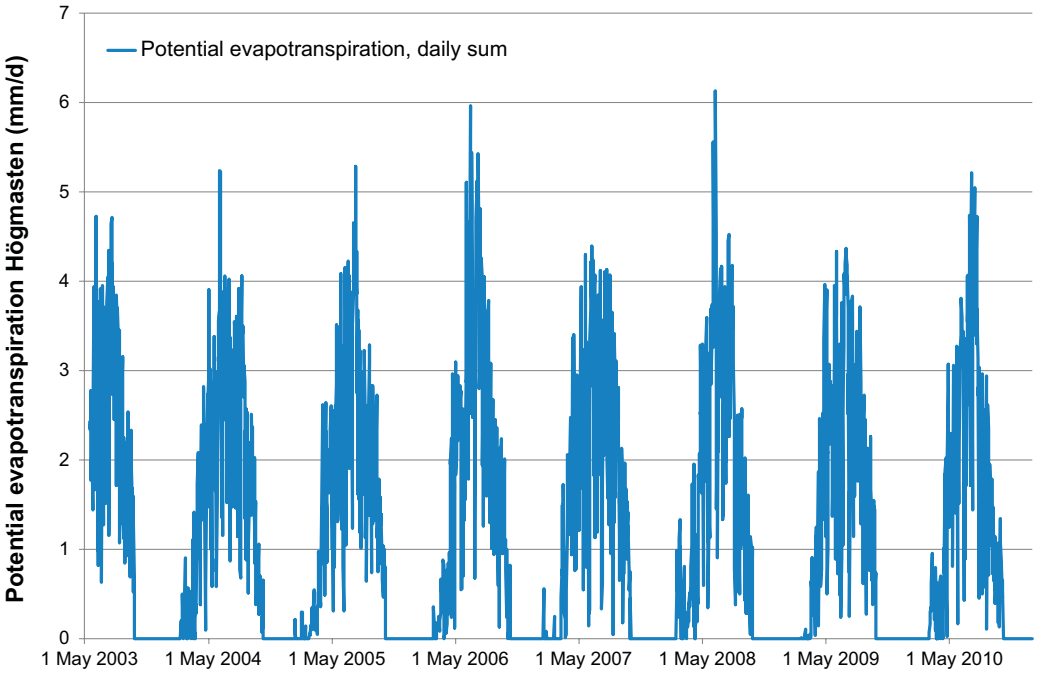

Figure 2-10. *Time-series plot of daily accumulated PET (potential evapotranspiration) for the period 2003–2010 (Högmasten meteorological station).*

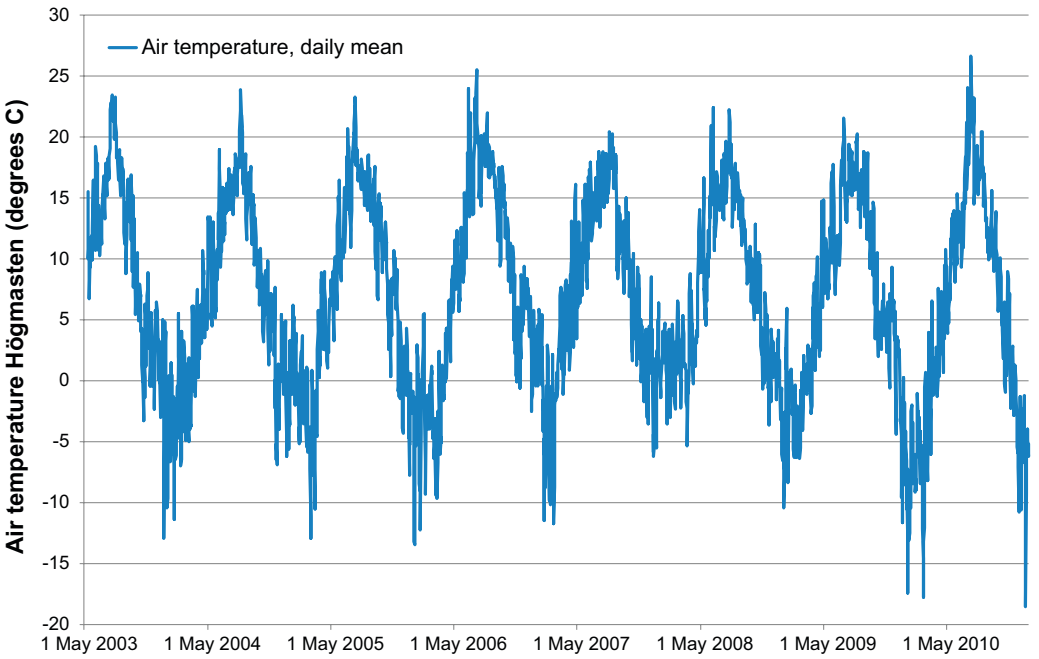

Figure 2-11. *Time-series plot of daily average near-surface air temperature (Högmasten meteorological station).*

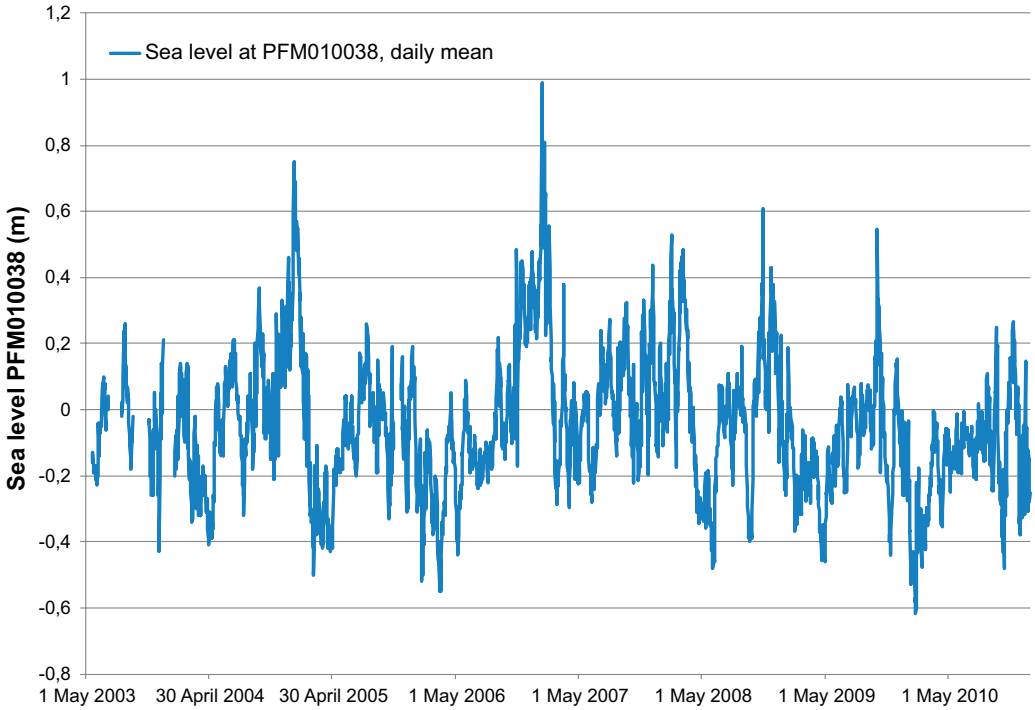

Figure 2-12. *Time-series plot of daily average sea level at gauging station PFM0100038.*

For the full seven-year period 2004–2010, the average annual precipitation, PET and near-surface air temperature was 589 mm, 509 mm, and 6.7°C, respectively. For the full three-year period 2004–2006 of the corresponding SDM-Site data sets (Johansson 2008), the average annual precipitation was less (537 mm) whereas the average annual PET and near-surface air temperature was identical (509 mm) and almost identical (6.9°C) to the prolonged data set of this study. The MIKE SHE modelling of SDM-Site and SR-Site (Bosson et al. 2008, 2010) used meteorological data from two SKB meteorological stations (Högmasten and Storskäret). The Storskäret station was decommissioned in 2007, and only Högmasten data are used in the present MIKE SHE model setup.

As described further in Section 3.3, quality check and calibration of the present-day regional model were performed by comparing modelling results with hydrological and hydrogeological monitoring data (see summary in Werner et al. (2013)) from the Forsmark site. The data sets used for quality check and model calibration include daily averages of groundwater levels in regolith (groundwater-monitoring wells) and rock (percussion boreholes), surface-water levels and stream discharges. The present study uses the same set of groundwater-monitoring wells, percussion boreholes, surface-water level and stream-discharge gauging stations as was used in the SDM-Site and SR-Site MIKE SHE modelling. For an overview of the locations of these monitoring installations, see Bosson et al. (2008, 2010).

2.1.7 Vegetation and land use

As one of the inputs to evapotranspiration calculations in MIKE SHE, temporally variable vegetation parameters, such as leaf-area index and root depth, must be specified for each type of vegetation and land-use type represented in the model domain. The assignment of present vegetation and land-use types and associated parameters in MIKE SHE (Section 3.1.6) is a simplification of the detailed vegetation and land-use map presented in Löfgren (2010). Figure 2-13 shows a map of present vegetation types implemented in MIKE SHE. As shown in the figure, vegetation and land-use types are in the MIKE SHE model setup divided into water, deciduous forest, coniferous forest, mixed forest, arable land, wetland and artificial fill.

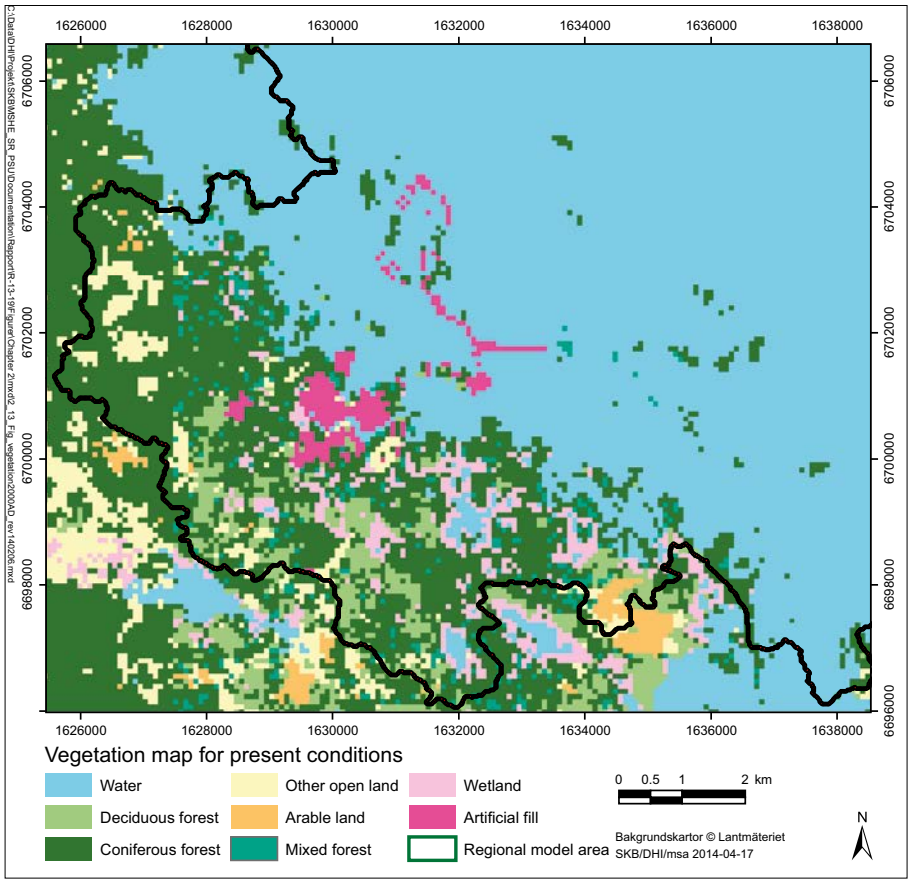

Figure 2-13. *Vegetation types implemented in MIKE SHE.*

2.1.8 SFR representation in MIKE SHE

Figures 2-14 and 2-15 show the layout of the existing SFR 1 facility and also the planned SFR 3 facility (layout version L1). The SFR 1 rock caverns (1BMA, 1BLA, 2BTF and 1BTF) are located at c –70 to –90 m elevation, whereas the Silo in SFR 1 has its bottom level at –133 m elevation. The planned SFR 3 rock caverns (1BRT, 2BLA, 3BLA, 4BLA, 5BLA and 2BMA) are located at c –120 to –140 m elevation, parallel to the SFR 1 rock caverns. The existing SFR 1 facility is implemented in the MIKE SHE model setup for description of present conditions, whereas both layouts (SFR 1 and SFR 3) are used as starting positions for particle tracking in models of future conditions (see Sections 2.3 and 5.8).

In the present-day model setup, SFR 1 has been implemented as pipe links with reduced (i.e. atmospheric) pressure in MOUSE, which is a modelling tool originally developed for urban hydrology purposes and pipe-flow hydraulics (DHI Software 2010). The water flow from MIKE SHE to MOUSE (i.e. the inflow of groundwater to the SFR 1 facility) is included as a sink term in MIKE SHE. For further details on the representation of SFR 1 and the integration of MIKE SHE and MOUSE, see Mårtensson and Gustafsson (2010) and Mårtensson et al. (2010).

It is noted that the subsurface cooling-water tunnels from the Forsmark nuclear power plant (Carlsson and Christiansson 2007) are not included in the present-day model setup. These tunnels are not pressurised and they are not empty even at zero power production at the plant, but rather act as links between communicating vessels in the form of surge pools at the power plant and the sea (Ulf Modin, FKA-F12CT, personal communication 2012). It is therefore assumed that they do not act as pressure boundaries or drains in the rock that must be accounted for in the model setup.

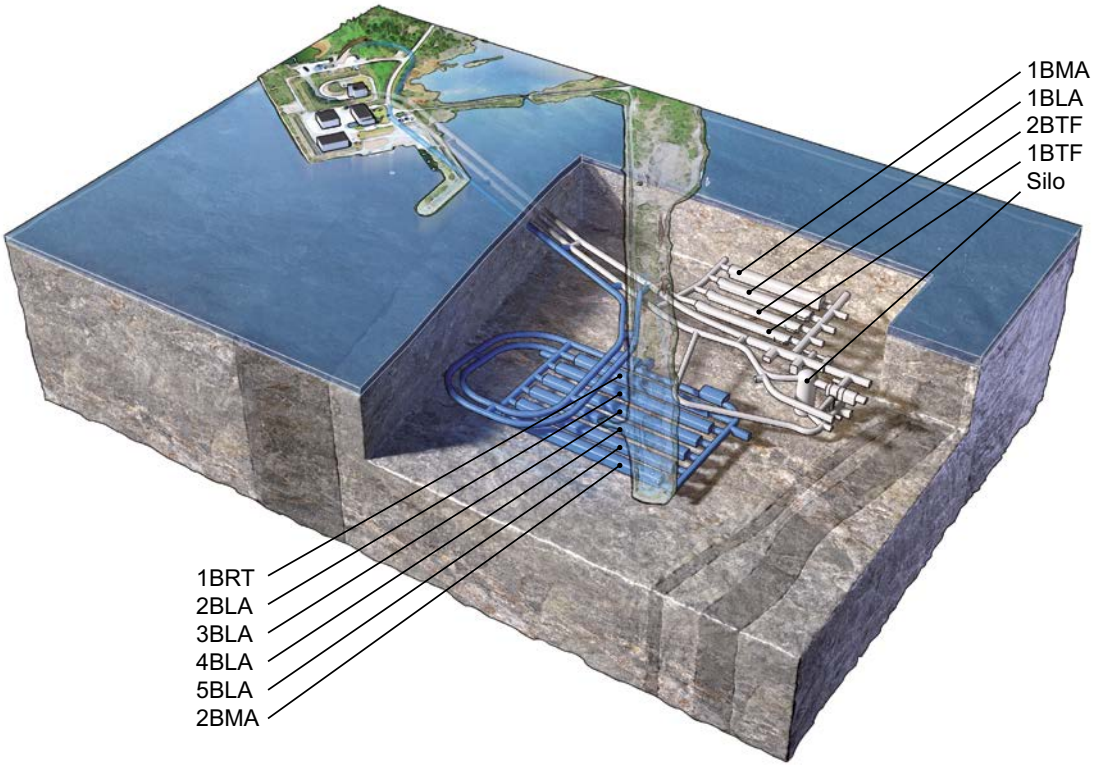

Figure 2-14. *Side view of the layout of waste-containing rock caverns and Silo of the existing SFR 1 facility (grey), and rock caverns of the planned SFR 3 facility (blue).*

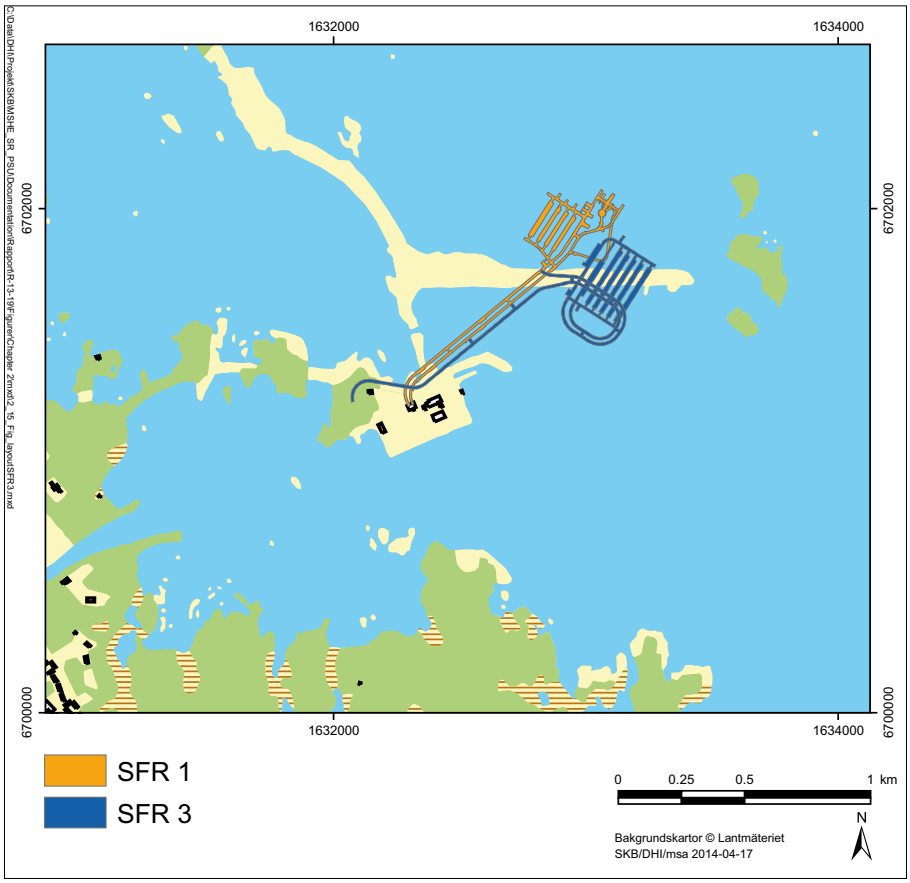

Figure 2-15. *Plan view of SFR 1 (orange) and SFR 3 (blue; layout version L1). In the MIKE SHE model for present conditions, SFR 1 is implemented using the MOUSE modelling tool.*

2.2 Data and models representing future conditions

2.2.1 Climate, topography, bathymetry and shoreline displacement

Climate

Meteorological parameters required for MIKE SHE calculations include precipitation, near-surface air temperature and potential evapotranspiration. The main climate cases in the SR-PSU project, global warming and extended global warming, are characterised by a warmer and wetter climate compared to present conditions (SKB 2014b). Specifically, the global warming climate case has a maximum temperature increase of c 3–4°C (at c 2700 AD), whereas the extended global warming climate case has a maximum temperature increase of c 6°C (at c 3000 AD). The maximum precipitation increase compared to present conditions is estimated to c 25–30%.

Two temperate climate cases, present-day climate and a possible wetter and warmer future climate, are considered in this study to analyse the hydrological responses to shifts in climate and landscape shifts (i.e. shoreline and vegetation). These two temperate climate cases are identical to those of Bosson et al. (2010). The influence of periglacial conditions and permafrost is described separately (Section 5.8).

The present-day climate case is represented by locally measured meteorological data during a selected period (October 1, 2003–September 30, 2004; average of the Högmasten and Storskäret meteorological stations). During the period 2003–2007, the selected one-year period has an accumulated precipitation that is close to that of the reference normal period 1961–1990, both on a monthly and annually basis (Bosson et al. 2010). Specifically, the selected one-year period, which in the following is referred to as the normal year, has an annual average air temperature of 6.4°C (minimum –13.2°C and maximum 23.4°C) and an accumulated precipitation of 583 mm. The annual average air temperature for the normal year is almost identical to the annual average for the period 2004–2010 (6.7°C). Moreover, the accumulated precipitation during the normal year (583 mm) is slightly above the estimated annual average (559 mm) for the reference normal period (Johansson 2008) and close to the annual average precipitation (589 mm) for the period 2004–2010 (Section 2.1.6).

The wetter and warmer climate case is represented by meteorological data available in Kjellström et al. (2009). Specifically, Kjellström et al. (2009) present meteorological data for a wet period of 50 years, having an annual average precipitation of c 1,280 mm. In this data set, Bosson et al. (2010) found a three-year period that includes both a very wet year and a year with an accumulated precipitation that is close to the 50-year average. The chosen period, which in the following is referred to as the wet and warm climate case, has an annual average air temperature of 7.7°C (minimum –16.1°C and maximum 24.2°C). The annual average precipitation is c 1,500 mm, i.e. almost three times the accumulated precipitation during the normal year. For further details on data-selection processes and meteorological data for the normal year and the wetter and warmer period, see Bosson et al. (2010).

Topography, bathymetry and shoreline displacement

For each future time considered in this report, Brydsten and Strömgren (2013) present data on ground-surface topography and bathymetry of lakes and the sea. The maps in Figure 2-16 show the modelled topography and bathymetry at 3000, 5000 and 11000 AD. Green colours represent areas above sea level, whereas blue areas are surface waters (lakes or the sea).

Future shoreline displacement, as described in Brydsten and Strömgren (2013), is taken into account in the MIKE SHE modelling. Specifically, the location of the shoreline at 3000 AD (–5.92 m elevation), 5000 AD (–16.60 m elevation) and 11,000 AD (–41.97 m elevation) is used to define the sea boundary at these times. Figure 2-17 shows the present shoreline and land areas formed due to shoreline displacement, implemented in the MIKE SHE regional and local model areas between 2000–3000 AD, 3000–5000 AD and 5000–11,000 AD. The sea has left the regional and local model areas at 11,000 AD (Brydsten and Strömgren 2013). As can be seen in the upper figure of Figure 2-17, in MIKE SHE at 11,000 AD a small sea area is kept in the north as a boundary condition for the regional model.

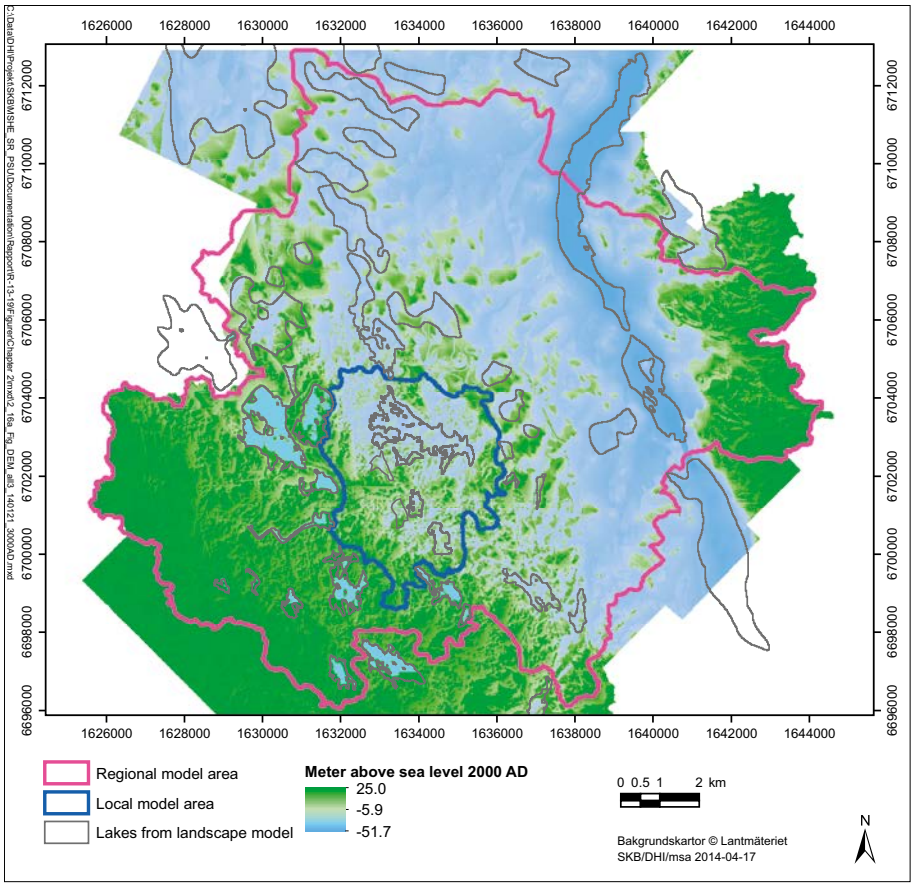
1626000
1628000
1630000
1632000
1634000
1636000
1638000
1640000
1642000
1644000
6712000
6710000
6708000
6706000
6704000
6702000
6700000
6698000
6696000
Regional model area
Local model area
Lakes from landscape model
Meter above sea level 2000 AD
25.0
-5.9
-51.7
0 0.5 1 2 km
Bakgrundskartor © Lantmäteriet
SKB/DHI/msa 2014-04-17
N

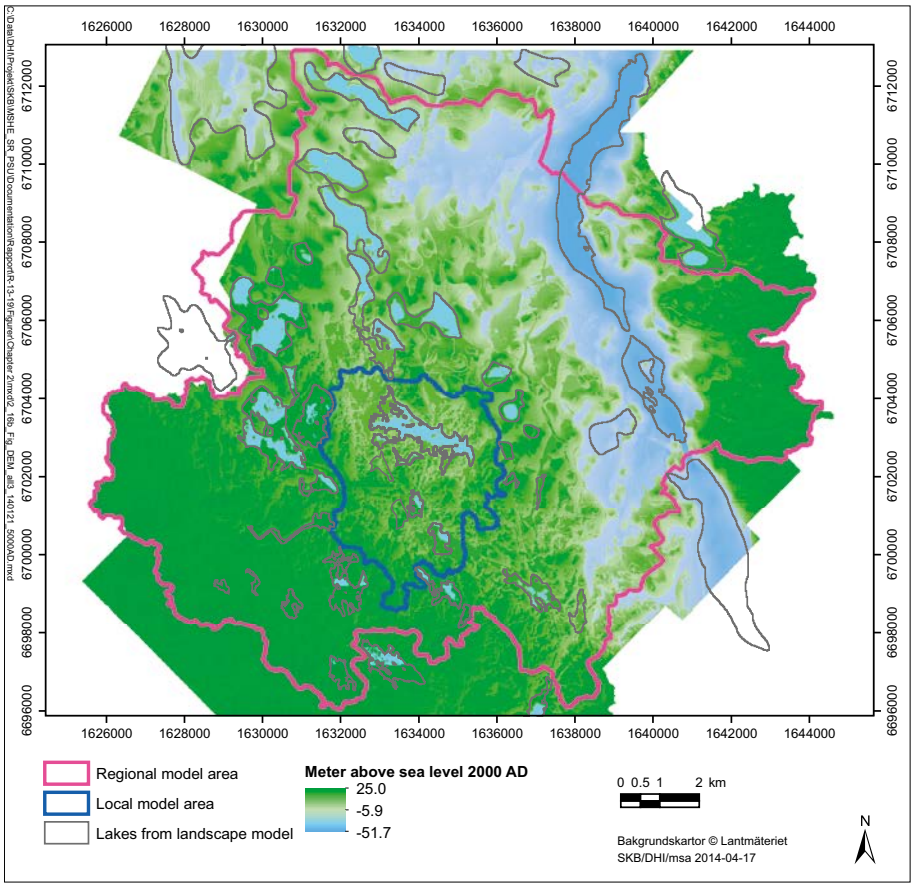
1626000
1628000
1630000
1632000
1634000
1636000
1638000
1640000
1642000
1644000
6712000
6710000
6708000
6706000
6704000
6702000
6700000
6698000
6696000
Regional model area
Local model area
Lakes from landscape model
Meter above sea level 2000 AD
25.0
-5.9
-51.7
0 0.5 1 2 km
Bakgrundskartor © Lantmäteriet
SKB/DHI/msa 2014-04-17
N

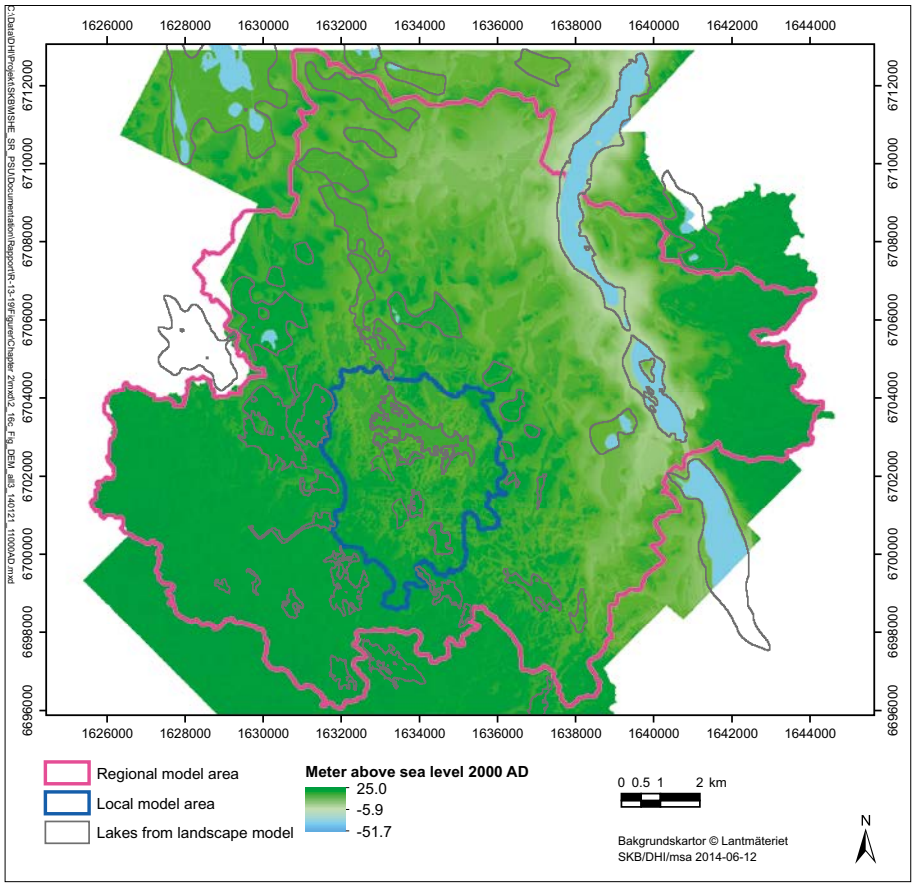

Figure 2-16. *Ground-surface elevation and bathymetries (m elevation) at 3000 AD (upper figure), 5000 AD (middle figure) and 11000 AD (lower figure). For orientation, the maps show the extents of the MIKE SHE regional and local model areas (Sections 3.1.1 and 3.3.2), and the largest extents of future lakes in the landscape model (Brydsten and Strömgren 2013).*

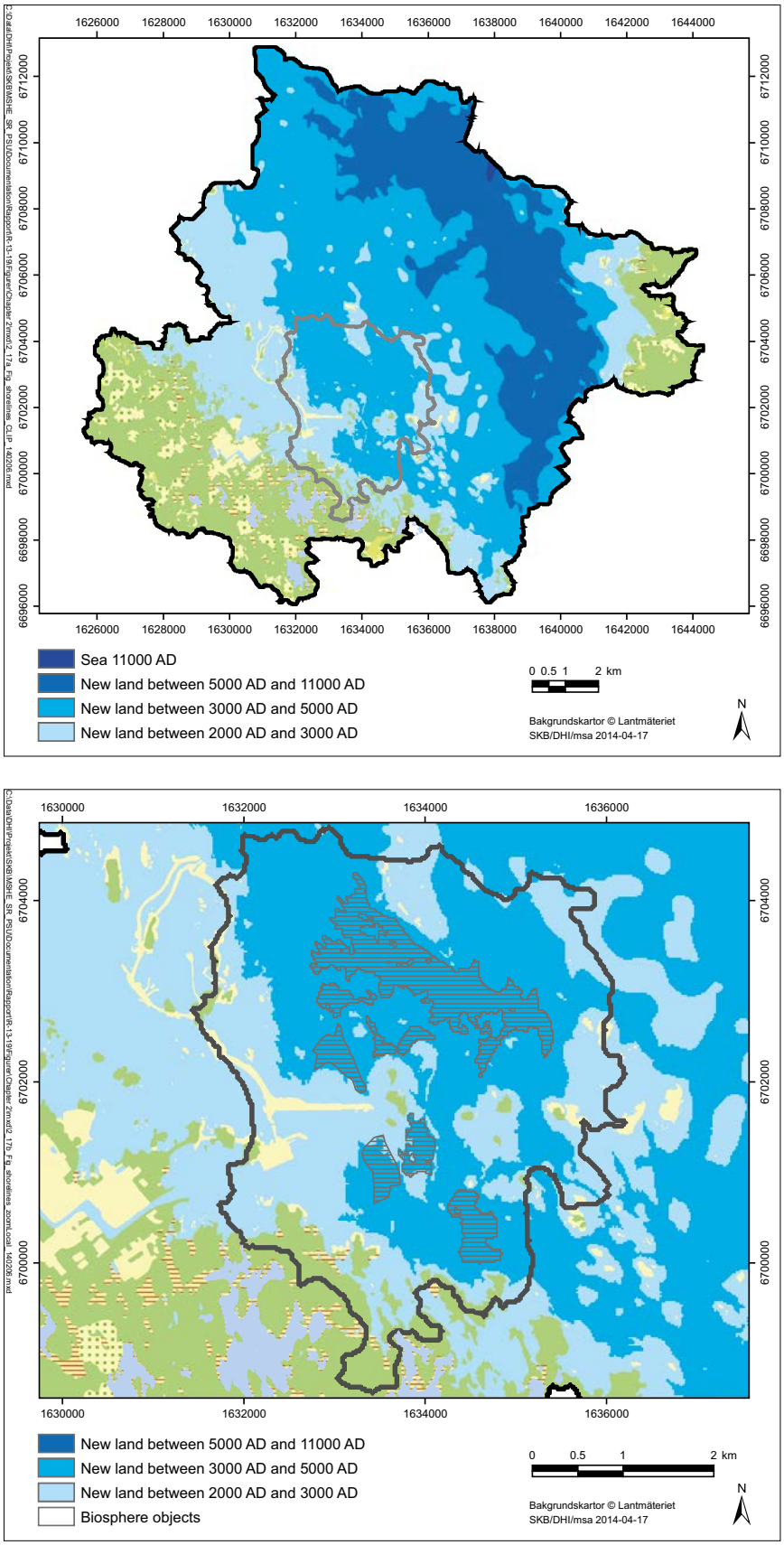

Figure 2-17. *MIKE SHE regional (upper figure) and local model area (lower figure, including delineated biosphere objects), showing the present sea shoreline and land areas formed due to shoreline displacement between 2000–3000 AD, 3000–5000 AD and 5000–11,000 AD. There is no sea in the regional and local model areas at 11,000 AD (Brydsten and Strömgren 2013), but in MIKE SHE a small sea area is kept in the north as a boundary condition for the regional model.*

2.2.2 Regolith, vegetation and land use

Regolith

Data on surface distribution, depth and stratigraphy of regolith at each of the considered future times are described in Brydsten and Strömgren (2013). Figure 2-18 shows the modelled spatial distribution of regolith at 3000, 5000 and 11,000 AD, classified according to regolith types utilised in MIKE SHE (cf Section 2.1.4). The surface distribution of regolith will continuously change due to continued accumulation of sediment and peat and due to sediment erosion on the sea floor. Moreover, the proportional distribution of different regolith types in terrestrial areas will change due to shoreline displacement. In particular, it can be expected that the proportion of terrestrial areas with clay, and hence the proportion of arable land, will increase as the broad and presently submerged Öregrundsgrepen valley is uplifted.

As a result of shoreline displacement, new lakes will be formed and subsequently filled with gyttja and peat. In present terrestrial areas, the proportion of peat will increase significantly due to infill of shallow lakes and formation of a peat cover on low-lying wetlands. The proportion of peat-covered areas is also affected by the climate. Specifically, in a colder climate a large proportion of the landscape will likely be covered by peat, formed in mires that are mixtures of fens and bogs. A wetter climate promotes the formation of bogs, whereas a warmer climate with higher evapotranspiration may prevent bog development.

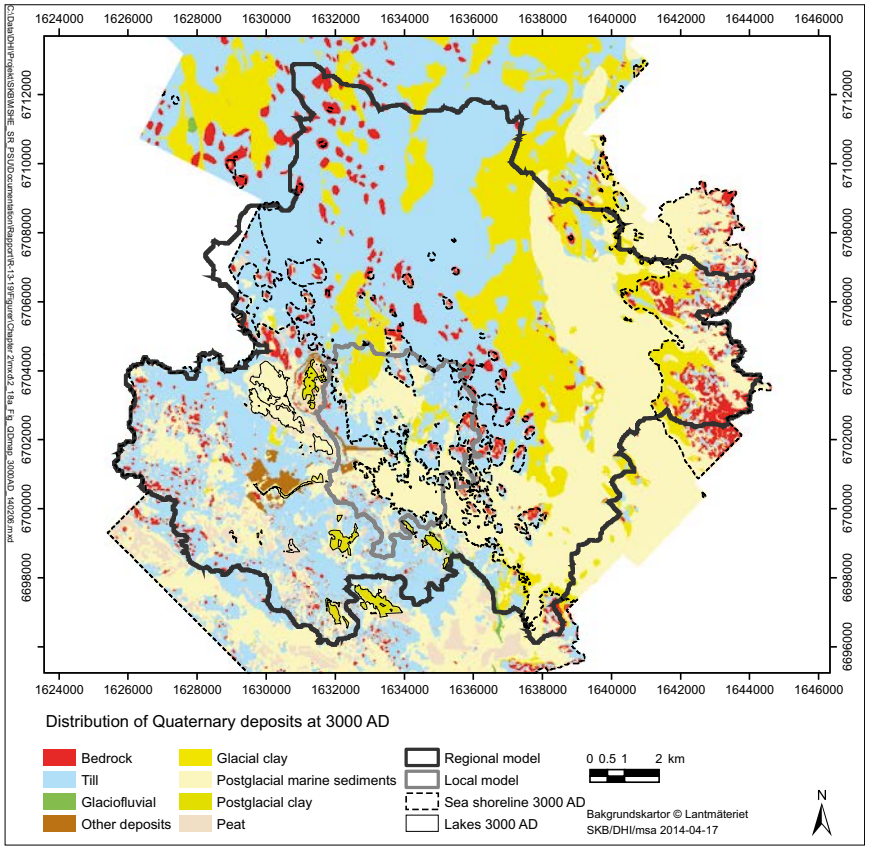

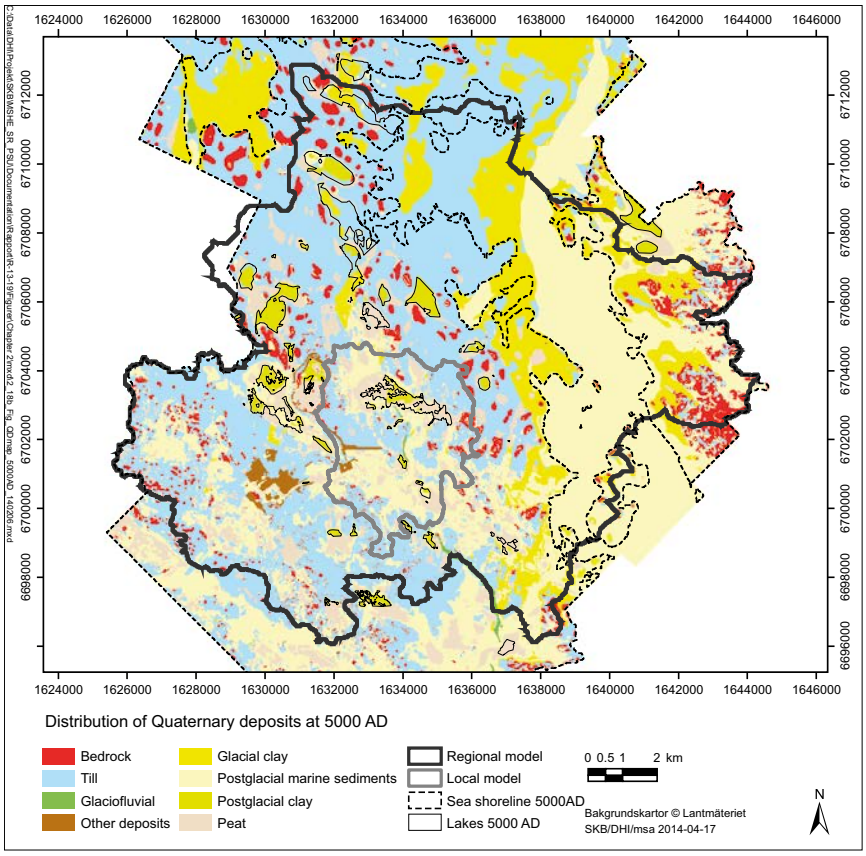

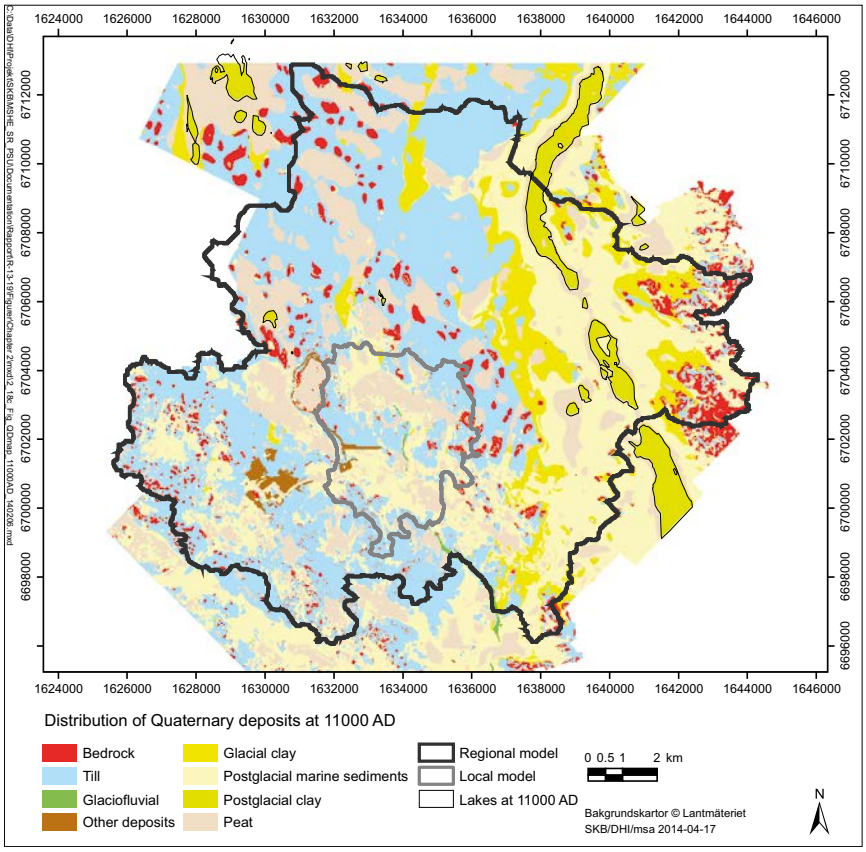

Figure 2-18. *Maps showing surface distribution of regolith at 3000 AD (upper figure), 5000 AD (middle figure), 11,000 AD (lower figure), and sea and lake shorelines at each time according to Brydsten and Strömgren (2013). Note that the regolith types Postglacial marine sediments and Postglacial clay are merged to the type Clay gyttja and gyttja in the corresponding 2000 AD map (Figure 2-2).*

Vegetation and land use

Spatially and temporally variable vegetation parameters (e.g. leaf-area index and root depth) are required in the whole model domain at each time for evapotranspiration calculations in MIKE SHE. A map of vegetation and land use, including associated parameters, was produced for each time (3000, 5000 and 11,000 AD) using the same methodology as described in Bosson et al. (2010). Specifically, Bosson et al. (2010) compared the map of surface distribution of regolith of Hedenström and Sohlenius (2008) with the vegetation map of Löfgren (2008, 2010), and thereby identified the dominating vegetation type associated to each regolith type. The coupling between regolith type and type of vegetation and land use of Bosson et al. (2010) was adapted to the maps of surface distribution of regolith at each considered time (Figure 2-18), see Table 2-3. The resulting maps of vegetation and land use are shown in Figure 2-19.

Table 2-3. Assigned types of vegetation and land use for different regolith types.

Regolith type	Type of vegetation or land use
Exposed rock	Scots-pine dominated forest
Till	Needle-leaved forest
Glacial clay	Arable land
Postglacial clay	Arable land
Thin layer of postglacial clay	Wetland
Other types of regolith	Needle-leaved forest

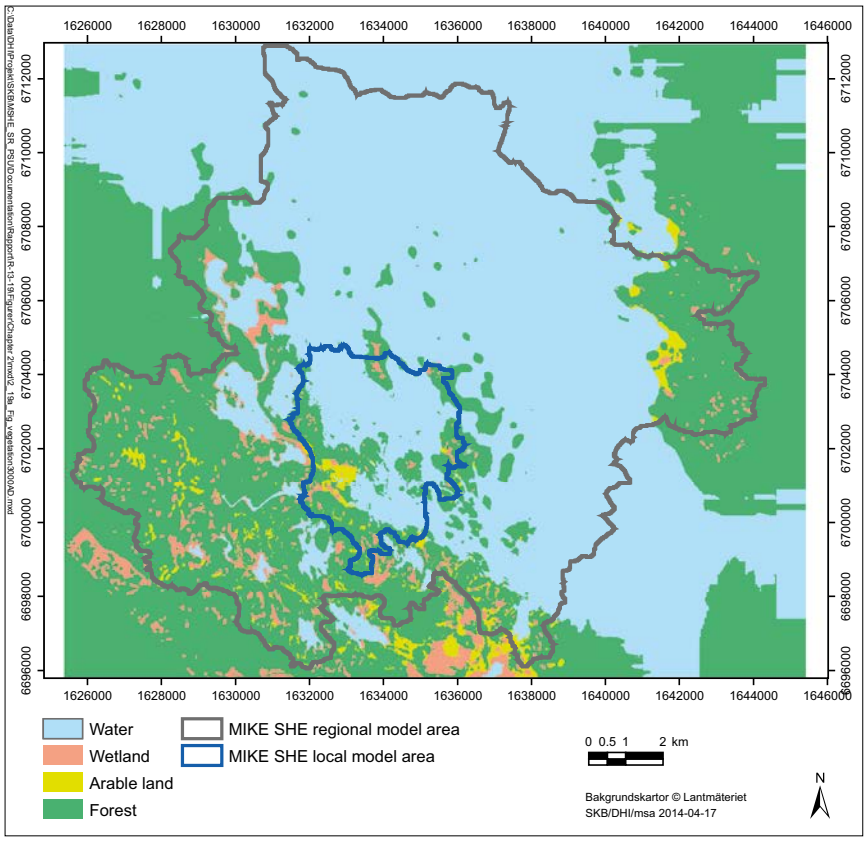

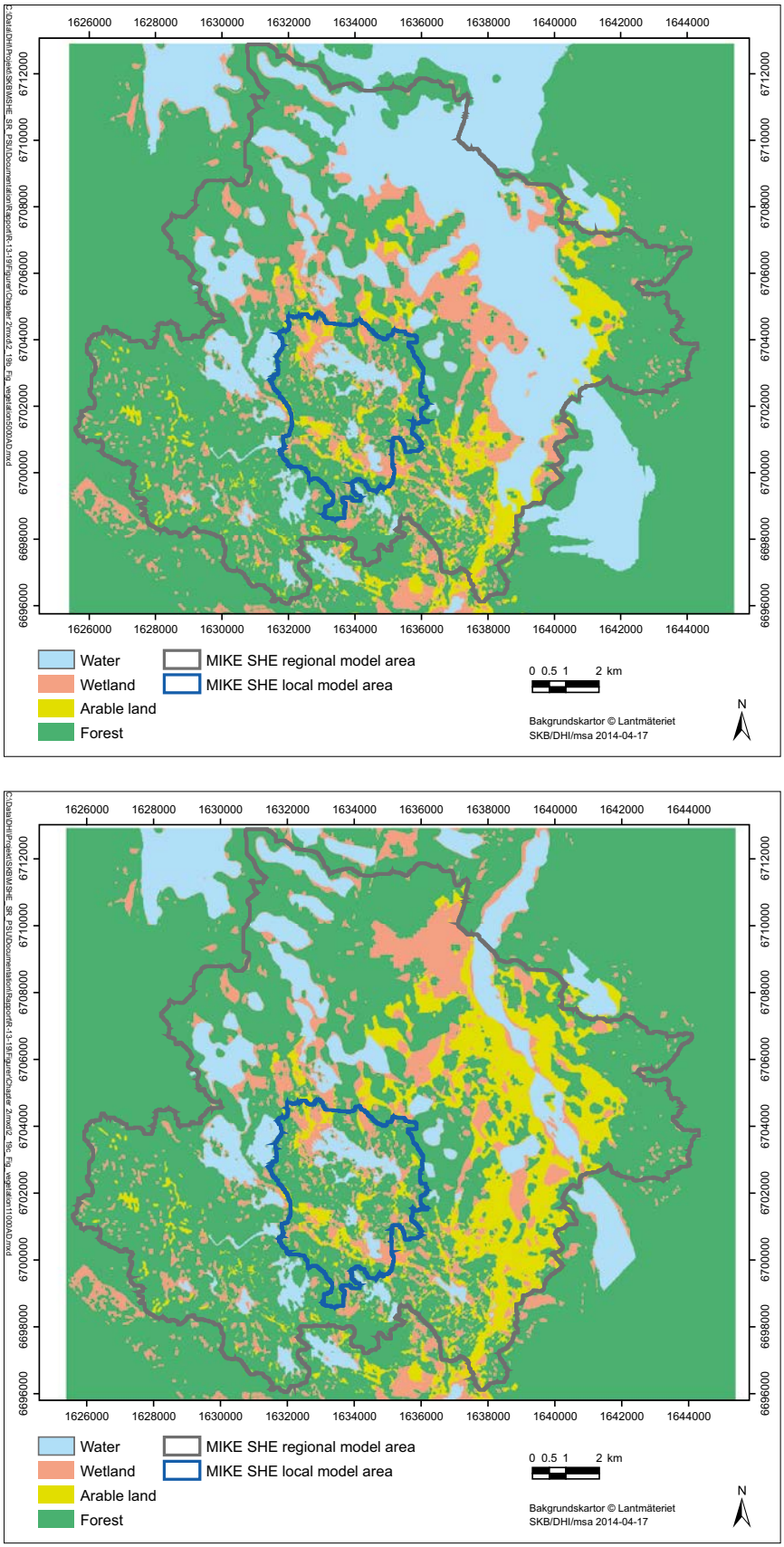

Figure 2-19. *Maps showing modelled surface distribution of vegetation types at 3000 AD (upper figure), 5000 AD (middle figure) and 11,000 AD (lower figure).*

2.2.3 Locations of catchment-area boundaries, lakes and streams

The overview map in Figure 2-20 shows future catchment areas, lakes (maximum extents are shown) and streams within the MIKE SHE regional model area, according to the landscape modelling (Brydsten and Strömgren 2013). Figure 2-21 details the temporal development of the stream network as a result of shoreline displacement during the period 3000–11,000 AD. At each time, MIKE SHE uses associated catchment-area boundaries in terrestrial areas as no-flow boundaries of the regional model area (red line in Figure 2-20). As can be seen in Figures 2-20 and 2-21, two streams and their associated stream discharges cross the downstream parts of the model-area boundary, which otherwise is described as a no-flow boundary. Moreover, three streams and their associated discharges cross the upstream part of the model-area boundary, in the west, south, and east.

Catchment-area boundaries, lakes and streams are identified by Brydsten and Strömgren (2013) using the present-day DEM (Strömgren and Brydsten 2013), whereas the DEM associated to each considered future time (cf Section 2.2.1) is used to define lakes and streams in the MIKE 11 channel-flow modelling tool. Therefore, compared to the stream network of Brydsten and Strömgren (2013), in MIKE 11 it was required to adjust some local stream stretches and cross-section elevations to obtain a numerically stable match between stream sections and the DEM (see also Section 3.4.3). The implications of these adjustments in terms of hydrological connections between biosphere objects are described in Section 7.2.

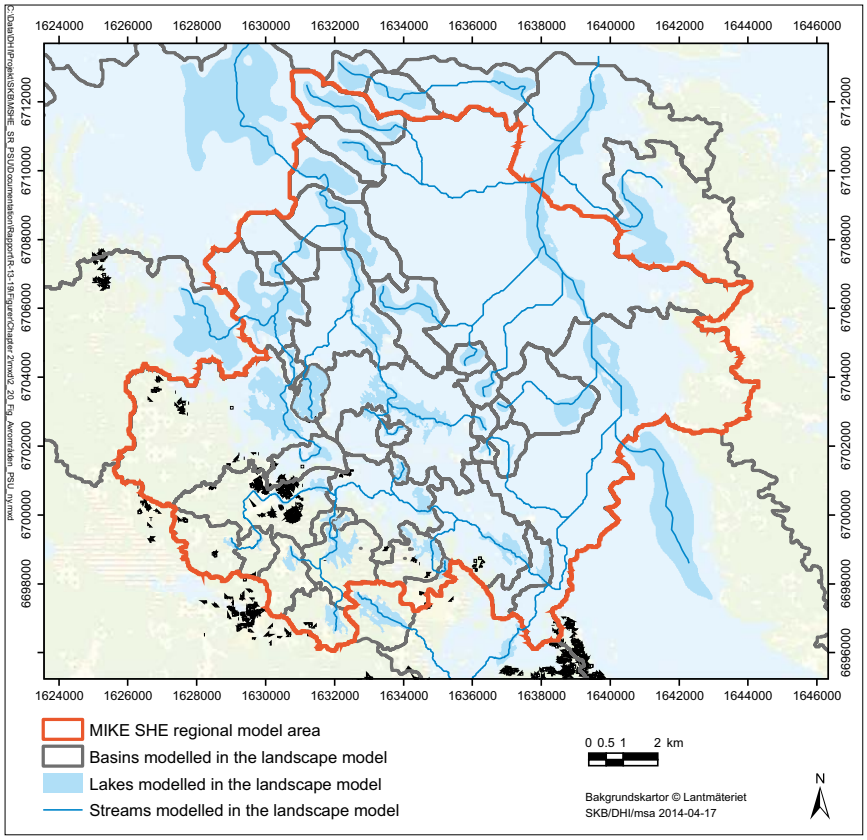

Figure 2-20. *Future catchment areas (basins), lakes and streams within the MIKE SHE regional model area (Brydsten and Strömgren 2013). The red line represents the MIKE SHE model-area boundary.*

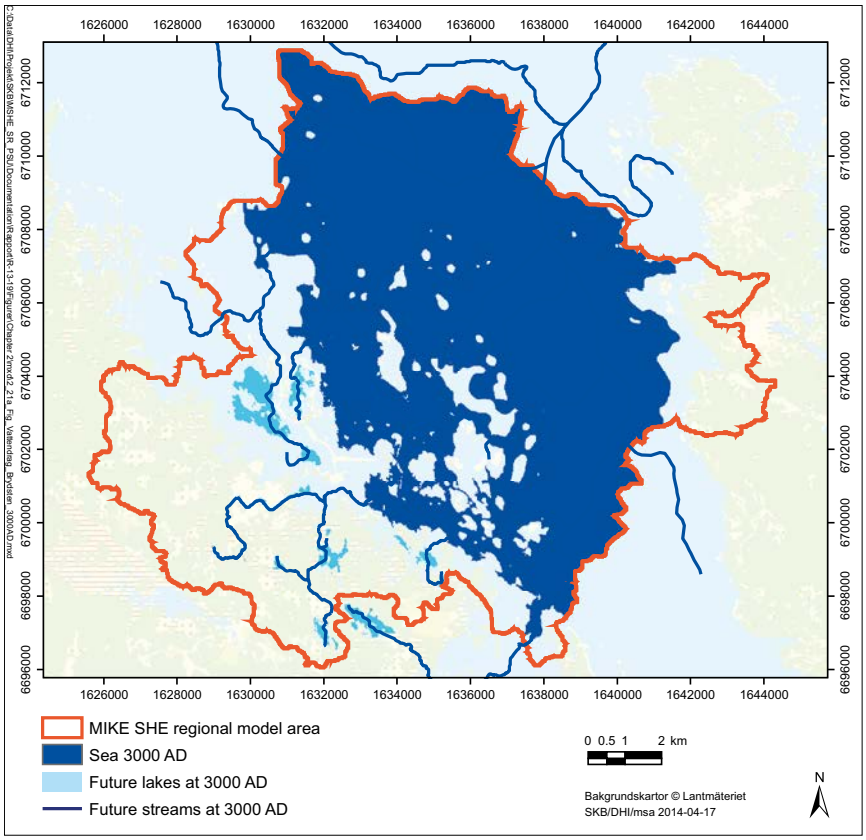
1626000
1628000
1630000
1632000
1634000
1636000
1638000
1640000
1642000
1644000
6712000
6710000
6708000
6706000
6704000
6702000
6700000
6698000
6696000
MIKE SHE regional model area
Sea 3000 AD
Future lakes at 3000 AD
Future streams at 3000 AD
0 0.5 1 2 km
N
Bakgrundskartor © Lantmäteriet
SKB/DHI/msa 2014-04-17

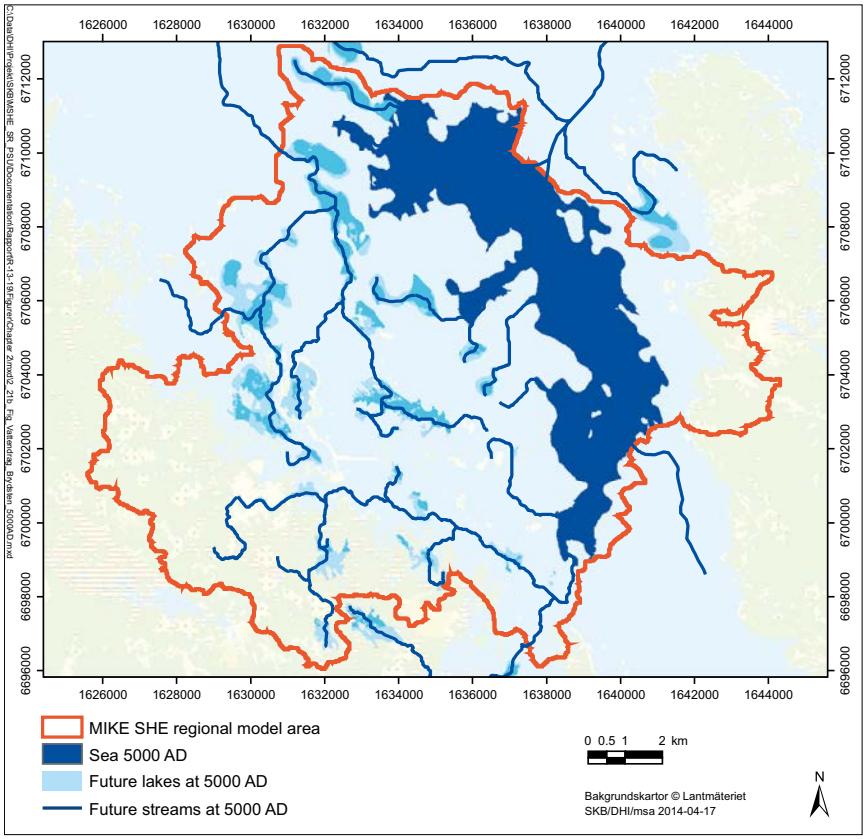
1626000
1628000
1630000
1632000
1634000
1636000
1638000
1640000
1642000
1644000
6712000
6710000
6708000
6706000
6704000
6702000
6700000
6698000
6696000
MIKE SHE regional model area
Sea 5000 AD
Future lakes at 5000 AD
Future streams at 5000 AD
0 0.5 1 2 km
N
Bakgrundskartor © Lantmäteriet
SKB/DHI/msa 2014-04-17

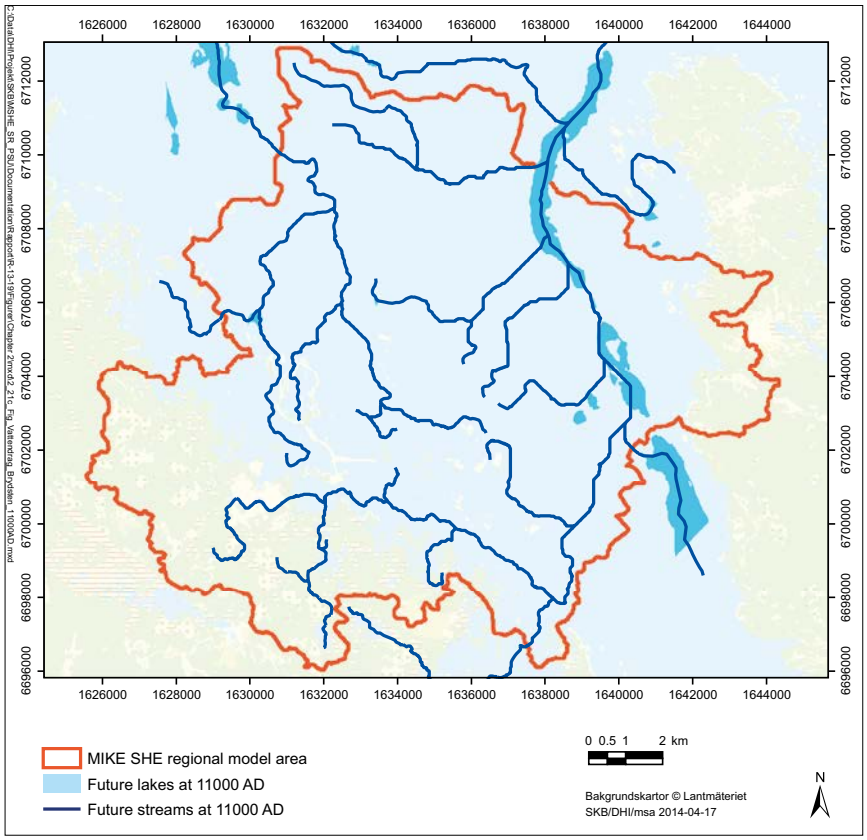

Figure 2-21. *Future lakes, streams and sea shoreline within the MIKE SHE regional model area at 3000 AD (upper figure), 5000 AD (middle figure) and 11,000 AD (lower figure) (Brydsten and Strömgren 2013).*

2.3 Delineation of biosphere objects

2.3.1 Biosphere objects for temperate conditions

The groundwater-flow modelling tool DarcyTools was used to identify discharge locations at the interface between rock and regolith for temperate climate conditions. Delineations of so called biosphere objects in the landscape were based on preceding simulations, whereas the modelling results of Odén et al. (2014) and Öhman et al. (2014) were used to check these delineations. Biosphere objects are areas that may be affected by a potential future release of radionuclides from SFR, which implies that delineation and characterisation of such objects and their temporal development are important issues within the SR-PSU project. Their delineations are inputs to the MIKE SHE modelling, for calculation of water balances and flow parameters required for radionuclide transport and dose calculations (see Chapter 7).

Similar to the particle-tracking method of MIKE SHE (cf Section 1.1.3), discharge locations are in DarcyTools identified by tracking inert "water parcels" as they are advected by groundwater flow in the model volume. Specifically, discharge locations in this case refer to those locations where particles, released from SFR 1 and SFR 3 into a three-dimensional groundwater-flow field, exit at the rock-regolith interface.

Specifically, Odén et al. (2014) calculated discharge locations for particles released in stationary, DarcyTools-calculated groundwater-flow fields at the times 2000, 2500, 3000, 3500, 5000, and 9,000 AD. Figure 2-22 illustrates discharge locations, in the form of particle densities (number of particles per m^2), calculated for the times 3500, 5000 and 9000 AD using the base-case setup of the rock that was also delivered to MIKE SHE (BASE_CASE1_DFN_R85), cf Section 2.1.3. In the particle tracking, 1,000,000 particles were distributed among SFR 1 and SFR 3 facility parts, proportional to facility volume, and the particles released from each facility part were released uniformly within each facility volume. It is noted that the flow-modelling domain of Odén et al. (2014) is enlarged to the north compared to that of Öhman et al. (2013) (cf Figure 2-5).

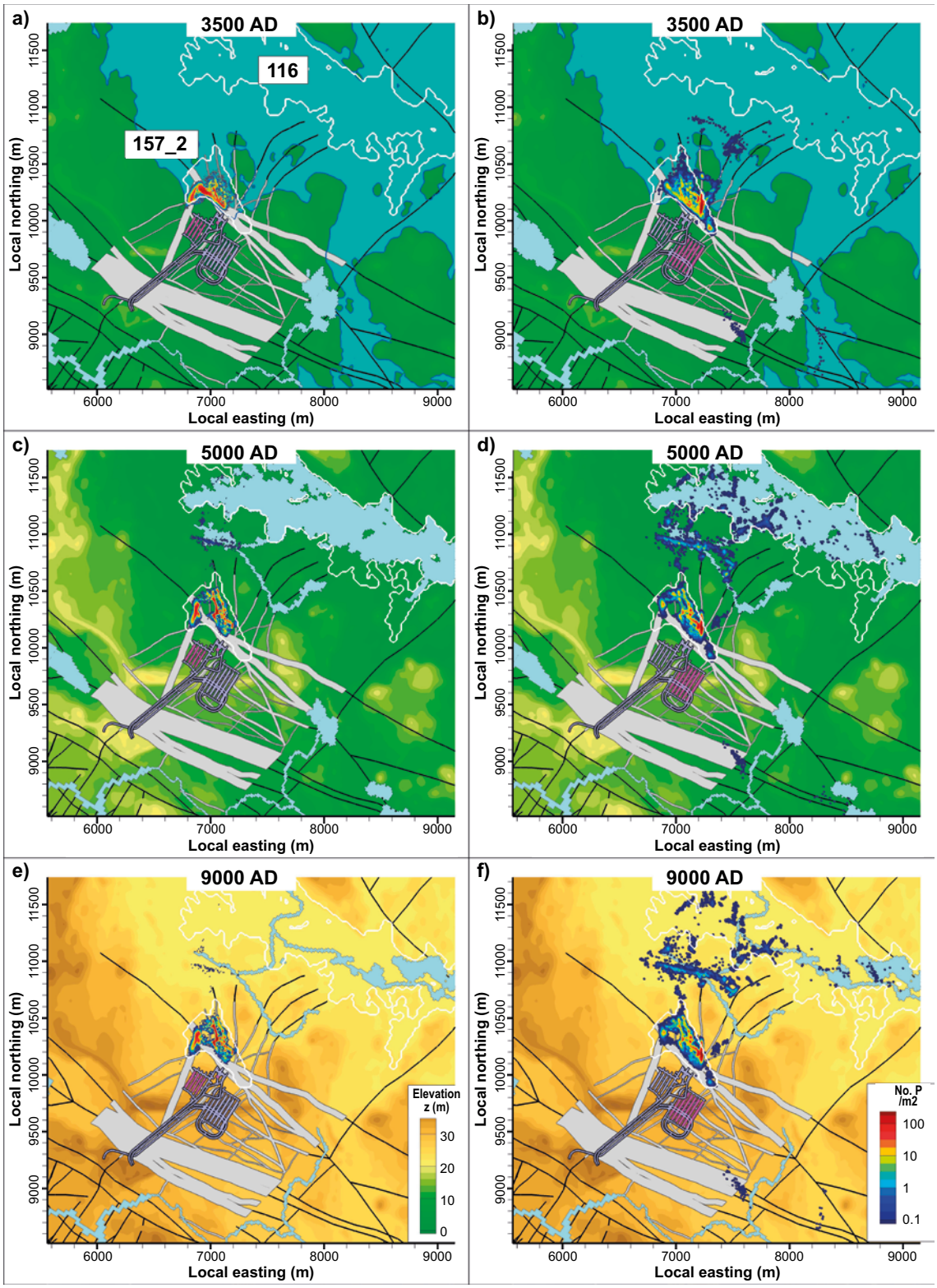

Figure 2-22. *Overview maps of DarcyTools-calculated discharge locations at the interface between rock and regolith at the times 3500, 5000 and 9000 AD (Odén et al. 2014). Left: Discharge locations for particles released from SFR 1. Right: Discharge locations for particles released from SFR 3.*

Based on the discharge-location calculations and also other types of information related to landscape development, seven biosphere objects are delineated (Figure 2-23; for further details, see SKB 2014a):

- **Biosphere object 116:** A lake is formed (i.e. separated from the sea) at 4500 AD and it is infilled (transformed into a wetland) at 9800 AD.
- **Biosphere object 121_1:** This object is a lake that is formed at 3900 AD and infilled at 6300 AD.
- **Biosphere object 121_2:** This object is separated from the sea at 3000 AD and thereafter transformed into a wetland, without passing a lake stage.
- **Biosphere object 157_1:** This object is a lake that is formed at 4500 AD and infilled at 5700 AD.
- **Biosphere object 157_2:** This object is separated from the sea at 3000 AD and thereafter transformed into a wetland, without passing a lake stage.
- **Biosphere object 159:** This object is a lake that is formed at 4000 AD and infilled at 7000 AD.
- **Biosphere object 160:** This object is a lake that is formed at 3300 AD and infilled at 8500 AD.

Discharge-location densities are strongly correlated to the local topography and ground-surface intercepts of deformation zones (Odén et al. 2014). According to Figure 2-22, discharge locations for particles that in DarcyTools are released from SFR 1 are rather independent of shoreline displacement. Most of the SFR 1 discharge locations are found within a low-lying area north of SFR 1, in the vicinity of the junction between two steeply dipping deformation zones. Discharge locations for particles released from SFR 3 are located north of the SFR facility but also southeast of SFR 3, which likely is due to the influence of the SFR pier on groundwater flow in the vicinity of SFR. Up to 5000 AD, discharge locations for particles released from SFR 3 demonstrate a larger dependence on shoreline displacement. After 5000 AD, discharge locations are more dependent on the ground-surface topography than continued shoreline displacement.

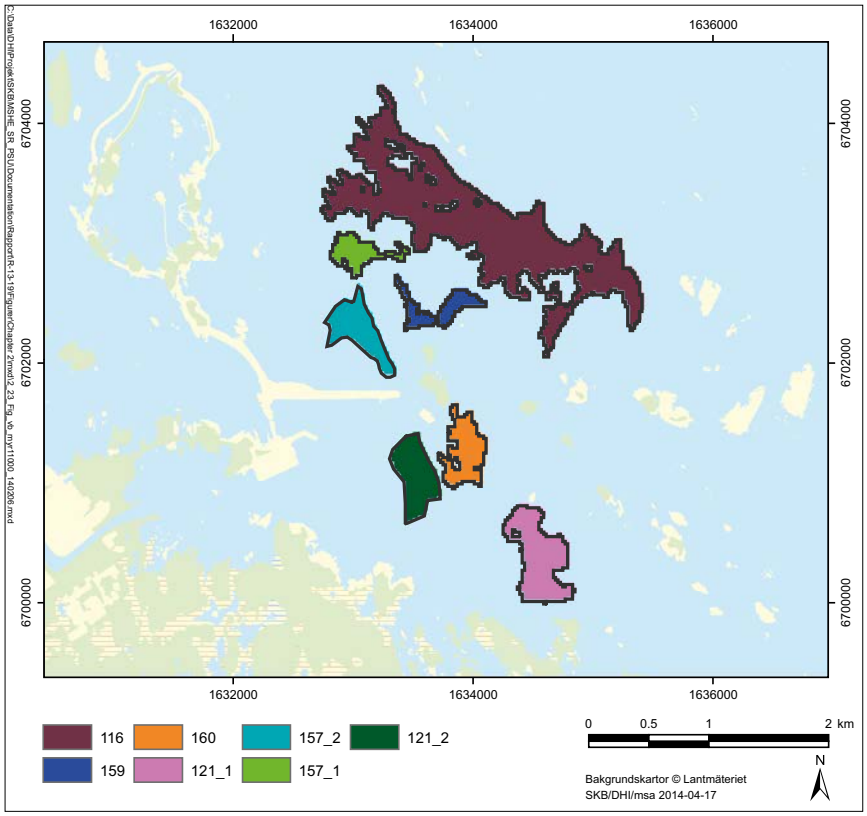

Figure 2-23. *Overview map showing the seven delineated biosphere objects.*

As shown in Figure 2-22, there is a high density of DarcyTools-calculated discharge locations at the rock-regolith interface within biosphere object 157_2, which is a low-lying area north of SFR 1. For instance, using the DarcyTools model setup at 5000 AD, Odén et al. (2014) found that c 4% of the groundwater flow from the rock to the regolith within the boundaries of biosphere object 157_2 passes SFR waste-disposal facilities. Moreover, they concluded that from the SFR 1 facility, many groundwater flow paths in the rock converge to this specific area due to enclosure of three deformation zones, two steeply dipping and one gently dipping zone just below SFR 1.

2.3.2 Discharge areas for periglacial conditions with permafrost

As described further below (Section 5.8), Odén et al. (2014) used DarcyTools to simulate steady-state groundwater flow in rock and taliks for permafrost conditions. The figures below show discharge locations at the interface between rock and regolith for a case with shallow permafrost (–60 m elevation), for two variants in terms of the locations of potential taliks. Specifically, Figure 2-24 shows discharge locations for a variant with taliks at the two lakes present at 20,000 AD (Brydsten and Strömgren 2013), whereas the discharge locations in Figure 2-25 are for a variant with taliks both at lakes and streams present at 20,000 AD (Brydsten and Strömgren 2013), and also at small surface waters according to the MIKE SHE simulations for temperate conditions at 11,000 AD.

As can be seen in Figure 2-24 (lake taliks only), groundwater flow from the unfrozen system below the permafrost to the active layer, superimposing the permafrost, is primarily influenced by the governing regional hydraulic gradient. For this simulation case, less than 1% of the particles released at SFR discharge north of SFR, whereas more than 99% discharge at the two lakes at the north-eastern DarcyTools model boundary. It should be noted that in this case, some high-elevation small surface waters (cf above) were also used as hydraulic boundary conditions, in order to mimic a regional-scale hydraulic gradient from depth to the discharge locations (Odén et al. 2014).

According to Figure 2-25 (potential taliks at lakes, streams and small surface waters), a higher density of potential taliks increases the influence of the local topography on the groundwater-flow pattern, specifically the influence of topographical differences between taliks. For this simulation case discharge locations are located to areas north of SFR but not at the two lakes at the north-eastern model boundary.

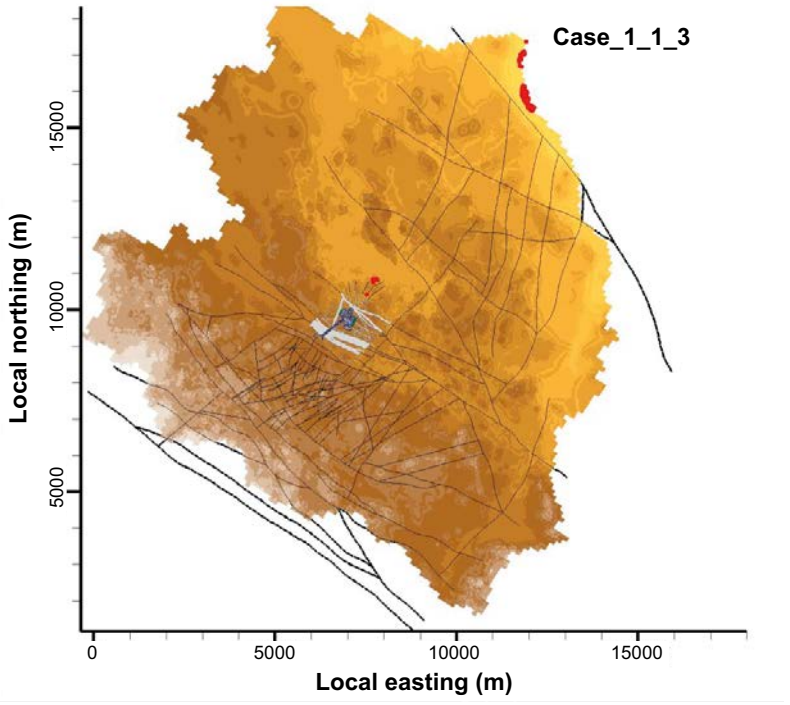

Figure 2-24. *Overview map of discharge locations (red) for a periglacial simulation representing shallow permafrost (down to –60 m elevation) and taliks at the two lakes present at 20,000 AD according to the landscape modelling (Odén et al. 2014).*

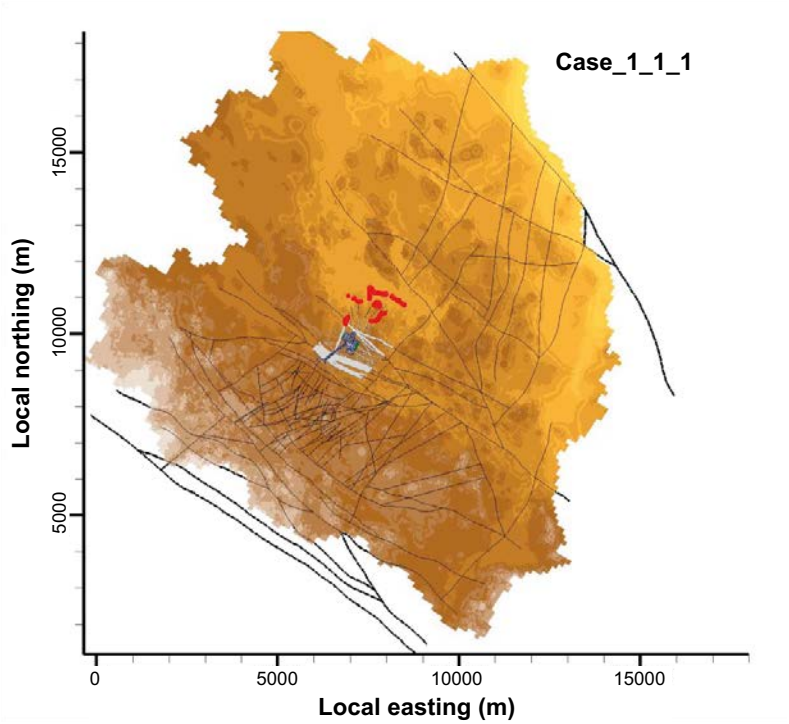

Figure 2-25. *Overview map of discharge locations (red) for a periglacial simulation representing shallow permafrost (down to –60 m elevation) and taliks both at lakes and streams present at 20,000 AD according to the landscape modelling, and also at small surface waters according to the MIKE SHE simulations for temperate conditions at 11,000 AD (Odén et al. 2014).*

3 Setup of MIKE SHE water-flow models

3.1 Regional model for present conditions

3.1.1 Model domain and grid

The MIKE SHE regional model domain (Figure 3-1) has an area of c 180 km^2 and a vertical extent down to –634 m elevation. The model boundaries follow water divides according to the DEM (Strömgren and Brydsten 2013), and they are therefore adjusted compared to the MIKE SHE regional model in SR-Site (Bosson et al. 2010).

In the horizontal direction, the regional model has a grid size of 80 m, whereas the grid size varies with depth in the vertical direction. The regolith is divided into two calculation layers (see description in Section 3.1.4) and the rock is divided into 14 layers, with a vertical discretization of 16 m in the upper 100 m of the rock and 32 m down to –234 m elevation. Below this elevation, there are three calculation layers, with a thickness of 80 m, 128 m and 192 m, respectively, down to the bottom of the model domain.

3.1.2 Lakes and streams

Lake thresholds, and cross sections and bottom elevations of streams described in Section 2.1.5 were implemented in MIKE 11. Moreover, parameters characterising the bed resistance in streams (the so called Manning number, M) and the water exchange between MIKE 11 and MIKE SHE (leakage coefficient) are equivalent to those of Bosson et al. (2008, 2010).

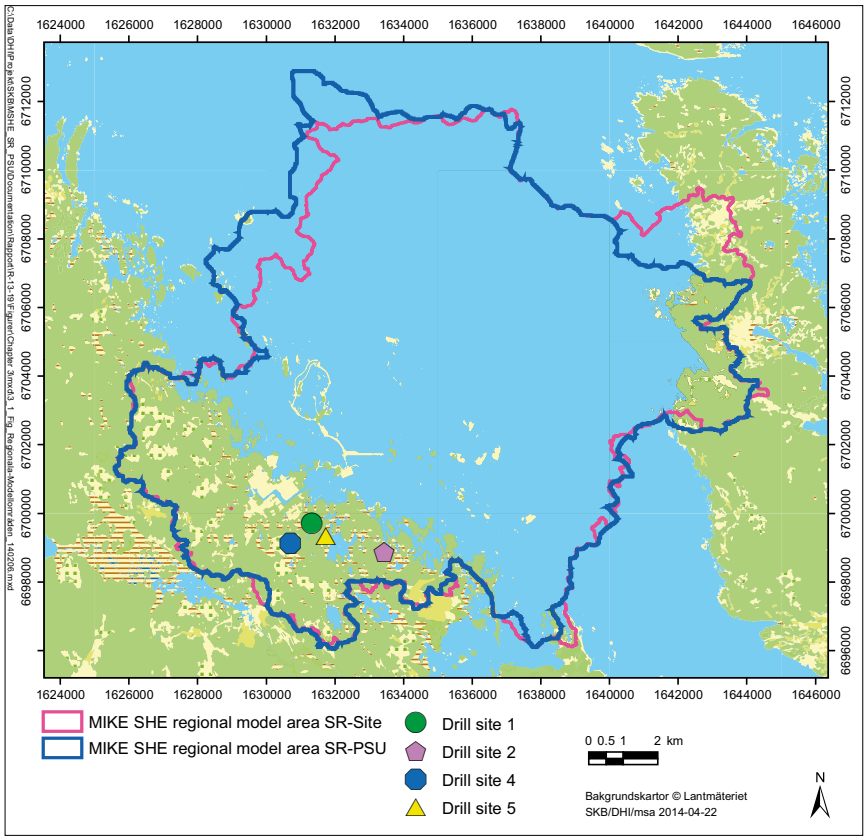

Figure 3-1. *MIKE SHE regional model area in the SR-PSU project, and the MIKE SHE regional model area in SR-Site (Bosson et al. 2010). The drill sites shown on the map are discussed in Section 4.3.*

3.1.3 The unsaturated zone

Numerical calculations of transient water flow in the unsaturated zone are generally very time consuming. Therefore, in order to reduce the simulation time MIKE SHE simulates unsaturated flow in a limited number of grid cells. The selection of grid cells to be included in these simulations is based on a classification system, according to which similar vertical grid-cell columns (in terms of e.g. RDM, vegetation and land use, and depth to the groundwater table) are grouped together. Unsaturated water flow is then calculated for one randomly chosen grid-cell column from each group. To ensure proper calculation of evapotranspiration processes in ponded areas, unsaturated water flow is calculated in all grid cells in such areas. The vertical grid-cell discretization used in this study is the same as that used in Bosson et al. (2010), with a resolution of 0.1 m in the depth interval 0–1 m below ground surface and coarser discretization at larger depths (see Bosson et al. 2010 for details).

3.1.4 The saturated zone

In MIKE SHE, there is a distinction between geological (regolith and rock) layers and calculation layers. Specifically, hydrogeological parameters are assigned to geological layers, whereas flow calculations consider calculation layers. Geological layers defined by the RDM are the basis for the model parameterisation of the regolith (see Sections 2.1.2 and 2.1.4). In the MIKE SHE regional model setup, the regolith is divided into two calculation layers (Section 3.1.1). At locations where the RDM consists of more than two regolith layers, the hydrogeological properties of the calculation layers are obtained by spatial averaging of the regolith-layers properties (for details on the averaging procedure, see Bosson et al. (2010)).

As described in Section 2.1.3, it was required to perform spatial averaging of the hydrogeological-properties data set delivered from DarcyTools, due to the vertical and horizontal discretizations of the MIKE SHE model and its limited capability to represent anisotropic hydrogeological properties in the horizontal plane. Specifically, the MIKE SHE model represents the rock with a vertical spatial resolution of 16 m down to –100 m elevation, whereas the delivered data set has a vertical spatial resolution of 4 m down to –170 m elevation and 16 m below this level. Moreover, the DarcyTools delivery contains anisotropic hydrogeological-properties data in the horizontal plane (i.e. $K_x \neq K_y$), which cannot be handled in MIKE SHE.

In accordance with the methodology of Bosson et al. (2010), the vertical hydraulic conductivity (K_v) of each MIKE SHE grid cell was calculated as the harmonic mean of the corresponding DarcyTools grid cells. The methodology chosen to calculate K_h (isotropic horizontal hydraulic conductivity) was based on tests of different alternatives. Specifically, down to –170 m elevation in the rock the arithmetic mean of the hydraulic conductivity in each of the two horizontal directions (K_x and K_y) delivered from DarcyTools was first calculated for each MIKE SHE grid cell. This was followed by calculation of K_h as the geometric mean of these two averages.

3.1.5 Boundary and initial conditions and time stepping

In MIKE SHE, the upper boundary condition is represented as daily time series of precipitation and potential evapotranspiration (PET), whereas near-surface air temperature is required to calculate snow accumulation and snow melt during simulation. No water flow is assumed to occur across the bottom boundary at –634 m elevation. Groundwater divides are assumed to coincide with surface-water divides, delineated according to the DEM (Strömgren and Brydsten 2013). Hence, in onshore (land) areas no water flow is assumed to occur across external model boundaries. In offshore (sea) areas of the model domain, the sea is represented by a geological layer of highly permeable material and a time-varying head equal to time series of measured sea level (cf Werner et al. 2013).

Due to the thickness of the upper calculation layer, near-surface groundwater flow in the high-conductive uppermost part of the regolith is represented as subsurface drainage at a depth of 0.5 mbgs in terrestrial parts of the model area. Subsurface drainage acts to route water from the upper part of the saturated zone to the nearest surface water (i.e. the MIKE 11 network or the sea), whereas the subsurface-drainage response time is determined by a drainage time constant. For further details on the implementation of subsurface drainage in MIKE SHE Forsmark models, see Bosson et al. (2008, 2010).

MIKE SHE simulations were run using locally measured meteorological data (precipitation, PET and near-surface air temperature) and sea-level data for the period May 15, 2003–December 31, 2007. Only transient simulations have been conducted, and initial conditions were generated by cycling the simulated period twice, followed by production of the simulation results summarised in Section 4.4. The simulations of the present study use the same maximum time step for each MIKE SHE compartment as those presented in Bosson et al. (2010).

3.1.6 Vegetation and overland flow parameters

Temporally variable vegetation parameters, such as leaf-area index and root depth, must be specified for each type of vegetation and land-use type represented in the model domain (cf Section 2.1.7). In the present study, the MIKE SHE-model setups representing both present and future conditions use the vegetation-parameter set described in Bosson et al. (2008, 2010). Moreover, calculation of overland flow is required for MIKE 11 calculations as overland flow provides lateral runoff to the MIKE 11 stream network. The associated overland-flow parameters, such as Manning number and detention storage, are in the present study identical to those of Bosson et al. (2008, 2010).

3.2 Models for future conditions

3.2.1 Future times

MIKE SHE models were established to represent hydrological and near-surface hydrogeological conditions at the future times 3000, 5000 and 11,000 AD. Note that in MIKE SHE calculations of future conditions, the term time is used to signify a certain point in time (e.g. 3000 AD) that the model setup is intended to represent. The term time should not be confused with time steps used internally in transient MIKE SHE simulations (cf Sections 3.1.5 and 3.2.5). At 3000 AD, the coast-line is located immediately downstream of SFR according to the modelled shoreline displacement (cf Section 2.2.1). 5000 AD represents an intermediate stage, with co-existing lakes and mires within the regional MIKE SHE model area. At 11,000 AD, all former lakes within the MIKE SHE regional model area are transformed to terrestrial areas (Brydsten and Strömgren 2013).

3.2.2 Model domain and grid

Local models (Figure 3-2) were established and used to generate modelling results for each future time (one model for each time), whereas the objective of the corresponding regional models (one model for each time) primarily was to obtain time-varying external boundary conditions for the local models.

At each future time, the regional model has the same horizontal resolution as the present-day regional model (80 m). The horizontal resolution of the local models is 20 m, and in these models the regolith is divided into 4 calculation layers (two in the regional models). Moreover, down to –90 m elevation each calculation layer in the rock of the regional model is in the local models divided into two calculation layers, which results in 23 calculation layers in the rock (14 in the regional models).

3.2.3 Lakes and streams

Figure 3-3 shows the sea shoreline and future lakes (maximum extents) according to Brydsten and Strömgren (2013), and the MIKE 11 stream network at 3000, 5000 and 11,000 AD. The starting point for the definition of the MIKE 11 stream network at each time is the stream network presented by Brydsten and Strömgren (2013), cf Figure 2-21. Their network is based on the 2000 AD DEM (Section 2.1.1), and some stream stretches and cross-section elevations are adjusted in MIKE 11 to fit the corresponding DEM at each time (cf Section 3.1.2). As the Forsmark streams are very small and their widths are below the resolution of the DEM, each DEM defines the bank level. Based on typical geometries of present-day streams, most streams in the MIKE 11 stream network are assigned a width of 2 m and a depth of 1 m.

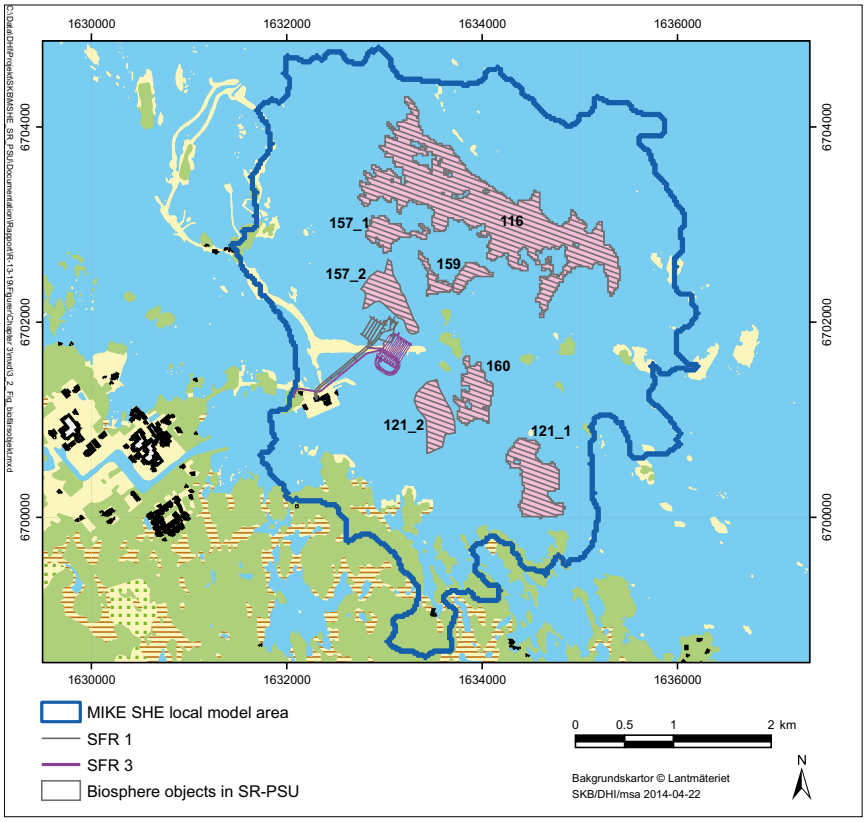

Figure 3-2. *MIKE SHE local model area (cf MIKE SHE regional model area in Figure 3-1). The map also shows the footprint of SFR 1 (i.e. existing parts of the SFR facility) and SFR 3 (i.e. its planned extent). The map also shows delineated biosphere objects within the local model area.*

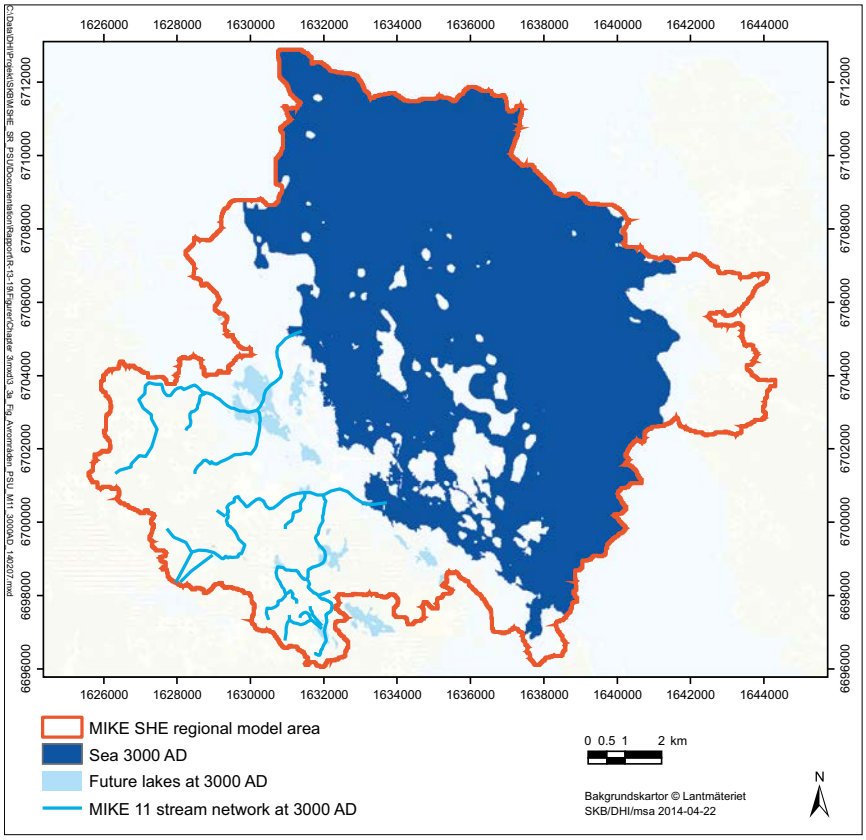

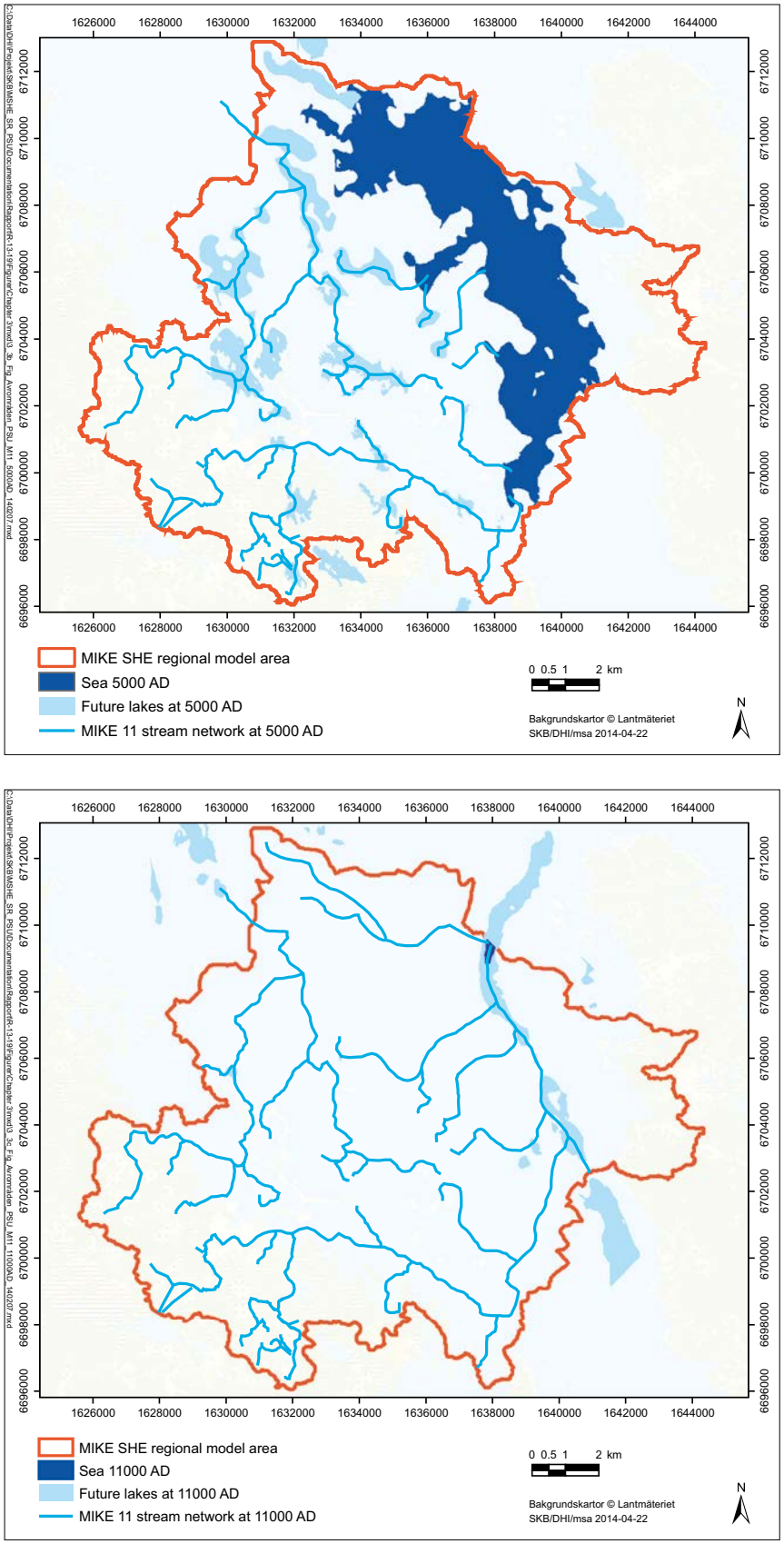

Figure 3-3. *Overview maps of the MIKE SHE regional model area, showing the sea within the MIKE SHE regional model area and future lakes (maximum extents) according to Brydsten and Strömgren (2013), and the MIKE 11 stream network at 3000, 5000 and 11,000 AD. There is no sea in the regional model area at 11,000 AD (Brydsten and Strömgren 2013), but in MIKE SHE a small sea area is kept in the north as a boundary condition for the regional model.*

3.2.4 The unsaturated and saturated zones, vegetation and overland flow

In each time-step specific MIKE SHE model setup, grid-cell column classifications and selections for calculation of water flow in the unsaturated zone were performed according to the methods described in Section 3.1.3. At each time, the regolith-layer model in MIKE SHE was established based on the associated regolith depth and stratigraphy model (Brydsten and Strömgren 2013). For each regolith type present in models of future times, the hydrogeological properties are identical to those of the present-day MIKE SHE model setup (Section 2.1.4), including parameter adaptations and adjustments presented in Section 4.3. Moreover, at each time, the hydrogeological properties of the rock are identical to those presented in Section 2.1.3. The present study uses the same set of vegetation and overland flow parameters as that of Bosson et al. (2008, 2010).

3.2.5 Boundary and initial conditions and time stepping

MIKE SHE-simulations were run using the meteorological data sets described in Section 2.2.1. The regional model for each time (3000, 5000 and 11,000 AD) is used to generate time-varying external boundary conditions for the corresponding local model. Initial conditions, in terms of hydraulic heads and depths of overland water, were also extracted from the regional models. Table 3-1 lists time steps (MIKE SHE internal) and model control parameters used in the local models.

Table 3-1. MIKE SHE-internal time steps and model control parameters of the local models. OL = overland flow, UZ = unsaturated zone, SZ = saturated zone.

Parameter	Value
Initial time step	1 h
Maximum allowed OL, UZ, ET time step	1 h
Maximum allowed SZ time step	3 h
MIKE 11 time step	2 s
Maximum Courant number OL	0.75
Maximum profile water balance error, UZ/SZ coupling	0.001 m
Maximum allowed UZ iterations	50
Iteration stop criteria	0.002
Time step reduction control: Maximum water balance error in one node (fraction)	0.03
Maximum allowed SZ iterations	80
Maximum head change per SZ iteration	0.05 m
Maximum SZ residual error	0.005 m/d
Saturated thickness threshold	0.05 m

4 Modelling and results for present conditions

4.1 Introduction

As part of SDM-Site, Johansson (2008) presents a description of present hydrological and near-surface hydrogeological conditions in Forsmark, based on evaluation of meteorological, hydrological and hydrogeological monitoring data up to the end of March, 2007 (Johansson and Öhman 2008) and numerical modelling using MIKE SHE (Bosson et al. 2008). Werner et al. (2013) compile and analyse corresponding, prolonged data sets up to the end of 2010, primarily to check conceptual models and to present sets of monitoring data used in the MIKE SHE (the present report) and DarcyTools modelling (Öhman 2010, Öhman and Follin 2010a, b, Öhman et al. 2012, 2013, Odén et al. 2014, SKBdoc 1346469).

Hence, the description of present hydrological and near-surface hydrogeological conditions in this chapter is kept relatively short, as it is focused on checking modelling results (using updated data and models available for the SR-PSU project) against models and descriptions presented in Johansson (2008).

4.2 Wells and water-resources management

All public water supplies in the Municipality of Östhammar are based on groundwater (Werner et al. 2010). The closest public water supply is located at the esker Börstilåsen, some kilometres southeast of SFR. According to the municipal comprehensive planning, there are no future needs for public water supplies in areas close to SFR. At present, c 30% of the inhabitants in Östhammar obtain their drinking water from private wells. The owner of the Forsmark nuclear power plant has previously drilled a number of boreholes in rock to prospect for water, but these boreholes are now abandoned. Today, there are some private wells (in regolith or drilled in rock) in land areas along the coast. Analyses of the well water show that the water quality varies from potable to non potable. Some wells are not used as drinking-water supplies but instead used for other purposes, e.g. irrigation of garden plots (Werner et al. 2010).

According to a regional analysis of well density (both wells in regolith and wells drilled in rock), the current well density varies between c 0.2 and 2 wells per km^2 depending on size and location of the analysed area (Kautsky 2001). The current well density is 0.2–0.9 wells per km^2 in different sub-areas within an area close to SFR (size 400 km^2) and 0.5–2 wells per km^2 in different sub-areas within northern Uppland (size 3,300 km^2).

Current water handling in Forsmark includes groundwater diversion from SFR, a cooling-water canal from the sea to the Forsmark nuclear power plant and cooling-water tunnels from the plant to the sea, the use of Lake Bruksdammen as a local water supply, and a groundwater-drainage system at the nuclear power plant. The groundwater inflow SFR has declined gradually over time since its completion. Specifically, the inflow was 720 L/min in 1988 and c 285 L/min in 2010 (Öhman et al. 2013), which corresponds to a 60% decrease in 23 years. There are no land improvements or drainage activities registered in public records. However, there are shallow ditches in the forests (the ditches are constructed for drainage purposes) and the lake outlet from Lake Eckarfjärden has previously been lowered in order to lower the level of the lake. Some minor natural springs have been observed in the area (see, for example, Nilsson and Borgiel 2005), but no springs are registered in public records.

4.3 MIKE SHE model calibration

Quality check and calibration of the MIKE SHE regional model were performed by comparing modelling results with hydrological and hydrogeological monitoring data (see summary in Werner et al. 2013) from the Forsmark site. As part of this process, the following main adaptations and adjustments were made of the initial regional model setup:

- Adaptation of unsaturated-zone classification (Section 3.1.3) and drainage-time constants (Section 3.1.5) to the RDM (Sohlenius et al. 2013a). Moreover, in order to improve model performance the subsurface-drainage level (cf Section 3.1.5) at Lake Eckarfjärden was changed from 0.5 to 0.75 mbgs.
- Increase of the horizontal (K_h) and the vertical hydraulic conductivity (K_v) for layer Z4a (representing gyttja/clay gyttja) by a factor of 30. Hence, for gyttja/clay gyttja K_h and K_v were both increased from the originally assigned value of $1.5 \cdot 10^{-8}$ m/s to $4.5 \cdot 10^{-7}$ m/s (cf Table 2-2).
- Increase of K_h and K_v for layer Z4b (representing glacial clay) by a factor of 30 below lakes. Hence, for glacial clay K_h and K_v were increased from the originally assigned value of $1.5 \cdot 10^{-8}$ m/s to $4.5 \cdot 10^{-7}$ m/s (cf Table 2-2). However, the originally assigned values of K_h and K_v were kept for lakes underlain by a clay layer (L3) in a previous version of the RDM (Hedenström et al. 2008), i.e. Bolundsfjärden, Puttan, Gällsboträsket, Eckarfjärden, Fiskarfjärden, Vambörsfjärden, Stocksjön and Lillfjärden.

Table 4-1 compares MAE (mean absolute error; absolute values of the differences between measurements and model outputs) and ME (mean error; differences between measurements and model outputs) data for the four gauging stations for the calibrated model setup of Bosson et al. (2010) and the present, calibrated model setup. Note that the MAE and ME data shown in the table for the present model setup consider some additional months of monitoring data compared to Bosson et al. (2010). According to the table, there are rather small MAE differences between the two model setups. In terms of surface-water levels, MAE is somewhat higher for the present setup compared to that of Bosson et al. (2010), whereas the opposite is noted in terms of stream discharges. However, the corresponding ME values for the present setup is positive and higher than those of Bosson et al. (2010), which implies that the present model setup to a larger extent underestimates surface-water levels and stream discharges compared to the model setup of Bosson et al. (2010).

Figures 4-1 and 4-2 show time-series plots of measured and model-calculated stream discharges at the discharge-gauging stations downstream Lake Eckarfjärden (gauging station PFM002668) and upstream Lake Bolundsfjärden (gauging station PFM005764) for the SDM-Site and SR-Site models of Bosson et al. (2008, 2010) and the present SR-PSU model setup. Specifically, it is noted that the model-calculated stream discharge downstream of Lake Eckarfjärden is lower in the present model setup compared to the Bosson et al. (2008, 2010) setups. The model-calculated accumulated stream discharge downstream of Lake Eckarfjärden is c 80% of the measured accumulated discharge, whereas the corresponding result was 87% in SDM-site (Bosson et al. 2008) and 112% in SR-Site (Bosson et al. 2010). Part of this stream-discharge deficit is propagated to the inlet to Lake Bolundsfjärden, which is located downstream of Lake Eckarfjärden. As Lake Eckarfjärden is located close to the upstream boundary of the MIKE SHE regional model area, i.e. relatively far from SFR, it is judged that the stream-discharge deficit has minor or no effects for the hydrological conditions at SFR and downstream areas in the modelling of future conditions.

Table 4-1. Comparison of MAE (mean absolute error) and ME (mean error) data in terms of surface-water levels (m) and stream discharges (m^3/s) for the calibrated model setup of Bosson et al. (2010) and the present calibrated model setup.

	Bosson et al. (2010) (May 15, 2003–Mar. 31, 2007)		Present setup (May 15, 2003–Dec. 31, 2007)	
Surface-water level	MAE	ME	MAE	ME
Lake Eckarfjärden	0.0684	0.0031	0.0731	0.0485
Lake Gällsboträsket	0.1275	0.1139	0.1532	0.1425
Lake Bolundsfjärden	0.0404	0.0038	0.0563	0.0151
Stream discharge				
Downstream Lake Eckarfjärden (PFM002668)	0.0065	–0.0016	0.0036	0.0022
Downstream Lake Stocksjön (PFM002667)	0.0071	–0.0004	0.0048	0.0021
Downstream Lake Gunnarsboträsket (PFM002669)	0.0092	0.0026	0.0040	0.0068
Upstream Lake Bolundsfjärden (PFM005764)	0.0142	0.0006	0.0104	0.0050

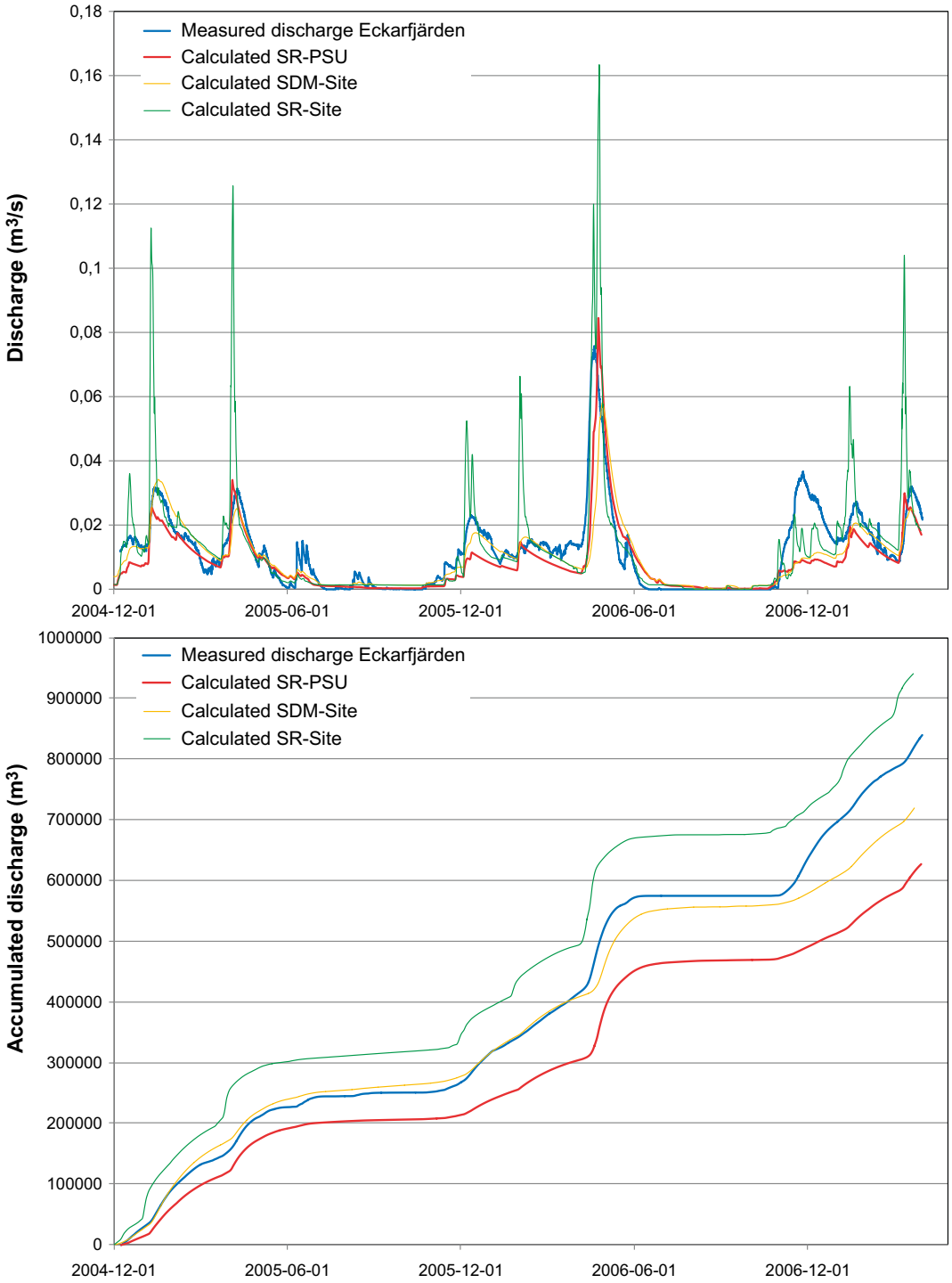

Figure 4-1. *Time-series plots of measured and model-calculated stream discharges downstream Lake Eckarfjärden (gauging station PFM002668). The upper plot shows time series of stream discharge, and the lower plot shows time series of accumulated discharge.*

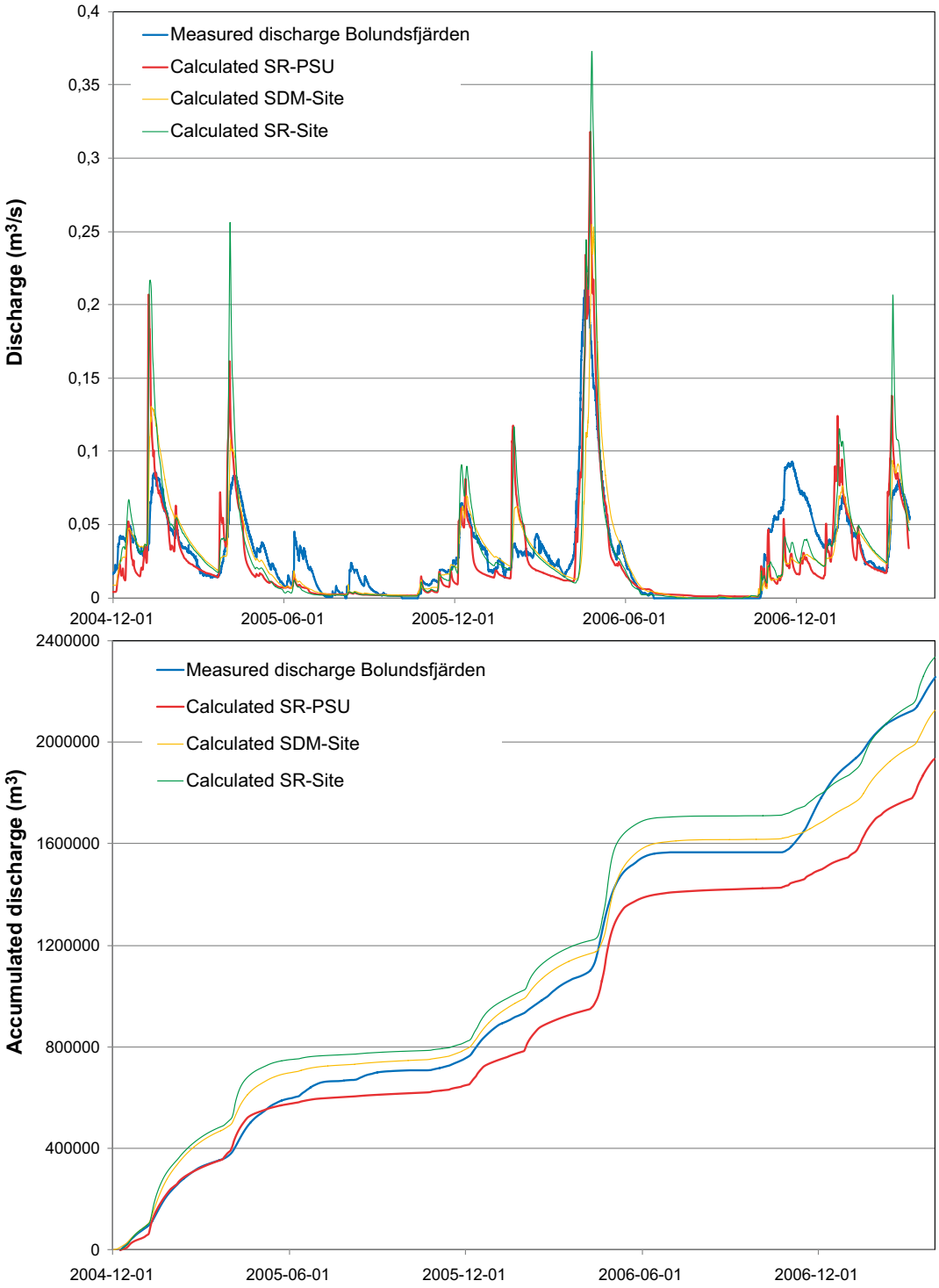

Figure 4-2. *Time-series plots of measured and model-calculated stream discharges upstream Lake Bolundsfjärden (gauging station PFM005764). The upper plot shows time series of stream discharge, and the lower plot shows time series of accumulated discharge.*

Table 4-2 compares MAE and ME data in terms of groundwater levels in regolith for the calibrated model setup of Bosson et al. (2010) and the present, calibrated model setup. As can be seen in this table, there are small MAE differences between the two model setups, whereas ME values are close to zero in both model setups. As exemplified in Figure 4-3, there are individual groundwater-monitoring wells for which MAE and ME are lower (e.g. SFM0003) in the present model setup compared to those of Bosson et al. (2008, 2010), whereas the opposite is noted for some wells (e.g. SFM036). Due to differences in the local topography, as described by the DEM, the MAE for groundwater-monitoring well SFM0036 is twice that of SR-Site. Specifically, in the present model setup the ground-surface elevation at SFM0036 is c 0.4 m lower than that of SR-Site. Both model setups include subsurface drainage at 0.5 m below ground, acting as a drainage for the groundwater level in regolith. The model-calculated groundwater level in SFM0036 is above the drainage level during two periods, associated with high sea levels in January, 2005 and January, 2007.

In order to check that the model reproduces directions of measured hydraulic gradients between regolith and rock, Figure 4-4 shows time-series plots of model-calculated groundwater levels in regolith and rock (percussion boreholes, denoted HFM) at the four drill sites 1, 2, 4 and 5 (see Figure 3-1 and Johansson 2008). In accordance with measurements (Johansson 2008, Werner et al. 2013), model-calculated groundwater levels in regolith are above groundwater levels in rock at drill sites 1, 2 and 5, whereas the opposite is noted for drill site 4.

Table 4-2. Comparison of MAE and ME data in terms of groundwater levels in regolith for the calibrated model setup of Bosson et al. (2010) and the present calibrated model setup.

	Bosson et al. (2010)		Present model setup	
Well ID	**MAE (m)**	**ME (m)**	**MAE (m)**	**ME (m)**
SFM0001	0.41	0.40	0.23	–0.12
SFM0002	0.40	–0.07	0.35	0.20
SFM0003	0.54	–0.54	0.34	0.15
SFM0004	0.43	0.43	0.46	–0.16
SFM0005	0.36	0.15	0.50	0.43
SFM0009	0.63	0.63	0.46	0.00
SFM0010	0.33	–0.03	0.34	0.01
SFM0011	0.20	0.19	0.68	0.68
SFM0012	0.10	–0.07	0.08	–0.07
SFM0013	0.46	–0.06	0.48	–0.39
SFM0014	0.00	0.10	0.12	0.06
SFM0015	0.05	–0.03	0.07	0.03
SFM0016	0.17	–0.16	0.08	–0.04
SFM0017	0.36	0.25	0.47	0.39
SFM0020	0.26	–0.07	0.46	0.16
SFM0021	0.39	–0.28	0.51	–0.29
SFM0023	0.06	–0.02	0.06	–0.03
SFM0028	0.32	–0.32	0.16	–0.12
SFM0030	0.45	–0.37	0.39	0.05
SFM0033	0.29	0.27	0.19	0.12
SFM0034	0.62	–0.33	0.70	0.70
SFM0036	0.35	0.33	0.66	0.66
SFM0039	0.05	–0.03	0.22	–0.22
SFM0057	0.87	–0.87	0.49	0.45
SFM0058	0.77	–0.69	0.44	–0.31
SFM0062	0.15	0.11	0.13	0.08
SFM0065	0.46	–0.45	0.37	–0.36
SFM0066	0.36	–0.35	0.27	–0.27
SFM0018	0.38	0.31	0.49	0.13
SFM0019	0.38	0.37	0.56	0.56
SFM0049	0.52	–0.39	0.64	0.64
Mean	**0.36**	**–0.05**	**0.37**	**0.10**

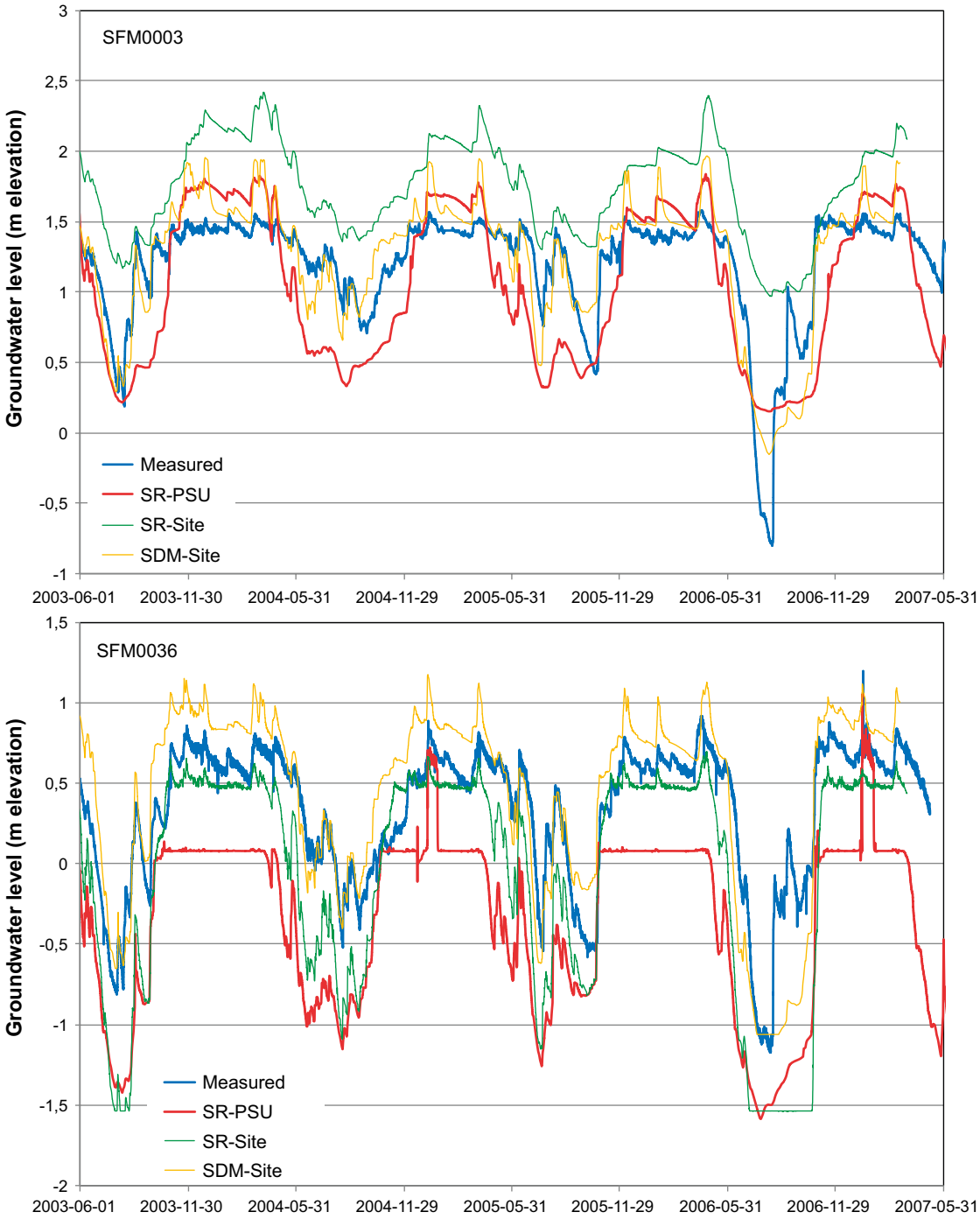

Figure 4-3. *Time-series plots of measured and model-calculated groundwater levels in regolith at groundwater-monitoring wells SFM003 (upper plot) and SFM0036 (lower plot). SR-PSU is the present model setup, whereas SDM-Site and SR-Site are the model setups of Bosson et al. (2008, 2010).*

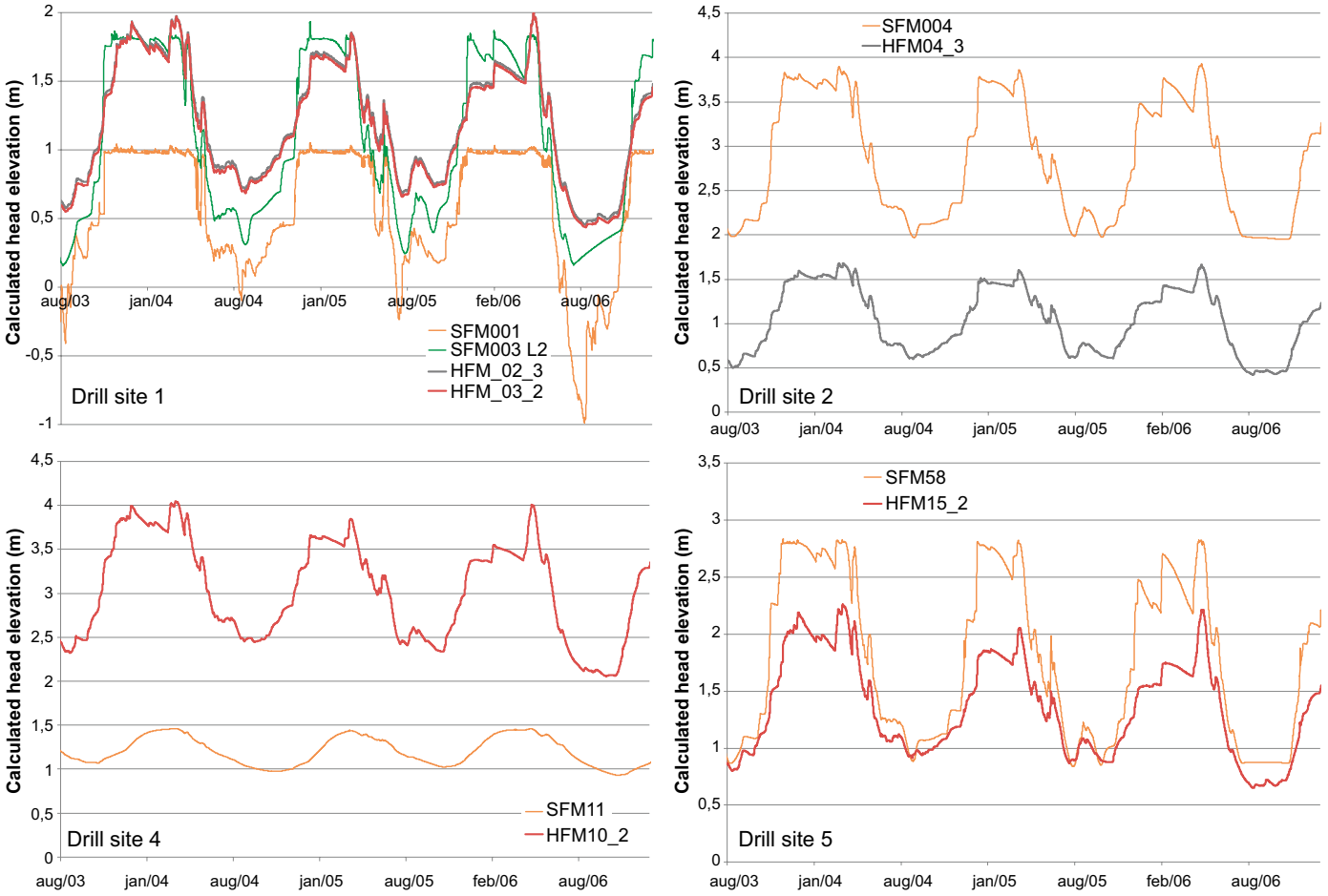

Figure 4-4. *Time-series plots of model-calculated groundwater levels in regolith and rock (percussion boreholes, denoted HFM) at drill sites 1, 2, 4 and 5.*

Table 4-3. Comparison of MAE and ME data in terms of groundwater levels in rock (percussion boreholes) for the calibrated model setup of Bosson et al. (2010) and the present calibrated model setup.

	Bosson et al. (2010)		Present model setup	
Borehole ID	MAE (m)	ME (m)	MAE (m)	ME (m)
HFM01_1	0.74	–0.74	0.50	–0.50
HFM01_2	0.97	–0.97	0.62	–0.62
HFM02_1	0.94	–0.94	0.56	–0.56
HFM02_2	0.96	–0.96	0.49	–0.49
HFM02_3	0.97	–0.97	0.47	–0.47
HFM03_1	0.92	–0.92	0.35	–0.34
HFM03_2	0.91	–0.91	0.34	–0.33
HFM04_1	0.44	–0.44	0.24	–0.21
HFM04_2	0.46	–0.46	0.31	–0.29
HFM04_3	0.24	–0.24	0.16	–0.01
HFM10_1	0.85	–0.85	0.66	–0.65
HFM10_2	0.53	–0.52	0.39	–0.34
HFM11_1	0.23	–0.15	0.25	0.25
HFM11_2	0.51	–0.49	0.18	0.02
HFM15_1	0.85	–0.85	0.49	–0.48
HFM15_2	0.70	–0.7	0.48	–0.45
HFM16_1	0.39	–0.38	0.35	–0.25
HFM16_2	0.39	–0.38	0.35	–0.25
HFM16_3	0.42	–0.41	0.35	–0.26
HFM20_2	0.17	–0.10	0.23	–0.11
HFM20_3	0.37	–0.37	0.26	–0.17
HFM20_4	0.66	–0.66	0.39	–0.27
HFM32_1	1.40	–1.40	1.16	–1.16
HFM32_2	1.36	–1.36	1.09	–1.09
HFM32_3	1.07	–1.07	0.78	–0.78
HFM32_4	1.08	–1.08	0.55	–0.55
HFM34_3	0.25	–0.23	0.19	–0.14
Mean	**0.70**	**–0.69**	**0.45**	**–0.39**

Table 4-3 compares MAE and ME data in terms of groundwater levels in rock (percussion boreholes) for the calibrated model setup of Bosson et al. (2010) and the present, calibrated model setup. According to this table, the average MAE and ME are lower for the present model setup compared to those of Bosson et al. (2010). Figure 4-5 shows examples of model-calculated groundwater levels in rock in the present model setup and those of Bosson et al. (2008, 2010).

4.4 Modelling results using the calibrated MIKE SHE model

4.4.1 Water balance

Water balances are calculated for land areas of the regional model area, using the water-balance tool in MIKE SHE. Specifically, water-balance results are extracted for the period Oct. 1, 2004–Sep. 30, 2007, which has an annual average precipitation of 523 mm and an annual average potential evapotranspiration of 529 mm. As shown in Appendix 1, evapotranspiration includes evaporation from snow, from the unsaturated and saturated zones and from ponded areas, and interception and transpiration by vegetation, whereas runoff includes stream discharge and boundary outflows. According to Figure 4-6, for the specified three-year period the annual average runoff (R) is c 113 mm/y (c 20% of the precipitation). This runoff is less than the estimated long-term annual average of 150–160 mm (Johansson 2008), and it is also lower than the annual average runoff of 175 mm calculated by Bosson et al. (2010). This is primarily due to less precipitation during the period considered here.

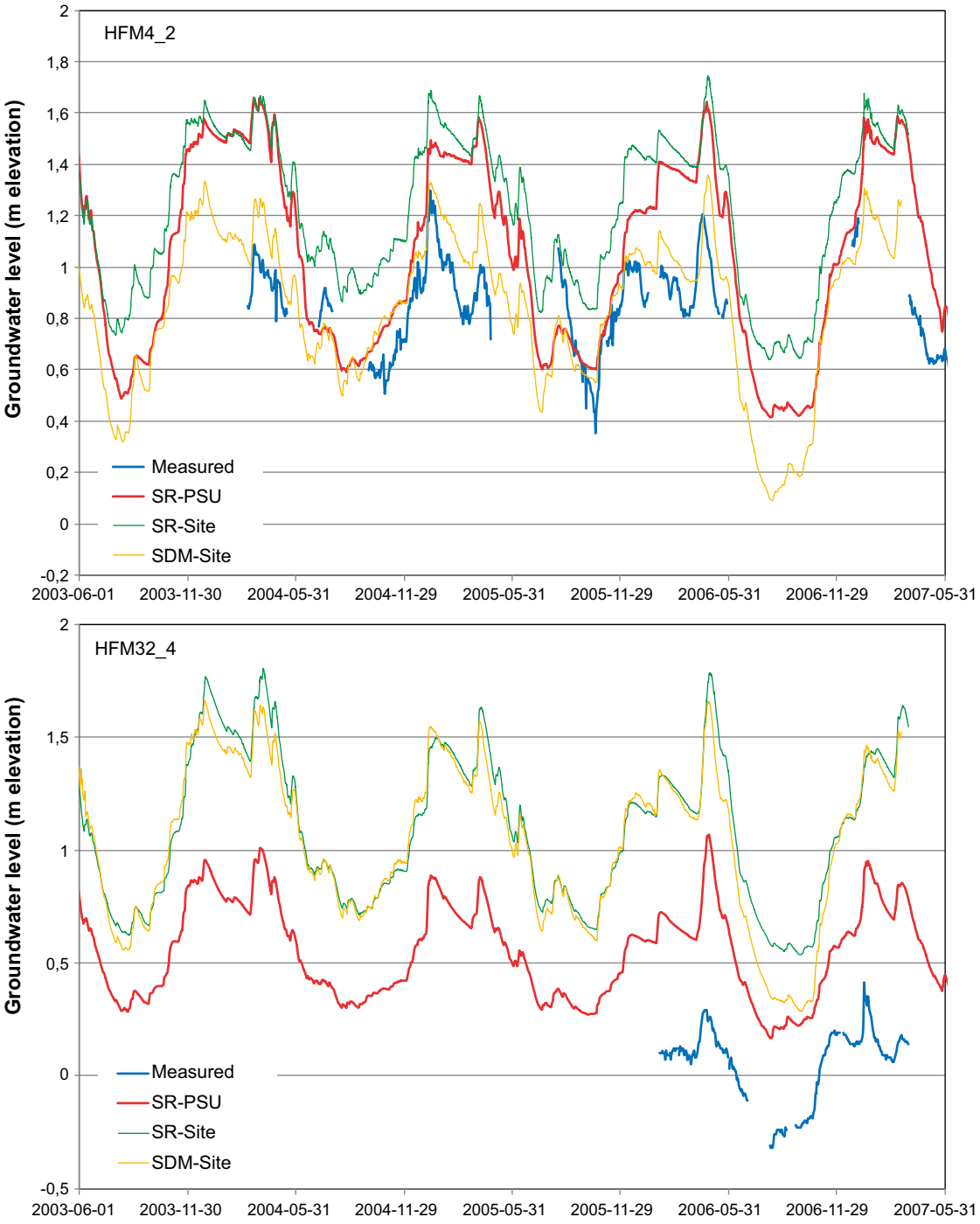

Figure 4-5. *Time-series plots of measured and model-calculated groundwater levels in rock in percussion borehole sections HFM04:2 (upper plot) and HFM32:4 (lower plot). SR-PSU is the present model setup, whereas SDM-Site and SR-Site are the model setups of Bosson et al. (2008, 2010).*

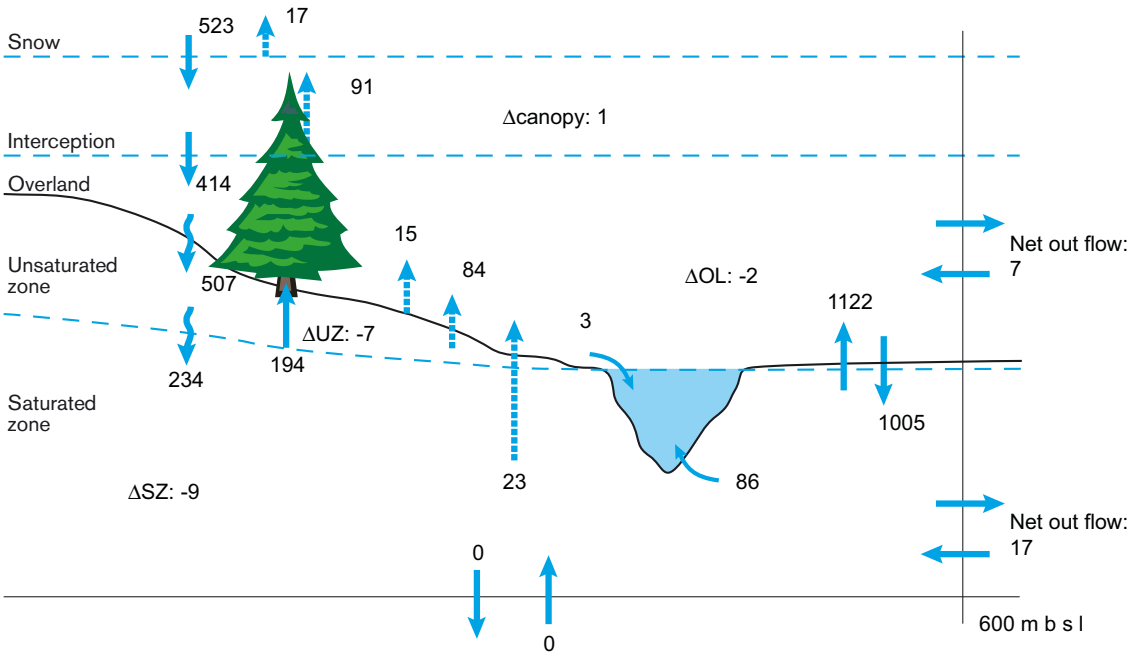

Figure 4-6. *Water balance (mm/y) for land areas at 2000 AD (Oct. 1, 2004–Sep. 30, 2007).*

Specifically, the estimated annual average precipitation is 559 mm for the reference normal period (Johansson 2008) and 583 mm for the normal year (Oct. 1, 2003–Sep. 30, 2004; cf Section 2.2.1), which was used to represent both present and future conditions in Bosson et al. (2010). Moreover, for the normal year used in Bosson et al. (2010) the annual average potential evapotranspiration was 508 mm, whereas it is 529 mm for the water-balance period considered here. In Bosson et al. (2010), the normal year was repeated three times and water-balance results were extracted for the last year, in order to reduce influence from the initial conditions. For the same reasons, the present simulations were run for a total time period of three years, including the normal year, whereas water-balance results are extracted for the total simulation period.

4.4.2 Vertical hydraulic-head differences in regolith and rock

Figures 4-7 and 4-8 show MIKE SHE-calculated annual average hydraulic-head differences in regolith (Figure 4-7) and rock (Figure 4-8) of the regional model area. As expected, there are upward gradients in local, low-elevated areas and downward gradients in local, high-elevated areas (cf Bosson 2008, 2010, Johansson 2008). There are upward gradients below the sea and in low-elevated areas also in the rock. Recharge-discharge patterns in the regolith are highly influenced by the local ground-surface topography, whereas there is less influence of the local topography on these patterns in the rock.

During dry periods, the overall groundwater recharge-discharge pattern in regolith is similar to average conditions. Due to the strong influence of evapotranspiration during such periods, vertical upward gradients increase and the total size of discharge areas increases (Johansson 2008). During wet periods, some groundwater discharge areas in the regolith switch into recharge areas. Specifically, in some areas evapotranspiration causes an upward groundwater flow during average and dry conditions, whereas during wet periods such areas switch into recharge areas.

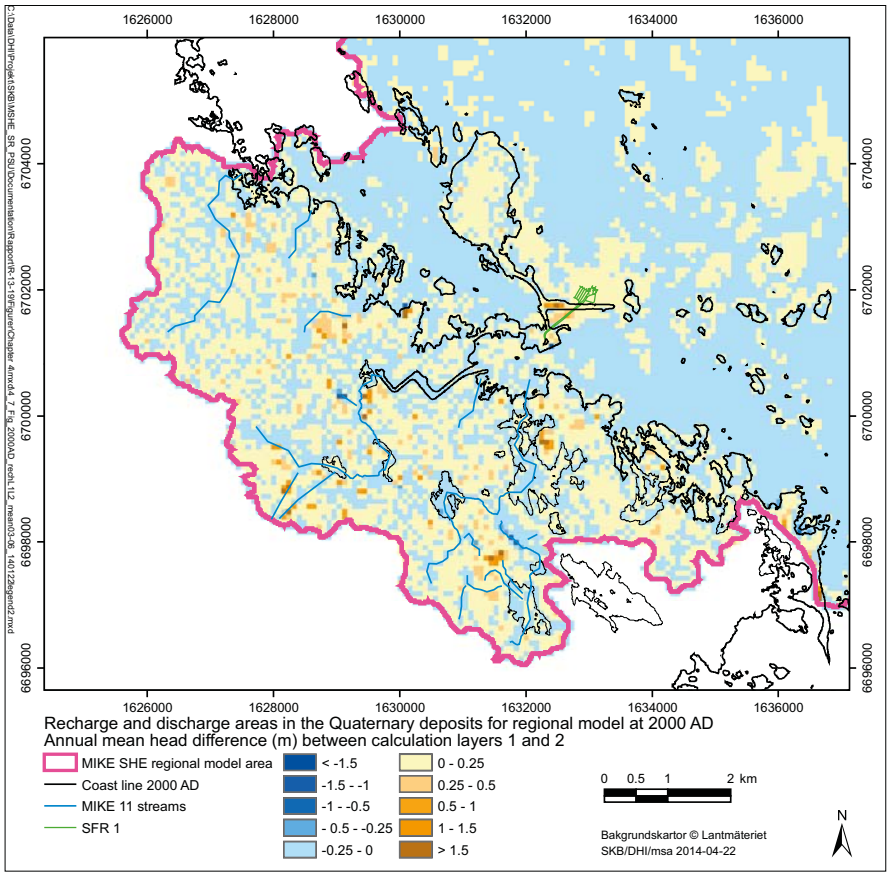

Figure 4-7. *MIKE SHE-calculated average hydraulic-head differences in the regolith (calculation layers 1 and 2) for the period Oct. 1, 2003–Sep. 30, 2006. Blue colours represent areas with upward gradients and red colours represent areas with downward gradients.*

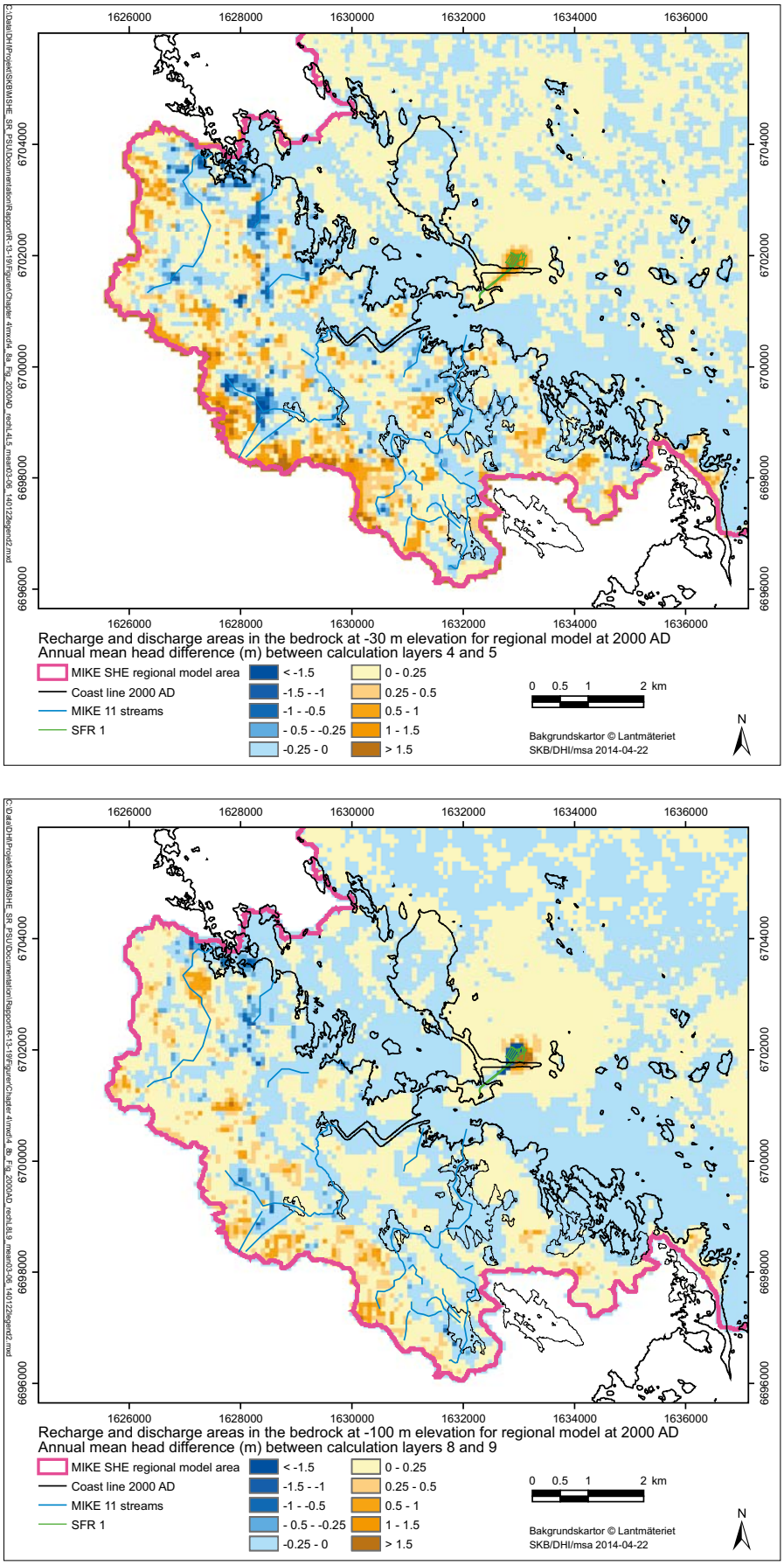

Figure 4-8. *MIKE SHE-calculated average hydraulic-head differences at c –30 m elevation (upper figure) and c –100 m elevation (lower figure) in the rock for the period Oct. 1, 2003–Sep. 30, 2006.*

4.4.3 Depth to the groundwater table

Forsmark is characterised by shallow depth to the groundwater table, and the average level of the groundwater table in the regolith is largely determined by the local ground-surface elevation (Johansson 2008). Figure 4-9 shows MIKE SHE-calculated average depth to the groundwater table in terrestrial parts of the regional model area for the period October 1, 2003–September 30, 2006. As illustrated in this figure, the groundwater table in the Forsmark area is shallow and generally the depth to the groundwater table is less than 1 m below ground surface in terrestrial areas.

Figures 4-10 and 4-11 shows the monthly average depth to the groundwater table during a wet period (April, 2006) and a dry period (August, 2006), respectively. Groundwater levels in regolith typically show a strong uniformity in their responses to drier summer conditions, and also in response to groundwater-recharge events associated with precipitation and snowmelt (Johansson 2008). As shown in Figure 4-10 (cf Section 4.4.2), during wet periods some groundwater discharge areas in the regolith switch into recharge areas, whereas the total size of discharge areas increases during dry periods (Figure 4-11).

4.4.4 Depth of overland water and stream discharge

MIKE SHE-calculated depths of overland water provide a possibility to check whether areas with overland water coincides with present lakes and mires. Figure 4-12 shows the annual average depth of overland water in terrestrial parts of the regional model area for the period October 1, 2003–September 30, 2006. Moreover, Figures 4-13, 4-14 and 4-15 show monthly average depths during a wet period (April, 2006), a dry period (August, 2006), and areas with overland-water depths exceeding 0.1 m during the wet and dry periods, respectively. Model-calculated areas with overland-water occurrence are within the boundaries of actual lakes and mires. Under wet conditions (Figure 4-13), there is a larger depth of overland water within the lakes and the total area with overland water is also larger.

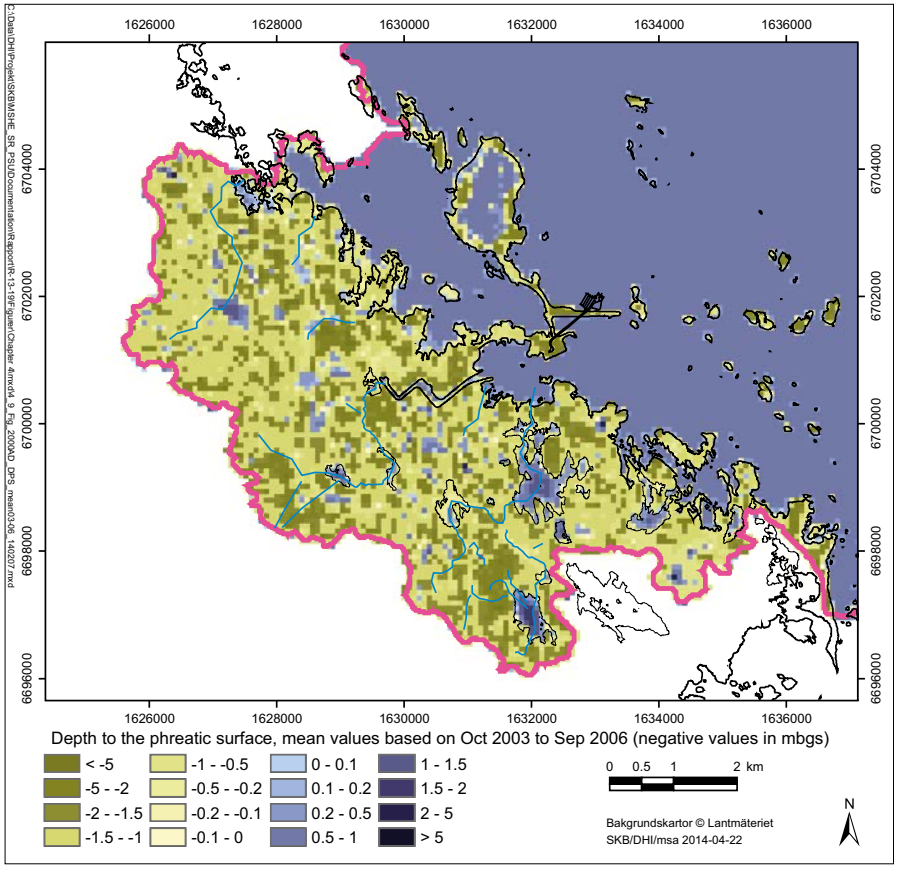

Figure 4-9. *MIKE SHE-calculated average depth to the groundwater table for the period Oct. 1, 2003–Sep. 30, 2006. Depths are shown as negative values, i.e. positive depths represent surface water.*

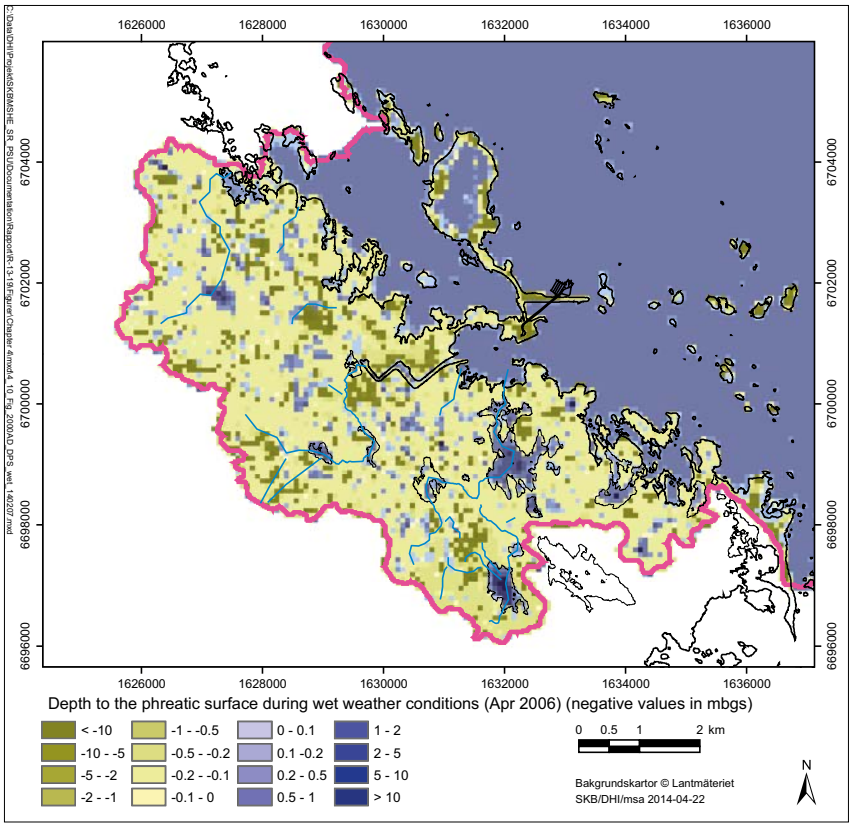

Figure 4-10. *MIKE SHE-calculated average depth to the groundwater table during a wet period (April, 2006). Depths are shown as negative values, i.e. positive depths represent surface water.*

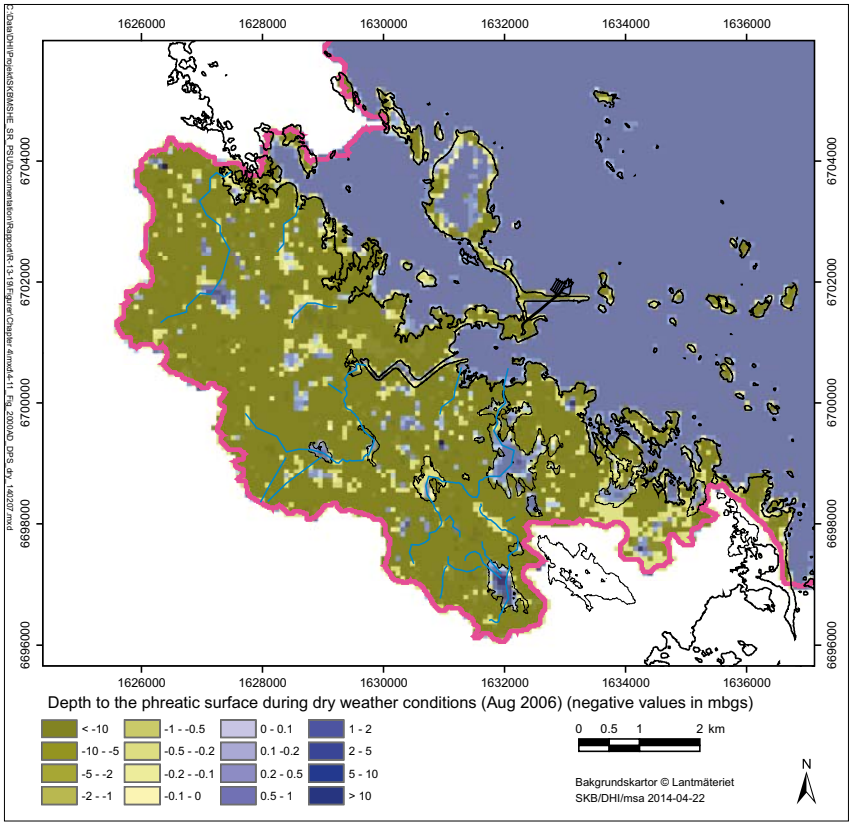

Figure 4-11. *MIKE SHE-calculated average depth to the groundwater table during a dry period (August, 2006). Depths are shown as negative values, i.e. positive depths represent surface water.*

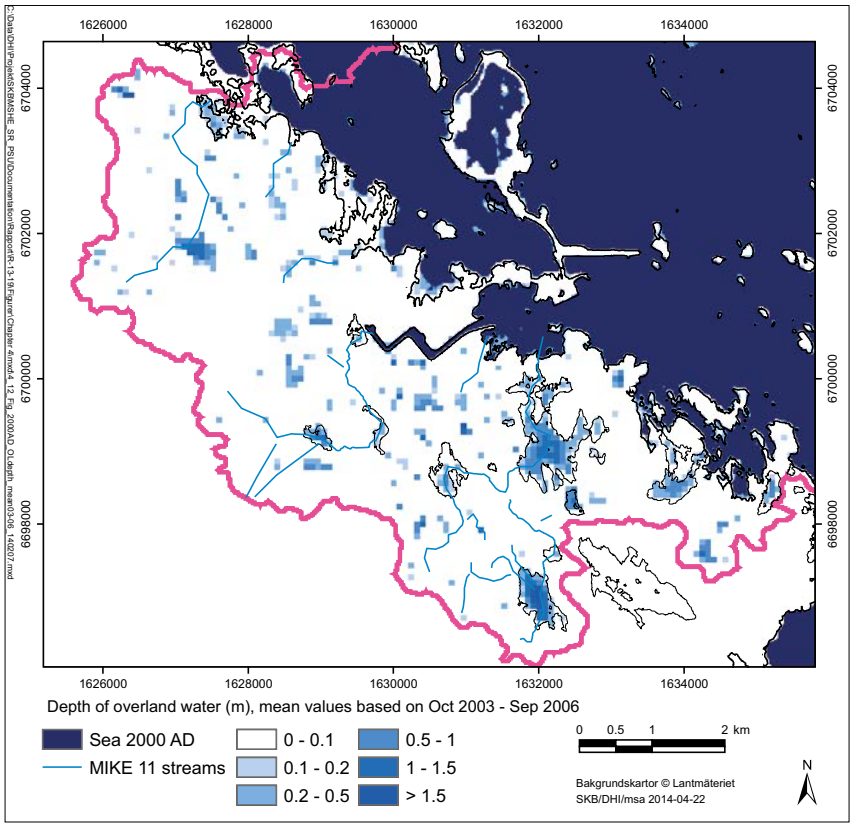

Figure 4-12. *MIKE SHE-calculated average depth of overland water for the period Oct. 1, 2003–Sep. 30, 2006.*

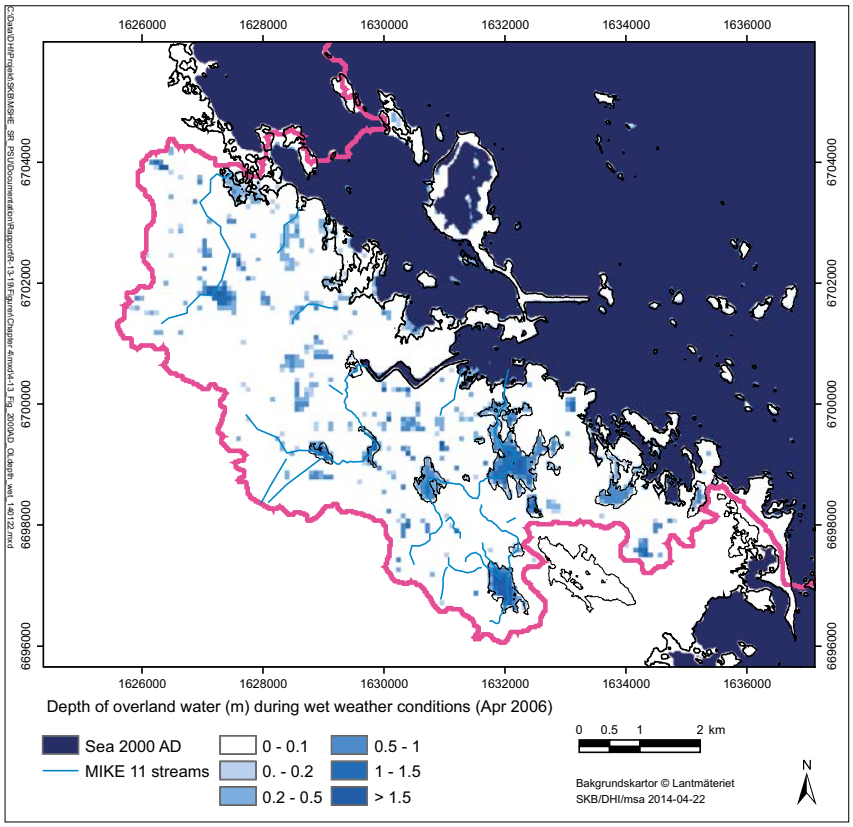

Figure 4-13. *MIKE SHE-calculated average depth of overland water during a wet period (April, 2006).*

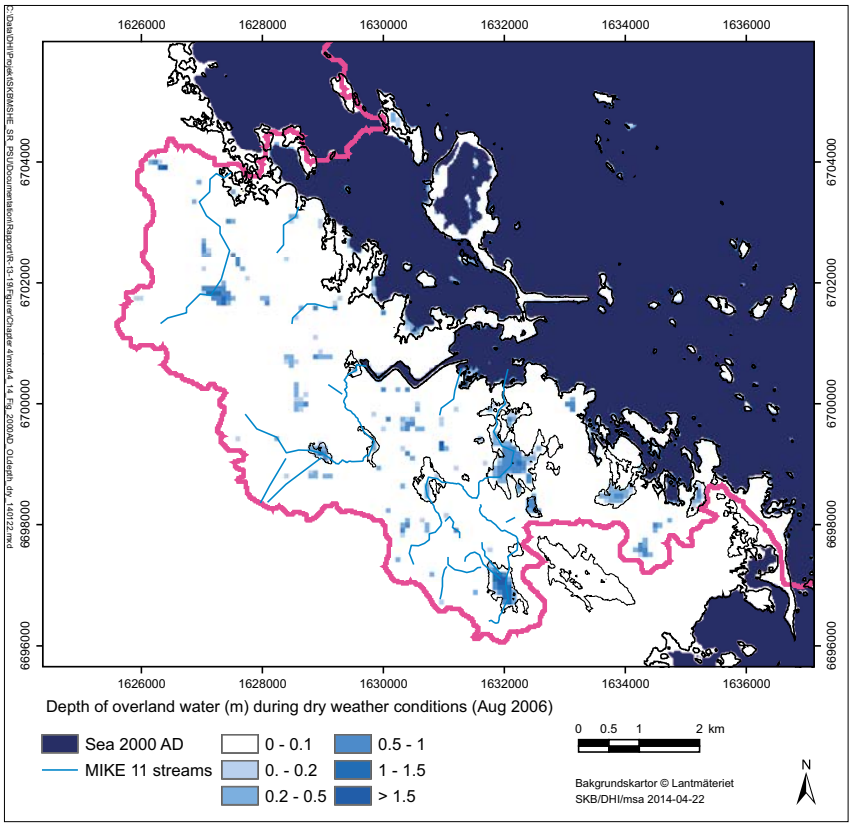

Figure 4-14. *MIKE SHE-calculated average depth of overland water during a dry period (August, 2006).*

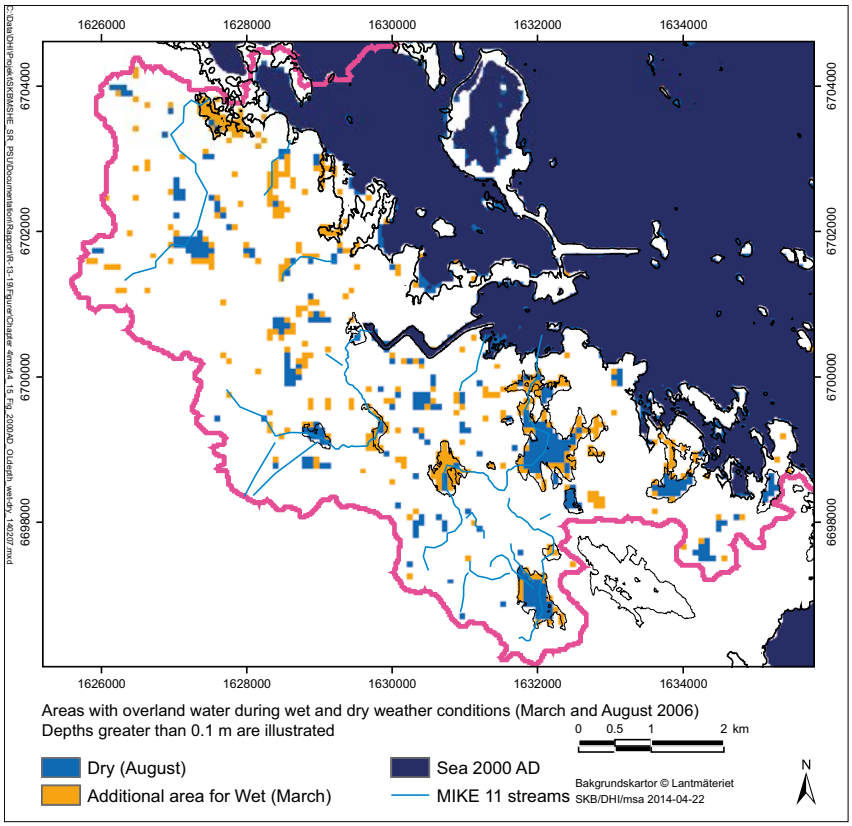

Figure 4-15. *MIKE SHE-calculated average depth of overland water exceeding 0.1 m during a dry (March) and a wet period (August, 2006).*

Figures 4-1 and 4-2 in Section 4.3 show time-series plots of MIKE 11-calculated stream discharges at the locations of gauging stations downstream Lake Eckarfjärden (PFM002668) and upstream Lake Bolundsfjärden (PFM005764). Most present-day streams in Forsmark are small and have very small or no discharge during dry periods during summer (Johansson 2008). Streams exhibit a well defined furrow along some stretches, in particular in forest areas where streams have been deepened for drainage purposes. However, stream-discharge paths are more diffuse in mire areas and downstream small ponds.

4.5 Residence times and inter-basin water exchanges of marine basins

The marine area outside Forsmark consists of the open-ended embayment Öregrundsgrepen, with a wide and deep boundary towards north and a narrow and shallower strait towards south. Most of the sea bottom consists of shallow and exposed hard bottoms (boulders or rock), interspersed by deeper valleys with soft bottoms. Based on the sea bathymetry according to the DEM (Strömgren and Brydsten 2013), the present-day marine area outside Forsmark is divided into 38 basins (Figure 4-16). Most of this coastal area is shallow (sea depth less than 10 m), except for the through Gräsörännan with sea depths exceeding 50 m. The salinity stratification in Öregrundsgrepen is generally weak. Local freshwater runoff produces slightly lower salinity compared to the Gulf of Bothnia (Aquilonius 2010). The direction of the flow through Öregrundsgrepen varies with time, but on an annual basis there is a net flow directed from north to south (Karlsson et al. 2010).

The sea-water flow in Öregrundsgrepen was calculated by the flexible-mesh modelling tool MIKE 3 FM (svn/SFR/SR-PSU/Indata/Marine/DHI_delivery_20121213/Utökning_TekniskPM_uppdateringForsmark_v_3_0.pdf) using site data from Forsmark, and results were extracted for each delineated basin in terms of inter-basin water exchanges (basin flow) and water residence times (HRT and AvA). According to the MIKE FM 3 calculations, the largest exchange flows are at the eastern part of the boundary towards north, from the Baltic to basin 105, whereas the largest inter-basin water exchange occurs across the embayment, between basins 114 and 184.

HRT (hydraulic residence time) of a basin is calculated as the basin volume divided by the annual gross inflow (or gross outflow) across its boundaries, i.e. the theoretical time required to replace the whole water volume. Moreover, AvA (average age) of a basin is the time that individual "water parcels" have spent within the model volume of Öregrundsgrepen. At the beginning of each modelled year, all water parcels have an age equal to zero. During the year, ageing water parcels present within the model are mixed with water parcels that enter the model area (initial age equal to zero).

The age concentrations in all model elements are used to calculate an average age per basin at each time during the modelled year. AvA for each basin is then calculated as the average age for all times, whereas remaining water parcels increase their age. The age in each model element is calculated and the average for all elements is calculated at each time step during the year. For a more detailed description of the modelling methodology, the MIKE 3 FM tools and the parameters basin flow, HRT and AvA, see Karlsson et al. (2010).

According to calculations, HRT varies between less than two hours (basin 178) to c 25 days (basin 118). The average HRT of all basins is c 1.5 days, whereas the average for the whole of Öregrundsgrepen (i.e. the whole MIKE FM 3 model area) is approximately one week. AvA in the 38 basins was calculated to vary between 13 and 29 days (19 days on average). Water turnover is more rapid in the deeper areas close to the open sea, whereas turnover is slower in the partly isolated shallow basins 117 and 118 (see Figure 4-16).

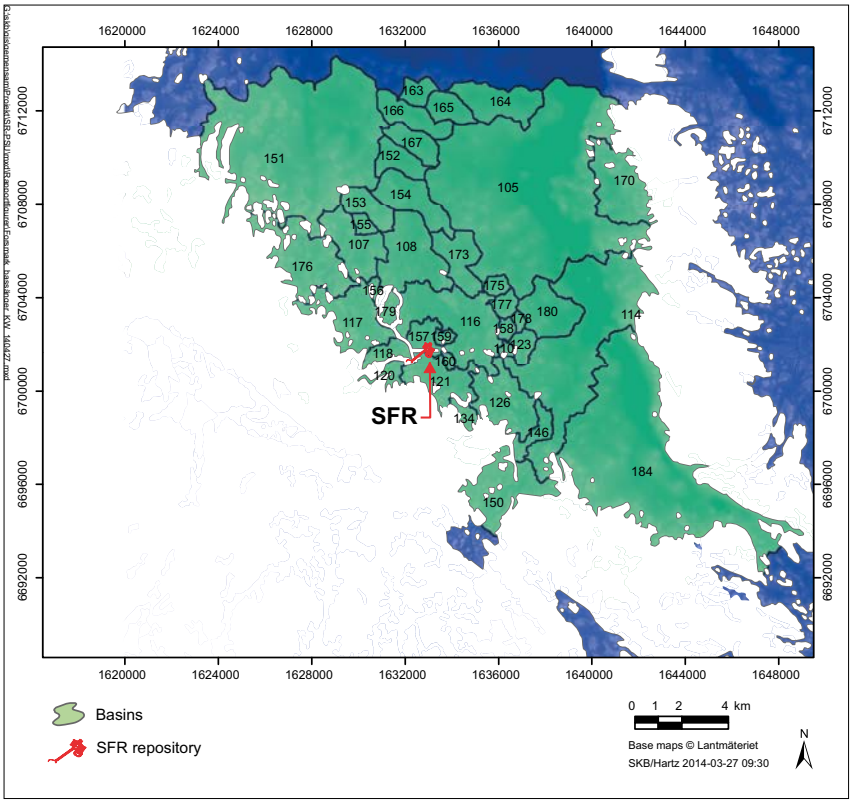

Figure 4-16. *Coastal basins (delineated based on the DEM) outside Forsmark. The inlet to the cooling-water canal for the Forsmark nuclear power plant is visible in basin 120, and the location of the SFR facility is indicated on the map.*

5 Modelling and results for future conditions

5.1 Introduction

The objectives of the descriptions and modelling of future hydrological and near-surface hydrogeological conditions are to support delineations of biosphere objects (cf Section 2.3.1), to deliver parameters to the modelling of radionuclide transport in biosphere objects (Chapter 7), and to support analyses of different water-management activities in the future Forsmark landscape (Chapter 6).

The descriptions and modelling results presented in the following sections are focused on the MIKE SHE local model area. The corresponding regional models (one for each future time) are primarily used to generate time-varying external boundary conditions for the local models (cf Section 3.2.2), which include the delineated biosphere objects. The MIKE SHE modelling results are focused on the normal year (cf Section 2.2.1), whereas the influence of periglacial conditions with permafrost on water flow in the surface system and interactions with groundwater in the rock are discussed in Section 5.8.

5.2 Water balance

Water balances are calculated for the local model area using the water-balance tool in MIKE SHE (see Table 5-1 and Appendix 1). In order to investigate influences of future shoreline displacement, landscape development and climate, water balances are calculated for different times, land areas and climate cases. Specifically, water balances are calculated for the times 5000 and 11,000 AD, for land areas at each specific time and also for areas constituting land at 3000 AD. The normal year is represented using locally measured meteorological data for the period 1 Oct. 2003–30 Sep. 2004, whereas the influence of a possible wet and warm future climate (Kjellström et al. 2009) is investigated using the 5000 AD model setup.

For land areas at 5000 AD and for the normal year (accumulated precipitation 583 mm), the annual average evapotranspiration (ET) is c 410 mm/y and the annual average runoff (R) is c 175 mm/y (c 30% of the precipitation). As shown in Appendix 1, ET includes evaporation from snow, from the unsaturated and saturated zones and from ponded areas, and interception and transpiration by vegetation, whereas R includes stream discharge and boundary outflows. For land areas at 11,000 AD, the corresponding water-balance components are c 390 and c 195 mm/y, respectively. At 11,000 AD, all former lakes within the local model area are infilled and transformed to mires. This terrestrialisation reduces ET by 6% and increases R by 12% compared to 5000 AD.

At 5000 AD, for areas constituting land at 3000 AD, the annual average ET is c 400 mm/y and R is c 180 mm/y. At 11,000 AD, also for areas constituting land at 3000 AD, the annual average ET is c 370 mm/y and R is c 210 mm/y. Hence, terrestrialisation between 5000 and 11,000 AD of the 3000 AD land area reduces ET by 8% and increases R by 13%.

Table 5-1. Summary of MIKE SHE-calculated water balances at 3000, 5000 and 11,000 AD. MS = MIKE SHE, P = precipitation, ET = evapotranspiration and R = runoff.

Time	Climate	Evaluated area	P (mm/y)	ET (mm)y)	R (mm/y)
3000 AD	Present	Land 3000 AD	583	329	256
5000 AD	Present	Land 3000 AD	583	404	182
5000 AD	Present	MS local model area	583	411	174
5000 AD	Wet and warm	MS local model area	1,539	1,144	457
11,000 AD	Present	Land 3000 AD	583	372	207
11,000 AD	Present	MS local model area	583	388	195

The 5000 AD water balances for the land area at 5000 AD and for the 3000 AD land area, respectively, show that the distance to the shoreline has relatively small overall effects on ET (2% larger for the land area at 5000 AD) and R (4% less for the land area at 5000 AD). At 11,000 AD, the corresponding differences are 4% (ET) and 6% (R). Similar to the conclusions drawn by Bosson et al. (2010), the present water-balance calculations show that for a given land area, landscape development in the form of lake terrestrialisation has larger, but still not dramatic, effects on the water balance compared to shoreline displacement (Figure 5-1).

The wet and warm climate is characterised by significantly more precipitation (c 1,500 mm per year) compared to the normal year (cf Section 2.2.1). For land areas at 5000 AD, the MIKE SHE-calculated annual average ET is high (c 1,140 mm per year), with R being approximately 150% higher than the normal-year R (c 450 mm/year) or c 30% of the precipitation (Appendix 1).

5.3 Vertical hydraulic-head differences in regolith and rock

Figures 5-2 to 5-5 show MIKE SHE-calculated annual average vertical hydraulic-head differences for the normal year in the regolith of the local model area at 3000 AD (Figure 5-2), 5000 AD (Figure 5-3), 11,000 AD (Figure 5-5), and in the regional model area at 11,000 AD (Figure 5.4). As expected, there are upward gradients in local, low-elevated areas and downward gradients in local, high-elevated areas. Sub-sea vertical hydraulic-head differences in the regolith are small, and most of the sea in the model area acts as groundwater-discharge areas. However, there is groundwater recharge in some marine areas, e.g. parts of the biosphere objects 116 and 157_1.

Subsequent to emergence from the sea (5000 and 11,000 AD, Figures 5-3 and 5-4), recharge-discharge patterns in the regolith are highly influenced by the local ground-surface topography, which is also the case in present land areas (cf Section 4.4.2). Shoreline displacement reduces downward hydraulic-head differences in the SFR pier and also affects recharge-discharge patterns in the rock, but there is less influence on these patterns from the local topography (Appendix 1). At 5000 AD, recharge-discharge patterns in the rock are rather unaffected by a wet and warm climate (Appendix 1).

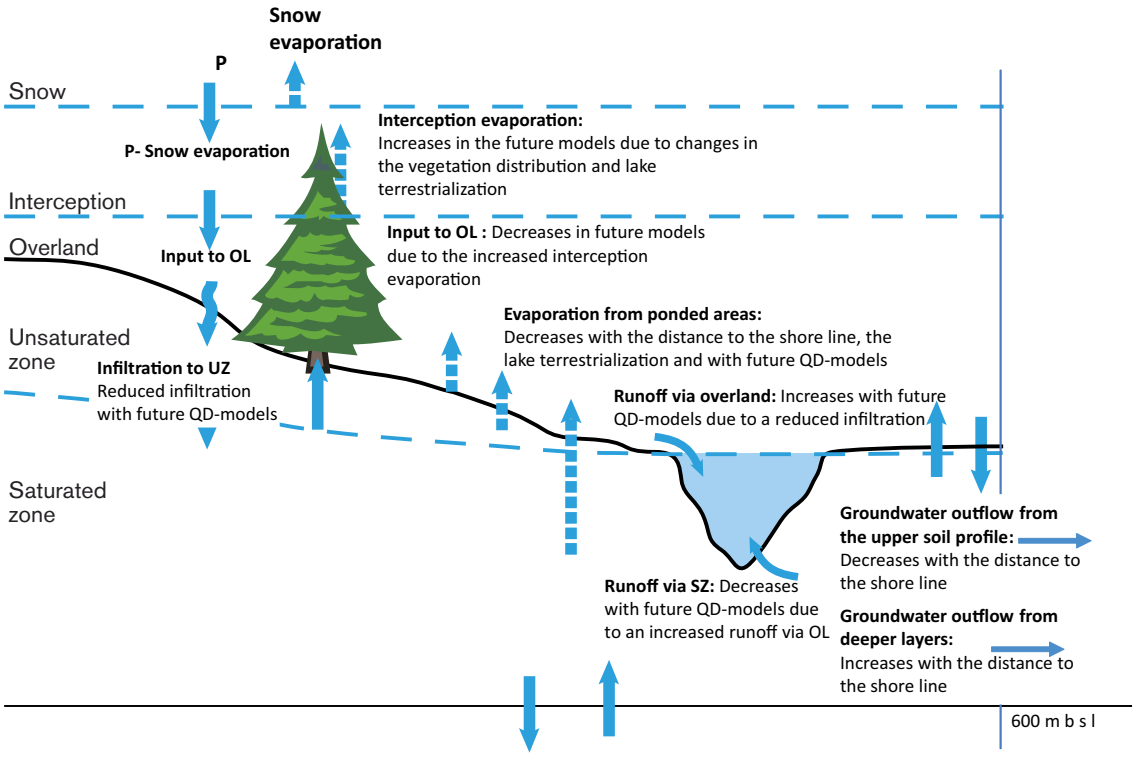

Figure 5-1. *Summary of main water-balance effects from shoreline displacement and landscape development (Bosson et al. 2010).*

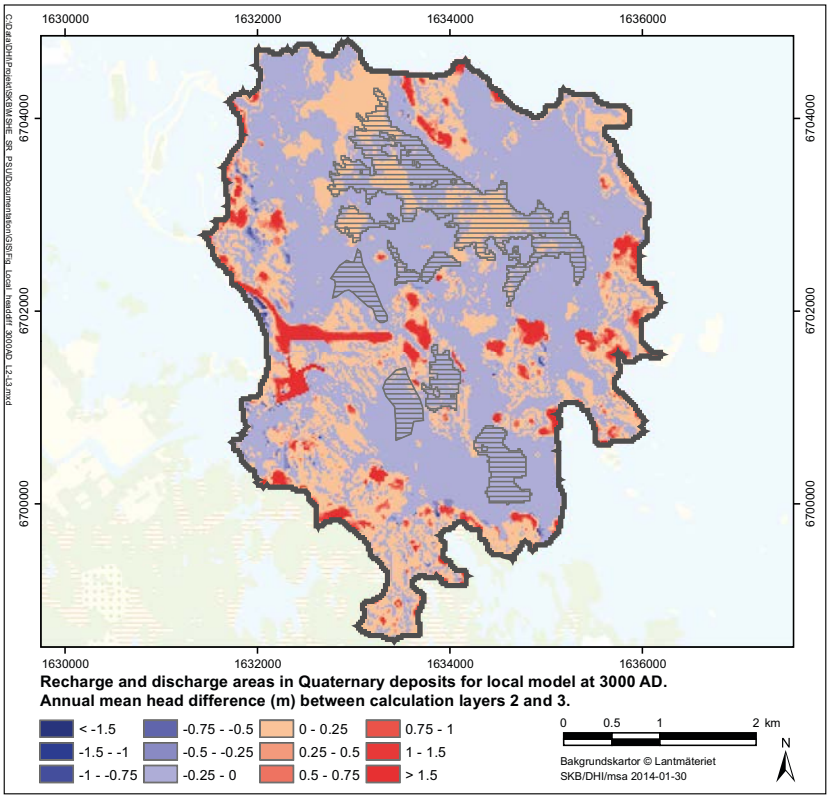

Figure 5-2. *MIKE SHE-calculated annual average hydraulic-head differences in the regolith (calculation layers 2 and 3) at 3000 AD (MIKE SHE local model area). Blue colours represent areas with upward gradients and red colours represent areas with downward gradients. Dashed areas are delineated biosphere objects.*

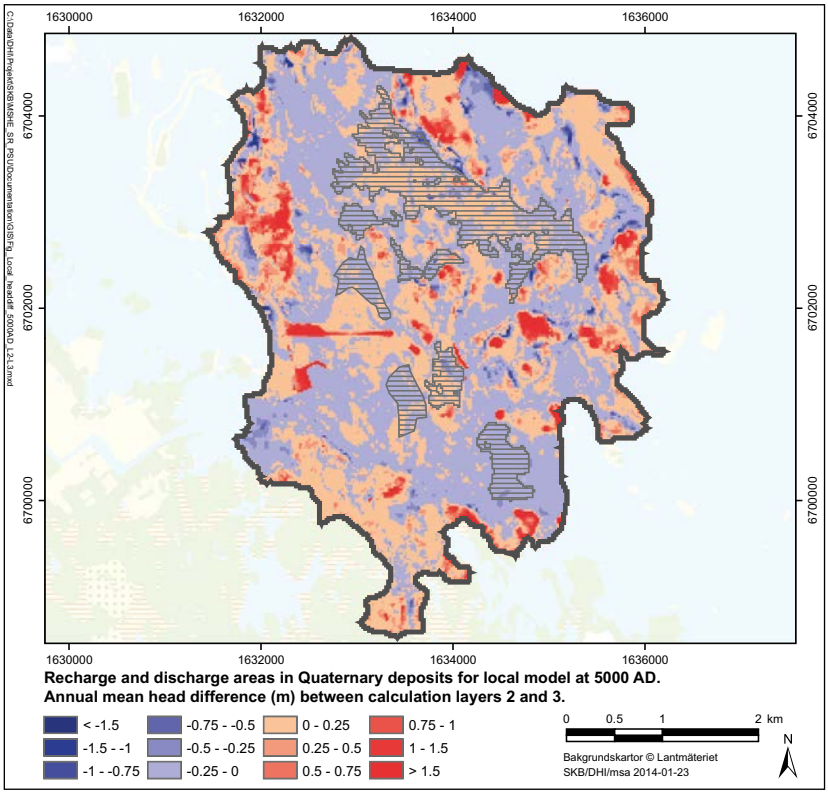

Figure 5-3. *MIKE SHE-calculated annual average hydraulic-head differences in the regolith (calculation layers 2 and 3) at 5000 AD (local model area). Blue colours represent areas with upward gradients and red colours represent areas with downward gradients. Dashed areas are delineated biosphere objects.*

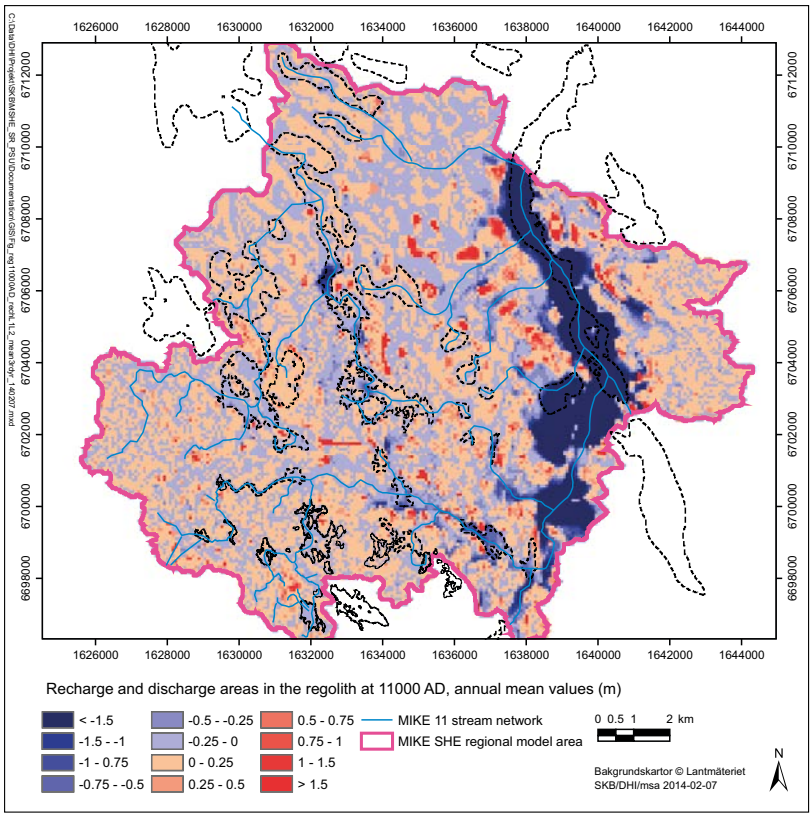

Figure 5-4. *MIKE SHE-calculated annual average hydraulic-head differences in the regolith (calculation layers 1 and 2) at 11,000 AD (regional model area). Blue colours represent areas with upward gradients and red colours represent areas with downward gradients.*

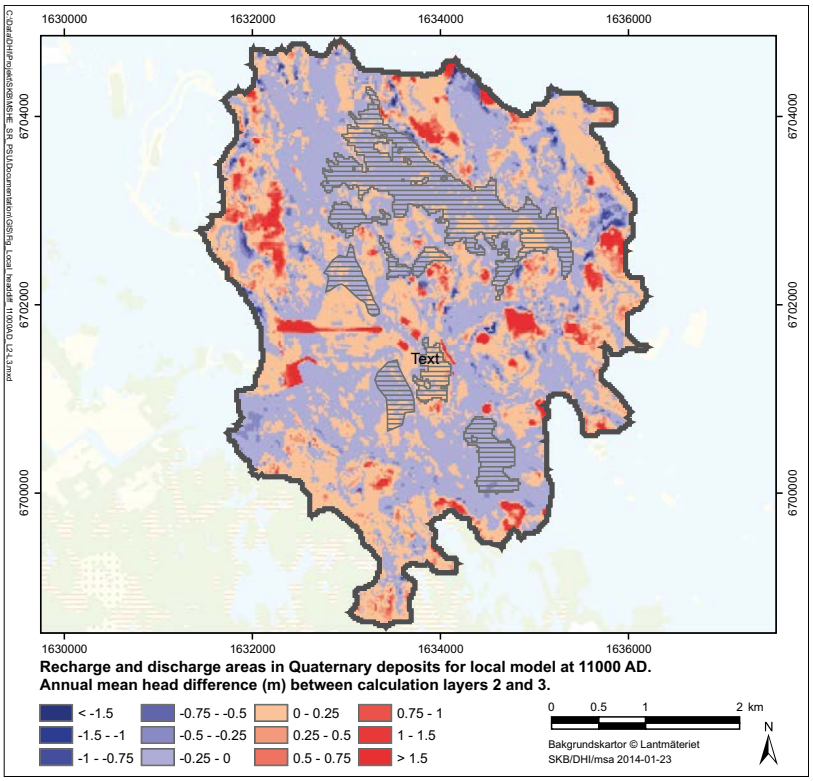

Figure 5-5. *MIKE SHE-calculated hydraulic-head differences in the regolith (calculation layers 2 and 3) at 11,000 AD (local model area). Blue colours represent areas with upward gradients and red colours represent areas with downward gradients.*

5.4 Depth to the groundwater table

Figure 5-6 shows MIKE SHE-calculated annual average depth to the groundwater table at 3000 AD. On average, the groundwater-table depth is 0.9 m below ground surface in terrestrial areas, and there is surface water (shown as positive values in the figure) in c 15% of the land area. If areas with surface water are excluded, the average depth to the groundwater table is 1.2 m at 3000 AD. As an illustration of annual groundwater-level amplitudes in the regolith (i.e. the difference in groundwater-table depths between a wet and a dry period), corresponding maps of groundwater-table depths during a wet (March) and dry period (August) are shown in Appendix 1 (total amplitude c 0.8 m).

Also at 5000 AD (Figure 5-7) there is surface water in c 15% of the land area, whereas the average depth to the groundwater table is 0.8 m in terrestrial areas. Excluding areas with above-ground water the average depth to the groundwater table is 1.1 m at 5000 AD, whereas the annual amplitude is c 1 m (see Appendix 1). Figure 5-8 shows a cumulative-frequency plot of annual average, maximum and minimum depths to the groundwater table at 5000 AD. As indicated in this figure, the annual groundwater-table amplitude is small in areas with a very shallow (0.2 m below ground or less) or deep groundwater table (more than 2 m), whereas the influence of dry and wet periods is larger in areas with intermediate depths to the groundwater table. The annual average groundwater-table depth is larger than 1 m in about 1/3 of the local model area. The corresponding fractions are 46% during dry periods (exemplified by August during the normal year) and 23% during wet periods (March). The depth to the groundwater table in the regolith is largely determined by the local ground-surface elevation. At 5000 AD, the spatial distribution of groundwater-table depths in terrestrial areas during a wet period of a wet and warm climate is rather similar to the distribution during the normal-year wet period Appendix 1). However, during dry periods of the wet and warm climate the groundwater table is located below ground surface in areas in the central parts of the local model area, being saturated during the normal-year dry period.

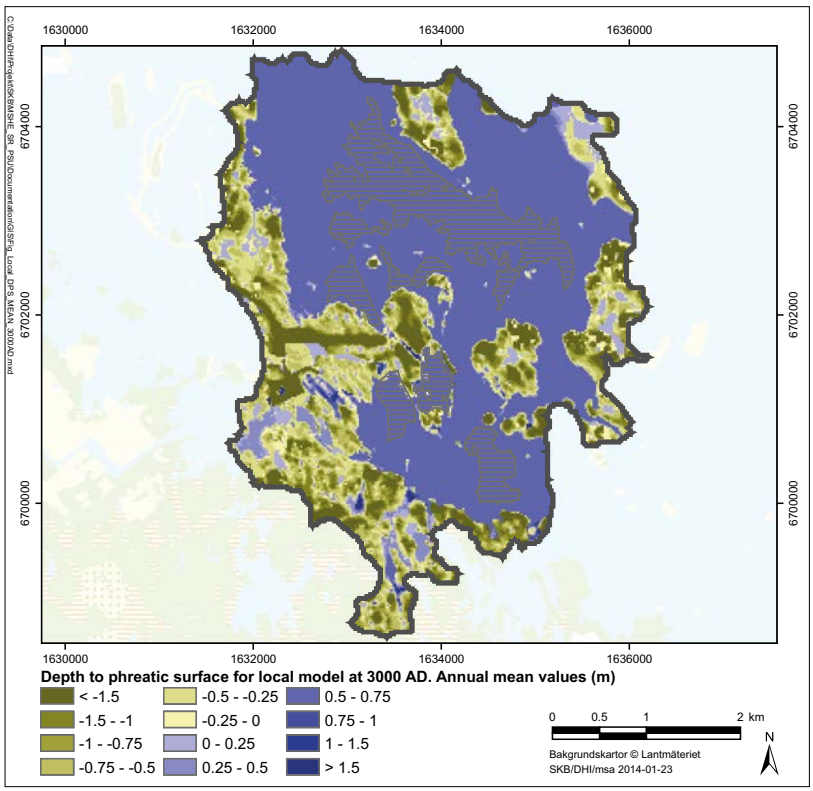

Figure 5-6. *MIKE SHE-calculated annual average depth to the groundwater table at 3000 AD (local model area). Depths are shown as negative values, i.e. positive depths represent surface water.*

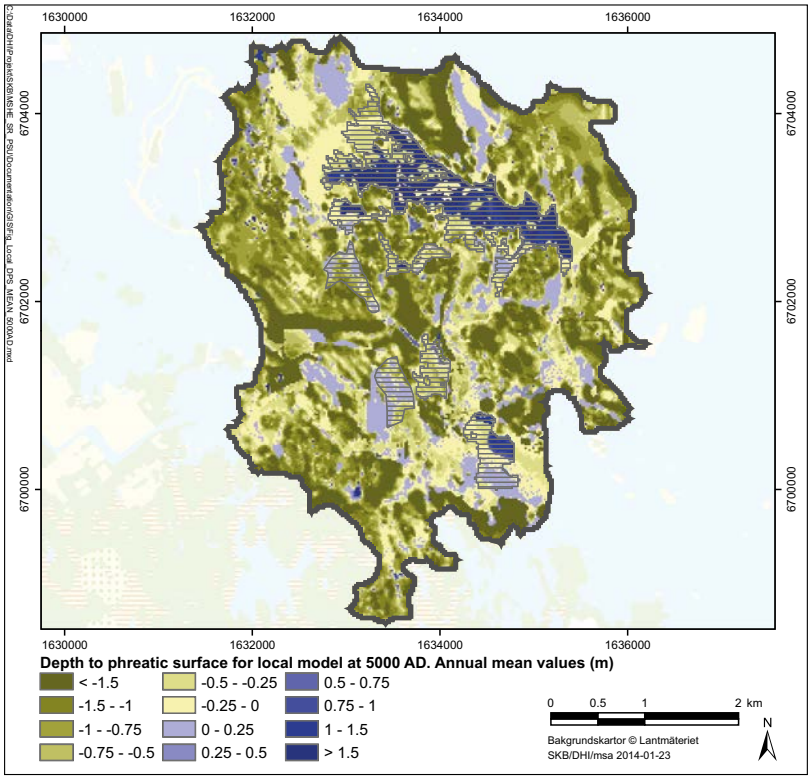

Figure 5-7. *MIKE SHE-calculated annual average depth to the groundwater table at 5000 AD (local model area). Depths are shown as negative values, i.e. positive depths represent surface water.*

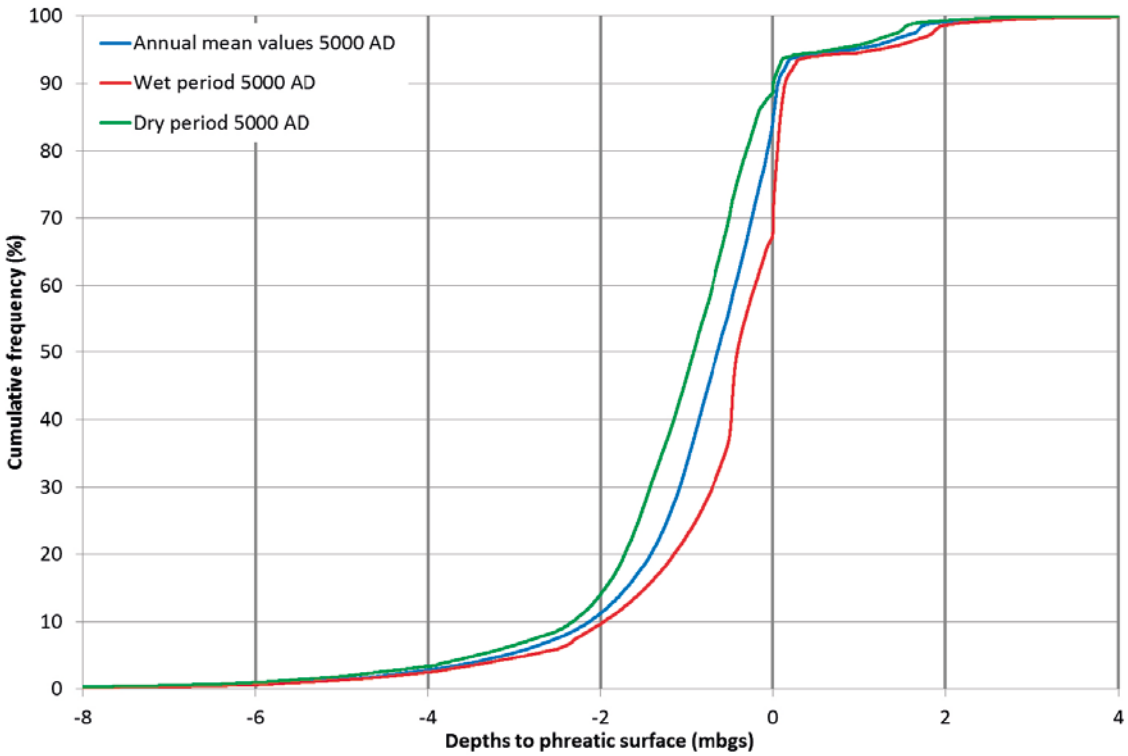

Figure 5-8. *Cumulative-frequency plot of MIKE SHE-calculated depths to the groundwater table at 5000 AD (annual average, wet period (April) and dry period (August)).*

Figure 5-9 shows MIKE SHE-calculated depths to the groundwater table at 11,000 AD, at which time the groundwater table is below ground surface also in former lakes. Even though all lakes within the local model area are terrestrialised at 11,000 AD (Brydsten and Strömgren 2013), according to Figure 5-9 there are areas with above-ground water. Corresponding maps of groundwater-table depths during a wet (March) and dry period (August) are shown in Appendix 1.

Figure 5-10 shows a cumulative-frequency plot of depth to the groundwater table at 3000, 5000 and 11,000 AD. Specifically, one 3000 AD graph considers the entire local model area (blue dotted line), whereas the other graphs only consider terrestrial areas at each time (e.g. solid blue line at 3000 AD). As seen in the figure, at 3000 AD c 45% of the local model area is land and 55% is sea. The cumulative-frequency graphs of groundwater-table depth in terrestrial areas 3000, 5000 and 11,000 AD are rather similar, whereas the graphs also demonstrate the effect of lake terrestrialisation in the form of decreasing lake depths (shown as positive values).

Figure 5-11 shows the same type of cumulative frequency-plot, in this case for areas constituting land at 3000 AD. This figure shows some effects of shoreline displacement in the form of increasing depths to the groundwater table. The depth is larger than 2 m in 16% of the terrestrial areas at 3000 AD (66% deeper than 0.5 m), whereas the corresponding fraction for the same land area is more than 20% at 5000 and 11,000 AD (more than 80% deeper than 0.5 m).

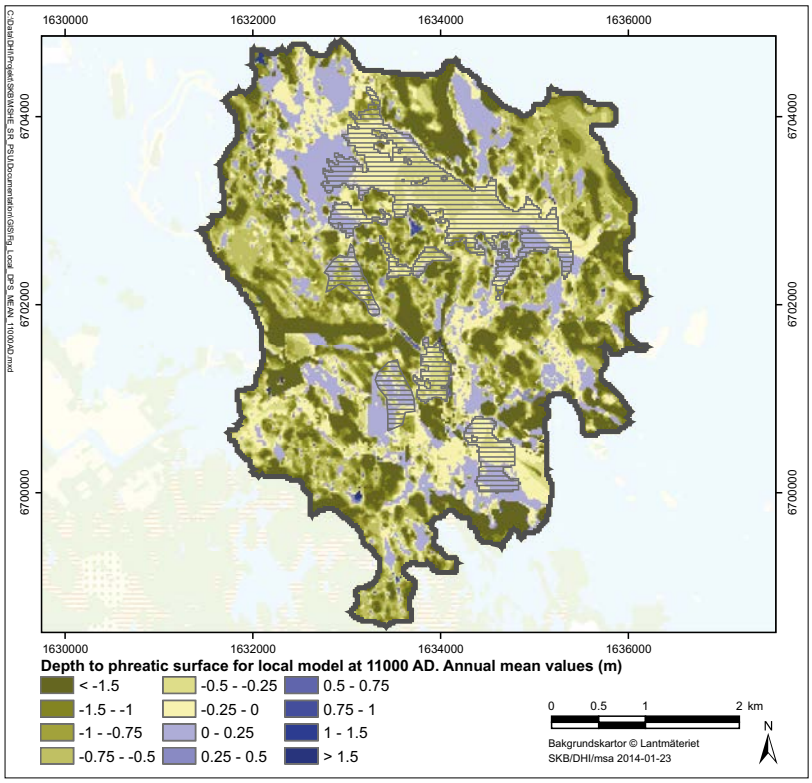

Figure 5-9. *MIKE SHE-calculated annual average depth to the groundwater table at 11,000 AD (local model area). Depths are shown as negative values, i.e. positive depths represent surface water.*

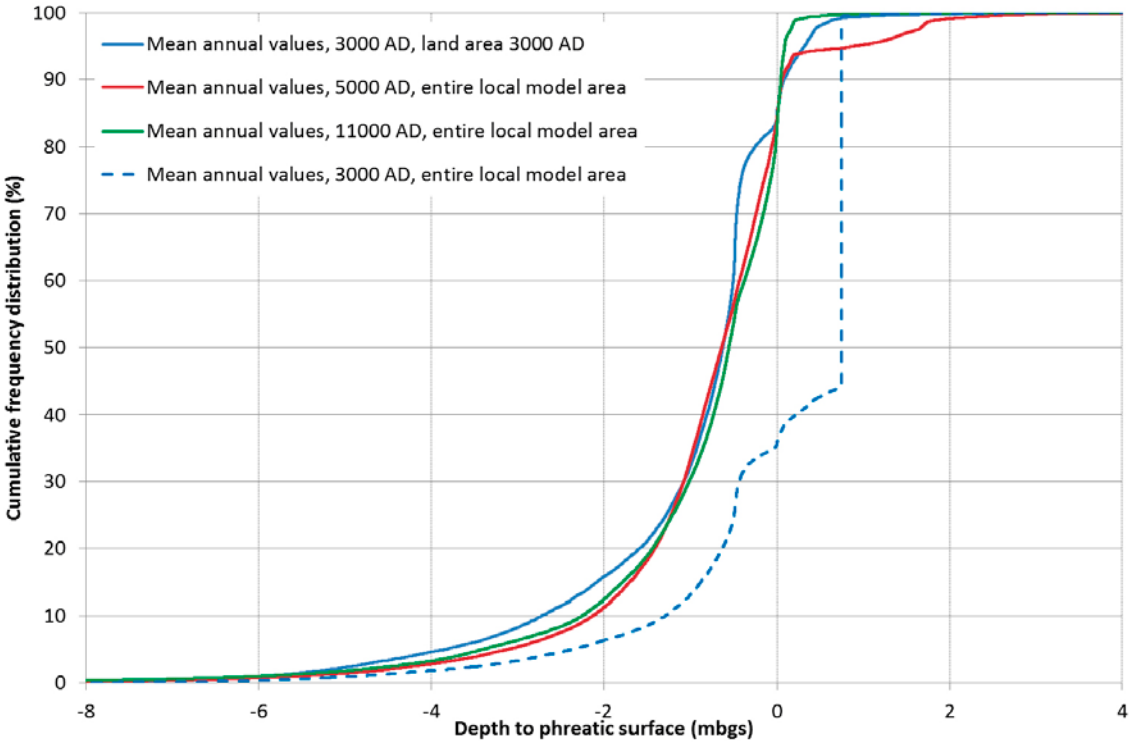

Figure 5-10. *Cumulative-frequency plot of MIKE SHE-calculated depths to the groundwater table in terrestrial areas at 3000, 5000 and 11,000 AD (solid lines), and in the whole local model area at 3000 AD (blue dotted line). Depths are shown as negative values, i.e. positive depths represent surface water.*

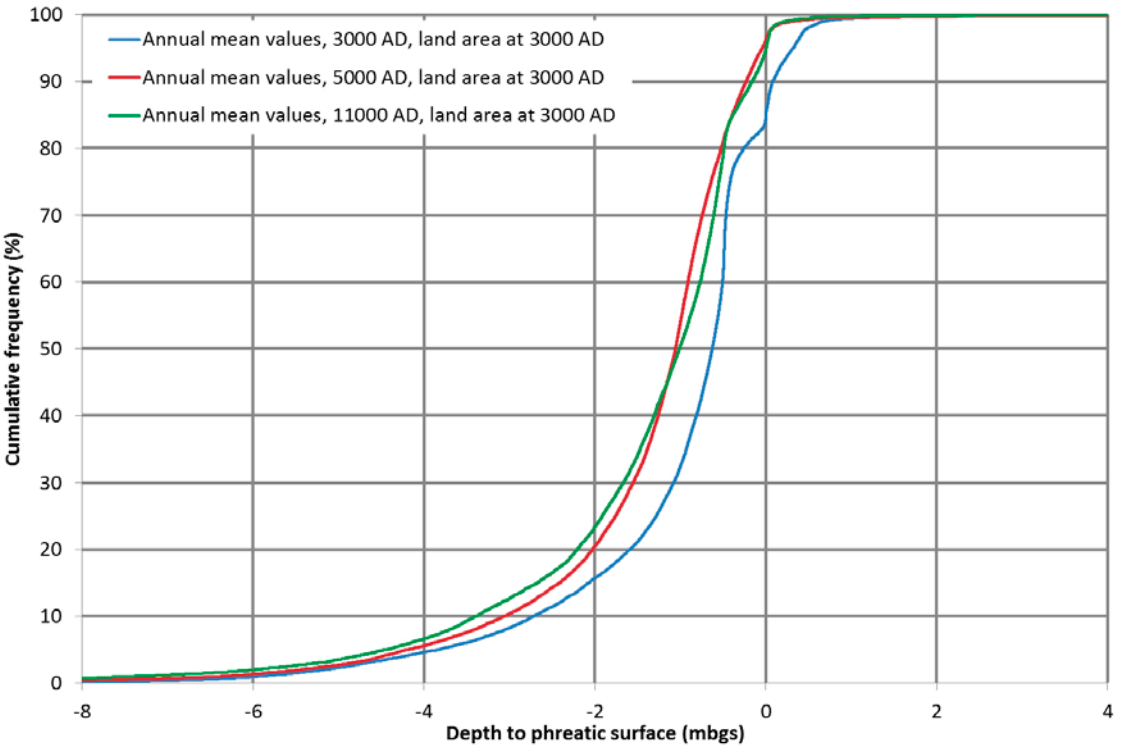

Figure 5-11. *Cumulative-frequency plot of MIKE SHE-calculated depths to the groundwater table at 3000, 5000 and 11,000 AD, in areas constituting land at 3000 AD. Depths are shown as negative values, i.e. positive depths represent surface water.*

5.5 Depth of overland water and stream discharge

Figure 5-12 shows the MIKE SHE-calculated annual average depth of overland (i.e. surface) water at 3000 AD. At this time 45% of the local model area consists of land and the SFR facility has emerged from the sea, whereas biosphere objects remain submerged even though some are close to the shoreline. At 3000 AD, there are no lakes within the local model area (Brydsten and Strömgren 2013). According to Figure 5-12, overland water primarily occurs in the vicinity of streams. Overland-water occurrences are shallow and above 0.5 m in depth in only 2% of the land areas. As illustrated by maps of overland-water depths during a wet (March) and a dry period (August) in Appendix 1, annual variations of overland-water depths are small.

Figure 5-13 shows the same type of map at 5000 AD, at which time the shoreline is outside of the local model area. At 5000 AD, there are lakes surrounded by mire areas in five biosphere objects, whereas two objects (121_2 and 157_2) consist of mire areas (no lake). There are parts of all objects with an annual average depth of overland water exceeding 0.1 m. Overland water is shallow (less than 0.2 m) in the two mire objects, whereas the average depth of overland water is above 0.5 m in the five lake-mire objects. As shown in Appendix 1, at 5000 AD there are larger differences between wet and dry periods compared to 3000 AD. Specifically, there are many dry areas during the dry period that contain a few decimetres of overland water during the wet period. At 5000 AD, the spatial distribution of overland-water depths in terrestrial areas is rather unaffected by a wet and warm climate (Appendix 1).

At 11,000 AD (Figure 5-14), there are no lakes within the local model area and all biosphere objects are transformed to mires. At this time, there are only some shallow (depth 0.1–0.2 m) overland-water occurrences in a few biosphere objects. As shown in Appendix 1, at 11,000 AD differences between wet and dry periods are similar to those at 5000 AD.

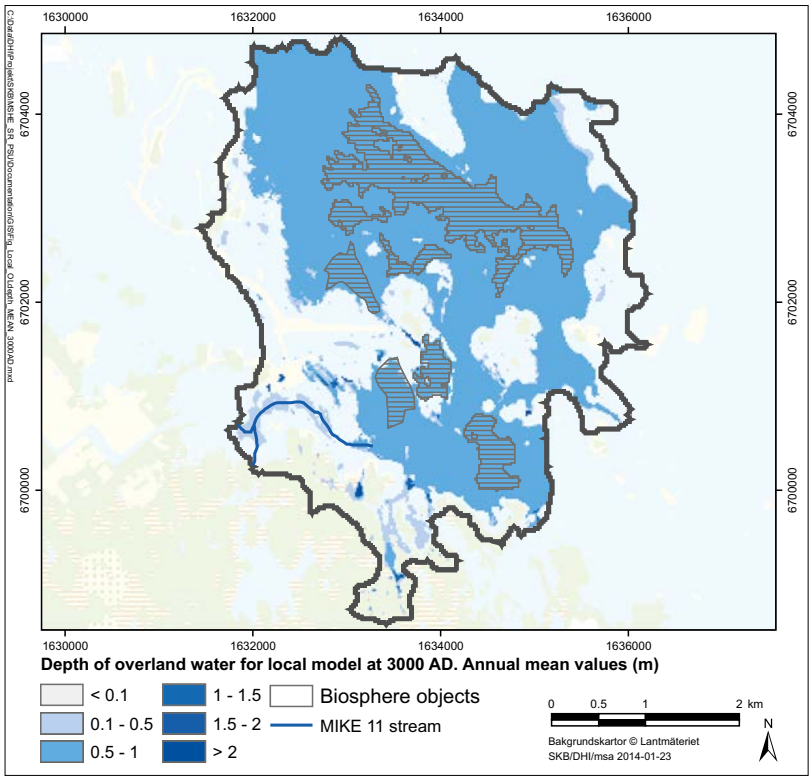

Figure 5-12. *MIKE SHE-calculated annual average depth of overland water at 3000 AD (local model area).*

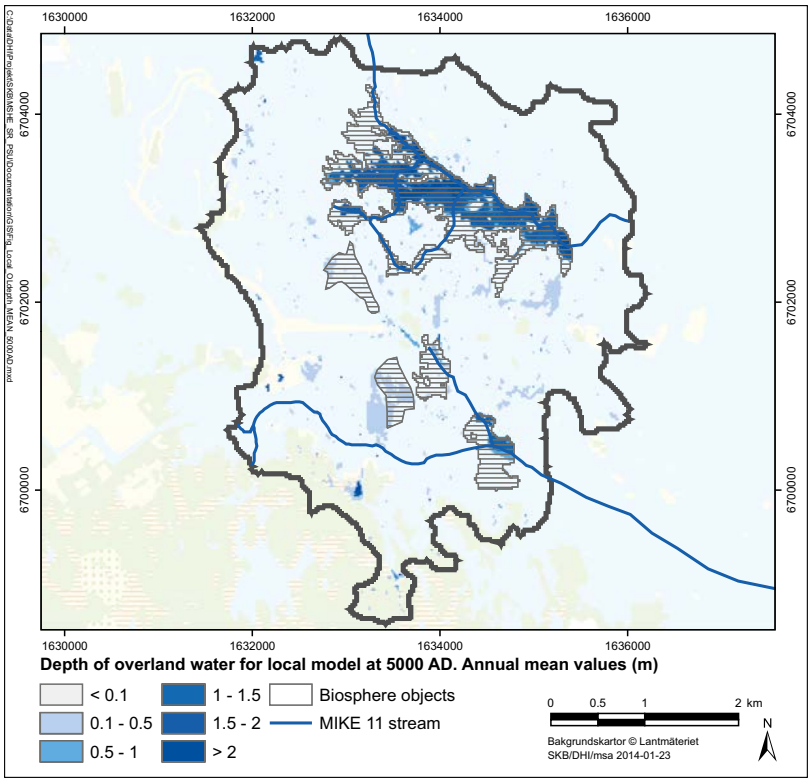

Figure 5-13. *MIKE SHE-calculated annual average depth of overland water at 5000 AD (local model area).*

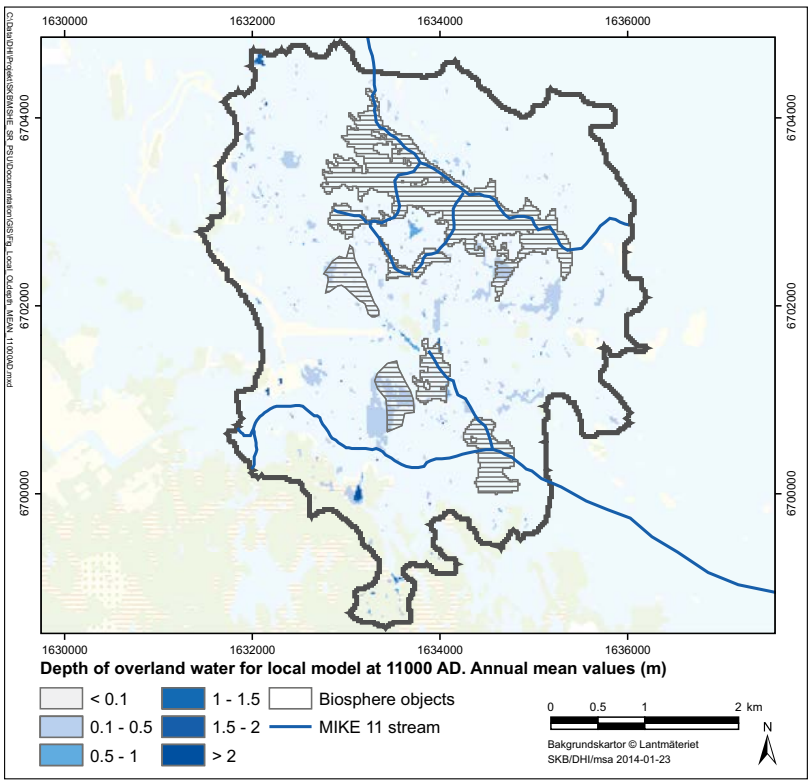

Figure 5-14. *MIKE SHE-calculated annual average depth of overland water at 11,000 AD (local model area).*

Figures 5-15 and 5-16 show stream discharges from biosphere objects 116 and 121_1 at 5000 and 11,000 AD. At 5000 AD biosphere object 116 (Figure 5-15) contains a lake (more than 50% of the object area) surrounded by mire areas, whereas the lake is transformed to mire at 11,000 AD. As shown in Figure 5-15, there are large differences in the hydrographs at 5000 AD (blue line) at 11,000 AD (red line). At 5000 AD the lake dampens and prolongs high-discharge peaks compared to 11,000 AD, and at 5000 AD the lake provides base flow and thereby more stream discharge during low-discharge periods. Compared to biosphere object 116, object 121_1 (Figure 5-16) demonstrates less lake dampening due to its smaller lake at 5000 AD.

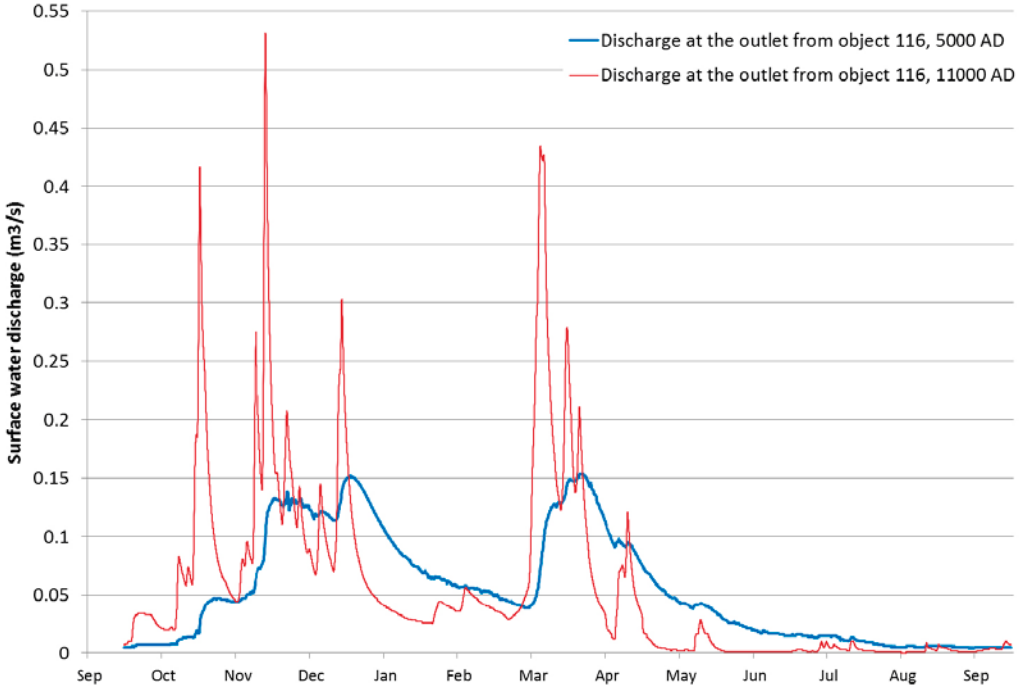

Figure 5-15. *MIKE 11-calculated stream discharge at the outlet from biosphere object 116 at 5000 and 11,000 AD.*

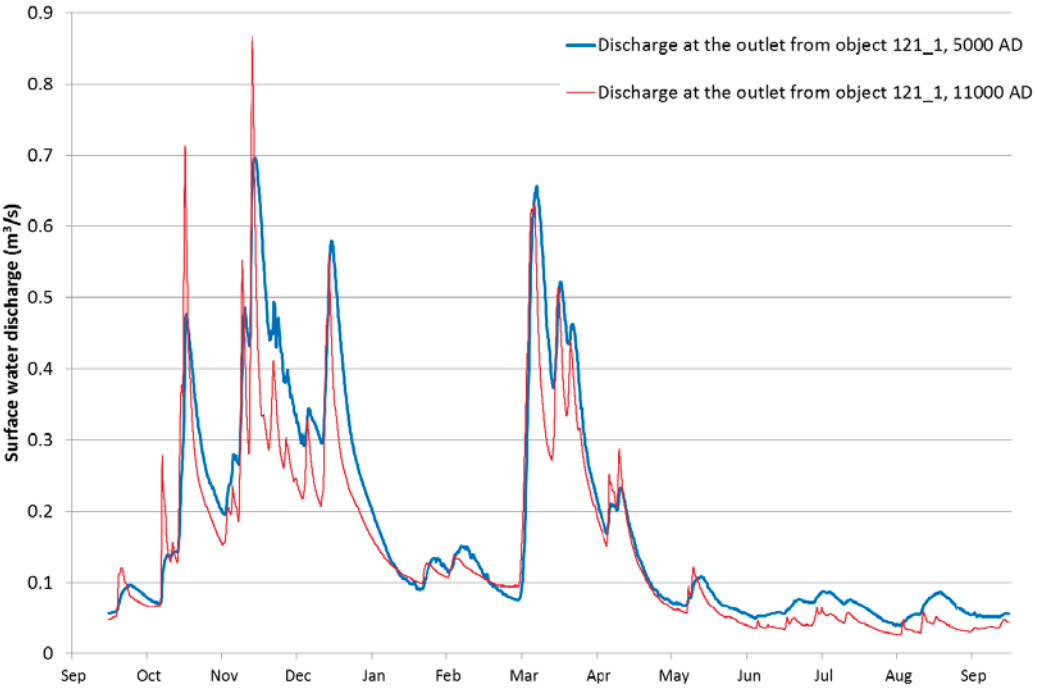

Figure 5-16. *MIKE 11-calculated stream discharge at the outlet from biosphere object 121_1 at 5000 and 11,000 AD.*

5.6 Residence times and inter-basin water exchanges of marine basins

Section 4.5 describes methodology, tools and modelling results in terms of present inter-basin water exchanges and water-residence times (hydraulic residence time (HRT) and average age (AvA)) in marine basins outside Forsmark. This section briefly describes future developments of these parameters, which were calculated in 1,000-year intervals from 0 to 9000 AD. The marine area outside Forsmark consists of the open-ended embayment Öregrundsgrepen, with a wide and deep boundary towards north and a narrow and shallower strait towards south. The open ends benefit flow through the embayment and inter-basin exchanges. The major factors influencing long-term changes of inter-basin water exchanges and water residence times are the long-term developments of the interchange between Öregrundsgrepen and the Baltic Sea, and the bathymetry of Öregrundsgrepen, which was determined from the DEM (Strömgren and Brydsten 2013). In the future, the exchange across the strait in the south (between basin 184 and the Baltic, see Figure 4-11) will continuously decrease as a result of isostatic rebound, which will also isolate basins from the sea.

At c 3000 AD, the strait is expected to close and turn Öregrundsgrepen into a bay, and at this point in time 30 basins (of the present 38) and 62 (of the present 92) inter-basin exchanges remain, including exchanges with the Baltic. During the period from 3000 to 5000 AD, a semi-enclosed archipelago is expected to develop, and at 5000 AD only 17 basins and 7 inter-basin exchanges remain. After 5000 AD, the number of basins and inter-basins exchanges continue to decrease, resulting in three basins and three basin exchanges at 6000 AD, two basins and two exchanges at 7000 AD (between basin 105 and the Baltic and between basins 105 and 114) and only one coupling (between basin 105 and the Baltic) at 9000 AD.

According to the MIKE FM 3 calculations, the largest exchange flows at 3000 AD are at the eastern part of the boundary towards north, between basin 105 and the Baltic, and between basin 164 and the Baltic. The largest inter-basin water exchange also occurs in the northern part of Öregrundsgrepen, across the boundary between basins 164 and 105. Also during the period 4000–6000 AD the largest exchange flows are between basin 105 and the Baltic, whereas the largest inter-basin water exchange is between basins 164 and 105 during the period 4000–5000 AD. At 6000 AD the largest inter-basin water exchange will occur across the remaining part of the embayment, between basins 114 and 184.

During the period 3000–5000 AD, the shortest HRT varies between 4–7 hours (basins 175, 165 and 164), whereas the shortest HRT increases to c 20 days at 6000 AD (basin 114). The shortest HRT is observed for basin 114 during the period 6000–8000 AD (10–20 days), and for basin 105 at 9000 AD (c 25 d). Between 3000 and 5000 AD, the longest HRT (basin 184) fluctuates between 4 and 30 days, whereas the longest HRT is more stable (25–30 days for basin 105) during the period 6000–9000 AD. The shortest AvA was calculated to vary between 11 and 17 days during the period 3000–8000 AD, whereas the shortest AvA increases to 35 days at 9000 AD. During the same period, the longest AvA varies between 19 days (7000 AD) and 50 days (4000 AD).

5.7 MIKE SHE-analyses of discharge locations and solute travel times

In order to check the identification of biosphere objects (cf Section 2.3.1) and to quantify solute travel times in the regolith of biosphere objects, particle tracking was performed using the MIKE SHE local model setups at the times 5000 and 11,000 AD. For each time, 100 imaginary particles were released per MIKE SHE model cell that intersects disposal rooms of SFR 1 and SFR 3 (Figure 5-17). The released particles were subsequently transported in a transient groundwater flow field using meteorological data for the period October 1, 2003–September 30, 2004. In total, 9,800 particles were released from SFR 1 and 16,200 particles from SFR 3. The 5000 AD simulation was run for a time period of 200 years, whereas the 11,000 AD simulation was run for a time period of 500 years. It should be noted that in MIKE SHE, particles are tracked in the saturated zone and hence exit the tracking domain at the groundwater table, surface waters (MIKE 11 and OL) or boundaries of the local model domain.

The upper map of Figure 5-17 shows particle-release locations at SFR 1 and SFR 3, and associated discharge locations for the 5000 AD simulation. As can be seen in the figure, particles released at SFR 1 discharge at biosphere object 157_2, whereas particles released at SFR 3 discharge at biosphere objects 157_2 and 121_2. These results are in overall agreement with the discharge locations at the interface between rock and regolith for the corresponding DarcyTools calculations (Section 2.3.1). However, DarcyTools-calculated discharge locations are also located further north of those calculated by MIKE SHE, both for particles released at SFR 1 and SFR 3. As shown in the bottom map of Figure 5-17, particles that exit the saturated zone in biosphere object 157_2 are mainly located to low-lying areas of the object. In terms of discharge locations, the results of the 11,000 AD simulations (not shown) are similar to the results of the 5000 AD simulations.

According to the dynamic regolith depth and stratigraphy model (Brydsten and Strömgren 2013) at 5000 AD there are organic sediments in the lowest-lying areas of the object, and a relatively thick layer of glacial clay in the northern part of the object. The average thickness of till in the object is approximately 2.5 m, with an assigned horizontal and vertical hydraulic conductivity of $7.5 \cdot 10^{-6}$ and $7.5 \cdot 10^{-7}$ m/s (Table 2-2). Areas with shallow (less than 0.25 m) depth to the groundwater table occur in four parts of the object (cf Sections 5.4 and 7.5.1), whereas annual average depths of overland water generally are less than 0.25 m (cf Section 5.5). Potential arable land is located to the northern part of the object (cf Section 6.4), along a low-lying "trough" towards biosphere object 157_1.

All particles that are released from SFR 1 in the 5000 AD simulation reach the bottom of the regolith at biosphere object 157_2 in c 2 years, whereas it takes another few years for them to exit the tracking domain in the regolith (in total, 99% of the released particles exit the domain during the simulated time period of 200 years). Hence, the MIKE SHE particle-tracking calculations indicate longer and more distributed solute travel times in the regolith of biosphere object 157_2 than travel times in the rock from SFR 1 to the object.

60% of all particles that are released from SFR 3 in the 5000 AD simulation reach the bottom of the regolith in biosphere objects 121_2 and 157_2 during the simulated time period of 500 years. These reach the bottom of the regolith in c 6 years, which indicate longer travel times in the rock from SFR 3 to biosphere objects than travel times from SFR 1 to biosphere object 157_2. Moreover, the MIKE SHE modelling results indicate longer travel times in the rock from SFR 3 to biosphere object 121_2 than to object 157_2. 55% of the released particles exit the tracking domain during the simulated time period of 500 years. Particles than remain in the rock after 500 years are those released in areas with downward hydraulic gradients in the rock, and they are hence moving relatively slowly towards the surface system. In terms of solute travel times in rock and regolith, the overall behaviour of the 11,000 AD simulations are similar to that of the 5000 AD simulations.

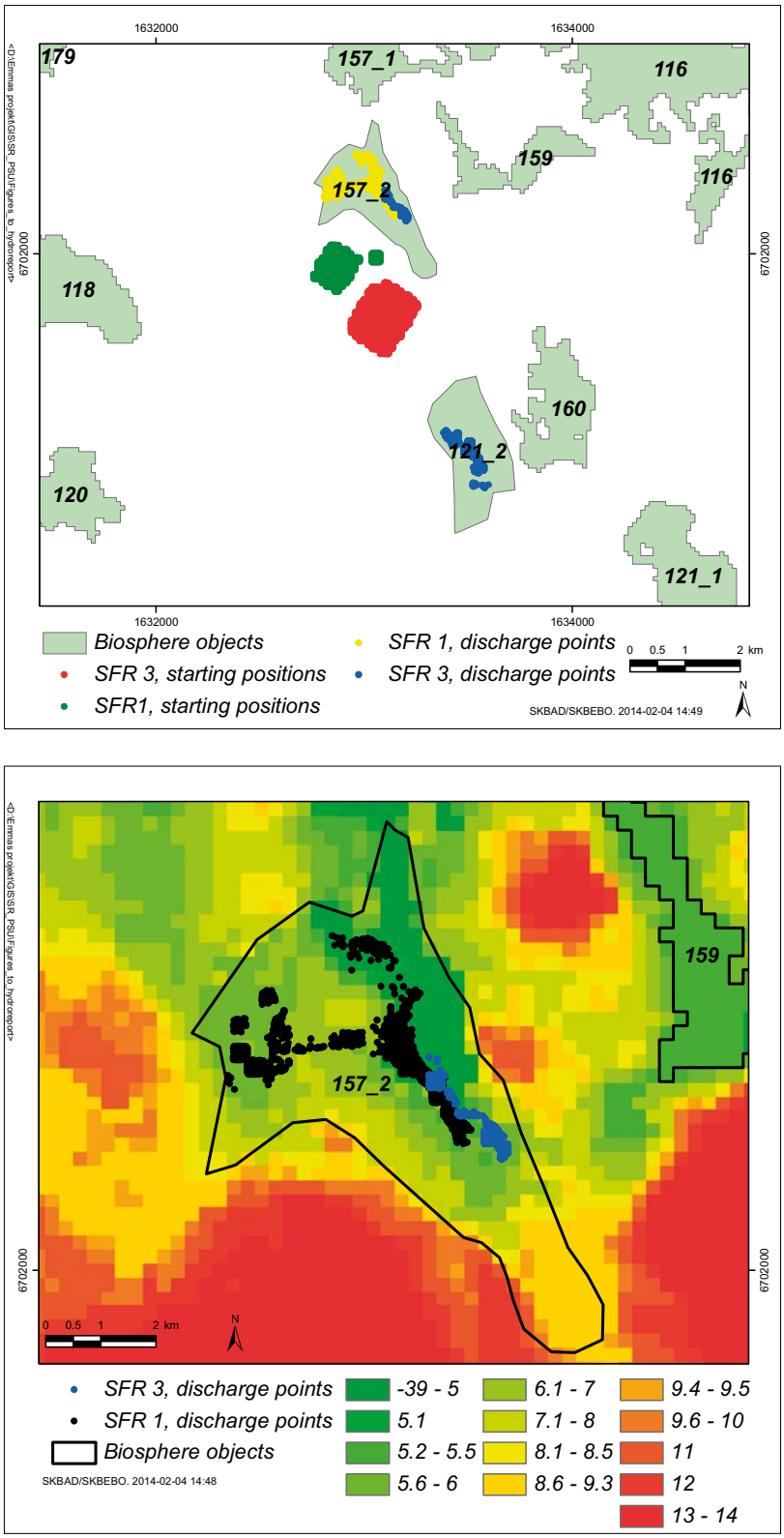

Figure 5-17. *Upper figure: Release (starting) and discharge locations (discharge points) for the MIKE SHE 5000 AD particle tracking. Lower figure: Zoomed map showing discharge locations in biosphere object 157_2 and ground-surface elevations.*

5.8 Analyses of periglacial conditions and permafrost

5.8.1 General description of permafrost features and hydrology in periglacial environments

The hydrology of periglacial environments is influenced by ice, snow and frozen ground. The water balance and the hydrological cycle are strongly affected by the presence of permafrost (White et al. 2007), which controls the distribution and routing of water across the landscape (Quinton and Carey 2008). The hydrologically active period, with stream flow and redistribution of water on the ground surface and in the active layer (see explanation below), is relatively short. The main hydrological event of the year is the snow melt period. The snow water balance has to be taken into account because sublimation, i.e. direct phase transition from solid to gas, and snow blowing events might cause considerable water losses during the winter period (McDonald et al. 2010, Reba et al. 2011, Bosson et al. 2013). The presence of permafrost reduces groundwater recharge and discharge relative to unfrozen conditions (Bosson et al. 2012). As shown in both theoretical and empirical studies (Frampton et al. 2011, 2013, Ge et al. 2011, Bosson et al. 2013, Grenier et al. 2013, Kane et al. 2013), the exchange of deep and shallow groundwater occurs via taliks.

Taliks denote unfrozen pockets of water located above, below or within frozen ground (French 2007). In areas of continuous permafrost, taliks are often located below lakes, due to the ability of surface water to store and vertically transfer heat energy. The potential for a lake to maintain a talik depends on the lake area, the lake depth and the permafrost depth (Hartikainen et al. 2010). In particular, an open talik is an area of unfrozen ground that is open to the ground surface but otherwise enclosed in permafrost (cf Figure 5-18). Through taliks are unfrozen ground exposed to the ground surface and to a larger mass of unfrozen ground below, whereas closed taliks are unfrozen ground enclosed in permafrost. Through taliks are important elements in a permafrost landscape, since they connect the unfrozen groundwater flow system at depth to the active layer on the ground surface. The active layer is an upper layer, which is subject to cyclic freeze and thaw and hence frozen or unfrozen depending on weather conditions. In the following, the active period refers to the period of the year when the active layer is fully thawed, whereas the frozen period is when the active layer is fully frozen. Between active and frozen periods, there are periods of thawing and freezing conditions.

As described in Section 5.8.2, in the SR-PSU project the above-mentioned features and processes are taken into account in DarcyTools modelling for delineation of discharge areas for periglacial conditions with permafrost (cf Section 2.3.2). Moreover, Sections 5.8.3–5.8.5 present modelling and results concerning periglacial hydrology and near-surface hydrogeology at Forsmark, based on further analyses of MIKE SHE modelling results from SR-Site.

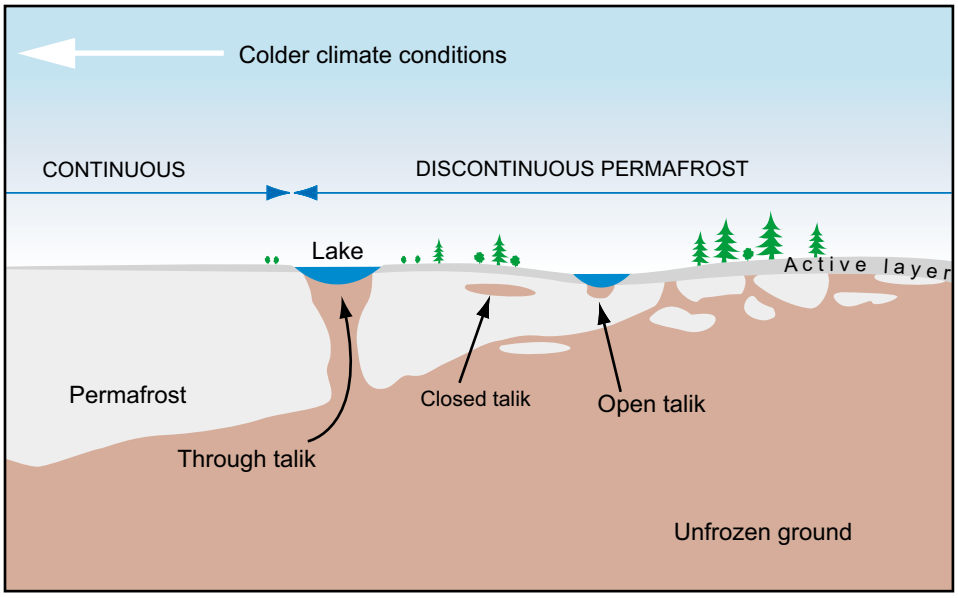

Figure 5-18. *A schematic profile through a permafrost area with an active layer and different types of taliks (Bosson et al. 2010).*

5.8.2 DarcyTools modelling of permafrost conditions

As part of the SR-PSU project, Odén et al. (2014) used DarcyTools to simulate steady-state groundwater flow in rock and taliks for permafrost conditions. The simulations were done for three variants of the hydrogeological model of the rock, the base case and two bounding variants. Specifically, in terms of disposal-facility cross flows for temperate conditions, the base case represents a median-flow case, whereas the two bounding variants represent a low- and a high-flow case, respectively.

In the DarcyTools permafrost modelling, locations of potential taliks associated with lakes and streams are taken from the landscape model at 20,000 AD (Brydsten and Strömgren 2013), at which time only two lakes are present within the DarcyTools model area. These lakes are represented as upper boundary conditions for temperature and also for hydraulic head, which is set equal to the lake threshold according to the landscape model, whereas streams are represented as upper boundary conditions for temperature. Outside of the talik areas, the upper boundary conditions are represented as a fixed temperature and a fixed hydraulic head. The latter represents the location of the groundwater table, which is assumed to be located in the active layer close to the ground surface. The lateral boundary conditions are similar to those used for simulations of temperate conditions, i.e. no groundwater flow (and in the permafrost simulations no flux of heat), whereas the bottom boundary condition is represented as no groundwater flow but with a specified heat flux.

Moreover, in one simulation case (see further below) a set of additional small surface waters (ponds and peat bogs) are also defined as potential taliks. Specifically, the locations of such small surface waters, and associated potential taliks, are taken as the locations of areas with at least 0.5 m of overland water in the MIKE SHE simulations for temperate conditions at 11,000 AD (cf Section 5.5).

Three different permafrost depths were investigated, namely shallow permafrost down to c –60 m elevation, and deeper permafrost down to c –85 m (within SFR-1) or –90 m elevation (below SFR-1). Moreover, locations of potential taliks were defined according to three variants: (1) All surface waters, including lakes and streams at 20,000 AD according to the landscape modelling by Brydsten and Strömgren (2013), as well as small surface waters according to the MIKE SHE simulations for 11,000 AD, (2) lakes and streams according to the landscape modelling, and (3) only lakes according to the landscape modelling. Section 2.3.2 describes the SR-PSU results of the DarcyTools permafrost modelling, in terms of discharge locations at the interface between rock and regolith.

5.8.3 MIKE SHE modelling of periglacial hydrology and near-surface hydrogeology at Forsmark

As described in Section 2.2.1, periglacial conditions are not considered in the MIKE SHE model setup of the SR-PSU project. The locations and extents of future lakes and streams (Section 3.2.3), which control the locations of taliks, are similar to those of SR-Site. The results of the MIKE SHE modelling of periglacial conditions and permafrost presented by Bosson et al. (2010) are therefore considered to be relevant also for the SR-PSU project.

The results of Bosson et al. (2010) were further analysed and elaborated by Bosson et al. (2012, 2013). In particular, the water balance of the Forsmark site was investigated for different landscape settings in terms of topography, regolith, vegetation and shoreline elevation, climate settings (air temperature, potential evapotranspiration and precipitation), and existence and thickness of permafrost (Table 5-2). Specifically, for the future-landscape cases (1b–2c in Table 5-2) the shoreline is situated at –31.42 m elevation, which corresponds to the shoreline at 10,000 AD. Figure 5-19 shows the considered model area (which is similar to the MIKE SHE regional model area in SR-PSU, cf Section 3.1.1) for flow and particle-tracking simulations, and the locations of through taliks in cases 2b (permafrost depth 100 m) and 2c (permafrost depth 240 m). As shown in Figure 5-19, the number of taliks depends on the permafrost depth, and larger permafrost depths result in fewer taliks (Bosson et al. 2012).

Table 5-3 (Section 5.8.3) summarises the climate characteristics for each of the considered cases, and the resulting surface-water fractions (lakes and wetlands), hydrological flows and flow ratios. Temperate climate data (cases 1a–b) are from Johansson (2008), whereas periglacial climate data (cases 2a–c) are from Kjellström et al. (2009). Specifically, for the temperate-climate cases the mean annual air temperature (MAAT) is +6.4°C and the annual accumulated precipitation (AAP) is 583 mm, whereas MAAT is –7°C and AAP is 412 mm in the periglacial-climate cases. Moreover, the annual accumulated potential evapotranspiration (AAPET) is 420 mm in cases 1a–b, and 216 mm in cases 2a–c.

Table 5-2. Simulation cases for different landscape and climate settings (Bosson et al. 2012).

Case	Landscape (topography, regolith, vegetation, shoreline)	Climate (air temperature, precipitation, potential evapotranspiration)
1a	Present	Temperate
1b	Future	Temperate
2a	Future	Periglacial (no permafrost)
2b	Future	Periglacial (100 m permafrost)
2c	Future	Periglacial (240 m permafrost)

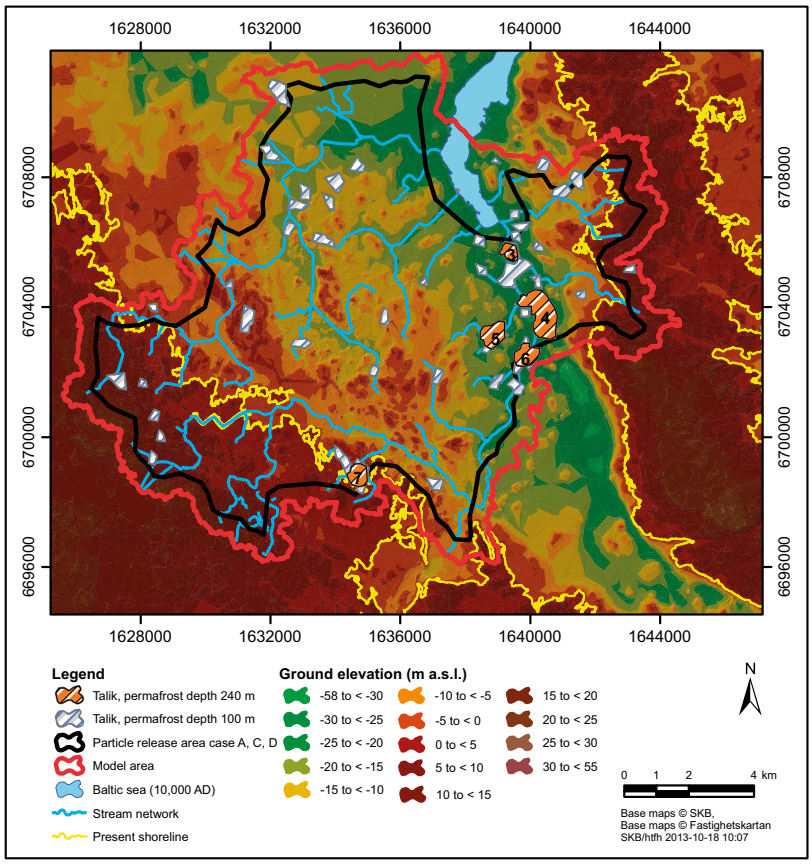

Figure 5-19. *Model area, particle-release area and through taliks in the permafrost cases 2b (permafrost depth 100 m) and 2c (permafrost depth 240 m) (Bosson et al. 2012).*

5.8.4 MIKE SHE results – water balance and intra-annual dynamics

According to Table 5-3, the modelling results show a slightly larger proportion of lakes (surface-water depth > 0.3 m) and wetlands (surface-water depth 0.01–0.3 m) for cases 2a–c (periglacial climate) compared to the present-landscape case with a temperate climate (case 1a), due to less evapotranspiration (ET). Furthermore, permafrost reduces the infiltration capacity of the regolith, which increases ground-surface storage in cases 2b–c (future landscape, periglacial climate and permafrost) compared to case 2a (same as 2b–c, but no permafrost). It can also be noted that there is more surface-water runoff for cases 2b–c compared to case 2a. In a permafrost landscape, large part of the snowmelt occurs when the active layer is still frozen, hence preventing infiltration. Moreover, once the active layer is thawed the thin active layer (thickness 1 m) is quickly saturated and ET is smaller in a periglacial climate in the Forsmark case, which promote ground-surface storage, ponding and surface-water runoff.

The modelling results demonstrate that for a temperate climate, the cumulative runoff increases more or less continuously (Figure 5-20) and groundwater recharge and discharge occur throughout the year, whereas for a periglacial climate (both without and with permafrost) snowmelt is the main hydrological event of the year (cf above). For a periglacial climate, snow accumulation occurs during a longer period and groundwater recharge and discharge only occur during the active period. In cases 2a–c, the snowmelt rate exceeds the infiltration capacity of the regolith and creates surface-water runoff. In the temperate cases (1a–b) and the periglacial case without permafrost (2a), groundwater flow in the uppermost regolith is the largest part of the runoff. In the permafrost cases (2b–c), surface water has the largest contribution to runoff. Moreover, permafrost delays groundwater discharge to streams compared to the non-permafrost case (2a). In case 2a, groundwater discharge occurs immediately after initiation of snowmelt, whereas in a permafrost landscape (cases 2b–c) the active layer has to thaw before groundwater recharge can take place. Thawing of the active layer is initiated more or less simultaneously as the snowmelt in spring, and continues until fully thawed conditions are reached in the beginning of the summer.

The results of Bosson et al. (2012) show a complexity in the hydrological responses to changes in landscape and climate settings. Specifically, the results demonstrate that a warmer or colder climate is not necessary similar to a wetter or drier landscape. The periglacial climate cases 2a–c, which are characterized by less precipitation and potential evapotranspiration compared to a temperate climate, may be viewed as drier conditions from a climate perspective. However, a periglacial climate may be characterized by more ground-surface storage and runoff, and hence wetter conditions from a landscape perspective.

5.8.5 MIKE SHE results – exchange of deep and shallow groundwater

Figure 5-21 shows model-calculated vertical groundwater flux (volumetric flow normalized over the whole model area) as function of elevation for cases 1b and 2b–c. Fluxes are calculated as total groundwater recharge minus total groundwater discharge, i.e. downward fluxes are positive. Results are shown for areas that correspond to inland through taliks, the sea bay, and the total area of inland through taliks and the sea bay (cf Figure 5-19). For all considered cases, the vertical groundwater flux decreases with depth. For the temperate case (1b), only a fraction (less than 5%) of the total groundwater discharge occurs in areas that constitute through taliks under periglacial conditions with permafrost.

Table 5-3. Climate characteristics and resulting hydrological flows for cases 1a–2c. MAAT = mean average annual air temperature, AAP = annual accumulated precipitation, AAPET = annual accumulated potential evapotranspiration, R = runoff, ET = evapotranspiration, Rgw = groundwater recharge. The percentage of lakes and wetlands refer to the ratio between their total surface area and the total land area (Bosson et al. 2012).

Case	Climate			Lakes and wetlands (%)	Abs. hydrological flows			Flow ratios (–)		
	MAAT (°C)	AAP (mm)	AAPET (mm)		R (mm)	ET (mm)	R_{gw} (mm)	ET/AAP	R/AAP	R_{gw}/AAP
1a	6.4	583	420	15	175	405	124	0.69	0.30	0.21
1b	6.4	583	420	13	186	403	136	0.69	0.32	0.23
2a	–7	412	216	16	204	211	109	0.51	0.50	0.26
2b	–7	412	216	19	217	194	56	0.47	0.53	0.14
2c	–7	412	216	18	217	193	55	0.47	0.53	0.13

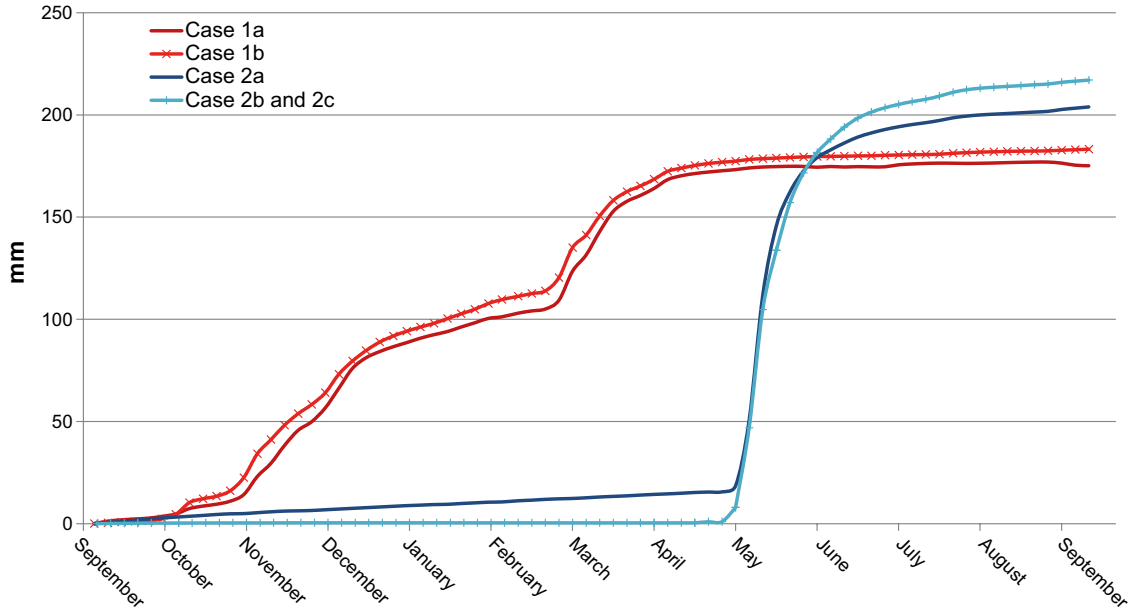

Figure 5-20. *Model-calculated runoff (R) for cases 1a–b (temperate climate), 2a (periglacial climate, no permafrost), and 2b–c (periglacial climate and permafrost) (Bosson et al. 2012).*

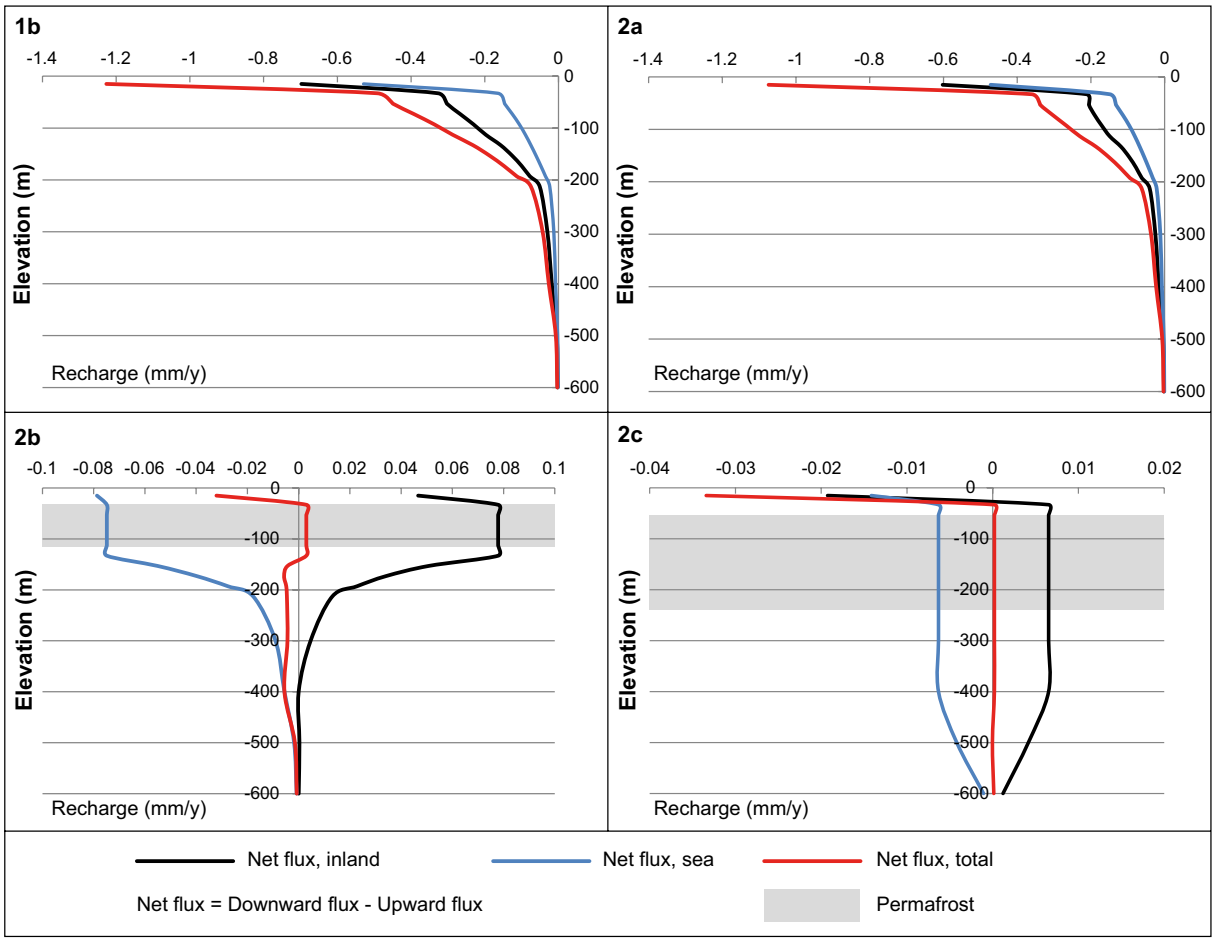

Figure 5-21. *Vertical groundwater flux (volumetric flow normalized by model area) as function of elevation for cases 1b and 2a–c (Bosson et al. 2013). Fluxes are calculated as total groundwater recharge minus total groundwater discharge, i.e. downward fluxes are positive. Results are shown for areas that correspond to inland through taliks (black dashed lines), the sea bay (blue dotted lines), and the total area of inland through taliks and the sea bay (red solid lines).*

Hence, groundwater fluxes decrease significantly and change predominant directions relative to temperate conditions. Specifically, in cases 2b–c the exchange between deep and shallow groundwater is restricted to talik areas, and inland talik areas that act as groundwater recharge areas in these cases are groundwater-discharge areas for temperate conditions (case 1b). Moreover, vertical groundwater fluxes are smaller for a reduced number of taliks. For permafrost conditions, the main groundwater flow takes place between recharge taliks in inland areas and the (unfrozen) sea, even though some inland taliks act as groundwater-discharge areas. Vertical groundwater fluxes are constant with depth within the permafrost, fluxes increase with depth above the permafrost layer in talik areas, and decreases with depth below the permafrost.

Bosson et al. (2013) performed forward particle tracking (particle release at –400 m elevation) to analyse groundwater flow paths for the future-landscape cases 1b (temperate), 2b (periglacial, permafrost depth 100 m; 45 through taliks) and 2c (periglacial, permafrost depth 240 m; 7 through taliks), cf Table 5-2. As shown by the discharge locations in Figure 5-22, in the presence of permafrost (cases 2b and 2c) the exchange between deep and shallow groundwater occurs in through-talik areas and on the (unfrozen) sea bottom. In particular, almost 50% (case 2b; permafrost depth 100 m) and almost 90% (case 2c; permafrost depth 240 m) of the particles that reach the regolith during the simulated period of 5,000 years discharge at the sea bottom (Bosson et al. 2013). In the temperate case (1b) groundwater discharge areas are located to lakes, wetlands and streams. In the temperate case (1b), approximately 20% of the discharging particles reach the regolith in areas that are through taliks in cases 2b–c. Hence, there are quite different discharge-location patterns for temperate conditions and periglacial conditions with permafrost.

Groundwater-flow path lengths and associated solute travel times are longer when permafrost is present, and they also increase with permafrost depth (Figure 5-23). In particular, in the temperate case (1b) the mean flow-path length (from –400 m elevation to the regolith) is c 1,000 m, whereas the corresponding lengths are c 3,000 m and c 5,000 m in the permafrost cases 2b and 2c, respectively. By releasing particles in the regolith (not shown here), Bosson et al. (2013) concluded that in the permafrost cases (2b–c) the longest travel times are in the unfrozen rock below the permafrost, whereas the shortest travel times are through the taliks.

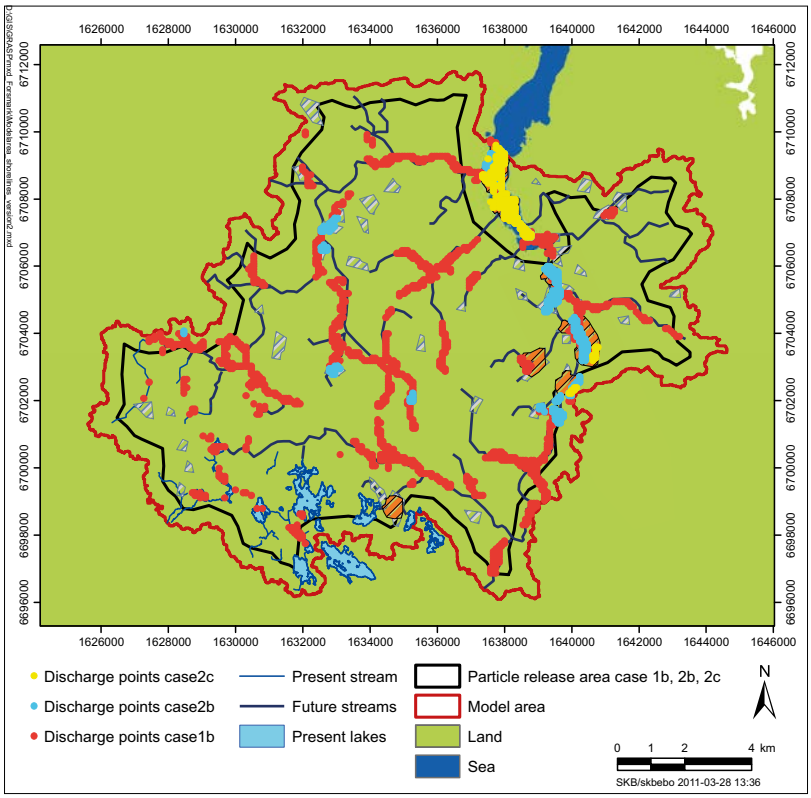

Figure 5-22. *Discharge locations (discharge points) at the regolith for particles released at –400 m elevation in the rock for cases 1b, 2b and 2c (cf Table 5-1).*

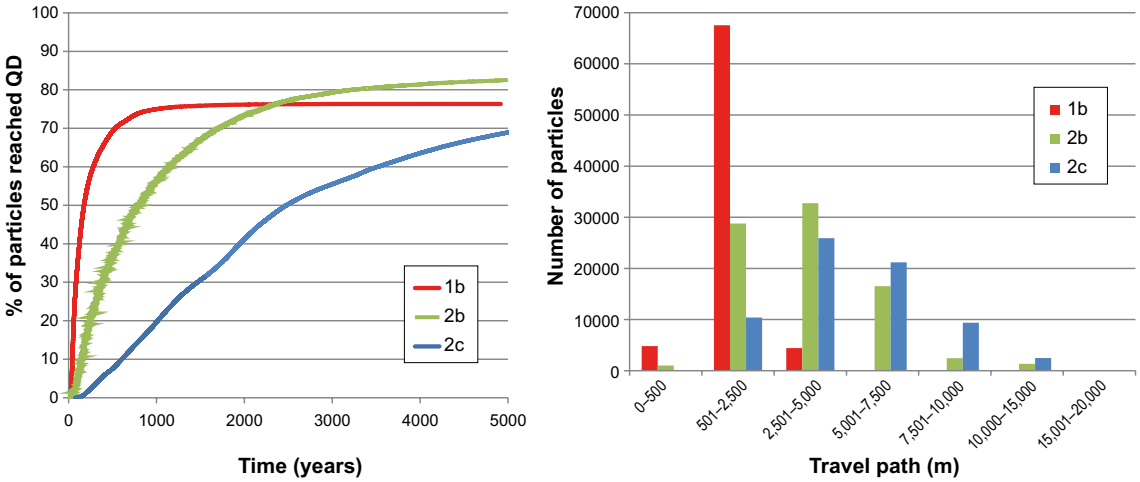

Figure 5-23. *Breakthrough curves (left) at the regolith and associated flow-path lengths (right) for particles released at –400 m elevation in cases 1b and 2b–c (Bosson et al. 2013).*

Areas that for temperate conditions act as inland groundwater-discharge areas can for permafrost conditions constitute recharge areas associated to through taliks. For such conditions, through taliks are the only available inland pathways through the permafrost and they tend to be located to topographical low points in the landscape. Hence, a shift from temperate to periglacial conditions with permafrost changes recharge-discharge patterns at the ground surface and the exchange between deep and shallow groundwater. Theoretical and empirical studies indicate that for periglacial conditions with permafrost, topographical differences between taliks govern the spatial pattern of groundwater recharge and discharge (Bosson et al. 2013). The main groundwater discharge occurs at the most downstream through talik (the sea bay in the Forsmark case).

6 Water-resources management and wells in the future Forsmark landscape

This chapter concerns water-resources management inhabitants of the future Forsmark landscape. Specifically, the first part of the chapter presents modelling and results on hydrological issues related to agriculture and drainage (Section 6.1), whereas the remaining Sections 6.2–6.5 are focused on water uses for humans, cattle and irrigation. Section 6.2 provides data on the total water use of different types of self-sufficient communities and associated potential water supplies. Sections 6.3–6.4 contain hydrogeological analyses of wells in regolith and wells drilled in rock, whereas Section 6.5 gives recommendations for handling of future water uses in the SR-PSU project.

6.1 Hydrology and water-resources management of agricultural land

6.1.1 Background and objectives

Agriculture is a main food contributor for future, self-sufficient agricultural communities in the Forsmark landscape. The SR-PSU model of transport and accumulation of radionuclides in the biosphere (Saetre et al. 2013b) considers three exposure scenarios associated to agricultural land:

- The use of contaminated hay (winter fodder) and manure (fertilizer) in infield-outland farming representing a self-sufficient Iron-age family.
- Modern-farming drainage of lake-mire systems.
- Cultivation of vegetables and potatoes on a garden plot by a small household, using contaminated water for irrigation and fertilizers from sea macrophytes (algae) or ash from wood or peat.

In order to enable analyses of these exposure scenarios, the radionuclide model takes into account a number of radionuclide-transport and transformation processes in agricultural land, e.g. percolation, groundwater uptake, decay, degassing, and mineralisation. In support of the radionuclide-transport modelling, this section provides a description of main hydrological processes and parameters associated to agricultural land, specifically related to water-resources management in the form of modern-farming drainage for a temperate climate. Hence, processes such as decay, degassing and mineralisation are not discussed here.

The present arable land in northern Uppland is mostly located to areas with water-deposited clay. Only a small part of the land area in Forsmark is covered by such regolith, whereas the proportion of potential arable land likely will increase in the future as the broad and presently submerged Öregrundsgrepen valley is uplifted (cf Section 2.2.2). Parts of the clay and sand dominated areas of Öregrundsgrepen will initially be covered by low-lying, shallow lakes and wetlands, which successively will be covered with a layer of fen peat. Parts of these shallow wetlands can probably be relatively easily drained and cultivated, and it is therefore assumed that modern-farming drainage and cultivation primarily occur in regolith consisting of peat and postglacial sediments. In the landscape development model (SKB 2014a), it is assumed that all present and future wetlands with a peat-layer thickness exceeding approximately 1.5 m are cultivated. As the fen-peat accumulation rate is low (Sohlenius et al. 2013b), it takes long time for cultivation to be suitable in uplifted areas.

6.1.2 Conceptual description of water flow in agricultural land

Compartmentalisation and water-flow processes

The SR-PSU model of radionuclide transport and accumulation in agricultural land (Saetre et al. 2013b) considers upward and downward water flow in a compartment denoted regoUp. This compartment represents a biologically active layer above the groundwater table; it is affected by ploughing and bioturbation, and it is where crops take up water, nutrients and trace elements by their roots. The water content in the root zone, which is influenced by the depth to the groundwater table during the growing

season, is one main factor for crop yield. Many crops have an optimal growth for a groundwater-table depth of 1 mbgs (e.g. Feddes 1971), whereas grass species suitable for hay production demonstrate high growth rates for a groundwater-table depth of c 0.5 mbgs (Mueller et al. 2005).

In a hydrological context, the regoUp compartment can be considered as the unsaturated zone in soil with a shallow depth to the groundwater table. Specifically, from below and up regoUp extends from the top of the capillary fringe to the ground surface. The capillary fringe is a tension-saturated zone above the groundwater table, in which the pressure head (negative above the groundwater table) is above the so called air-entry (or bubbling) pressure head, i.e. the pressure head at which air enters the largest pore (e.g. Gillham 1984). The vertical extent of the capillary fringe in peat is typically on the order of 0.3–0.4 m, and it can be up to 0.6 m in highly decomposed peat (Verry 1997). Hence, an unsaturated zone in peat (i.e. regoUp) that extends 0.5 mbgs corresponds to a groundwater-table depth of 0.8–0.9 mbgs if the capillary fringe has a vertical extent of 0.3–0.4 m.

During the growing season, water required for crop growth is added to the regoUp compartment by precipitation and it is lost by evapotranspiration. During periods when the water content is higher than the field capacity of the soil, water is also lost by downward percolation towards the groundwater table. The field capacity is the water content at cessation of drainage of a soil profile, whereas water is unavailable for crops at water contents at or below the wilting point. The field capacity and the wilting point are usually defined as the soil-specific water content at pressure heads of –1 m (i.e. the pressure head 1 m above the groundwater table in a soil profile with no vertical water flow) and –150 m, respectively (e.g. Grip and Rodhe 1994).

In addition to precipitation, water can also be added to regoUp by groundwater uptake, i.e. by a combination of capillary rise and upward water-flow from the groundwater table (e.g. Schlotzhauer and Price 1999, Mueller et al. 2005, Ayars et al. 2006, Singh et al. 2006, Logsdon et al. 2009). For agricultural land with a shallow groundwater table, it has been found that this process, which is driven by evapotranspiration during dry periods (zero precipitation), may be large part of the total crop-water supply during the growing season (e.g. Mueller et al. 2005).

Percolation – parameterisation of downward water flow

As outlined above, percolation is here defined as downward water flow through the unsaturated regoUp compartment towards the groundwater table. In agricultural land, the percolation flux (percolation flow per unit area) varies in space and time as a result of e.g. soil and crop type, depth to the groundwater table, precipitation intensity, and variations of near-surface air temperature. Bosson et al. (2010) present MIKE SHE-calculated annual average percolation fluxes for the Forsmark area at 2000, 5000 and 10,000 AD. For these times, the average percolation flux is c 200 mm/y for the normal year. As the ratio between percolation and runoff was close to one in these simulations, long-term discharge statistics can be used to infer corresponding statistics for the percolation flux. For instance, Larsson McCann et al. (2002) and Bosson et al. (2010) present and analyse data from the Vattholma discharge-gauging station (located some 50 km southwest of Forsmark) for the 83-year period 1917–2000. For a wet and warm climate, the MIKE SHE-calculated average percolation flux is c 260 mm/y (Bosson et al. 2010), which is within the range for the 1917–2000 record for Vattholma.

Groundwater uptake – parameterisation of upward water flow

As outlined above, groundwater uptake is here defined as upward water flow through the unsaturated regoUp compartment, from the groundwater table across the capillary fringe. In agricultural land in Sweden, the upward water flux (groundwater-uptake flow per unit area) from the groundwater table is normally less than 10 mm/d and typically c 1 mm/d during dry periods (Johansson 1973/74). For instance, using water-balance calculations for different types of crops, for an agricultural land in the south-central coastal area of Sweden Johansson and Klingspor (1977) estimated the upward water flux to be 20–90 mm for a growing season during a normal year and 65–115 mm during a dry year.

Moreover, in an experimental study of different types of agricultural soils and depths to the groundwater table, Mueller et al. (2005) found that the upward water flux per growing season was 10–60 mm for spring barley, 20–250 mm for winter wheat, and 80–300 mm for pasture grasses for various soils and groundwater depth levels. Specifically, the results of their study showed that upward fluxes were higher for smaller depths to the groundwater table. Based on the studies by

Johansson and Klingspor (1977) and Mueller et al. (2005) it is suggested that as a long-term annual average, the groundwater uptake in a drained mire with a shallow depth to the groundwater table is set in the range 20–65 mm for barley and 80–300 mm for hay.

6.1.3 Hydrological effects of drainage

General

Drainage has been practised in Sweden for a long time to obtain arable-land areas and improve their productivity, possibly since the 12th century, and drainage operations are legally regulated in Sweden since the 13th century (Gustafsson 1955). Iron-age farmers (here denoted infield-outland farmers) choose fairly dry soils for cultivation and likely did not drain their fields (Gustafsson 1955). More advanced drainage techniques that were introduced during 18th century enabled drainage of peat and heavy clays, and the increased food demand during the 18th to 20th centuries resulted in extensive drainage of wetlands and lakes (Persson 2011). During the last decades, the demand for arable land has decreased. However, the demand may increase in the future, e.g. due to increasing global food demand.

Due to drainage-caused subsidence (see further below) it may be difficult to maintain the function of the drainage system for agricultural land consisting of peat and postglacial deposits. In particular, fens in former lakes are often underlain by thick layers of easily compacted gyttja, which complicates long-term agriculture. Longer-term agriculture may be possible in agricultural land consisting of thin peat layers underlain by clay and sand, as these areas are not as sensitive to compaction.

Drainage depth and subsidence

As mentioned above, many crops and grass species have optimal growths for a groundwater-table depth of 0.5–1 mbgs, and an unsaturated zone in peat (i.e. regoUp) that extends 0.5 mbgs corresponds to a groundwater-table depth of 0.8–0.9 mbgs if the capillary fringe has a vertical extent of 0.3–0.4 m. Due to factors such as seepage-face related inflow resistance to ditches (Gillham 1984, Kao et al. 2001, Chahar and Vadodaria 2008), inflow resistance to drainage pipes (e.g. Kohler et al. 2001) and resulting groundwater-table depths between drains (e.g. Cooke et al. 2001, Ritzema 1994), the drainage must be at a lower level than the desired depth to the groundwater table. In Sweden, open and tile ditches in agricultural land have typically been dug to 1.2–1.5 mbgs (Gustafsson 1955), which likely is sufficient to obtain an unsaturated zone in peat that extends 0.5 mbgs if the drains are closely separated.

Due to drainage-caused subsidence, some time after drainage it will be required to deepen the drainage in order to maintain the desired depth to the groundwater table (e.g. Juhlin-Dannfelt 1923). Peat subsidence following drainage is mainly due to compaction and oxidation. The initial compaction can be as high as 30 mm/y (Kasimir-Klemedtsson et al. 1997), whereas the continued subsidence due to peat oxidation is slower. The total subsidence can hence be 1–1.5 m during a 50-year period, which is the length of the time period during which cultivation of a peat area likely can occur.

Effects on groundwater recharge-discharge and runoff

As described above, the SR-PSU modelling of transport and accumulation of radionuclides in agricultural land (Saetre et al. 2013b) considers downward (percolation) and upward water fluxes (groundwater uptake) in the regoUp compartment, i.e. the biologically active layer above the groundwater table. Moreover, the associated parameterisation takes into account modern-farming drainage of lake-mire systems. However, there are hydrological effects of drainage that are not taken into account in the SR-PSU project. For instance, near-surface drains act as line sinks and constitute line-shaped groundwater discharge areas (e.g. Strack 1989). Hence, groundwater recharge-discharge patterns are changed in the vicinity of drains, which, depending on their depth, locally can collect and diverge also groundwater entering the regolith from below.

Drainage may also affect the total runoff from the agricultural land, the runoff dynamics (e.g. magnitude and longevity of flow peaks) and the distribution of runoff between overland flow and groundwater flow (e.g. Seuna 1981, Bjerketorp and Johnson 1986, Lundin 1994, Beheim 2006, Holden et al. 2006). Initially after drainage, the total runoff is typically increased due to the increased depth to the groundwater table and the associated evapotranspiration reduction. With time, subsidence by compaction and increased decomposition may lead to a decrease of the total runoff. The effects of drainage on runoff dynamics are more complex and depends on factors such as soil hydraulic properties, mire type and drainage intensity (e.g. Holden et al. 2006).

6.2 Future water uses and supplies

6.2.1 Background and objectives

The objective of this section is to provide input to calculations of radiological exposure to a representative individual of the most exposed group, specifically in terms of water uses and supplies associated to self-sufficient communities in the Forsmark landscape. Potential exposure pathways for radionuclides to members of such communities, related to their water uses, include ingestion of contaminated water, ingestion of milk or meat from cattle consuming contaminated water, and ingestion of crops irrigated by contaminated water.

Section 6.2.2 presents estimates of water demands of different types of self-sufficient communities, which in Section 6.2.3 are compared to capacities and hydrochemical characteristics of potential ground- and surface water supplies in the future Forsmark landscape. Moreover, estimated water demands serve as input to hydrogeological analyses related to water discharge (withdrawal) from wells in regolith and rock, respectively (Sections 6.3–6.4).

6.2.2 Water uses of self-sufficient communities

Present and historical water uses

The present-day household water consumption in Sweden is on average c 180 L/d per person, distributed on drinking and food preparation (10 L), WC (35 L), washing-up the dishes (35 L), washing-up clothes (25 L), personal hygiene (65 L) and other uses (10 L) (Svenskt Vatten 2005). This water consumption, which is above the global average (Hoekstra and Chapagain 2007), reflects the fact that the main part of the current Swedish population inhabits urban areas connected to public water works. The household water consumption is less in countries in which the main part of the population inhabits rural areas, with private and/or smaller-scale water supplies. For instance, a typical household water consumption in Sweden was below 10 L/d per person in rural areas during the 19th century, excluding washing of clothes and water consumed by cattle (Hult 2011). Gleick (1996) and WHO (2011) present per capita water consumption as a function of service level (i.e. type of and distance to water supply), including taps in the house (100–200 L/d), tap on yard (50 L/d), access within 1 km round trip (20 L/d) and access more than 1 km round trip (5 L/d). Moreover, survey data on present water uses in Sweden (e.g. Westrell et al. 2006) show that households connected to municipal water supplies consume more water than households using private wells in regolith, and significantly more than households using private wells drilled in rock. In a study of basic water needs for humans, Gleick (1996) recommends a minimum water supply of 50 L/d per person.

Types of self-sufficient communities

In the SR-PSU project, self-sufficient communities are divided into the following four types (cf Saetre et al. 2013a), here presented by increasing level of technological sophistication (see summary in Table 6-1):

- **Hunter-gatherers:** Stone-age cultures from the Mesolithic and middle Neolithic periods serve as a reference for the most exposed group in terms of intake of radiologically contaminated marine or terrestrial natural food. From historical records, it is reasonable to assign a group size of some 30–40 members (40 is used here), who only can use surface water (i.e. water from lakes or streams) to fulfil their water demands. This type of community does not keep any cattle, and it is not involved in agricultural activities that require irrigation water.
- **Infield-outland farmers:** Stationary infield-outland farmers during the Iron Age serve as a reference for the most exposed group in terms of radiological exposure from food cultivated on land, fertilised by contaminated manure (originating from wetland haymaking). Based on estimated future wetland productivity in the Forsmark area and the level of technological sophistication associated to this type of community, it is reasonable to assign a group size of two households (some 10 members), who could use either surface water or groundwater from a well in regolith to fulfil their water demands. This type of community does keep cattle, but their agricultural methods do not involve the use of water for irrigation.

- **Modern farmers:** 19th century farmers serve as a reference for the most exposed group in terms of radiological exposure from food cultivated on a contaminated wetland (dominated by peat and clay gyttja) that is subject to land improvement and drainage. Based on a typical size of a cultivated, drained wetland in the Forsmark area and level of technological sophistication associated to this type of community, it is reasonable to assign a group size of two households (some 10 members), who could use either surface water, water from a well in regolith or water from a well drilled in rock to fulfil their water demands. This type of community does keep cattle, but their agricultural methods do not involve the use of water for irrigation.
- **Garden-plot household:** A present-day, small family household serves as a reference for the most exposed group in terms of radiological exposure from food cultivated on a small garden plot (dominated by glacial clay) irrigated by contaminated water. A group size of 5 members is assigned for this type of community, who could use surface water, water from a well in regolith or water from a well drilled in rock to fulfil their water demands. This type of community which is self-sustained with respect to consumption of vegetables and root-crop, does not keep any cattle but their horticultural methods involve the use of water for irrigation.

Water consumption by humans

Drinking water

In principle, there are two ways to estimate the drinking-water needs for an individual, either based on the needs set by the human physiology (and associated fluid-intake recommendations) or based on statistics on actual fluid intakes. Both demonstrate large variability depending on factors such as climate, activity level and diet, and such factors are reasonable to take into account for the present purposes.

The daily water losses from a human body (urine, insensible losses, faeces and sweat) must be balanced by water gains through direct intake of water or other fluids, water contained in food and water generated by metabolism (oxidation of food). Based on physiological data, ICRP (1975, 2002) presents the daily fluid balance for a "reference man" for the purposes of radiological risk analyses. According to the water balance for an adult male (with a weight of 73 kg), the total daily water losses are 2.9 L/d (the corresponding sum for an adult female is c 2.2 L/d). These losses must then be balanced by direct intake of water or other fluids (2.6 L/d) and metabolism (0.3 L/d). For a reference intake of 0.7 L/d of water contained in food (ICRP 1975), the need of an adult male for direct intake of water or other fluids is hence 1.9 L/d. In SAR-08, Avila and Bergström (2006) assumed daily water losses of 2.95 L/d and that the sum of intake of water contained in food plus water generated by metabolism equals 1 L/d, which hence yields a need for direct intake of water or other fluids of 1.95 L/d.

Gleick (1996) reports results of various physiological studies of human water requirements, suggesting a minimum requirement for fluid replacement of 3 L/d under average temperate conditions. WHO (2011) recommends a direct fluid intake of 2 L/d, as an average for both males/females and for all ages. The recommended minimum fluid intake was 2.9 L/d during NASA's early space flights, and the National Academy of Sciences (1977) recommends a water intake of 2–4.5 L/d depending on energy intake in food. Members of future, self-sufficient communities are likely involved in hard and prolonged physical activities, which, in combination with a potentially warmer climate during part of the assessment period, put their fluid needs above present-day averages. For instance, US Army (2008) recommends a water intake of 6–11 L/d for field personnel active in temperate climates. A direct fluid intake of 2 L/d for adults is recommended by US EPA (2000) to be used in risk analyses related to drinking water in the USA, which is also recommended for corresponding risk analyses in Sweden (Westrell et al. 2006).

Table 6-1. Characteristics and water uses of different types of self-sufficient communities.

Type of community	Group size (no. of individuals)	Water uses		
		Human needs	Cattle	Irrigation
Hunter-gatherers	40	x		
Infield-outland farmers	10	x	x	
Modern farmers	10	x	x	
Garden-plot household	5	x		x

There are few surveys of present-day drinking habits that are relevant for the present purposes and/or for a reference man defined for the purposes of radiological risk analyses. Most such surveys are focused on risks associated to intakes of tap water, whereas a large part of current fluid intakes are fluids other than tap water. Moreover, current average physical activities are likely less hard and less prolonged compared to members of self-sufficient communities, who also are likely to lose more water during work in a warmer climate than today (cf above).

For instance, French survey data presented in Antoine et al. (1986), which is referred to by ICRP (2002) and Avila and Bergström (2006), show an average intake of tap water and other fluids of c 1.3 L/d (0.5 m^3/y). However, the average intake of water contained in food in that study was 1 L/d, which corresponds to an average direct intake of water and other fluids of 1.6 L/d if the reference value of 0.7 L/d (cf above) is used. The total average water intake in the study was 2.7 L/d, which is within the interval for daily water losses for a mixed male/female group according to ICRP (1975, 2002). Moreover, US survey data presented in Ershow and Cantor (1989), also referred to in ICRP (2002) and Avila and Bergström (2006), show an average water intake of 1–1.6 L/d (0.4–0.6 m^3/y), including direct intake of water, water added to other beverages and water added to food during preparation. However, the survey data do not take into account the intake of water contained in food or other fluid intakes (e.g. milk or soft drinks). In fact, in the Ershow and Cantor (1989) study the average tap-water intake (c 1 L/d) was just 55% of the total average water intake, which was 2 L/d (US EPA 2011). In a recent Swedish survey (Westrell et al. 2006), the average water intake was c 1.9 L/d. This average includes tap water and bottled water, but not other fluid intakes (e.g. milk or soft drinks).

Assuming that water is the only source for direct fluid intake, 2 L/d per person (slightly higher than the value used in SR-Site) is used here as one of the inputs to estimate total water demands for different types of self-sufficient communities. This drinking-water need is supported by, for instance, the needs set by the human physiology (e.g. ICRP 1975, 2002) and fluid-intake recommendations in terms of human health (WHO 2011) and for risk-analysis purposes in Sweden and USA (US EPA, 2000, Westrell et al. 2006).

Food preparation, personal hygiene and other human needs

In the present study, the present-day water use for food preparation in Sweden is used (10 L/d per person), meeting typical demands in both developed and undeveloped countries (Gleick 1996). The demand for personal hygiene is set to 10 L/d per person, which is within the recommended interval to meet basic human needs (Gleick 1996) but below the present-day consumption (Svenskt Vatten 2005). Other water uses are set to 10 L/d per person, i.e. equal to the present-day consumption.

Total human water demands

The estimated total human water demands are summarised in Table 6-2. The total human water demand sums up to c 35 L/d per person, which is in between the likely per capita water consumption for the service levels tap on yard (50 L/d) and access within 1 km round-trip (20 L/d) according to WHO (2011).

Water consumption by cattle

For infield-outland farmers, it is assumed that a typical iron-age community with a group size of 10 individuals keeps a mixed herd of livestock of 25 cattle units, consisting of 12 cows, 5 heifers, 5 oxen, 8 pigs and 26 sheep (Widgren 1979, Saetre et al. 2013a). An estimate of the water need for this mixed herd of livestock can be based on the food need (in terms of carbon) for dairy and beef cows. According to Nordén et al. (2010), the food need is equivalent to 7 and 4 kgC/d for dairy and beef cows, respectively, with a corresponding water need of 70 and 40 L/d. With a carbon content of hay of 46% (Löfgren 2010) one then obtains a water need of c 4.5 L/kg hay (dry weight). One cattle unit requires c 5 kg hay/d during winter (Widgren 1979, Saetre et al. 2013a), which yields a water need of c 22.5 L/d for the mixed herd of livestock. The water need per cattle unit is here assumed to be 25 L/d, in order to account for a somewhat larger need during the summer period. The total water need for the mixed herd of livestock kept by a typical iron-age community can then be estimated to 625 L/d.

Table 6-2. Human water demands of self-sufficient communities.

Type of demand	Water demand ($L \cdot p^{-1} d^{-1}$)	Type of community	No. of individuals	Total demand ($L \cdot d^{-1}$)
Drinking	2	Hunter-gatherers	40	80
		Infield-outland f.	10	20
		Mod. farmers	10	20
		Garden-plot hh.	5	10
Food preparation	10	Hunter-gatherers	40	400
		Infield-outland f.	10	100
		Mod. farmers	10	100
		Garden-plot hh.	5	50
Pers. hygiene	10	Hunter-gatherers	40	400
		Infield-outland f.	10	100
		Mod. farmers	10	100
		Garden-plot hh.	5	50
Other (incl. washing of clothes)	10	Hunter-gatherers	40	400
		Infield-outland f.	10	100
		Mod. farmers	10	100
		Garden-plot hh.	5	50
Sum	~35	Hunter-gatherers	40	~1,400
		Infield-outland f.	10	~350
		Mod. farmers	10	~350
		Garden-plot hh.	5	~175

For modern farmers, it is assumed that a typical self-sufficient farm with a group size 10 individuals keeps 8 dairy and/or beef cows and one horse (Saetre et al. 2013a). According to Nordén et al. (2010), the water need of a beef cow is c 40 L/d, whereas the water need for a horse is c 30 L/d (Jordbruksverket 1999). The total water need for the livestock kept by a typical industrial-age agriculture community can then be estimated to 350 L/d.

Water demands for irrigation

According to Table 6-1, it is assumed that the garden-plot horticulture involves the use of irrigation water. In principle, it could be assumed that modern farmers use traditional irrigation techniques (e.g. channel irrigation) as sprinkler irrigation was not used until the beginning of the 20th century (Juhlin-Dannfeldt 1923, Hallgren 1955, Dahlgren 1974, Alinder 1984, 1986, Armstrong 1985). However, potential arable land that could be used by modern farmers in the future Forsmark landscape is found in previous mire areas, i.e. local low-lying areas where there will be no need for irrigation.

Based on the needs to grow potatoes and vegetables for a garden-plot household with a group size of 5 individuals, their garden requires an approximate area of 150 m^2. Based on Johansson and Klingspor (1977), the irrigation need is set to 90 mm during a normal year and 125 mm during a dry year; the latter can also be considered to represent the irrigation need during a warmer climate. This yields c 36 L/d for a normal year and 51 L/d for a dry year. In the estimate of the total water needs for a modern-agriculture community, the water need for irrigation of a small garden plot is set to 40 L/d.

Total water demands

The estimated total water demand for each type of self-sufficient community is summarised in Table 6-3. As can be seen in the table, the total water demand is highest for hunter-gatherers (1,400 L/d per person), which is due to the large size of a typical group (40 individuals). Infield-outland farmers and modern farmers have the same human water needs (350 L/d) for a typical group size of 10 individuals, whereas the total demand is somewhat higher (975 L/d) for the former community type due to the larger number of cattle. In comparison, the water demand for a household with a garden plot is quite small (215 L/d), due to the typically small group size of 5 individuals and modest irrigation-water demands.

Table 6-3. Total water demands ($L \cdot d^{-1}$) of self-sufficient communities.

Type of community	Human needs	Cattle	Irrigation	Total
Hunter-gatherers	1,400	0	0	1,400
Infield-outland farmers	350	625	0	975
Modern farmers	350	350	0	700
Garden-plot household	175	0	40	215

6.2.3 Water supplies in the future Forsmark landscape

Table 6-4 summarises the types of water supplies assumed to be used by different types of self-sufficient communities. As shown in the table, it is assumed that surface-water supplies (lakes and streams) can be used by all types of communities. Regarding groundwater in the regolith, there is historical evidence of pits dug in the vicinity of surface waters or deepening and reinforcing of natural springs during the Neolithic era (10,000–7000 BC), when there was a shift towards farming and relatively stationary settlements (e.g. Andersson 2009, Schyman 2009). The oldest known well in regolith (8100–7500 BC) is located in Israel (Galili et al. 1993). In Europe, there are records from early wells constructed from wood c 5500–5000 BC (Persson and Larsson 2011, Tegel et al. 2012). It is therefore assumed that all types of communities except hunter-gatherer communities have the abilities to dig and utilise pits or wells in regolith.

There are historical records of manual drilling of more than 100 m deep water wells in rock in China during the first centuries AD (Kuhn 2004) and manual rock drilling took place in mines in Sweden from the 17th century (Atlas Copco 2012). The first patented machine-powered rock drill was a steam-powered percussion drill invented by J. J. Couch in Philadelphia (USA) in 1849. This was followed by a large number of patents of rock-drilling machines in USA and Europe during the period 1850–1875, such as S. Ingersoll's compact, steam-powered rock drill in USA in 1871. The technology of drilling water wells in rock was therefore rather mature in the beginning of the 20th century (e.g. Bowman 1911), and the first Swedish rock drill was launched in 1905 (Atlas Copco 2012). It is hence assumed that modern (i.e. industrial-age) farmers and horticulture households have access to drill and utilise wells in rock.

Surface-water supplies

Figure 6-1 shows the locations of future lakes (maximum extents) and streams in the Forsmark landscape (cf Section 3.2.3). The figure also shows MIKE 11 stream sections at which stream-discharge time series are extracted for comparison with typical total water demands (see further below). Based on Figure 6-1 and the locations of delineated biosphere objects (Figure 2-23 in Section 2.3.1), Table 6-5 lists potential surface-water supplies that may be used by self-sufficient communities utilising each biosphere object and/or areas in the vicinity of objects.

Table 6-4. Types of water supplies that could be used by self-sufficient communities.

	Type of water supply		
Type of community	Surface water	Pit/well in regolith	Well drilled in rock
Hunter-gatherers	x		
Infield-outland farmers	x	x	
Modern farmers	x	x	x
Garden-plot household	x	x	x

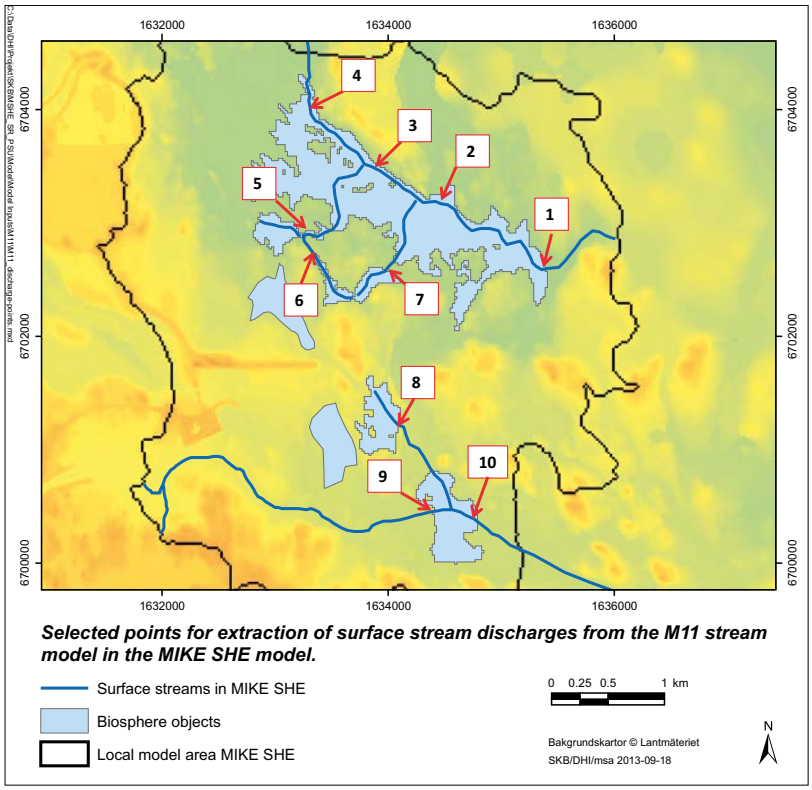

Figure 6-1. *Map of future lakes (maximum extents) and streams, and MIKE 11 stream sections at which stream-discharge times series are extracted for comparison with typical total water demands of self-sufficient communities.*

Table 6-5. Potential surface-water supplies that may be utilised by self-sufficient communities that inhabitate each of the seven delineated biosphere objects.

Biosphere object	Potential lake supplies	Lake life length	Potential stream supplies (stream section in Figure 6-1)
116	Lake 116	4500–9800 AD	Yes (within object, s. 1–4)
121_1	Lake 121_1	3900–6300 AD	Yes (within object, s. 9–10)
121_2	Lake 160	3300–8500 AD	Yes (outlet from Lake 160, s. 8)
157_1	Lake 157_1	4500–5700 AD	Yes (within object, s. 5)
157_2	Lake 157_1/ Lake 159	4500–5700 AD/ 4000–7000 AD	Yes (outlet from Lake 157_1, s. 5) /outlet from Lake 159, s. 6)
159	Lake 159	4000–7000 AD	Yes (within object, s. 6)
160	Lake 160	3300–8500 AD	Yes (within object, s. 8)

According to the description in Section 2.3.1, five of the biosphere objects (116, 121_1, 157_1, 159 and 160) contain lakes, whereas objects 121_2 and 157_2 contain wetlands that are formed after emergence from the sea, without passing a lake stage. Accordingly, communities that inhabit areas in the vicinity of the five lake objects may utilise the associated lakes to satisfy their water demands during the time frames of lake life lengths (Table 6-5). Moreover, communities utilising the wetland objects (121_2 and 157_2) may use surface water from lake objects 121_1, 157_1 and 159, as these lakes are located within manageable distances (say, 400–500 m) from the associated settlements. This distance is supported by archaeological findings (from the period c 500 BC–500 AD) on the west coast of Sweden, which indicates that distances from iron-age settlements to surface-water supplies on average was on the order of 400 m (Schnell 1966, Carlie 2005, Persson and Larsson 2011).

Except for object 121_2, streams are located within manageable distances for inhabitants of all objects. It should be noted that based on the 2000 AD DEM, Brydsten and Strömgren (2013) define a stream from biosphere object 160 to object 121_2 (cf Section 3.2.3), whereas the MIKE 11 stream network defines the stream from object 160 (section 8 in Figure 6-1) to object 121_1. Most present-day streams in Forsmark are small and tend to dry out during dry summer periods (Section 4.4.4). MIKE 11 stream-discharge time series are therefore used to assess the potential of future streams as surface-water supplies, given typical total water demands of self-sufficient communities. Table 6-6 summarises MIKE 11 modelling results for the meteorological normal year (cf Section 2.2.1) at the times 5000 AD and 11,000 AD. Modelling results are shown in terms of annual average (Q_{av}), maximum (Q_{max}) and minimum discharges (Q_{min}). Moreover, the table shows the total time during which the MIKE 11-calculated discharge is below 1 m^3/d, which approximates a typical total water demand.

According to Table 6-3 in Section 6.2.2, the total water demand for a self-sufficient community is estimated to vary between c 1,400 L/d (hunter-gatherers) and c 200 L/d (garden-plot household). As seen in Table 6-6, annual average stream discharges vary between 1 L/s in small streams and 150 L/s in large streams. Hence, annual average stream discharges, both at 5000 AD and 11,000 AD, are sufficient to fulfil water demands for all types of self-sufficient communities. Specifically, annual average stream discharges are approximately one to four orders of magnitude larger than the demands. However, seasonal fluctuations are large and small streams tend to have small discharges (< 1 m^3/d) or be dry during 20–60% of the year.

It is noted that for some streams the average and maximum discharge are higher at 11,000 AD than 5000 AD, whereas there are longer periods with low or no discharge at 11,000 AD (cf Section 5.5). One explanation is that lakes are smaller at 11,000 AD, and therefore within the catchment areas of streams evapotranspiration is less compared to 5000 AD. Moreover, the larger proportion of lakes at 5000 AD acts to lower discharge peaks and maintains longer baseflow periods compared to 11,000 AD. At 11,000 AD, stream discharges demonstrate faster and more pronounced responses to rainfall and snow melt than at 5000 AD. Below is a brief summary regarding surface-water supplies for future inhabitants at each of the seven biosphere objects:

- **Biosphere object 116:** The lake in biosphere object 116 will exist 4500–9800 AD. According to the MIKE 11 analysis (stream sections 1–4 in Figure 6-1 and Table 6-6), at 5000 AD the stream that passes through the biosphere object on average carries c 3 L/s and has low (< 1 m^3/d) or no flow during approximately 10% of the year in its upstream part (MIKE 11 stream section 1). The average flow increases and the length of periods with no or low flow decreases downstream; the annual average flow is more than 50 L/s and there is water flow at all times at MIKE 11 stream section 4. The average stream flow is larger at 11,000 AD, at which time the stream flow is characterised by larger flow peaks but also longer periods with no or low flow. For biosphere object 116, it can hence be concluded that a lake and a stream with sufficient flow will be available as water supplies during the period 4500–9800 AD. After the lake period, water-supply demands will still be fulfilled by utilising the stream, with sufficient flow at least in its downstream parts (cf MIKE 11 stream sections 3 and 4 in Figure 6-1).
- **Biosphere object 121_1:** The lake in biosphere object 121_1 will exist 3900–6300 AD. According to the MIKE 11 analysis (stream sections 9–10 in Figure 6-1 and Table 6-6), at both 5000 and 11,000 AD the flow in the stream that passes through the biosphere object is sufficient to fulfil the demands for all types of communities. For biosphere object 121_1, it can hence be concluded that a lake and a stream with sufficient flow will be available as water supplies during the period 3900–6300 AD. After the lake period, the stream still satisfies the water-supply demands.
- **Biosphere object 121_2:** No lake will be formed in biosphere object 121_2 (Brydsten and Strömgren 2013). As mentioned above, Brydsten and Strömgren (2013) define a stream from biosphere object 160 to object 121_2 based on the 2000 AD DEM, whereas the MIKE 11 stream network defines the stream from object 160 to object 121_1. Inhabitants in the eastern part of the biosphere object may utilise the lake in the neighbouring biosphere object 160 (the lake exists 3300–8500 AD) and/or the stream that passes through that object (see further below).

- **Biosphere object 157_1:** The lake in biosphere object 157_1 will exist 4500–5700 AD. According to the MIKE 11 analysis (stream sections 5 and 6 in Figure 6-1 and Table 6-6), at 5000 AD the stream that enters and passes through the biosphere object on average carries c 1–10 L/s and has low (< 1 m^3/d) or no flow during approximately 10–20% of the year. The average stream flow is larger at 11,000 AD, at which time the stream flow is characterised by larger flow peaks but also longer periods with no or low flow. For biosphere object 157_1, it can hence be concluded that a lake and a stream with sufficient flow will be available as water supplies during the period 4500–5700 AD. After the lake period, water-supply demands may partly be fulfilled by utilizing the stream. However, periods with low or no flow are longer after the lake period.
- **Biosphere object 157_2:** No lake or stream will be formed in biosphere object 157_2 (Brydsten and Strömgren 2013) (see comments below). However, inhabitants may utilise the lakes in the neighbouring biosphere objects 157_1 and 159 (these lakes exist 4500–5700 and 4000–7000 AD, respectively) and/or the stream at the outlet from the lake in object 157_1.
- **Biosphere object 159:** The lake in biosphere object 159 will exist 4000–7000 AD. According to the 5000 AD MIKE 11 analysis (stream sections 6 and 7 in Figure 6-1 and Table 6-6), the stream that passes through the biosphere object on average carries c 1 L/s and has low (< 1 m^3/d) or low flow during approximately 20% of the year. The average stream flow is similar at 11,000 AD, whereas the stream flow at this time is characterised by longer periods with no or low flow. For biosphere object 159, it can hence be concluded that a lake and a stream with sufficient flow will be available as water supplies during the period 4000–7000 AD. After the lake period, water-supply demands may partly be fulfilled by utilising the stream. However, periods with low or no stream flow are longer after the lake period.
- **Biosphere object 160:** The lake in biosphere object 160 will exist 3300–8500 AD. According to the 5000 AD MIKE 11 analysis (stream section 8 in Figure 6-1 and Table 6-6), the stream that passes through the biosphere object on average carries c 1 L/s and has low or no flow (< 1 m^3/d) during approximately 5% of the year. At 11,000 AD, the average stream flow is less and there are longer periods with no or low flow. For biosphere object 160, it can hence be concluded that a lake and a stream with sufficient flow will be available as water supplies during the period 3300–8500 AD. After the lake period, water-supply demands may partly be fulfilled by utilising the stream. However, periods with low or no stream flow are longer after the lake period.

Table 6-6. Summary of annual average (Q_{av}), maximum (Q_{max}) and minimum (Q_{min}) stream discharges at stream sections 1–10 (Figure 6-1) at 5000 and 11,000 AD.

Stream section (biosphere object)	5000 AD (L/s)				11,000 AD (L/s)			
	Q_{av}	Q_{max}	Q_{min}	Q < 1 m^3/d (%)	Q_{av}	Q_{max}	Q_{min}	Q < 1 m^3/d (%)
1 (116)	2.7	32.6	0.0	9.3	4.6	49.0	0.0	24.4
2 (116)	22.8	83.0	0.0	0.3	24.9	216.0	0.0	17.4
3 (116)	27.5	85.4	0.0	0.6	30.5	298.0	0.0	4.54
4 (116)	54.0	153.9	4.4	0.0	55.3	531.0	0.0	0.5
5 (157_1)	9.1	83.0	0.0	11.9	14.0	105.0	0.0	23.6
6 (159)	1.2	10.6	0.0	22.7	1.4	17.0	0.0	43.3
7 (159)	1.4	19.3	0.0	0.1	1.2	15.0	0.0	36.1
8 (160)	1.4	17.1	0.0	4.0	0.7	13.0	0.0	61.4
9 (121_1)	158.7	478.0	36.3	0.0	138.9	745.0	26.0	0.0
10 (121_1)	176.3	695.8	39.3	0.0	148.9	866.0	26.0	0.0

As mentioned above, according to Brydsten and Strömgren (2013) no lakes will be formed in biosphere objects 121_2 and 157_2, and no stream will be formed in object 157_2. Brydsten and Strömgren (2013) identified lakes and streams using the present-day DEM (cf Section 2.2.3), and neither the stream network by Brydsten and Strömgren (2013) nor the MIKE 11 stream network includes a stream between biosphere objects 157_2 and 157_1. In the absence of a stream in the MIKE 11 network, MIKE SHE transfers surface water as overland water, i.e. water above the ground surface. Analysis of the MIKE SHE-calculated overland-water flow in the area between objects 157_2 and 157_1, using the DEM at 5000 and 11,000 AD, respectively, shows that the depth of overland water is shallow in this area. Specifically, the annual average overland-water depth is on the order of 0.05 m, it typically varies between c 0.01 and 0.08 m during the year and the area dries out during dry periods in the summer. The annual average overland-water flow from biosphere object 157_2 to object 157_1 is c 5 L/s, with wet-period peaks of 30–50 L/s.

Hence, the analysis above shows that the overland-water flow in the area between objects 157_2 and 157_1 is on the same order of magnitude as the calculated stream discharges in streams identified by Brydsten and Strömgren (2013), at least during periods of the year (cf Table 6-6). Hence, in terms of water flow it cannot be ruled out that surface water in the area between objects 157_2 and 157_1 may be used as water supply in the future. In the Forsmark area, there are many present analogues to the flow conditions between objects 157_2 and 157_1, i.e. mires and small ponds with no clearly defined stream outlet (cf Section 4.4.4). From a water-supply perspective, diffuse overland-water outflow is generally difficult to collect and not aesthetically appealing. Hence, from practical and water-quality perspectives, it is likely that the area between objects 157_2 and 157_1 will be rejected as water supply. The influence of stream discharge between biosphere objects 157_2 and 157_1 on the water balance of object 157_2 is analysed in Section 7.5.2.

Groundwater supplies in regolith

As described above, it is assumed that pits or wells in regolith can be dug and utilised by all types of self-sustaining communities, except hunter-gatherers. According to Table 6-3 in Section 6.2.2, the total water demand for these self-sufficient communities is estimated to vary between c 1,000 L/d (infield-outland farmers) and c 200 L/d (garden-plot household). In Sweden, pits and wells dug in till have historically been the most common type (Engqvist and Olsson 1974), simply because till is the most widespread type of regolith and also due to the typically shallow groundwater table in terrain dominated by till. Hence, pits and wells in till are analysed in the present study. The maximum well capacity (Q_{max}) for a pit or well in till can be estimated as (e.g. Engqvist and Olsson 1974)

$$Q_{max} = T_{dug\ well} \cdot s_{max}$$

where $T_{dug\ well} = K_h \cdot d_{till}$ is the total transmissivity of a well of depth d_{till} in till, with a horizontal hydraulic conductivity of K_h, and s_{max} is the maximum drawdown of the water level in the well. The average till thickness (d_{till}) in present marine areas outside Forsmark is approximately 6 m (Sohlenius et al. 2013a). Assuming that the upper 1 m of a well in regolith is cased and that the initial groundwater table is located at ground surface (s_{max} = 5 m), $K_h = 7.5 \cdot 10^{-6}$ m/s (Section 2.1.4) yields a total transmissivity $T_{dug\ well} = 3.75 \cdot 10^{-5}$ m^2/s and a maximum well capacity of c $2 \cdot 10^{-4}$ m^3/s. This is equivalent to c 700 L/h (17,000 L/d), which is typical for a well in till in Sweden (Engqvist and Olsson 1974, Engqvist et al. 1978, Pousette et al. 1981). Hence, this calculation example shows that it is possible for future, self-sufficient communities of the considered types and sizes to dig pits or wells in regolith with capacities sufficient for their water demands. A quantitative hydrogeological analysis related to water discharge from pits or wells in regolith is presented in Section 6.3.

Groundwater supplies in rock

As described above, it is assumed that wells in rock can be drilled and utilised by modern farmers and garden-plot households, with a total water demand of c 700 L/d and c 200 L/d, respectively. The maximum well capacity (Q_{max}) for a well drilled in rock can be estimated as

$$Q_{max} = T_{drilled\ well} \cdot s_{max}$$

where $T_{drilled\ well} = K_h \cdot d_{well}$ is the total transmissivity of a well of depth d_{well} in rock, having a horizontal hydraulic conductivity of K_h, and s_{max} is the maximum drawdown of the water level in the well.

A typical depth of a well drilled in rock (d_{well}) can be estimated using data from the SGU Well Archive (© Geological Survey of Sweden, SGU), delivered to SKB in 2011. At time of the delivery, the archive contained data for totally 408,048 private wells in Sweden. A similar analysis, based on a previously delivered data set (c 210,000 wells), was presented by Gentzschein et al. (2007). Wells depths are here analysed for approximately the same area as in the previous study (cf Figure 1-3 of Gentzschein et al. 2007). In the recent data delivery, it is noted that locations of wells may be inaccurate (up to 100 m, in some cases up to 250 m). The boundaries of the analysed area, adjusted to take into account a location inaccuracy of 250 m, are therefore set at 1606944 m (W), 1667152 m (E), 6715726 m (N) and 6658390 m (S) in the coordinate system RT 90 2,5 gon V/0:15. Figure 6-2 presents a plot of cumulative frequency (i.e. the ogive) of well depths (mbgs) for the totally 5,164 wells located within the analysed area.

The average well depth (mbgs) for the data shown in Figure 6-2 is 76 m, whereas the median depth is 64 m. Wells drilled in rock are normally cased across the regolith, which has an average thickness of c 4 m in terrestrial areas (Sohlenius et al. 2013a). Hence, the average and median well depths in rock are some metres less than the well depth from ground surface. Gentzschein et al. (2007) obtained an average well depth in rock of 56 m and a median depth of 51 m (1,945 wells). The larger average and median depths obtained in the present analysis could also be explained by the fact that during recent years, most private wells have been drilled for geo-energy production. Such wells are typically deeper than water-supply wells. Also taking this into account, a reasonable, typical depth in rock for a water-supply well (d_{well}) is here set to 60 m.

Based on hydraulic tests in 64 core boreholes at the SFR facility, the median hydraulic conductivity in the depth interval 0–100 m is estimated to c $1.5 \cdot 10^{-7}$ m/s (SKBdoc 1350092). For d_{well} = 60 m, the total transmissivity $T_{well} = 9 \cdot 10^{-6}$ m^2/s and the maximum well capacity (Q_{max}) is c $5.4 \cdot 10^{-4}$ m^3/s. This is equivalent to c 1,900 L/h (more than 46,000 L/d), which is c 20% of the maximum well capacity estimated for present land areas upstream SFR (Löfgren 2010). It should also be noted that Q_{max} only may be attained using modern, high-capacity pumping equipment, providing large hydraulic gradients (full drawdown in the well) and 3-dimensional groundwater flow towards a well. Estimated water demands are very small compared to Q_{max}, and the natural (undisturbed by well discharge) groundwater flow passing a well drilled in rock is miniscule compared to Q_{max}.

The calculation example above shows that it is possible for future, self-sufficient communities of the considered types and sizes to drill a well in rock with a capacity that is sufficient for their water demands. A hydrogeological analysis related to water discharge from wells drilled in rock is presented in Section 6.4.

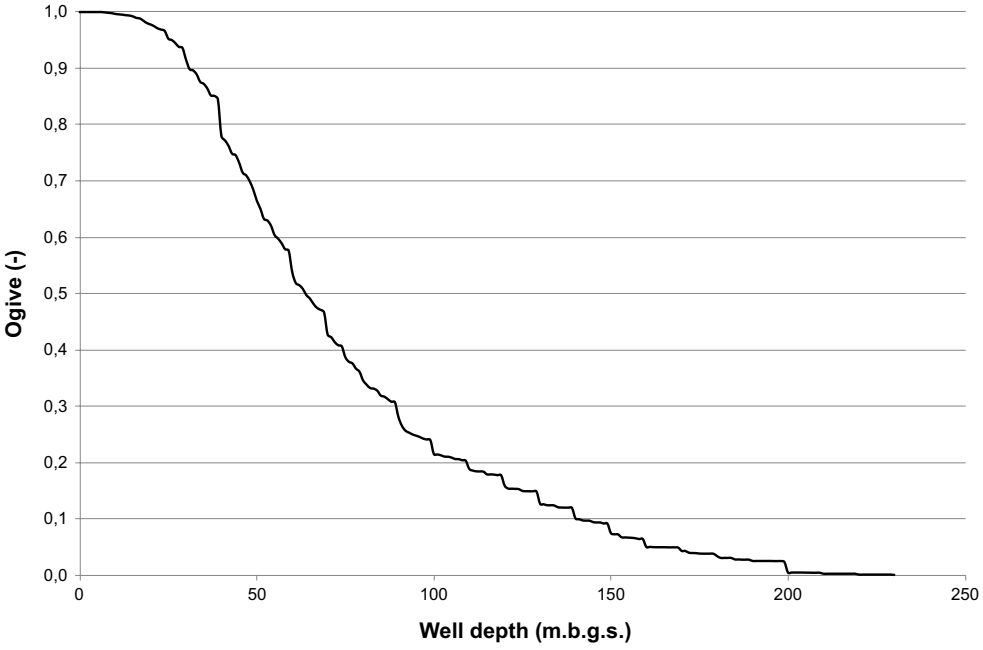

Figure 6-2. *Cumulative frequency (i.e. ogive) plot of well depths (metres below ground surface) for 5,164 wells drilled in rock within an area in northern Uppland.*

Chemical characteristics of future water supplies

Chloride, iron and sulphate are here used to assess whether water from potential supplies in the future Forsmark landscape will appear as potable from a water-quality perspective. There are no health-based guidelines for these chemical parameters (WHO 2011), but they can quite easily be detected in water by their taste and/or smell. Hence, a potential water supply with a high content of chloride, sulphate and/or iron is likely to be considered unsuitable for drinking- or irrigation-water purposes (e.g. Jonsson 1977, Håkansson and Kreuger 1986), even without access to analytical methods. The descriptions below consider local groundwater-chemistry data from Forsmark (Tröjbom et al. 2007, Andersson 2010, Nilsson et al. 2011) and regional data from northern Uppland, delivered to SKB in 2011 from the SGU Well Archive (© Geological Survey of Sweden, SGU).

Chloride gives water a salty taste. The taste threshold depends on the associated cation but is normally in the range 200–300 mg/L (WHO 2003a, 2011). For assessment of public and private water supplies in Sweden, the taste threshold is commonly assumed to be 300 mg/L, which is about 1/10 of the present chloride concentration in the Baltic Sea (c 2,800 mg/L). Figure 6-3 shows the present chloride concentration in groundwater in the Forsmark area, plotted as function of sampling elevation in the rock. There is a quite large spread of the chloride concentration in groundwater sampled in the upper c 100 m of the rock, whereas the chloride concentration is above the taste threshold (300 mg/L) below c –100 m elevation. According to an analysis of the regional groundwater-chemistry data from northern Uppland, there is no clear correlation between the chloride concentration in groundwater in the rock, the well depth and/or the local ground-surface elevation (equivalent to the distance to the sea shoreline), see Appendix 2.

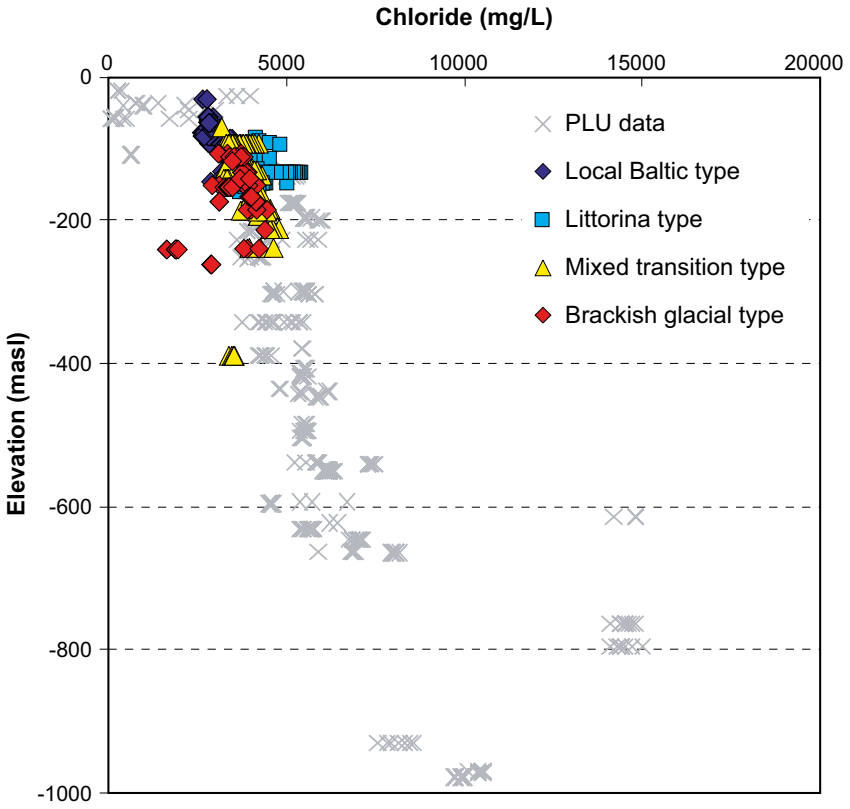

Figure 6-3. *Chloride concentration in groundwater in rock in the Forsmark area, plotted as function of sampling elevation (Nilsson et al. 2011).*

Iron gives water a bad smell and a taste of tinplate. Moreover, it has been found that iron stains laundry if the iron concentration is above 0,3 mg/L, whereas iron concentrations of up to 1–3 mg/L can be acceptable for drinking-water purposes (WHO 2003b, 2011). Figure 6-4 shows the iron concentration in groundwater in the Forsmark area, plotted as function of sampling elevation in the rock. There is a quite large spread of the iron concentration in groundwater sampled in the upper c 100 m of the rock, whereas most iron concentrations above the acceptance threshold (3 mg/L) are found in the approximate elevation interval –100 to –200 m. According to an analysis of the regional groundwater-chemistry data from northern Uppland, there is no clear correlation between the iron concentration in groundwater in the rock, the well depth and/or the local ground-surface elevation (Appendix 2).

Hydrogen sulphide gives water a smell of rotten eggs. The taste threshold depends on the associated cation but is normally in the range 250–1,000 mg/L, and it is commonly assumed that sulphate concentrations above 500 mg/L gives the water a noticeable bad taste (WHO 2004, 2011). Figure 6-5 shows the sulphate concentration in groundwater in the Forsmark area, plotted as function of sampling elevation in the rock. There is a quite large spread of the sulphate concentration in groundwater sampled in the upper c 100 m of the rock, whereas observed sulphate concentrations are above the acceptance threshold (500 mg/L) only in a narrow depth interval around c –100 m elevation. According to an analysis of the regional groundwater-chemistry data from northern Uppland, there is no clear correlation between the sulphate concentration in groundwater in the rock, the well depth and/or the local ground-surface elevation (Appendix 2).

From a water-supply perspective, the chemical characteristics of present groundwater in regolith and surface waters in lakes and streams are useful analogues for the likely characteristics of future ground- and surface waters. At present, groundwater in regolith in Forsmark is characterised by high chloride concentrations (at some locations above the taste limit) in local low-lying areas, whereas groundwater does not have a salty taste in local higher-elevated areas (Tröjbom et al. 2007). Moreover, in local low-lying areas iron and sulphate concentrations are higher than those found in most wells in regolith in Sweden. Concentrations are below the acceptance limit for sulphate, whereas at some locations the iron concentration is above the acceptance limit.

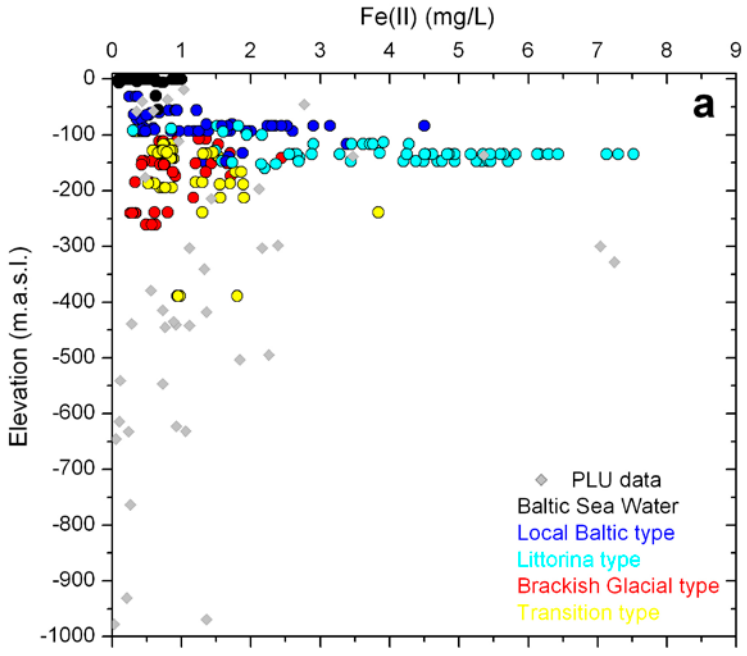

Figure 6-4. *Iron(II) concentration in groundwater in rock in the Forsmark area, plotted as function of sampling elevation (Nilsson et al. 2011).*

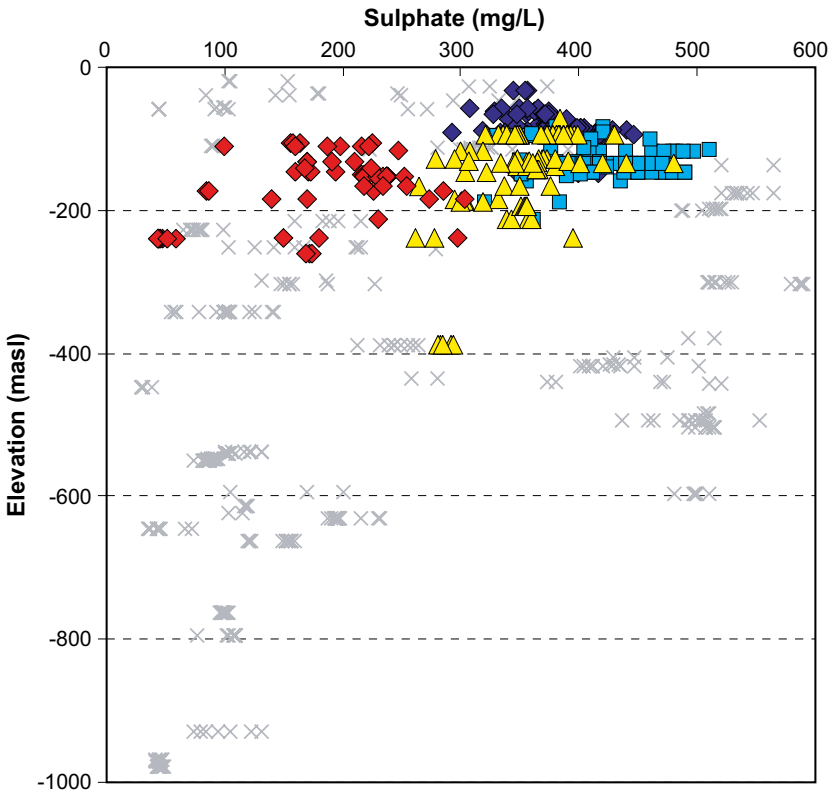

Figure 6-5. *Sulphate concentration in groundwater in rock in the Forsmark area, plotted as function of sampling elevation (Nilsson et al. 2011).*

Present lakes are characterised as oligotrophic hardwater lakes, with high pH, high concentrations of major ions and high electrical conductivity (Andersson 2010). Lake waters have high concentrations of dissolved organic carbon, which in combination with the moderate water colour is unusual. Present streams are also characterised by high pH and moderate water colour (Andersson 2010). The highest chloride concentrations (temporally above the taste limit) have been recorded in the near-coastal lakes Bolundsfjärden, Norra Bassängen, and Fiskarfjärden, due to occasional sea-water intrusion during periods with high sea level (e.g. Johansson 2008). Hence, in the future Forsmark landscape, it is likely that lakes recently separated from the sea may be disregarded as water supplies due to periodically salty taste. Iron concentrations in present lake waters are generally low, whereas iron concentrations in present stream waters are similar to or higher than those of most streams in northern Uppland. However, iron concentrations in both lakes and streams are well below the acceptance limit. Sulphate concentrations in present lake waters are typical for the region, i.e. higher than those of most Swedish lakes (but below the acceptance limit), whereas sulphate concentrations in stream waters are relatively low.

From a water-quality perspective, considering factors such as bad taste and/or smell, no type of potential water supply (groundwater from rock or regolith, surface water from lakes or streams) can be disregarded in an analysis of water uses in the future Forsmark landscape. The exceptions are groundwater from wells drilled at depths larger than typical (deeper than 100 m), which likely will be considered unsuitable due to high concentrations of chloride, iron and sulphur. Moreover, depending on local conditions, some water-supply localities may be disregarded by future, self-sufficient inhabitants, including groundwater from wells in low-lying areas and lakes recently separated from the sea. There are current wells located close to the sea shoreline in Forsmark that are characterized by bad-tasting water (Werner et al. 2010). Data from the SGV well Archive (© Geological Survey of Sweden, SGV) on 1,200 wells in the coastal area around Forsmark and on the Gräsö Island (Figure 6-6) show that 95% of the wells are located in areas where the ground surface elevation is at least 2.5 m above sea level.

6.3 Analysis of wells in regolith

6.3.1 Radionuclide concentration in a well in regolith

This section presents a methodology to utilise the framework of calculating radionuclide release (Bq/y) from rock to till at biosphere objects (SKB 2014e), specifically for calculation of the radionuclide concentration in wells in regolith. As illustrated in Figure 6-6, the capture zone (or strictly, capture volume) for a well is defined as the volume of regolith and rock that contributes to the well discharge (Q_{well}), whereas the influence area is the area in which the hydraulic head is influenced by well discharge. Hence, by definition, at steady-state conditions the sum of groundwater recharge (to the groundwater table) and groundwater discharge (from below) to the capture zone equals Q_{well}.

The starting point for the analysis is a case with only groundwater discharge to RegoLow, which is the till layer above rock according to the terminology for compartment modelling of radionuclide transport in the biosphere (Saetre et al. 2013b). For this case (see illustration in Figure 6-6)

$$Q_{well}/Q_{RegoLow,\ bo} \approx (Bq/y)_{cz}/(Bq/y)_{RegoLow,\ bo}$$

where bo denotes biosphere object and cz is the capture zone in RegoLow. According to this expression the ratio between the well discharge Q_{well}, which is equal to the groundwater discharge within the capture zone, and the total groundwater discharge to RegoLow within the biosphere object ($Q_{RegoLow,\ bo}$, which is assumed to be unaffected by the well discharge) is approximately equal to the ratio between the radionuclide release from the rock to RegoLow within the capture zone ($(Bq/y)_{qz}$) and the radionuclide release to RegoLow within the biosphere object ($(Bq/y)_{RegoLow,\ bo}$). It should be noted that Q_{well} is assumed to be equal to the groundwater discharge within the capture zone. Hence, in case of recharge of uncontaminated groundwater to the groundwater table, Q_{well} overestimates the size of the capture zone and it thereby also proportionally overestimates the radionuclide release from the rock to RegoLow within the capture zone.

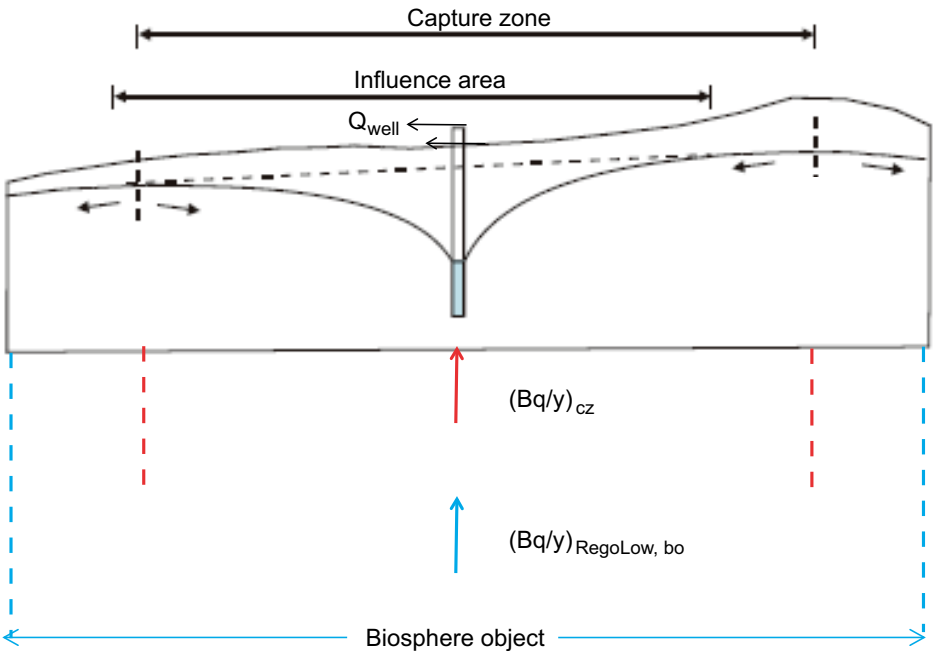

Figure 6-6. *Illustration of the concepts capture zone, influence area, and radionuclide releases to RegoLow within a biosphere object, $(Bq/y)_{RegoLow,\ bo}$, and within the capture zone, $(Bq/y)_{cz}$.*

The radionuclide concentration in RegoLow, within the boundaries of the biosphere object, can be written as $C_{RegoLow,\ bo} = (Bq/y)_{RegoLow,\ bo}/Q_{RegoLow,\ bo}$, and the radionuclide concentration in RegoLow within the capture zone can be written as $C_{cz} = (Bq/y)_{cz}/Q_{well}$. From these expressions, we have

$$(Bq/y)_{cz} \sim (Q_{well}/Q_{RegoLow,\ bo})\cdot(Bq/y)_{RegoLow,\ bo.}$$

If this expression is inserted into the expression for C_{cz} given above, we obtain

$$C_{cz} = \{(Q_{well}/Q_{RegoLow,\ bo})\cdot(Bq/y)_{RegoLow,\ bo}\}/Q_{well},$$

which can be simplified to

$$C_{cz} = (Bq/y)_{RegoLow,\ bo}/Q_{RegoLow,\ bo}$$

Hence, given the framework of calculating radionuclide release (Bq/y) from rock to till at biosphere objects (SKB 2014e), the radionuclide concentration in RegoLow within the boundaries of the biosphere object (except for the capture zone), is approximately equal to the concentration within the capture zone and the concentration in the well, i.e. $C_{RegoLow,\ bo} \approx C_{cz} \approx C_{well}$.

This concept can readily be extended to also account for radionuclide release to RegoLow in the form of recharge of contaminated water to the groundwater table. For such a case, the radionuclide concentration in RegoLow, within the boundaries of the biosphere object (except for the capture zone) is

$$C_{RegoLow,\ bo} = \{(Bq/y)_{RegoLow,\ recharge} + (Bq/y)_{RegoLow,\ discharge}\}/Q_{RegoLow,\ bo}$$

where $Q_{RegoLow,\ bo}$ is the sum of groundwater discharge from below and groundwater recharge to the groundwater table. The radionuclide concentration within the capture zone is then

$$C_{cz} = \{(Bq/y)_{cz\ (recharge)} + (Bq/y)_{cz\ (discharge)}\}/Q_{cz}$$

where $Q_{cz} = Q_{well}$ is the sum of groundwater discharge and groundwater recharge within the capture zone.

Since $\{(Bq/y)_{RegoLow,\ bo\ (recharge)} + (Bq/y)_{RegoLow,\ bo\ (discharge)}/\{(Bq/y)_{cz\ (recharge)} + (Bq/y)_{cz\ (discharge)}\}$ is approximately equal to $Q_{cz}/Q_{RegoLow,\ bo}$, also in this case we obtain the approximate relationships $C_{RegoLow,\ bo} \approx C_{cz} \approx C_{well}$.

The above expressions are valid for well-mixed conditions in RegoLow only, i.e. the assumption made in Saetre et al. (2013b). Specifically, it is assumed that there are no temporal or spatial variability of groundwater discharge and/or recharge (uncontaminated or contaminated) to RegoLow, neither within the boundaries of the biosphere object nor within the capture zone. In reality, groundwater discharge and recharge vary in both space and time, which implies that also the radionuclide concentration in RegoLow will vary.

The concepts described above indicate that the radionuclide concentration in a well in regolith depends on its location and the size of its capture zone in relation to locations and sizes of contaminated areas in RegoLow. The following sections quantify typical capture-zone sizes for discharges from wells in till at various locations, which can be related to sizes of contaminated areas in RegoLow.

6.3.2 Capture-zone calculations

As mentioned above, the capture zone for a well is defined as the volume of regolith and rock that contributes to the well discharge. A number of wells in till were implemented in the MIKE SHE local model setup for the meteorological normal year, at the time 5000 AD. The wells were represented as sinks with specified discharge in till, down to the rock surface. This mimics wells with intake screens across the whole till layer, whereas there also are well constructions with water intakes only at the well bottom (e.g. Agerstrand 1968). The discharge rate in each well was set to 975 L/d, which is equal the total water demand for an infield-outland agricultural community (Section 6.2.2). Totally nine wells were implemented, one in each biosphere object, except for the largest objects (116 and 121_1) in which two wells were implemented per object. The wells were located to areas with a till thickness of 3–4 m (4–5 m for one of the wells in biosphere object 121_1) according to the regolith depth and stratigraphy model (Brydsten and Strömgren 2013).

There is historical evidence that early wells were dug in the vicinity of surface waters (in some cases as deepenings and/or reinforcements of natural springs), whereas current-day wells typically are located to solid ground as a result of digging-technology improvements. In the present MIKE SHE model setup, in each biosphere object wells were located midway between the outer boundaries of biosphere objects and the closest surface water, defined as areas with a overland-water depth exceeding 0.1 m at all times during the simulated period (see example in Figure 6-7). Due to the long distances between wells, there were no inter-well interferences and all well discharges could be simulated in a single model setup.

Capture zones were identified using particle tracking. Specifically, particles were released continuously in all model cells representing the regolith for a simulation period of two years, using data on sea level, precipitation, potential evapotranspiration and near-surface air temperature for the period September, 2004–September, 2006. All released particles were tracked in a transient groundwater-flow field produced by cycling the two-year period 10 times, corresponding to a total simulation period of 20 years. The capture zone for each well was thereby identified as the release cells for particles that during the total simulated period reached MIKE SHE model cells representing the well.

As illustrated in Figure 6-8, for the assigned discharge rate (975 L/d) the influence areas of the hydraulic head-drawdown in till are rather small. The capture zones in regolith are even smaller in size, and they are also influenced by the local topography. Capture zones in regolith are therefore more irregular in shape than influence areas. In Figure 6-8, it can also be noted that the capture zones for most wells are not continuous. Specifically, many starting positions for particles reaching a well are separated from the others, which are located closer to the well. Such particles are released in the regolith far from the well and follow groundwater flow paths in the rock until they enter the capture zone in the regolith closer to the well. This implies that only the continuous particle-release positions in the vicinity of each well are of interest. The reason is that these particles illustrate the capture zone within the biosphere object, where radionuclide fluxes from the rock to RegoLow may enter the well (cf discussion above).

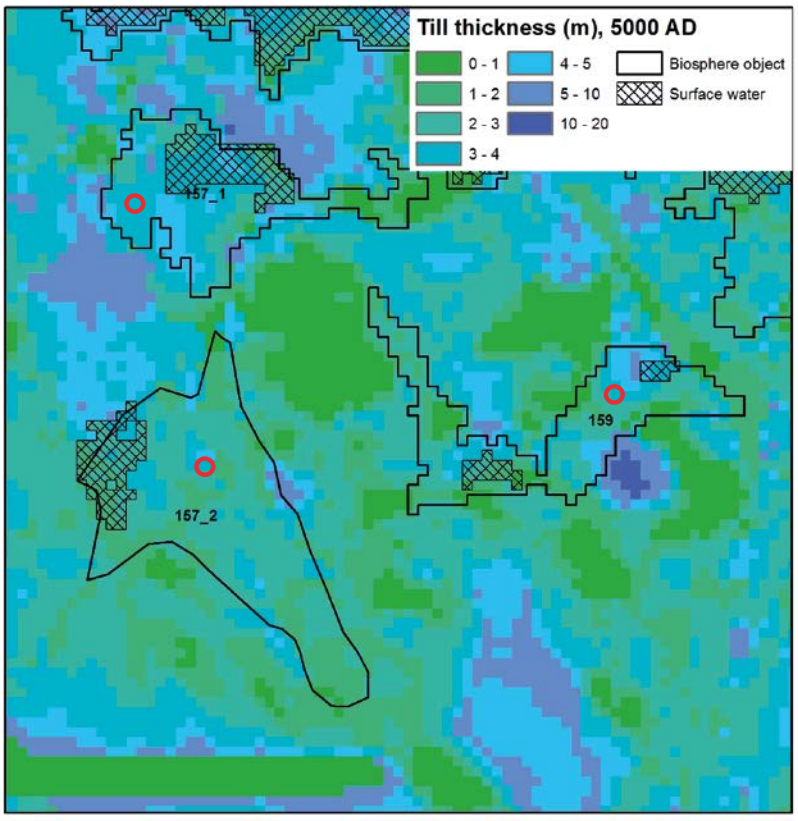

Figure 6-7. *Locations of three of the totally nine wells in till (red circles) implemented in the MIKE SHE model set at 5000 AD (biosphere objects 157_1, 157_2 and 159).*

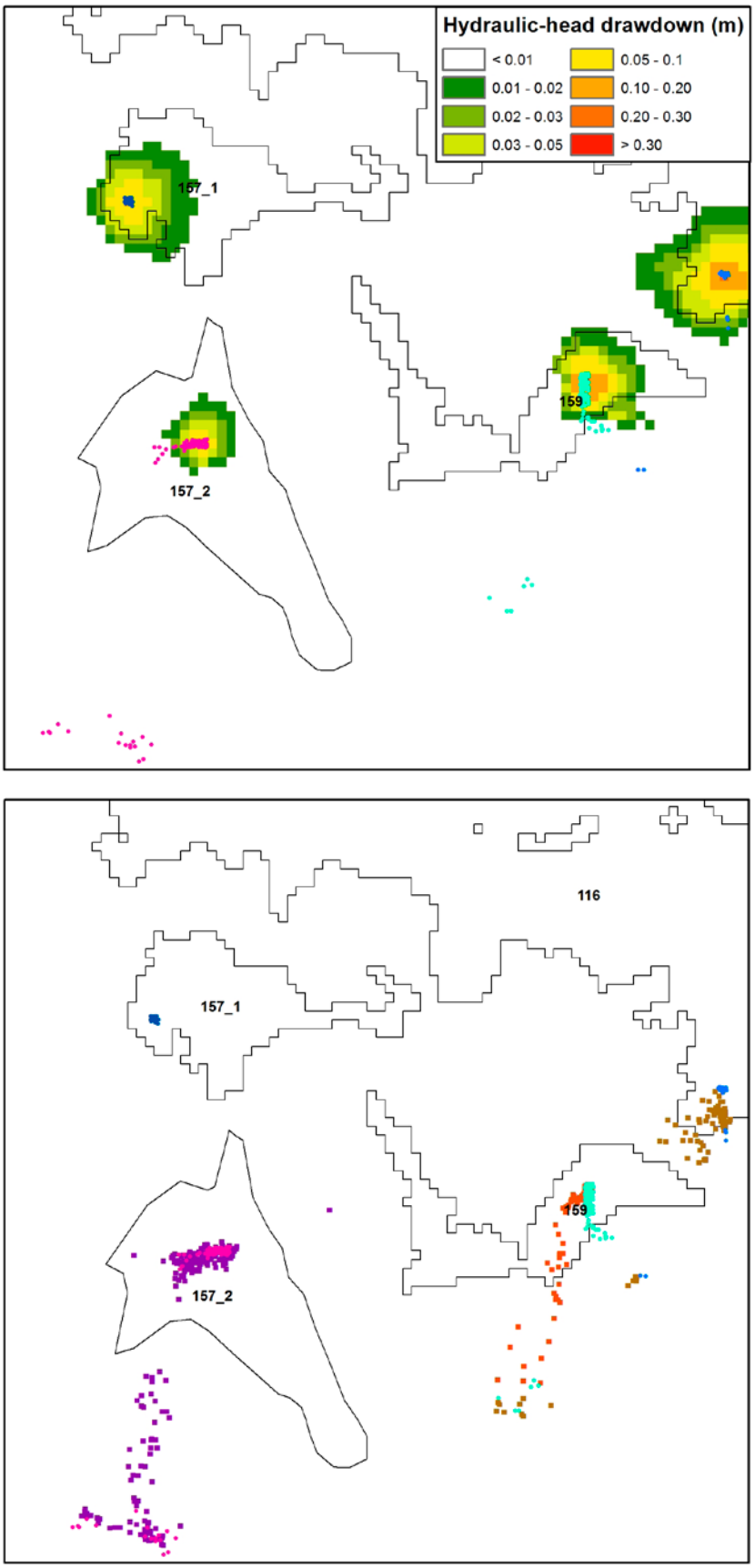

Figure 6-8. *Upper figure: MIKE SHE-calculated average hydraulic-head drawdown in till (RegoLow) and release cells in regolith (wells in biosphere objects 116, 157_1, 157_2 and 159). Lower figure: Corresponding release cells in both regolith and rock. The coloured dots represent release cells located in regolith or in rock, associated to the well in each biosphere object.*

Table 6-7 summarises the results in terms of influence areas (average hydraulic-head drawdown > 0.1 m) and capture zones in the regolith. As mentioned previously, only the continuous particle-release positions in the vicinity of each well are of interest. Using the well in biosphere object 157_2 as an example, its capture zone of 4,000 m^2, excluding separated starting positions located far from the well, is c 2% of the area of the biosphere object (167,600 m^2). The well discharge 356 m^3/y (975 L/d) is in fact 2% of the groundwater discharge from rock to RegoLow within the biosphere object (16,900 m^3/y; cf water balances in Chapter 7). Hence, the ratio between the capture zone and the object area is approximately equal to the ratio between the well discharge and the total groundwater discharge from the rock within the biosphere object. This illustrates that the previously presented underlying assumptions for calculating radionuclide concentrations in wells in regolith are appropriate. Moreover, the capture zone is c 8% of the area within the biosphere object with highest discharge-location density (47,200 m^2).

These modelling results show that for likely water needs of future, self-sufficient communities, capture zones for wells in till are smaller in size than the biosphere objects. Specifically, for biosphere object 157_2 the capture zone is also smaller than the potentially most contaminated area of RegoLow, which implies that for a realistic well discharge, a well in till cannot capture the whole contamination plume in RegoLow. Depending on the location of a well in regolith and its associated capture zone, the capture zone may only interfere with a certain part of the plume, and the water discharged from the well will be diluted with uncontaminated water from areas outside of the plume or the biosphere object (cf Figure 6-8).

6.4 Analysis of wells drilled in rock

6.4.1 Radionuclide concentration in a well drilled in rock

In the same manner as for wells in regolith (Section 6.3), this section presents a methodology to utilise the framework of calculating radionuclide release (Bq/y) from rock to till at biosphere objects (SKB 2014e), specifically for calculation of the radionuclide concentration in a well drilled in rock. It should be noted that the present analysis is focused on water-supply wells, i.e. not deep-rock drilling for exploration of geothermal energy, oil or ores (e.g. SKB 1999). The discharge from a water-supply well influences the groundwater flow field in the rock, and it may hence influence groundwater flow paths between the SFR facility and biosphere objects depending on its location, depth and the well discharge.

Table 6-7. Sizes of MIKE SHE-calculated influence areas (average hydraulic-head drawdown in till > 0.01 m) and captures zones in regolith.

Well in biosphere object	Influence area (m^2)	Capture zone (m^2)		
		Regolith	Regolith (continuous area in object)	Rock
116-a	53,200	7,600	800	81,600
116-b	66,000	2,000	1,600	15,200
121_1-a	36,400	400	400	4,400
121_1-b	45,200	400	400	2,800
121_2	10,000	12,000	8,400	18,400
157_1	44,000	400	400	0
157_2	18,400	9,600	4,000	30,400
159	33,200	5,600	4,400	11,600
160	16,800	1,600	1,600	0

In principle, the radionuclide release to a well drilled in rock can be calculated using models and parameters that describe groundwater flow and transport in the geosphere (SKB 2014e). Related to long-term safety of repositories for radioactive waste, the influence of discharge from drilled wells on groundwater flow paths have previously been investigated by Thunvik (1983), Axelsson et al. (1991), Holmén and Stigsson (2001a, b) and Kattilakoski and Suolanen (2000). Specifically, the study by Thunvik (1983) was focused on the effects on groundwater flow through a deep-rock repository, whereas Axelsson et al. (1991), Holmén and Stigsson (2001a, b) and Kattilakoski and Suolanen (2000) used a similar methodology as the one presented here to investigate effects on groundwater flow paths. Axelsson et al. (1991) and Holmén and Stigsson (2001b) assigned well discharges in their modelling, whereas Kattilakoski and Suolanen (2000) represented wells in the rock as model cells with atmospheric pressure, thereby producing well discharges equal to maximum well capacities.

Radionuclide releases to wells drilled in the rock in the vicinity of biosphere objects are here estimated in a simplified manner, using calculated radionuclide releases to biosphere objects without well discharge, $(Bq/y)_{bo}$. Specifically, the radionuclide release to drilled in rock a well, $(Bq/y)_{well}$, can be estimated as (see illustration in Figure 6-9)

$$(Bq/y)_{well} = \{(bo_{no\ well} - bo_{well})/bo_{no\ well}\} \cdot (Bq/y)_{bo}$$

in which $bo_{no\ well}$ denotes the number of groundwater flow paths in rock reaching the upper rock surface that are associated to a biosphere object without well discharge, and bo_{well} is the corresponding number in a case with well discharge. Hence, $bo_{no\ well} - bo_{well}$ is the number of groundwater flow paths reaching the well that is associated to the biosphere object without well discharge.

The radionuclide concentration in the well can then simply be calculated as

$$C_{well} = (Bq/y)_{well}/Q_{well}$$

which states that the mixing volume is equal to the well discharge, Q_{well} (cf Axelsson et al. 1991).

6.4.2 Well locations

Prior to modern geophysical methods, such as the VLF method developed during the 20th century, suitable locations to drill wells in rock were normally selected based on the practical experiences of farmers and drillers (e.g. Bowman 1911). As stated in Section 6.2.3, it is assumed that wells may be drilled in rock by modern farmers or a garden-plot community, with total water demands according to Section 6.2.2 (700 and c 200 L/d, respectively). In order to analyse the hydraulic influence of and radionuclide transport from the SFR facility to such wells, wells are here assigned in potential settlement areas in the vicinity of future arable land areas. These areas are identified on a landscape scale, based on historical information on typical locations of agricultural settlements during the 19th century and onwards. For instance, an analysis of well locations based on data from a previous delivery from the SGU Well Archive (© Geological Survey of Sweden, SGU) as part of the Östhammar pre study (SKB 2000), shows that almost all wells drilled in rock are located to solid ground (i.e. not immediately at shorelines or in peat areas) and that 80–90% of the wells are located within 100–200 m from arable land. In order to enable well drilling and to avoid sea-water intrusion, it can be assumed that the drilling area needs to be located at least 1 m above sea level (Werner et al. 2013).

As illustrated in Figure 6-10, future arable land are identified as areas with organic soils exceeding 1 m in depth, or areas with glacial-clay depths exceeding 0.3 m at 9500 AD according to the description in Brydsten and Strömgren (2013). Based on the criteria above, potential agricultural settlements and associated drilled wells are preferentially placed to shortcut groundwater flow paths from SFR to discharge locations at the interface between regolith and rock. Figure 6-10 shows the resulting 11 potential settlements, visualised as circles with a radius of 100 m within which settlements and associated drilled wells may be located in the future.

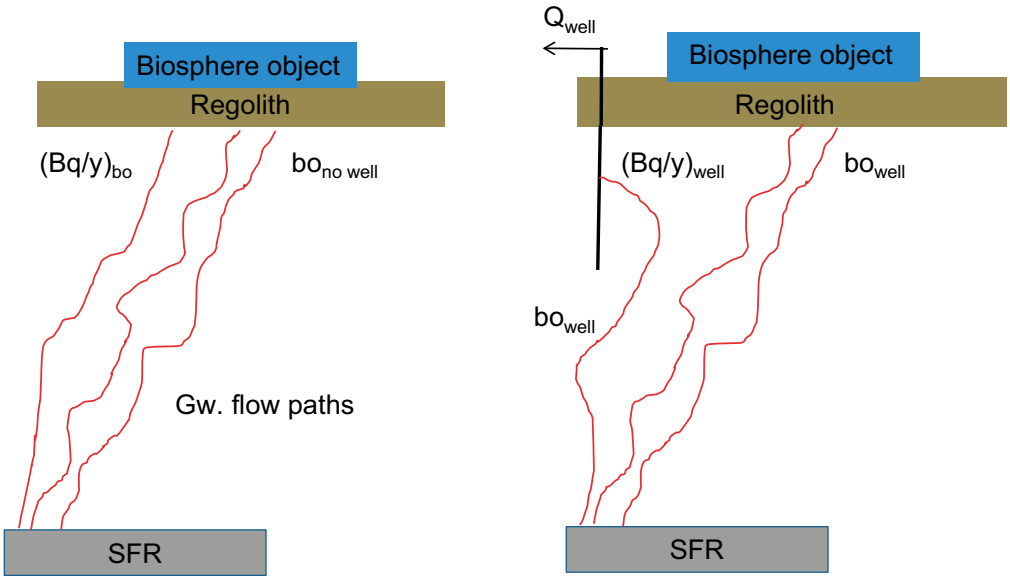

Figure 6-9. *Illustration of the proposed methodology for calculation of radionuclide release to wells drilled in rock, $(Bq/y)_{well}$, based on radionuclide releases to biosphere objects without well discharge, $(Bq/y)_{bo}$. $bo_{no\ well}$ denotes the number of groundwater flow paths in rock reaching the upper rock surface at a biosphere object without well discharge, and bo_{well} is the corresponding number in a case with well discharge.*

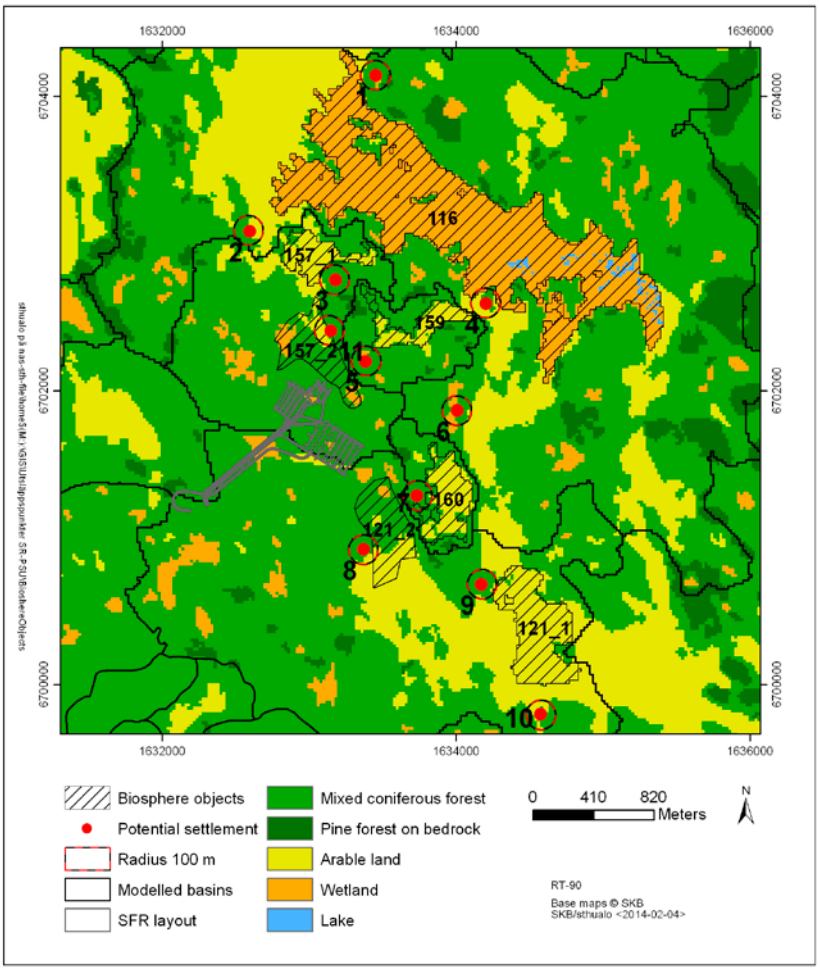

Figure 6-10. *Potential settlement areas (enumerated 1–11) in the vicinity of future arable land (yellow). For orientation, the map also shows basin boundaries, delineated biosphere objects and the footprint of the SFR facility.*

6.4.3 Setup of flow modelling and particle tracking

DarcyTools is a modelling tool specifically developed to analyse groundwater flow and transport in fractured rock. Wells drilled in rock within the circles shown in Figure 6-10 were therefore implemented in the DarcyTools base case model setup (HydroDFN case R85 and HCD base case) for 5000 AD (Öhman and Vistrand 2014). The flow modelling tool DarcyTools is described in Svensson et al. (2010) and the underlying flow-model setup is described in Odén et al. (2014).

According to the analyses in Section 6.2.3, a typical depth in rock for a water-supply well (d_{well}) can be set to 60 m. Moreover, the median hydraulic conductivity in the depth interval 0–100 m yields a maximum well capacity (Q_{max}) of c 46,000 L/d, i.e. much above the estimated total water demands of a self-sufficient community. A present-day well drilled in rock typically has a diameter of 0.115 or 0.140 m, corresponding to a well volume of 600–900 L for a 60 m deep well. Hence, for a well discharge of 700 L/d the water volume in the well is replaced approximately once per day. However, the maximum well capacity demonstrates large spatial variations depending on the hydrogeological properties of the rock at relevant depths. The total transmissivity (T) and the required drawdown (s) for Q_{well} = 700 L/d were therefore calculated for wells located at circle centres of Figure 6-10 using the hydrogeological rock parameterisation of the DarcyTools setup, see Table 6-8. Specifically, the total transmissivity T of each well was calculated as

$$T \approx \sum_{n} bK_{h,max}$$

where b = vertical extent and $K_{h,max}$ = maximum horizontal cell-wall conductivity of the n^{th} intersected DarcyTools model cell (each DarcyTools model cell has four side walls). Since wells drilled in rock typically are cased across the regolith (see further below), only K_h of the rock is included in the calculation of T. Moreover, the required drawdown s to produce the well discharge Q_{well} is calculated by

$$s \approx Q_{well}/T$$

where s refers to "rock drawdown" (s_{rock}), i.e. drawdown along the column of DarcyTools model cells intersected by the well (see discussion below). This relationship between s, T and Q_{well} is only an approximation (e.g. Bradbury and Rotschild 1985, Razack and Huntley 1991, Huntley et al. 1992, Meier et al. 1999) but it is considered as sufficient for the present purposes. The second column of Table 6-8 shows the total transmissivity T, from the interface between rock and regolith down to a depth of 60 m in the rock. The model setup takes into account that wells drilled in rock typically are cased across the regolith, and according to present standards c 4 m in rock. Specifically, current well-drilling regulations in Sweden (SGU 2008) require that wells are sealed at least 2 m into good rock and at least 6 m below the ground surface. The third and fourth columns of Table 6-8 show assigned well-casing lengths in rock and associated total transmissivities T ("w. casing"), from the casing bottom down to 60 m in the rock (the well bottom is extended downwards so that the effective well length is kept at 60 m). Note that the casing bottom is assigned at the first intersected DarcyTools cell wall after a minimum of 4 m well length in rock. The resulting casing lengths therefore vary, due to local variations of the vertical DarcyTools cell discretisation. The last column of Table 6-8 shows well discharge (Q_{well}) for s_{rock} = 10 m, i.e. 10 m drawdown along the column of DarcyTools model cells intersected by the well (calculated from the relationship $s \approx Q_{well}/T$).

The required rock drawdown (s_{rock}) to produce a well discharge of 700 L/d varies locally and should not exceed 60 m (i.e. maximum possible drawdown). s_{rock} is small for most wells but large at wells 1, 6 and 10, for which Q_{well} is below 700 L/d for s_{rock} = 10 m. The drawdown in an actual well drilled in rock (typically with a diameter of 0.140 m, cf above) is larger than s_{rock}, i.e. the calculated drawdown along the column of model cells representing the well (e.g. Andersson and Woessner 1992). This implies that a discretised groundwater-flow model must have very fine cell discretization in the vicinity of the well to give a proper representation of the drawdown in and immediately around the well. However, the present calculations are focused on larger-scale groundwater flow and transport, and not on the drawdown in or in the immediate vicinity of wells. The relationship between the drawdown (s_{well}) in a well with radius r_{well} and the drawdown along model-cell columns (s_{rock}) is

$$s_{well} = s_{rock} - \frac{Q}{2\pi T} \ln\left(\frac{r_e}{r_{well}}\right)$$

Table 6-8. Data on wells located at circle centres of Figure 6-10. T = transmissivity (m^2/s), K = hydraulic conductivity (m/s), b = vertical well extent, s_{rock} = "rock drawdown", and Q_{well} = well discharge (L/d).

Well	T = K·b (no casing)	Casing (m)	T = K·b (w. casing)	Est. Q_{well} (s_{rock} = 10 m)
1	$7.55 \cdot 10^{-6}$	4	$1.57 \cdot 10^{-8}$	13.6
2	$2.41 \cdot 10^{-4}$	5	$2.33 \cdot 10^{-4}$	201,226
3	$8.08 \cdot 10^{-5}$	4	$7.32 \cdot 10^{-5}$	63,262
4	$2.78 \cdot 10^{-5}$	7	$2.03 \cdot 10^{-5}$	17,556
5	$7.97 \cdot 10^{-6}$	4.5	$7.90 \cdot 10^{-6}$	6,827
6	$7.50 \cdot 10^{-6}$	5	$1.74 \cdot 10^{-9}$	1,5
7	$1.76 \cdot 10^{-5}$	4.5	$1.74 \cdot 10^{-5}$	14,990
8	$1.28 \cdot 10^{-5}$	5	$1.18 \cdot 10^{-5}$	10,187
9	$7.42 \cdot 10^{-5}$	4	$7.36 \cdot 10^{-5}$	63,564
10	$2.45 \cdot 10^{-7}$	4	$2.17 \cdot 10^{-7}$	187.7
11	$3.27 \cdot 10^{-5}$	5	$2.73 \cdot 10^{-5}$	23,622

Table 6-9. Simulated well discharge (Q_{sim}) for each well.

Well	Simulated Q_{well} (L/d)
1	102.6
2	699.9
3	700.0
4	700.0
5	700.0
6	152.1
7	700.0
8	715.4
9	700.0
10	690.9
11	700.0

where $r_e = 0.208a$ (Andersson and Woessner 1992). In the expression for r_e, $a = \Delta x = \Delta y$ is the side length of adjacent model cells. In the present case, DarcyTools model-cell side lengths adjacent to well locations are 8 or 16 m, which implies that the ratio between s_{rock} and s_{well} is c 0.6–0.7, for a well diameter of 0.140 m.

In order to find a proper DarcyTools modelling sequence (cf below) and also to test well capacities using DarcyTools, a test simulation was performed with all 11 wells active (Öhman and Vidstrand 2014). In each well, the well discharge (Q_{well} = 700 L/d) was assigned in the model cell having maximum horizontal hydraulic conductivity (the "pumped cell"), whereas all model cells representing the well were assigned a high vertical hydraulic conductivity ($K_v = 10^{-4}$ m/s). The upper and lower ends of each well (casing bottom and well bottom) were assigned a small vertical hydraulic conductivity ($K_v = 3 \cdot 10^{-11}$ m/s). The groundwater flow field was solved at steady state with fixed hydraulic heads in surface cells, obtained from the corresponding steady-state solution without wells (cf Odén et al. 2014). As shown in Table 6-9, the simulated well discharge (Q_{sim}) is lower than Q_{well} (700 L/d) for wells 1, 6 and 10 with small estimated well discharge (s_{rock} = 10 m) in Table 6-8.

The above results call for some slight relocations, within the circles in Figure 6-10, of some wells to areas with smaller required drawdown s (equivalent to higher maximum well capacity). These relocations were done using maps of s_{rock} (for Q_{well} = 700 L/d) covering areas c 200 by 200 m around each well position (see example in Figure 6-11). In the relocation process, some wells located to areas with sufficient well capacity were slightly relocated to areas with even larger potential to shortcut groundwater flow paths from SFR. Table 6-11 shows initial well coordinates and data on the relocated wells (relocated well coordinates, well-casing lengths in rock, total transmissivities T ("w. casing"), and estimated well discharge (Q_{well}) for s_{rock} = 10 m. Comparison between initial (Table 6-8) and relocated well locations (Table 6-10) shows that total transmissivities and well capacities are higher at the relocated positions, including wells 1, 6 and 10.

Table 6-10. Data on relocated wells. T = transmissivity (m^2/s), K = hydraulic conductivity (m/s), b = vertical well extent, s_{rock} = "rock drawdown", and Q_{well} = well discharge (L/d).

Well	Initial location		Relocated location		Casing (m)	T = K·b (w. casing)	Est. Q_{well} (s_{rock} = 10 m)
	Easting (RT 90)	Northing (RT 90)	Easting (RT 90)	Northing (RT 90)			
1	1633455	6704141	1633480	6704167	6	$1.27 \cdot 10^{-4}$	109,814
2	1632597	6703081	Not relocated		5	$2.33 \cdot 10^{-4}$	201,226
3	1633182	6702751	1633215	6702740	4	$1.65 \cdot 10^{-4}$	142,387
4	1634204	6702592	1634260	6702567	4	$9.62 \cdot 10^{-5}$	83,151
5	1633386	6702198	1633357	6702170	5.5	$8.81 \cdot 10^{-6}$	7,612
6	1634009	6701862	1633964	6701886	4.5	$9.78 \cdot 10^{-6}$	8,452
7	1633736	6701284	1633706	6701291	4.5	$4.49 \cdot 10^{-5}$	38,750
8	1633373	6700918	1633410	6700994	5	$8.44 \cdot 10^{-5}$	72,904
9	1634174	6700681	1634204	6700665	4	$9.65 \cdot 10^{-5}$	83,341
10	1634574	6699798	1634539	6699824	4	$2.47 \cdot 10^{-4}$	213,235
11	1633149	6702405	1633141	6702412	4.5	$2.87 \cdot 10^{-5}$	24,831

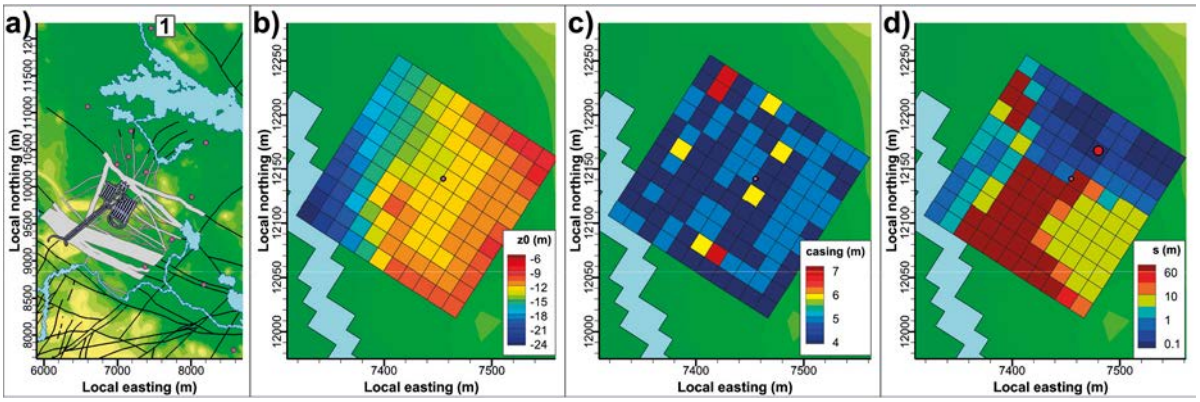

Figure 6-11. *Example of well relocation using maps of required s_{rock} (well 1). The initial well location is shown in a), well-bottom elevations (60 m well length in rock) are shown in b), casing lengths (minimum 4 in rock) are shown in c). Required s_{rock} and initial (small dot) and relocated well locations (large red dot) are shown in d).*

As mentioned previously, one objective of the test simulation was to investigate the impacts of different modelling sequences. Specifically, a steady-state simulation for temperate conditions in DarcyTools involves a recharge phase and a steady-state phase (Odén et al. 2014). The objective of the recharge phase is to obtain hydraulic heads in surface cells as upper boundary conditions for the steady-state phase, which aims to produce a high-precision groundwater-flow solution. When two recharge-phase solutions were compared, one without wells and one with all 11 wells active, there were some unanticipated results in the form of groundwater-table drawdown in areas far from wells. This is likely due to limitations of the recharge algorithm. It was therefore determined to base the well simulations on hydraulic heads in surface cells obtained from the recharge-phase calculations without wells, but to re-solve hydraulic heads by the recharge algorithm inside circles with radii of 700 m, centred at each well.

In the present case (cf above), the radionuclide concentration in a well drilled in rock can be calculated based on the number of groundwater flow paths from SFR that reach the well, the number of flow paths that are associated to a biosphere object and the radionuclide release to the biosphere object, $(Bq/y)_{bo}$, after passage of the geosphere for a case without wells. The flow paths needed to calculate radionuclide releases to wells and biosphere objects are quantified using particle-tracking techniques. Using the groundwater flow field for each well case, such techniques were therefore used to quantify groundwater flow paths between individual disposal rooms in SFR and each well. Specifically, the following particle-tracking simulations were performed for each well:

- Release of totally 10^6 particles within SFR 1 disposal rooms (1BTF, 2BTF, 1BLA, 1BMA and Silo, proportionally to facility volume) and forward tracking of particles.
- Release of totally 10^6 particles within SFR 3 disposal rooms (2BLA, 3BLA, 4BLA, 5BLA, 2BMA and 1BRT, proportionally to facility volume) and forward tracking of particles.

It can be noted that backward particle tracking, in which particles are released within the well and tracked backwards, can be used to calculate dilution effects in a well in terms of water volumes. Specifically, if b/B of the released particles that are tracked backwards originate at a certain storage facility, b/B of the water volume entering the well (Q_{well}) has passed the storage facility, whereas 1 – b/B of Q_{well} has not. On the other hand, if f/F of the released particles that are tracked forwards from a certain storage facility reaches the well, f/F of $Q_{facility}$ (the total groundwater flow that leaves the storage facility) contributes to Q_{well}. The relation between b/B and f/F is $b/B \sim q \cdot (f/F)$, where $q = Q_{facility}/Q_{well}$. In the present cases, $Q_{facility} < Q_{well}$ (the total groundwater flow that leaves the facility is less than the well discharge), and b/B is then always less than f/F. For each of the well cases, this relationship was checked by release of totally 10^6 particles within the well (within the "pumped cell") and backward tracking of particles. It was found that the number of particles leaving each storage facility at a certain location is proportional to the groundwater flow leaving the facility at that location, which implies that the relationship between b/B and f/F is linear and proportional to q as stated above.

6.4.4 Results of flow modelling and particle tracking

The simulations show that the simulated well discharges have negligible or no effects on groundwater flow through the waste-storage facility parts of SFR. Moreover, water balances of each well show that the inflow to the well equals the well discharge for almost all wells, which verifies that the well discharge is a proper representation of the mixing volume. The exceptions are wells 2 and 8–10, which are located to and surrounded by large areas with high maximum well capacities. This is particularly the case for well 2, in which the well discharge is c 37% of the inflow to the column of model cells representing the well. Depending on flow paths from SFR to such a well, it is possible that no flow paths enter the "pumped cell".

The results of the forward particle tracking are shown in Table A3-1 in Appendix 3 in terms of particle-capture ratios, i.e. the ratio between the number of captured particles at the "pumped cell" in each well and the number of particles released from each facility part of SFR 1 and SFR 3. As can be seen in the table, particles released at SFR 1 and SFR 3 are only captured in few of the wells and particle-capture ratios are small. Specifically, particles released at SFR 1 are captured in one of the wells (well 11) with a particle-capture ratio between 0.001% (2BTF) and 0.009% (Silo). Particles released at SFR 3 are captured in three wells (wells 3, 5, 11), with particle-capture ratios between 0.001% (from 3BLA to well 5) and 0.17% (from 3BLA to well 11).

6.4.5 Wells drilled in the well interaction area downstream of SFR

The previous analyses concern well locations associated to settlements in the vicinity of future arable land areas, i.e. wells that may be drilled and used by agricultural, self-sufficient communities (modern farmers and garden-plot households). It is considered to be less probable for water-supply wells to be drilled at other locations, not associated to arable land areas. However, it cannot be ruled out that future drilling of water-supply wells may occur also at other locations than those analysed above, i.e. at locations that are decoupled from any foreseeable land use by a self-sufficient community. The analysis presented below aims to delineate an interaction area for wells drilled at random locations downstream of SFR, i.e. the size of the area (or rather, volume) in which wells drilled in the rock may have the highest concentrations of radionuclides originating from SFR.

It can be assumed that rock drilling is feasible some period after the considered area has emerged from the sea. Specifically, it can be assumed that the drilling area needs to be located at least 1 m above sea level to enable drilling and to avoid sea-water intrusion (cf section of Well locations above). Already some hundreds of years after repository closure (e.g. SKB 2006), knowledge about the SFR repository may be lost.

The well interaction area was delineated using results of particle tracking for undisturbed conditions, i.e. groundwater-flow conditions without well discharge, for the DarcyTools base case model setup (HydroDFN case R85 and HCD base case) for 5000 AD (cf Odén et al. 2014). Specifically, particle trajectories associated to particle releases from individual SFR 1 and SFR 3 facility parts were extracted in piecewise 10-m elevation intervals from –80 to –10 m elevation in the rock, i.e. within the approximate total elevation interval relevant for drilled wells in the area downstream of SFR. Hence, the delineation of the well interaction area takes into account groundwater flow paths at relevant elevations in the rock, and it is not limited to discharge locations at the interface between rock and regolith (cf Section 2.3.1). Subsequently, trajectories for all elevation intervals and all particle releases were accumulated to visualise the extent of the contamination plume within the considered total elevation interval. Specifically, the well interaction area was delineated as the area (volume) of rock with high density of trajectories. Particle trajectories and the delineated well interaction area, with a size of 0.26 km^2, are shown in Figure 6-12.

The probability for a well to be located at random within the well interaction area can be calculated as its size (km^2) times the well density (number of wells per km^2). According to the regional analysis of well density (both wells in regolith and wells in rock) presented in Section 4.2, the current well density varies between c 0.2 and 2 wells per km^2 depending on size and location of the analysed area. The current well density is 0.2–0.9 wells per km^2 in different sub-areas within an area close to SFR (size 400 km^2) and 0.5–2 wells per km^2 in different sub-areas within northern Uppland (size 3,300 km^2). The well density is c 0.5 wells per km^2 in areas that emerged from the sea c 1,000 years ago, i.e. corresponding to approximately 4000 AD in the SR-PSU case. There is a peak (c 0.9 wells per km^2) for areas the emerged from the sea c 1,800 years ago (approximately 5000 AD in the SR-PSU case). Moreover, the well density is below 0.5 wells per km^2 in areas that emerged from the sea more than 2,000 years ago (i.e. beyond 5000 AD in the SR-PSU case).

The well density in a certain area depends on a number of factors other than the time since shoreline passage. For the present analysis, an average well density of 0.5 wells per km^2 is recommended for calculations of the probability for a well to be drilled at random within a given area. The well interaction area (Figure 6-12) has a size of 0.26 km^2, which for a well density of 0.5 wells per km^2 corresponds to a probability of 0.13 for a well to be drilled in rock at random within this area. In comparison, the delineated well interaction area for SFR 1 and SFR 3 is slightly larger than the corresponding area for SFR 1 (c 0.2 km^2) delineated by Holmén et al. (2001).

As mentioned above, the underlying analysis (Kautsky 2001) concerns data regarding both wells in regolith and wells in rock. The analysis is based on a previous delivery from the SGU Well Archive (© Geological Survey of Sweden, SGU) as part of the Östhammar pre study (SKB 2000). This delivery contains all reported wells that are constructed up to a specific point in time, but there is no information regarding abandoned wells. Hence, 0.5 wells per km^2 is likely an overestimation of the density of wells drilled in rock that are in actual use at a specific point in time.

It should be noted that within the relevant elevation interval (from –80 to –10 m elevation), the contamination plume (and in principle also the associated well interaction area) differs in size depending on the time for radionuclide release from SFR (cf discharge locations in Section 2.3.1). However, the well interaction area is delineated based on areas with high trajectory densities, which are relatively independent on the release time. The delineated well interaction area, which is based on analysis of trajectories at the intermediate time 5000 AD, is therefore relevant also for other times after the well interaction area emerges from the sea. However, since it is not considered feasible to drill water-supply wells in submerged areas, for times prior to emergence the actual (emerged) well interaction area equals the emerged part of the delineated well interaction area at a certain time.

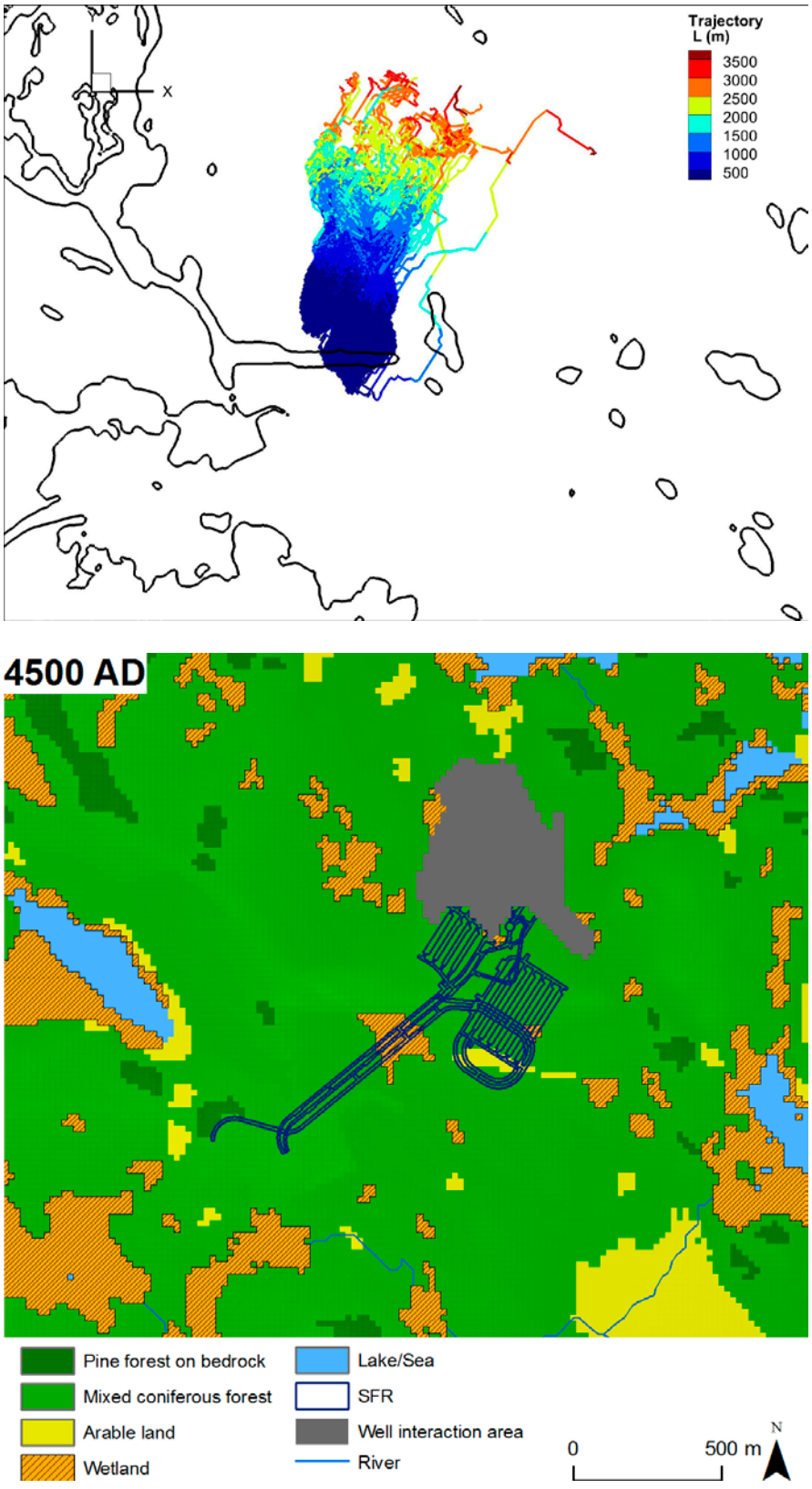

Figure 6-12. *Particle trajectories (upper figure) and delineated well interaction area on the 4500 AD landscape map (lower figure).*

No part of the well interaction area is yet emerged at 2500 AD. The emerged part is very small at 3000 AD (0.03 km^2) and also at 3500 AD (0.1 km^2). The emerged part increases to 0.2 km^2 at 4000 AD, and the whole well interaction area is emerged at 4500 AD. As mentioned previously, it can be assumed that the drilling area needs to be located at least 1 m above sea level to enable drilling and to avoid sea-water intrusion. The parts of the well interaction area that are 1 m or more above sea level at the corresponding times as above are obviously less than the emerged part (0.02 km^2 at 3000 AD, 0.06 km^2 at 3500 AD and 0.15 km^2 at 4000 AD). At 4500 AD, the whole emerged part of the well interaction area is at least 1 m above sea level.

Particle-capture ratios associated to discharges from wells drilled in rock within the well interaction area were analysed using the same DarcyTools model setup as described above, i.e. the base case model setup (HydroDFN case R85 and HCD base case) for 5000 AD, using a well discharge of Q_{well} = 700 L/d and the same methodology as for wells 1–11 (cf above), including 60 m deep wells cased across regolith and at least 4 m in rock. The locations of wells are based on the analysis of particle trajectories associated to particle releases from individual SFR 1 and SFR 3 facility parts (cf Tables A3-2 and A3-3 in Appendix 3). Specifically, wells are located to areas with high trajectory densities within the analysed elevation interval (–80 to –10 m elevation), i.e. those locations where well discharge likely results in high particle-capture ratios. As shown in Figure 6-13, totally 9 wells were analysed, located immediately downstream of SFR 3 (well 21), close to the Silo of SFR 1 (wells 22 and 27), and in fracture zones north (wells 23–26 and 29) and immediately northwest of SFR 1 (well 28). Table 6-11 shows data on wells 21–29 in terms of well coordinates, well-casing lengths in rock, total transmissivities T ("w. casing"), and estimated well discharge (Q_{well}) for s_{rock} = 10 m (cf Tables 6-8 and 6-10). As shown in the table, total transmissivities and well capacities are rather high at the locations of wells 21–29. The results of the particle-tracking calculations are summarised in Tables A3-2 (SFR 1) and A3-3 (SFR 3) in Appendix 3.

According to Tables A3-2 and A3-3 in Appendix 3, there are large particle-capture differences between facility part/well combinations. Hence, the facility-specific particle capture for an individual well depends on its location in relation to the extent of the associated contamination plume. For most wells capturing particles released from SFR 1 and SFR 3, the particle-capture ratio is on the order of 1–10%, whereas the largest particle captures are noted for well 29 (31.80% from 2BTF in SFR 1) and well 25 (13.04% from 1BRT in SFR 3).

However, from the tables in Appendix 3 it is noted that the average particle-capture ratio is rather constant among SFR facility parts (c 2–8% of the released particles). For all wells capturing particles released from SFR 1, the average particle-capture ratio per facility part is 5.61% (the average ratio per well is 6.75%), whereas the corresponding ratio for SFR 3 is 3.56% (the average ratio per well is 3.43%). Therefore, as an upper boundary for the safety assessment, a generic well drilled in rock at random within the contamination plume (well interaction area) downstream of SFR can be assumed to capture 10% of radionuclides released from any SFR facility part. This is obviously a conservative assumption, since only four of the tested wells in the plume capture particles from all SFR 1 repository parts (23, 25, 26 and 29), whereas six wells capture particles from all SFR 3 repository parts (22, 23, 25–27 and 29). Only three of the tested wells (23, 25 and 29) capture particles from all facility parts.

6.4.6 Influence of well discharge

According to the concepts described above, the radionuclide concentration in a well drilled in the rock is given by $C_{well} = (Bq/y)_{well}/Q_{well}$. Hence, the influence of well discharge on the radionuclide concentration in the well can be investigated by analysing the response on the particle-capture ratio for different Q_{well}. In the analyses above a well discharge (Q_{well}) of 700 L/d was used, resulting in a largest particle-capture ratio of 31.80% for well 29 (2BTF in SFR 1). In order to investigate the influence of Q_{well} on the particle-capture ratio for well 29, a set of simulations were performed using the following well discharges:

- Q_{well} = 1,000 L/d, which approximately corresponds to the present-day water demand for 5 individuals.
- Q_{well} = 1,400 L/d, i.e. twice the initially assigned well discharge (700 L/d).
- Q_{well} = 2,800 L/d, i.e. four times the initially assigned well discharge (700 L/d).

Table 6-11. Data on wells 21–29 (Figure 6-13). T = transmissivity (m^2/s), K = hydraulic conductivity (m/s), b = vertical well extent, srock = "rock drawdown", and Qwell = well discharge (L/d).

Well	Easting (RT 90)	Northing (RT 90)	Casing (m)	T = K·b (w. casing)	Est. Q_{well} (s_{rock} = 10 m).
21	1633292	6701935	4	$1.78 \cdot 10^{-4}$	153,619
22	1633206	6702055	4.5	$1.96 \cdot 10^{-4}$	169,690
23	1633124	6702315	5.5	$1.06 \cdot 10^{-5}$	9,167
24	1632838	6702210	5.5	$5.70 \cdot 10^{-5}$	49,239
25	1632892	6702382	4	$4.64 \cdot 10^{-5}$	40,090
26	1632971	6702480	4	$2.08 \cdot 10^{-5}$	18,006
27	1633171	6702140	4	$6.79 \cdot 10^{-6}$	5,863
28	1632771	6702058	4.5	$6.36 \cdot 10^{-5}$	54,985
29	1632971	6702264	5.5	$3.53 \cdot 10^{-5}$	30,491

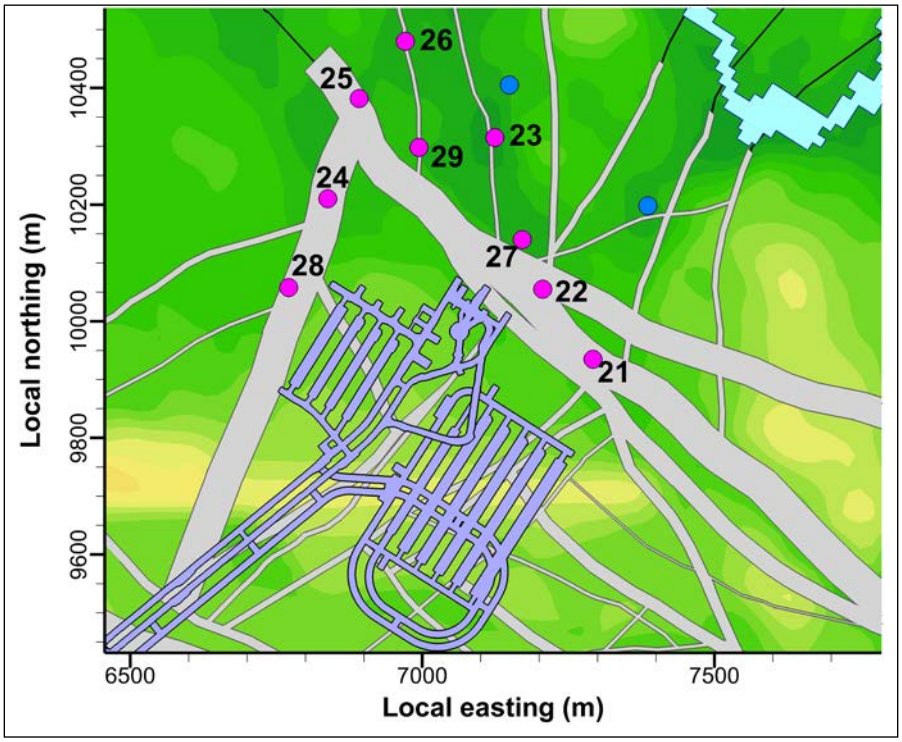

Figure 6-13. *Locations of analysed well locations (lilac dots, wells 21–29) in areas downstream of SFR 1 and SFR 3.*

The analysis was done using the same model setup as above. i.e. the DarcyTools base case model setup (HydroDFN case R85 and HCD base case) for 5000 AD. According to Öhman and Vidstrand (2014) there are negligible effects of Q_{well} on groundwater flow through SFR waste-storage facilities. As seen in Table A3-4 in Appendix 3, there is a clear response of increasing Q_{well} from well 29, in the form of increasing capture of particles released at all SFR facility parts. Table A3-5 in Appendix 3 compares well-discharge and particle-capture ratios, i.e. the ratios between tested Q_{well} values and the initial Q_{well} value (700 L/d), and corresponding particle-capture ratios. There is a linear relationship between Q_{well} and the particle-capture ratio for most SFR facility parts. Hence, the radionuclide concentration in well 29 (C_{well}) is not sensitive to Q_{well}, due to the underlying linear relationship between C_{well}, the radionuclide release to the well $((Bq/y)_{well})$ and the well discharge. Hence, an increase of the well discharge leads to an increase of the particle capture, proportional to the well-discharge increase, and the concentration in the well is therefore not affected.

6.4.7 Probability for an intrusion well

The areas above SFR 1 and SFR 3 will not be suitable for agricultural purposes, and, as mentioned previously, it is considered to be less probable for water-supply wells to be drilled at locations that are not associated to arable land areas. As for wells drilled in the contamination plume downstream of SFR (cf above), it cannot be ruled out that future drilling of water-supply wells may occur in areas above SFR 1 and SFR 3, i.e. at locations decoupled from any foreseeable land use by a self-sufficient community.

As was also mentioned previously, to enable drilling and to avoid sea-water intrusion, it can be assumed that rock drilling is feasible some period after the considered area has emerged from the sea. In the global warming and early periglacial climate cases (see SKB 2014b), the duration for a complete transformation to terrestrial conditions above SFR 1 and SFR 3 is c 1,000 years after closure. In addition, the drilling area needs to be located at least 1 m above sea level, which takes another 160 years after complete transformation. Different parts of the SFR facility will raise above sea level at different times. For simplicity, it is assumed that wells can be drilled above SFR 1 and SFR 3 at 3000 AD in the global warming and early periglacial climate cases. In the extended global warming climate case, due to an initial sea-level rise it is assumed that wells can not be drilled above SFR 1 or SFR 3 until at least 2,360 years after closure.

The probability for a well to be drilled into SFR can be calculated as the size of the well interaction area (km^2), which in this case can be set equal to the footprint area of SFR, times the well density (number of wells per km^2). As mentioned previously, an average well density of 0.5 wells per km^2 seems appropriate for calculations of the probability for a well to be drilled at random within a given area. The probability for an intrusion well must also take the well depth into account. Specifically, the waste-storage facilities in SFR 1 have their roofs at c –70 m elevation, whereas the roofs of the SFR 3 waste-storage facilities will be at c –120 m elevation. According to the DEM (Strömgren and Brydsten 2013), the elevation of the sea bottom above SFR 1 and SFR 3 is c –3 to –4 m. Hence, a well drilled in rock above SFR 1 or SFR 3 would intrude the facility at a depth of approximately 66 or 116 mbgs, respectively. According to the cumulative frequency plot of well depths in northern Uppland (Figure 6-2), the median depth is 64 mbgs (50% of the wells are deeper), whereas less than 20% of existing wells are deeper than 116 mbgs.

6.5 Recommendations for handling of future water uses in the SR-PSU project

In terms of water uses (humans, cattle and irrigation) of future, self-sufficient communities in the Forsmark landscape, the following approaches are recommended for identification of a representative of the most exposed group and for calculation of associated radiological exposure:

- **Hunter-gatherers:** The most exposed group uses water from the most contaminated surface-water supply (lake or stream), see Sections 6.2.2 and 6.2.3.
- **Infield-outland farmers:** The most exposed group uses the most contaminated water from a surface-water supply (lake or stream) or a well in regolith, see Sections 6.2.2–6.2.3 and 6.3.
- **Modern farmers:** The most exposed group uses the most contaminated water from a surface-water supply (lake or stream), a well in regolith or a well drilled in rock, see Sections 6.2.2–6.2.3 and 6.3–6.4.
- **Garden-plot household:** The most exposed group uses the most contaminated water from a surface-water supply (lake or stream), a well in regolith or a well drilled in rock, see Sections 6.2.2–6.2.3 and 6.3–6.4.

As mentioned in Section 6.2.3, even though the future stream network does not include a stream between biosphere objects 157_2 and 157_1, it cannot be ruled out that surface water in the area between these two objects may be used as water supply in the future. For agricultural communities that may use wells in regolith, it is recommended to calculate the radiological exposure using the maximum concentration in RegoLow in biosphere objects (Section 6.3). Moreover, for agricultural communities associated to larger areas of arable land, who may use wells drilled in

rock (Section 6.4), it is recommended to use a well discharge of 700 L/d and the maximum particle-capture ratio, among all studied wells (Figure 6-10), for each SFR facility part. The analysis may also use a safety factor (say, 2) to account for different types of uncertainties related to the maximum particle-capture ratio.

As described in Section 6.4, wells drilled in the contamination plume downstream of SFR and intrusion wells are considered to be less probable. In the former case, it is recommended to use the time-dependent part of the delineated well interaction area and the well density to estimate the time-dependent probability for a water-supply well to be drilled within the well interaction area. In order to calculate the radiological exposure from a well drilled within the well interaction area, it is recommended to use a conservative particle-capture ratio (10%) for any SFR repository part. As for wells drilled in the contamination plume downstream of SFR, it cannot be ruled out that future drilling of water-supply wells may occur in areas above SFR 1 and SFR 3. In this case, the well interaction area can be set equal to the footprint area of SFR, and the probability for an intrusion should also take into account well-depths statistics (Figure 6-2) versus the levels of waste-storage facilities in SFR 1 and SFR 3.

For a well drilled in the contamination plume and for an intrusion well, it is recommended to use a well discharge (Q_{well}) of 700 L/d in radiological-exposure calculations. This is equal to the water demand for a group of modern farmers and approximately midway between the water demand for a rural garden-plot household (c 200 L/d) and the present-day water use of 5 individuals (900 L/d) connected to public water works.

7 Hydrological descriptions and parameterisations of biosphere objects

7.1 Introduction and background

As described in Section 2.3.1, seven biosphere objects are identified based on discharge locations at the interface between rock and regolith, calculated using forward particle tracking in DarcyTools. This chapter describes MIKE SHE local-model outputs in terms of water-balance components for biosphere objects at the years 3000, 5000 and 11,000 AD, delivered to the radionuclide transport modelling (Saetre et al. 2013b).

Section 7.1 presents a background for the deliveries and Section 7.2 provides a description of the methodology for deriving water-balance components. The subsequent sections present and discuss some main modelling results for the normal year (Section 7.3) and for other climate cases (Section 7.4). Section 7.5 presents results of sensitivity analyses using biosphere object 157_2 as a case study, in terms of governing climate conditions and alternative sub-area delineations of the object. Finally, Section 7.6 gives an overview of the process of transforming water-balance components to radionuclide-transport modelling parameters.

At present, all seven biosphere objects (cf Figure 2-23) are submerged by the sea. Shoreline displacement, caused by isostatic rebound, is modelled by a continuous change of the state of submodels representing biosphere objects, from submerged to emerged conditions for wetlands or lakes (Brydsten and Strömgren 2013). Hence, the characteristics and properties of a particular biosphere object will change with time as a result of landscape development. In five of the biosphere objects (116, 121_1, 157_1, 159 and 160) a lake is formed subsequent to the isolation from the sea. At the end of the submerged period, for these objects the terrestrial period is initiated at the point in time when the associated lake threshold is at average sea level (top left and right in Figure 7-1). For these objects, the terrestrial period can be divided into an initial transition stage and a subsequent mature stage. The initial stage is associated with expanding wetland areas in a lake-mire complex, whereas at the mature stage the lake is gone and the wetland has reached its full extent. Subsequent to emergence, no lake is formed in objects 121_2 and 157_2 (bottom left and right in Figure 7-1) and the submerged period is terminated when the objects are fully emerged above average sea level.

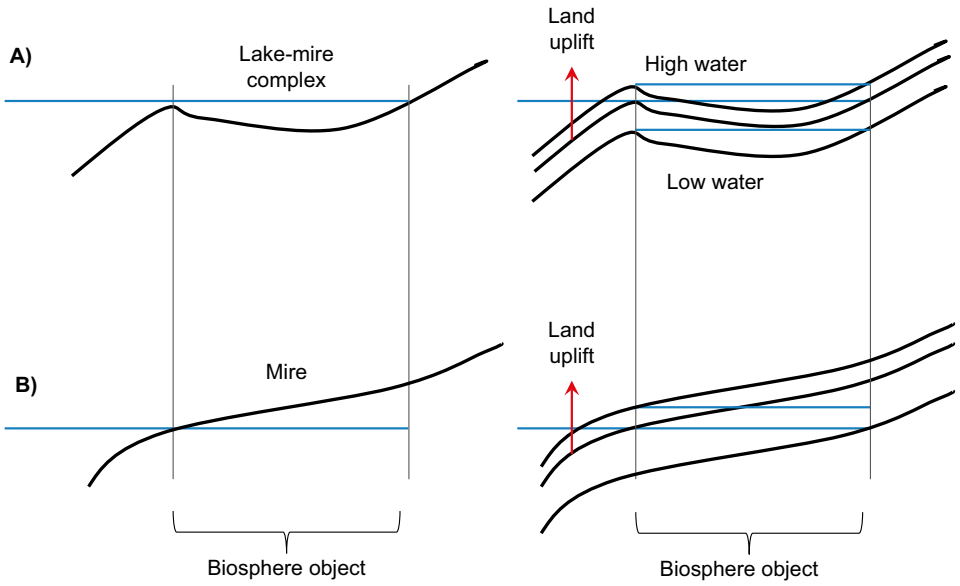

Figure 7-1. *Schematic illustrations of the transition from submerged to terrestrial conditions of biosphere objects as a result of isostatic rebound. A) Transition from sea bay to lake-mire complex. Conditions are intermediate during the period between isolation at extreme low sea level (left) and isolation at extreme high sea level (right). B) Transition from sea bay to wetland (no lake is formed). Conditions are intermediate during the period between full emergence at extreme low sea level (left) and full emergence at extreme high sea level (right).*

In the radionuclide-transport modelling (Saetre et al. 2013b) the continuous developments of individual biosphere objects are partly described using dynamic (time dependent) model parameters. For instance, depths and volumes of surface-water bodies, mire areas, peat-layer depths, stream flows, sedimentation, resuspension and aquatic primary production are examples of time-dependent model parameters (see Grolander 2013).

The radionuclide-transport modelling takes into account time-dependent effects of isostatic rebound on water fluxes during the transition from submerged conditions to a fully isolated lake (or mire). This transition period is initiated at the point in time when the lake threshold (or first land) of an object emerges above sea level during periods of extremely low sea level, set at –1.2 m below average sea level, whereas lake (or mire) isolation is completed when the lake threshold (or all land) is above sea level during periods of extremely high sea level water, set at 1.0 m above the average sea level (see descriptions of the parameters *threshold_start* and *threshold_stop* in Grolander (2013)).

The effect of landscape development on horizontal water fluxes are described using the time-dependent parameter *WF_landscape* (see Grolander 2013). Specifically, the exchange of water between marine basins are estimated using MIKE 3 (Sections 4.5 and 5.6), whereas MIKE SHE is used to estimate horizontal surface-water fluxes at two points in time; shortly after first lake isolation/land emergence (at low sea level) and after completion of mire expansion.

Vertical groundwater fluxes between regolith layers were modelled in MIKE SHE for submerged or terrestrial conditions. Specifically, groundwater fluxes were calculated representing (1) the submerged period, (2) conditions following lake isolation, and (3) the period when mire expansion is completed. It is assumed that vertical groundwater fluxes are stable during the submerged period (1) and during the terrestrial period subsequent to completion of mire development (3), whereas vertical fluxes depend on the progress of shoreline displacement between these stable states (2). It should be noted that time-dependent meteorological parameters and a time-dependent sea level are used to model also the stable states, i.e. the term stable only refers to the independence of shoreline displacement (Saetre et al. 2013b).

As shown in Table 7-1, for biosphere objects in which a lake is formed after isolation (top left and right in Figure 7-1), time-dependent vertical groundwater fluxes during the intermediate period are modelled by linear interpolation of fluxes calculated at initiation (low sea level) and completion (normal sea level) of isolation. For objects in which no lake is formed after isolation (bottom left and right in Figure 7-1), the corresponding interpolation uses fluxes calculated at the points in time when land first emerges (at low sea level) and when the object is fully emerged (at normal sea level). Moreover, vertical groundwater fluxes in the mire parts of objects are linearly interpolated during the period between completed lake isolation/land emergence and when completion of mire expansion (Saetre et al. 2013b).

Figure 7-2 shows compartments and fluxes for both limnic (lake) and terrestrial (wetland) systems, and it can also be used to clarify parameters delivered to the radionuclide-transport modelling of the submerged period. Blue arrows represent advective fluxes delivered from the MIKE SHE model. During the marine stage, i.e. at 3000 AD among the future times considered here, only fluxes represented by the blue vertical arrows in the aquatic part (right side) of Figure 7-2 are delivered, whereas no surface-water fluxes are calculated by MIKE SHE for the marine stage. For objects that contain both limnic and terrestrial systems at 5000 AD, parameters representing all inter-compartment fluxes (blue arrows denoted as “2” in Figure 7-2) are delivered to the radionuclide-transport modelling.

Table 7-1. Modelling of transition periods using interpolated vertical groundwater fluxes.

Ecosystem	Transition	Transition period	
		Start	End
Aquatic	Sea to lake	Lake isolation at low sea level	Lake isolation at high sea level
	Sea to mire (without lake stage)	First land above low sea level	All land above sea at high sea level
Mire	Mire expansion (both types above)	Lake isolation/all land above water at high sea level	Mire expansion completed

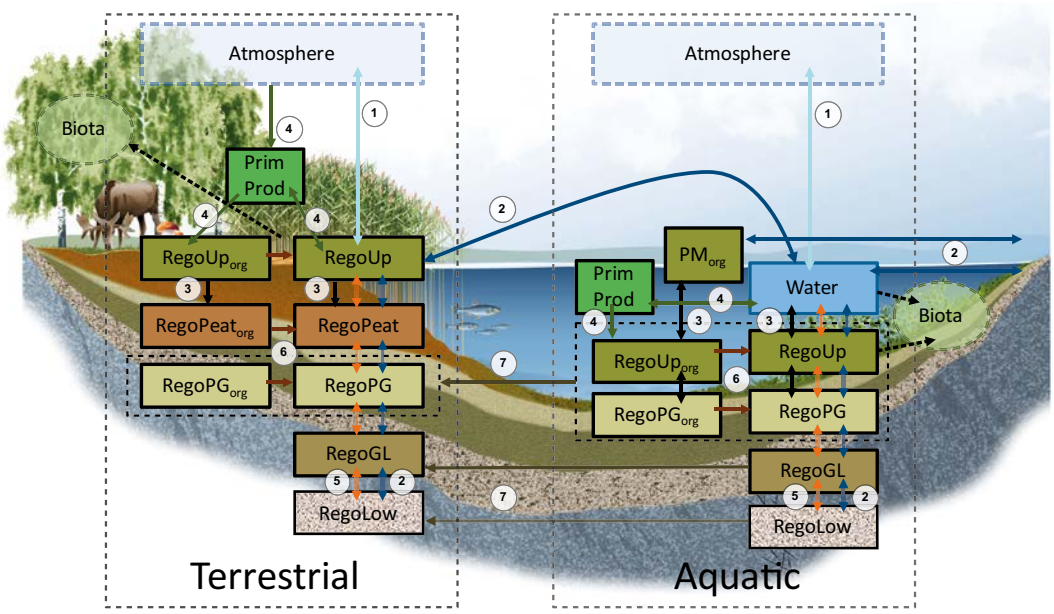

Figure 7-2. *Illustration of compartments and inter-compartment fluxes considered in the modelling of radionuclide transport and accumulation in lake-mire systems. For further details, see Saetre et al. (2013b).*

For biosphere objects that are terrestrialised immediately after the marine stage (121_2 and 157_2) MIKE SHE calculates vertical groundwater fluxes in the terrestrial part (left side) of Figure 7-2, whereas MIKE 11 calculates surface-water fluxes to downstream objects for biosphere objects that contain streams.

7.2 Methodology

Based on the water-flow calculations for the local MIKE SHE model area described in Chapter 5, water balances are derived for each of the seven biosphere objects included in the analysis. Specifically, water-balance components are extracted in the form of water flows into and out from each object and water flows between calculations layers of MIKE SHE, corresponding to radionuclide-model compartments (Figure 7-2). For objects that at a considered point in time consist of a lake area surrounded by a mire, three separate water balances are extracted to obtain fluxes (flow divided by area) for all arrows shown in Figure 7-2. Specifically, one water balance is extracted for the lake area, one for the mire area and one for the entire object. For objects that are submerged, or terrestrial objects that only consist of mire, one water balance is extracted for the entire object. For more details on issues related to extraction of water-balance components from MIKE SHE, see Bosson et al. (2010).

In MIKE SHE water balances, lakes are defined as areas with an annual minimum depth of overland water of 0.1 m at 5000 AD. Hence, in water-balance calculations lakes comprise areas that contain surface water during the entire simulated period. The definition above implies that lake extents in some cases differ slightly from lakes delineated as part of landscape modelling (cf Section 2.2.3).

At all biosphere objects associated with streams, in the MIKE 11 stream network streams enter at the upstream parts and exit at the downstream parts of objects (Figure 7-3). In the radionuclide-transport modelling (Saetre et al. 2013b), the lake area of objects is reduced with time by reducing its width, which implies that the associated stream enters and exits the lake at the same locations at all times. As shown in Figure 7-3, the MIKE SHE-definition of lakes described above implies that a lake may be transformed to mire areas along the entire lake circumference, and the associated stream may enter and/or exit a lake at different locations at different points in time. Moreover, in the radionuclide-transport modelling it is assumed that each object is associated with a single stream, whereas in the MIKE 11 stream network several streams may reach a lake at different locations along the lake shoreline. In such cases, the total MIKE 11-calculated stream discharges are added to represent the single stream in the radionuclide transport model.

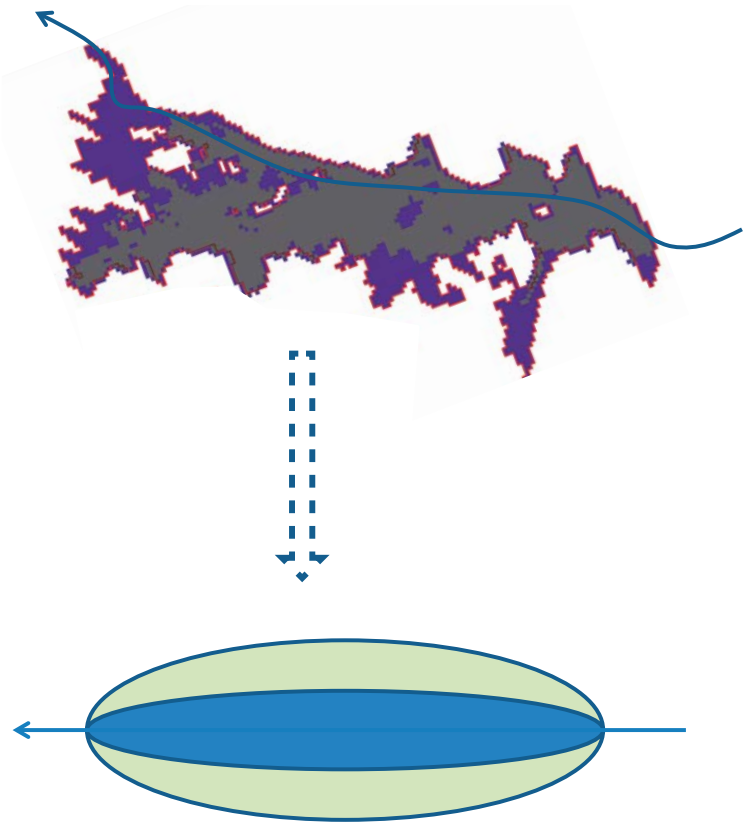

Figure 7-3. *Representation of lakes and streams in MIKE SHE (upper figure) and the corresponding conceptualisation in the radionuclide-transport model (lower figure). In the upper figure, grey areas represent the lake and lilac areas represent mire areas.*

Figure 7-4 and 7-5 illustrate hydrological connections between biosphere objects subsequent to emergence of associated areas. The catchment area for object 157_2 (Figure 7-4) has no upstream catchment area, and according to Brydsten and Strömgren (2013) there is no stream associated with the object (see further discussion in Chapter 6). As shown in Figure 7-4, surface water generated in object 157_2 and the stream associated with object 159 are directed towards object 157_1. Moreover, the stream associated with object 157_1 is directed towards object 116. Surface water also enters object 116 from a catchment denoted 158.

As mentioned in Section 2.2.3 the stream network by Brydsten and Strömgren (2013) is based on the 2000 AD DEM, and some stream stretches and cross-section elevations are adjusted in MIKE 11 to fit the corresponding DEM at each time. As shown in Figure 7-5, the MIKE 11 stream network defines a stream from object 160 to object 121_1, whereas Brydsten and Strömgren (2013) define a stream from biosphere object 160 to object 121_2, based on the 2000 AD DEM (cf Section 6.2.3). In MIKE SHE, precipitation reaching the ground surface will subsequently follow the ground-surface topography, and the reason for changing the stream direction in MIKE 11 is simply to catch surface water in a stream.

Figure 7-6 illustrates conceptual surface-water flows into and through a biosphere object containing a lake-mire complex. The MIKE SHE water-balance tool extracts water flows within the selected water-balance area, and total water flows passing across its boundaries. However, as MIKE SHE water balances do not provide information on the flow distribution along the boundary of the water-balance area, it is not possible to estimate the proportions between Q_{in}, Q_{catch} and Q_{mire} in Figure 7-6 from the water balances for the object area. There is neither any information on the proportion of return flows, i.e. water passing in and out across the boundary, for instance during flooding events. Furthermore, since the MIKE SHE water-balance tool only provides information on total water exchanges between MIKE SHE and MIKE 11 within the water balance area, the annual average stream in- and outflows divided by the object area (which provide fluxes in mm/y) are extracted separately from the MIKE 11 model and thereafter added to the MIKE SHE-calculated water balances.

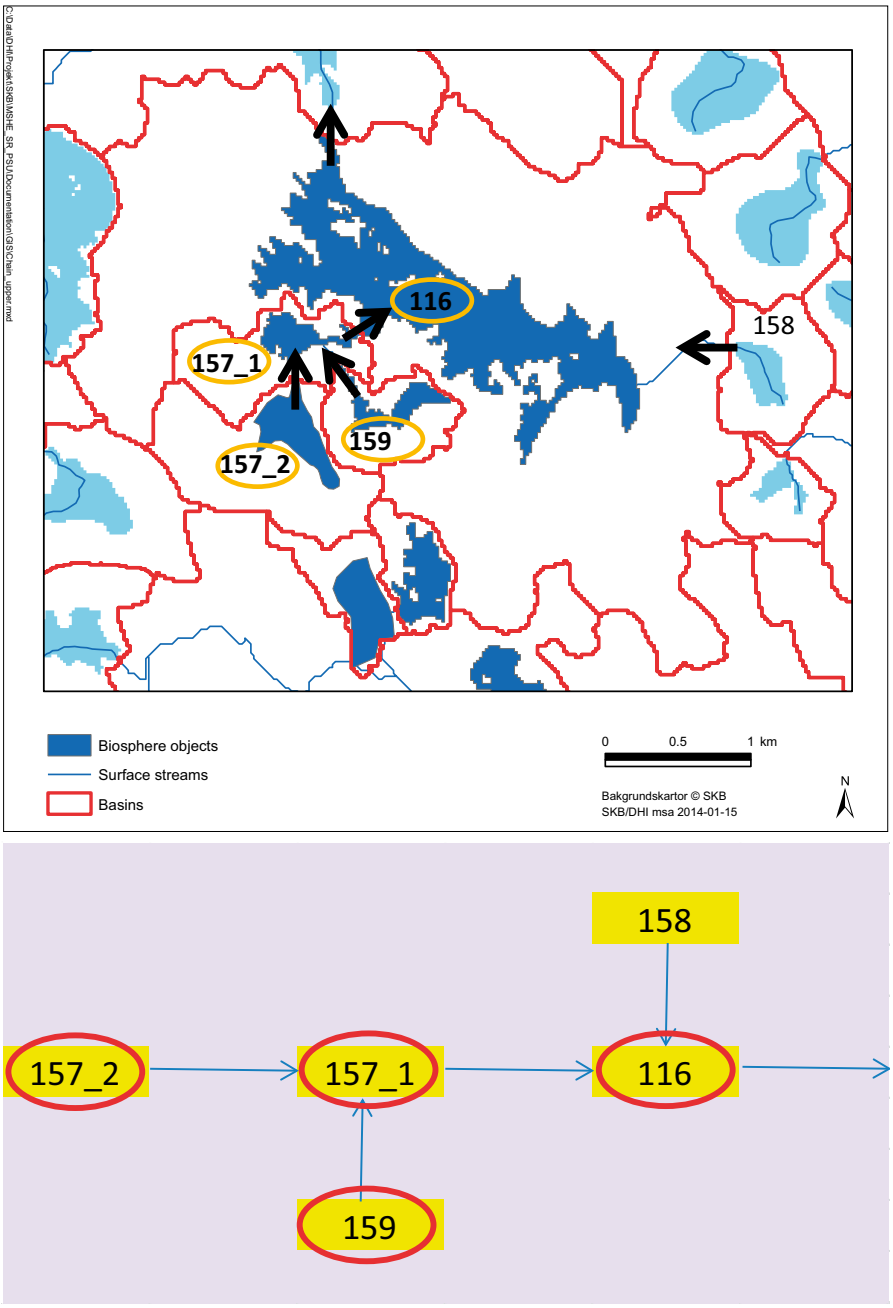

Figure 7-4. *Illustration of hydrological connection between biosphere objects (circumscribed in the bottom figure) 116, 157_1, 157_2 and 159, located north of SFR.*

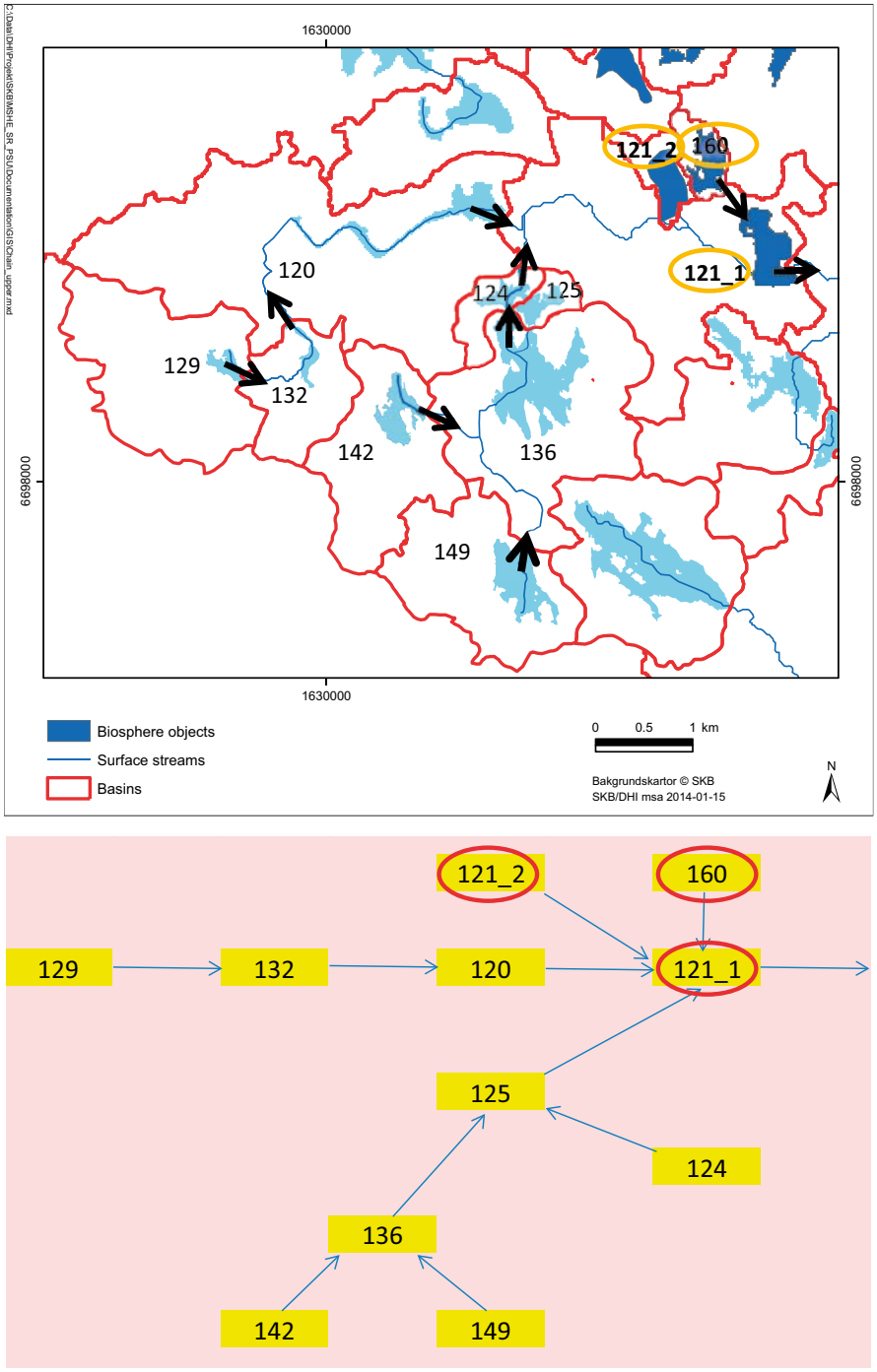

Figure 7-5. *Illustration of hydrological connection between biosphere objects (circumscribed in the bottom figure) 121_1, 121_2 and 160, located south of SFR.*

In Figure 7-6, water generated usptream of the lake inlet is denoted Q_{in}. If the catchment area of the object has no further upstream catchment areas, Q_{in} is the surface water generated only within the catchment area of the lake inlet (cf Figure 7.6). Otherwise, if there are further upstream catchment areas, Q_{in} is the total amount of surface water coming from all upstream catchment areas of the lake inlet. Surface water generated within the area corresponding to the catchment area of the stream outlet minus the catchment area of the stream inlet (Q_{catch}) reaches the mire area, from which Q_{mire} reaches the lake. Q_{out} is the total amount of surface water that leaves the object at the stream outlet from the lake.

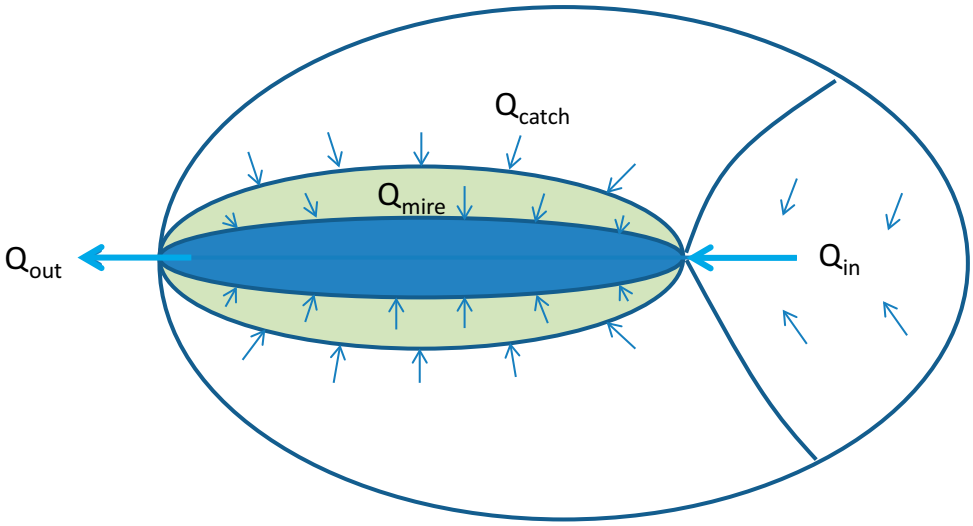

Figure 7-6. *Conceptual surface-water flows into and through a biosphere object containing a lake (blue) and a mire (green).*

The parameters in Figure 7-6 are calculated based on annual average runoffs and sizes of catchment areas and biosphere objects. Specifically, annual average runoffs are calculated by extracting separate water balances for each of the subareas (catchment areas and biosphere objects) with the MIKE SHE water-balance tool. In Tables 7-2 to 7-5 (catchment areas and biosphere objects north and south of SFR, at 5000 and 11,000 AD), the Basin columns contain runoff values calculated based on entire catchment areas, including biosphere objects, whereas the Basin_NOBJ columns consider catchment areas except biosphere objects. Moreover, the TOTAL_OBJ columns consider biosphere objects, whereas the Lake and Mire columns in Tables 7-2 to 7-5 consider lake and mire areas, respectively, of biosphere objects.

As illustrated in Figure 7-3, there is a discrepancy between how lakes are described in MIKE SHE and in the radionuclide model (Saetre et al. 2013b). In the radionuclide model, all surface water enters biosphere objects by the surface stream (Q_{in} in Figure 7-6), whereas in MIKE SHE water may also reach a lake by overland water outside of the stream, in particular during flooding events, but also if the area around the lake has a flat topography. The amounts of surface water entering and leaving objects are here estimated by extracting MIKE 11 stream-discharge data at or in the vicinity of stream inlets and outlets of biosphere objects. Subsequently, annual average discharges are calculated based on the resulting stream discharge time series, and these averages are normalised with the area of each biosphere object to obtain corresponding annual average fluxes (mm/y).

Table 7-2. MIKE SHE-calculated annual average runoff at 5000 AD for biosphere objects north of SFR.

Biosphere object	Runoff (mm/y)				
	Basin	Basin_NOBJ	TOTAL_OBJ	Mire	Lake
157_1	178	180	166	166	164
157_2	178	179	173	–	–
159	179	179	179	181	163
116	172	174	160	161	160

Table 7-3. MIKE SHE-calculated annual average runoff at 11,000 AD for biosphere objects north of SFR.

Biosphere object	Runoff (mm/y)		
	Basin	Basin_NOBJ	TOTAL_OBJ
157_1	191	196	164
157_2	192	194	180
159	203	212	169
116	189	193	165

Table 7-4. MIKE SHE-calculated annual average runoff at 5000 AD for biosphere objects south of SFR.

Biosphere object	Runoff (mm/y)				
	Basin	Basin_NOBJ	TOTAL_OBJ	Mire	Lake
160	181	182	181	182	165
121_2	173	187	162	–	–
121_1	176	177	161	160	164

Table 7-5. MIKE SHE-calculated annual average runoff at 11,000 AD for biosphere objects south of SFR.

Biosphere object	Runoff (mm/y)		
	Basin	Basin_NOBJ	TOTAL_OBJ
160	186	203	170
121_2	189	180	198
121_1	201	204	158

Figures 7-7 to 7-10 specify water-balance components extracted for submerged biosphere objects (Figure 7-7), biosphere objects with lake and mire areas (Figure 7-8), objects with mire and a former lake, transformed to mire (Figure 7-9) and for objects that are transformed to mire areas only (no lake) subsequent to emergence (Figure 7-10).

At 3000 AD all biosphere objects are submerged (cf Figure 7-7). In marine areas, the sea is represented in the upper MIKE SHE calculation layer (Rego1), whereas the regolith is represented in layers Rego2–Rego4. At 5000 AD the entire local model area is emerged and all biosphere objects, except for objects 121_2 and 157_2, are transformed into lake and mire areas (cf Figure 7-8). Specifically, for such objects water-balance components are extracted separately for the lake and the mire area. The regolith is represented in four calculation layers (Rego1–Rego4), of which the upper layer (Rego1) has a total thickness of 2.5 m in order to allow proper calculations of evapotranspiration processes (see Bosson et al. 2008).

In the delivery to the radionuclide-transport modelling, Rego1 was divided into two layers, with thicknesses of 0.5 m (Rego1a) and 2.0 m (Rego1b). Specifically, near-surface groundwater flow (subsurface drainage, see Section 3.1.5) is assigned to Rego1a, whereas other contributions are distributed according to relative thickness (20% to Rego1a and 80% to Rego1b). Accordingly, vertical groundwater flows are recalculated to obtain layer-wise water balances based on these distributions of horizontal flows.

Horizontal flows in the uppermost layer (blue compartments in Figure 7-8) are based on annual average runoff (Tables 7-2 to 7-5) and MIKE 11-calculated stream discharges. Specifically, stream discharges are assigned to lakes (the blue-marked components In MIKE 11 and Out MIKE 11). The Lake balance component is calculated under the assumption of water balance in the compartment representing the lake box. In a final step, all components in the lake and mire compartments are added to check the water balance.

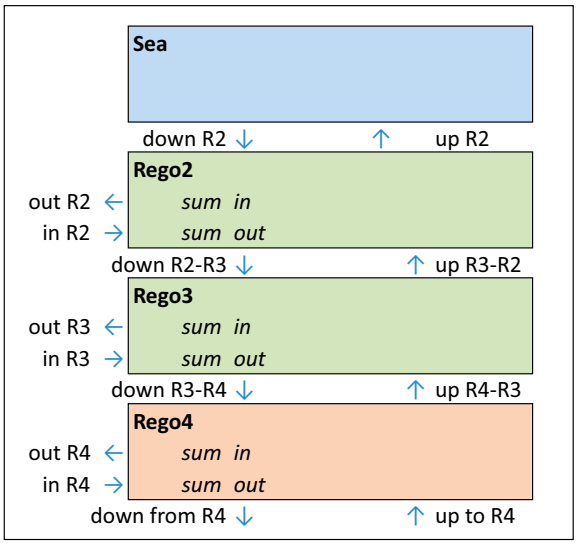

Figure 7-7. *Extracted water-balance components for submerged biosphere objects.*

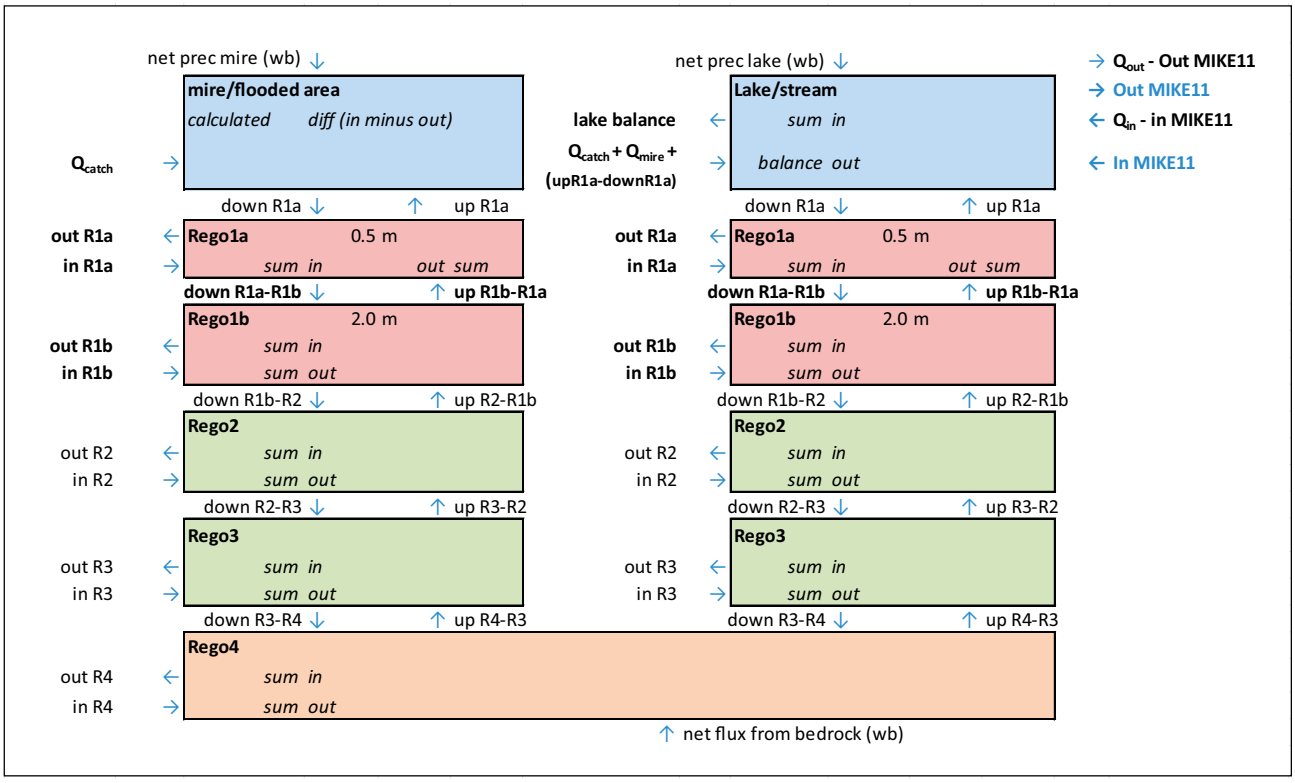

Figure 7-8. *Extracted water-balance components for biosphere objects with lake and mire areas. Components extracted from MIKE 11 are shown in blue.*

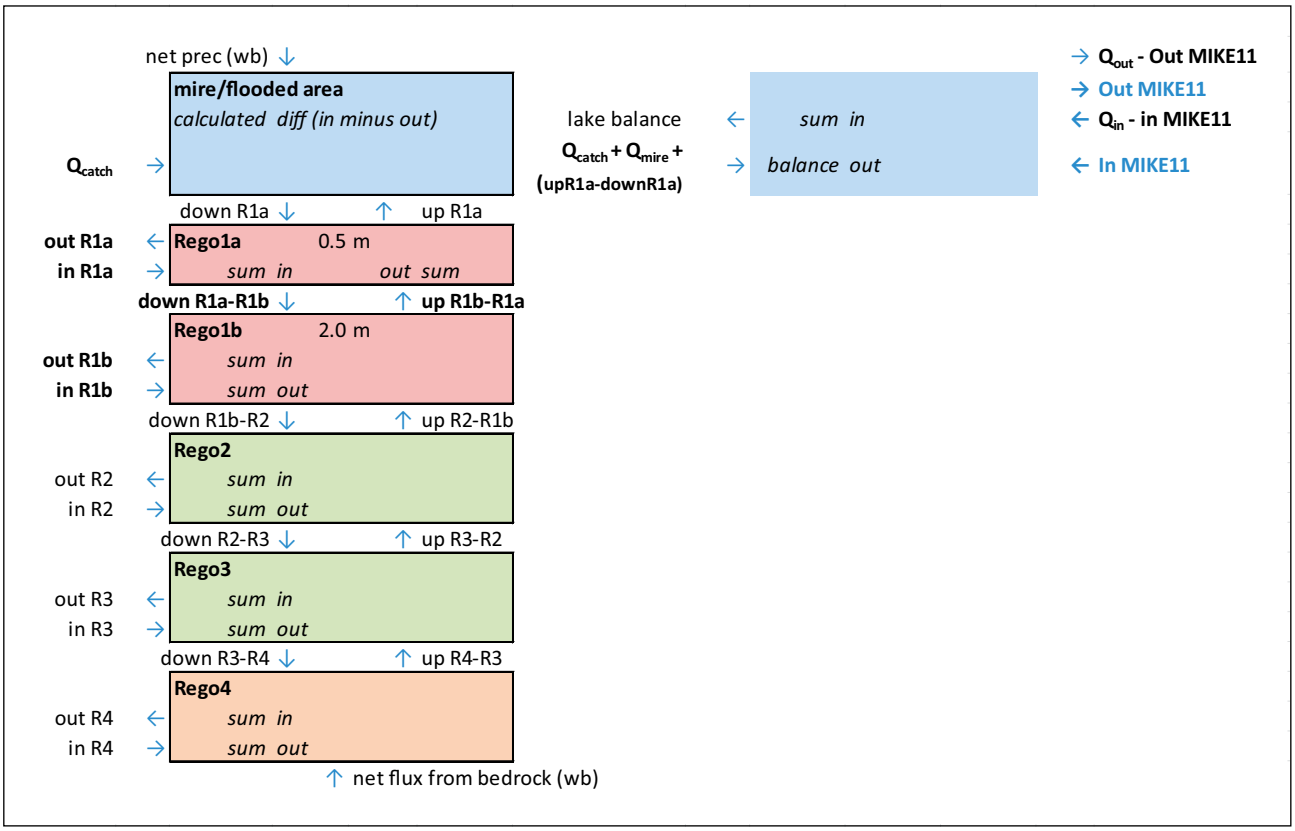

Figure 7-9. *Extracted water-balance components for biosphere objects with mire and a former lake, transformed to mire. Components extracted from MIKE 11 are shown in blue.*

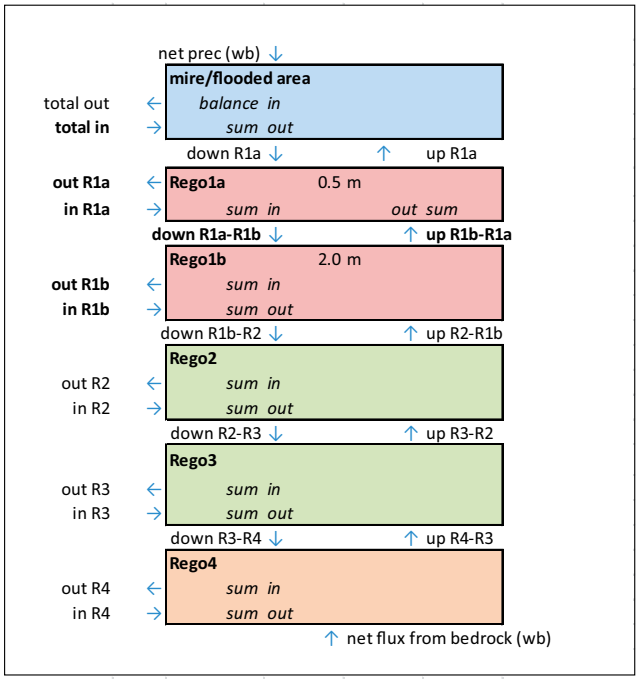

Figure 7-10. *Extracted water-balance components for biosphere objects that are transformed to mire areas only (no lake) subsequent to emergence.*

In the extraction of water-balance components for biosphere objects with mire and a former lake, transformed to mire (Figure 7-9), the water balance is extracted for the entire object only. Concerning biosphere objects that are transformed to mire areas only (no lake) subsequent to emergence (Figure 7-10), the Total out component is obtained as Q_{out} in Figure 7-6 in the absence of a stream.

7.3 Water balances for the normal year

This section presents a summary of the MIKE SHE calculations, whereas the calculated water-balance components and regolith-layer thicknesses for the seven biosphere objects are presented in Appendix 1 (cf Figures 7-7 to 7-10). In each water balance, flow components are normalised with the area of each object (Table 7-6). Note that areas of objects are different at the considered points in time. In some cases, it was required to adjust the area to facilitate interpretation of modelling results. For instance, at 3000 AD, when all objects are submerged some objects are located near the shoreline, which causes numerical instabilities in water-balance calculations. Therefore, near-shore model cells were excluded from relevant objects. Moreover, in order to separate water fluxes between lakes and mires at 5000 AD, lakes need to be surrounded by mire areas. Specifically, a cell defined as being part of a lake (overland-water depth exceeding 0.1 m, cf above) cannot be located at the object boundary. In such cases, some model cells were added for the purposes of water-balance calculations.

7.3.1 Results for the submerged period (3000 AD)

All biosphere objects are submerged at 3000 AD. Hence, the water-balance components shown in Figure 7-7 are extracted from MIKE SHE. Table 7-7 summarises the modelling results in terms of net vertical groundwater fluxes (flow divided by object area) between the four calculation layers of the local MIKE SHE model (Rego1–4). According to the table, net vertical fluxes are directed upwards for all objects. For most objects the net vertical flux is small, whereas the largest fluxes (c 20 mm/y) are calculated for object 121_1. Moreover, vertical fluxes are rather constant with depth in the regolith, which implies that horizontal fluxes are small.

Table 7-6. Object areas used in water-balance calculations.

Biosphere object	Object area (m^2)		
	3000 AD	5000 AD	11,000 AD
157_2	130,000	167,600	167,600
159	101,200	103,600	103,200
157_1	103,600	105,600	103,600
116	1,490,800	1,569,600	1,491,600
121_2	161,200	178,000	178,000
160	106,000	158,400	158,400
121_1	269,600	274,400	270,000

Table 7-7. Net vertical groundwater fluxes for biosphere objects during the submerged period (3000 AD).

Biosphere object	Vertical flux (mm/y)			
	Rock to Rego4	Rego4 to Rego3	Rego3 to Rego2	Rego2 to Rego1
116	0.5	0.5	0.5	0.6
121_1	24.8	20.3	19.9	19.8
121_2	5.1	5.0	4.8	4.7
157_1	0.1	0.0	0.1	0.5
157_2	7.0	7.1	7.1	7.0
159	3.2	3.2	3.9	4.1
160	1.4	1.3	0.9	1.0

7.3.2 Results for the lake-mire period (5000 AD)

Figure 7-11 displays delineations of lake and mire areas used in the 5000 AD water-balance calculations. Table 7-8 lists the relative proportions of lake and mire areas in each object at the year 5000 AD. As mentioned previously, there are no lakes in objects 121_2 and 157_2. Among the other objects, object 116 has the largest lake proportion (c 60%), whereas the lake in object 159 is smaller than 10% of its area.

Figure 7-12 shows an example of MIKE 11-calculated time series of stream discharge (object 116), which is used to estimate surface-water flows into, through and out from biosphere objects. The blue line represents stream inflow, the red line is stream outflow, and dotted lines represent corresponding annual averages. It is noted that outflow fluctuations are smaller than fluctuations of the inflow, which illustrates the flow-dampening effect of the lake. For reasons mentioned previously, average in- and outflows divided by the object area (providing fluxes in mm/y) are added to the MIKE SHE-calculated water balances, see Table 7-9.

Table 7-8. Relative proportions of lake and mire areas of biosphere objects at 5000 AD.

Biosphere object	% of total object area	
	Lake	Mire
157_2	–	100
159	8.1	91.9
157_1	23.9	76.1
116	57.5	42.5
121_2	–	100
160	8.8	91.2
121_1	27.7	72.3

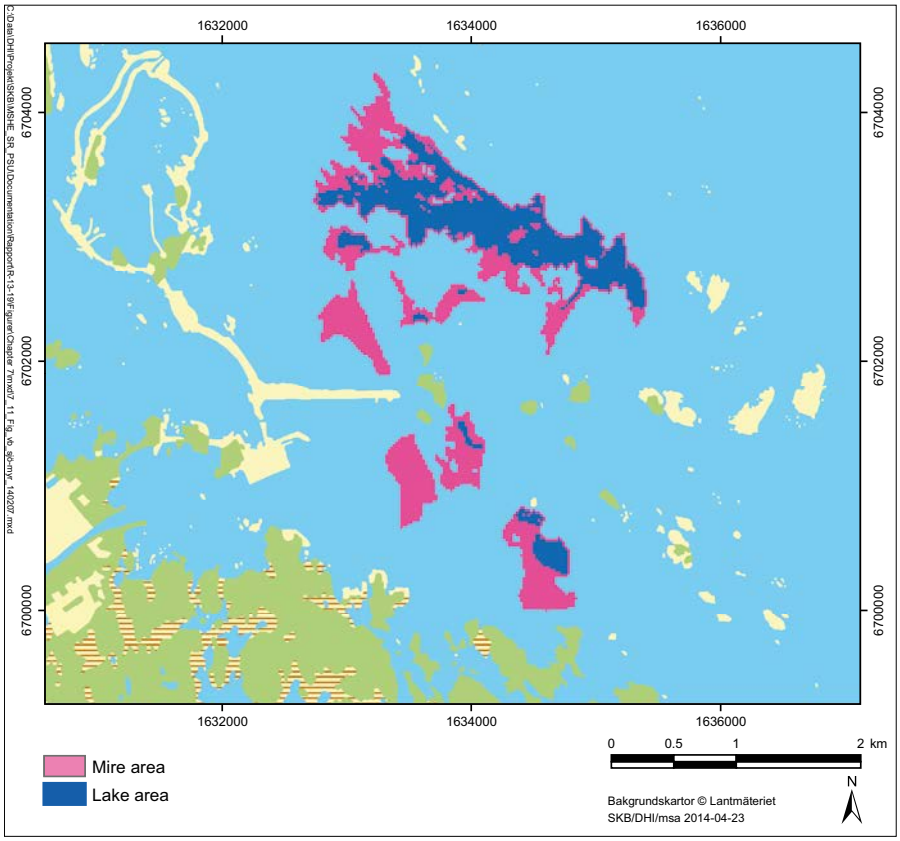

Figure 7-11. Delineated lake and mire areas of biosphere objects at 5000 AD (cf Figure 2-23).

Table 7-9. MIKE 11-calculated stream discharges (mm/y) at 5000 AD.

Biosphere object	Stream discharge (mm/y)			
	In	Out	Net	MIKE 11 stream discharge/MIKE SHE water balance (%)
116	304	1,084	780	100
121_1	19,487	20,264	777	97
157_1	418	3,344	2,925	99
159	0	776	776	89
160	0	270	270	120

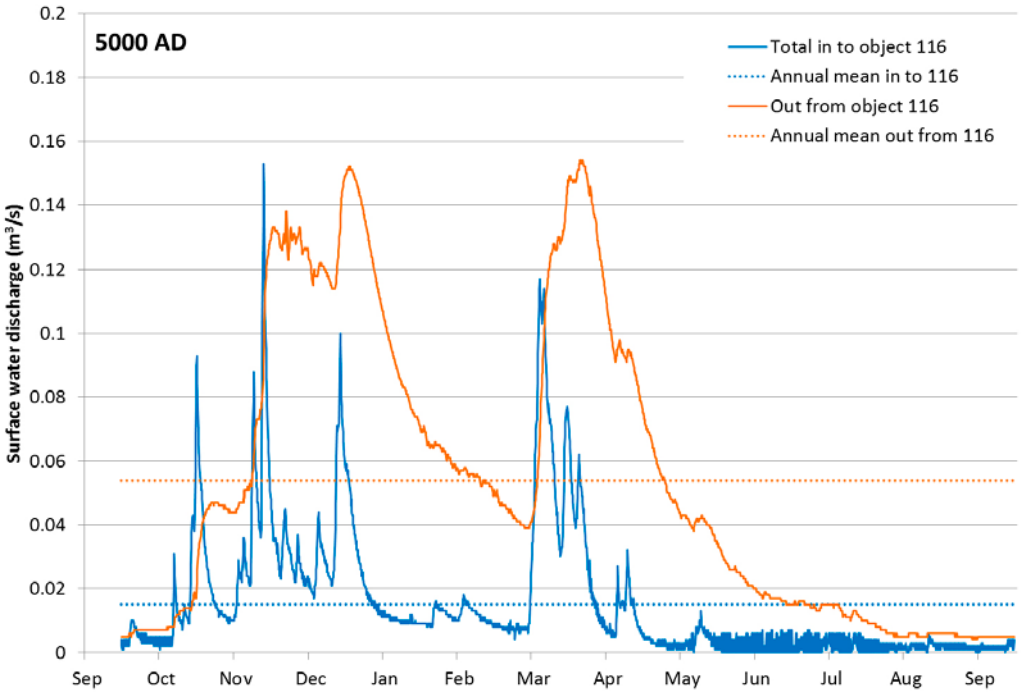

Figure 7-12. *MIKE 11-calculated stream discharges into (blue solid line) and out from (red solid line) biosphere object 116. Dotted lines represent corresponding annual averages.*

Due to the specific locations of cross sections of the MIKE 11 stream network, in some cases stream discharges, which are calculated midway between cross sections, are not calculated immediately up- or downstream of biosphere objects. This may lead to slight under- or overestimation of stream discharges entering and exiting objects. Moreover, due to differences in the original DEM and the MIKE SHE-interpolated topography, there may be minor discrepancies in terms of locations of ground- and surface water exchanges. However, as shown in the rightmost column of Table 7-9, there are generally good agreements between MIKE 11-calculated stream discharges and associated MIKE 11-components of the MIKE SHE water balances.

Table 7-10 shows net vertical groundwater fluxes (flow divided by the area of the biosphere object) at 5000 AD for biosphere objects north of SFR. Vertical net groundwater fluxes are small in all lakes located within biosphere objects north of SFR. However, there are large differences between objects in terms of net fluxes from rock to regolith. Specifically, object 157_2 has the largest flux from rock to regolith. Comparison with corresponding MIKE SHE modelling presented in Bosson et al. (2010) shows good agreement to the present results in terms of vertical groundwater flux from rock to regolith.

There are small vertical flux differences between most layers (Table 7-10), which show that net horizontal fluxes are small. The exception is the uppermost calculation layer (Rego1), indicating relatively large horizontal flows at shallow depth in the regolith (e.g. object 159). However, Table 7-10 indicates that horizontal fluxes in Rego1 are small in objects 157_1 and 116. In these objects, the net vertical groundwater flux is directed downwards from the surface to Rego1, from which groundwater is directed to the associated lakes.

Table 7-10. Net vertical groundwater fluxes at 5000 AD (mm/y) for biosphere objects north of SFR.

Biosphere object	Object	Mire				Lake			
	Rock to Rego4	Rego4 to Rego3	Rego3 to Rego2	Rego2 to Rego1	Rego1 to surface	Rego4 to Rego3	Rego3 to Rego2	Rego2 to Rego1	Rego1 to surface
157_2	101	102	108	117	208	–	–	–	–
159	29	32	35	35	240	3	5	13	25
157_1	8	12	17	24	–12	2	2	3	25
116	7	5	7	10	–5	2	0	1	33

In biosphere objects located south of SFR, net vertical groundwater fluxes from rock to regolith are rather high (Table 7-11), in particular in objects 121_1 and 121_2. In object 160, the net vertical flux is negative in the mire part, which implies that the flux is directed downwards, whereas the flux is directed upwards in the lake.

7.3.3 Results for the mire period (11,000 AD)

At 11,000 AD, all former lakes in the MIKE SHE local model area are transformed to mires. Figure 7-13 shows MIKE 11-calculated time series of stream discharge into and out from biosphere object 116 at 11,000 AD. Comparison with the corresponding 5000 AD results in Figure 7-12 shows less flow-dampening at the outflow, since the lake is absent at 11,000 AD. Moreover, it is also noted that discharge peaks are higher and of shorter duration at 11,000 AD.

Table 7-12 shows MIKE 11-calculated stream discharges into and out from biosphere objects at 11,000 AD. Ratios between MIKE 11-calculated stream discharges and corresponding MIKE SHE-calculated water-balance components are similar to those at 5000 AD (Table 7-9). Comparison between 5000 and 11,000 AD stream discharges shows small differences for object 159. For object 157_1 there is a distinct increase in the stream discharge, which can be noted both in the MIKE 11-calculated discharge and in the associated MIKE SHE water-balance components (the MIKE 11/ MIKE SHE ratio is unchanged). The reason for this increase is that at 5000 AD, surface water north of object 157_1 and west of object 116 is directed to object 116. At 11,000 AD part of this surface water is directed to object 157_1 and subsequently to object 116. As a result, the stream discharge in object 116 is similar at 5000 and 11,000 AD, whereas the difference is larger for object 157_1.

For objects 121_2 and 160, there is less stream discharge at 11,000 AD compared to 5000 AD, likely due to that parts of the surface water at 5000 AD enters the associated streams across the catchment border in the north-eastern part of object 160. Surface water directed to the northeast does not reach object 121_1.

Tables 7-13 and 7-14 show net vertical groundwater fluxes for all seven biosphere objects at 11,000 AD. Similar to the 5000 AD results (Table 7-10) differences between most layers are small, which show that net horizontal fluxes are small. The exception is the uppermost calculation layer (Rego1), indicating relatively large horizontal flows at shallow depth in the regolith (cf above).

Comparison with 5000 AD modelling results shows small net-flux differences and a slight increase in net fluxes from rock to regolith for most objects at 11,000 AD. In object 160, at 11,000 AD the former lake in object 160 has been transformed to a mire and the net flux is directed downwards, whereas the net flux in that object is directed downwards in its mire area and upwards in the associated lake at 5000 AD.

Table 7-11. Net vertical groundwater fluxes (mm/y) at 5000 AD for biosphere objects south of SFR.

Biosphere object	Object	Mire (mm/y)				Lake (mm/y)			
	Rock to Rego4	Rego4 to Rego3	Rego3 to Rego2	Rego2 to Rego1	Rego1 to surface	Rego4 to Rego3	Rego3 to Rego2	Rego2 to Rego1-	Rego1 to surface
121_1	67	42	42	41	17	19	20	22	55
121_2	39	39	43	52	72	–	–	–	–
160	12	–3	–7	–8	–91	10	13	19	46

Table 7-12. MIKE 11-calculated stream discharges (mm/y) at 11,000 AD.

Biosphere object	Stream discharge (mm/y)			
	In	Out	Net	MIKE 11 stream discharge/MIKE SHE water balance (%)
159	0	791	791	96
157_1	492	5,010	4,517	99
116	471	1,170	699	102
160	0	142	142	113
121_1	16,472	17,108	636	106

Table 7-13. Net vertical groundwater fluxes (mm/y) at 11,000 AD for objects north of SFR with outflow from object 116.

Biosphere object	Object	Mire (mm/y)			
	Rock to Rego4	Rego4 to Rego3	Rego3 to Rego2	Rego2 to Rego1	Rego1 to surface
157_2	116	117	125	10	300
159	31	39	42	50	288
157_1	10	14	19	24	34
116	7	9	12	15	31

Table 7-14. Net vertical groundwater fluxes (mm/y) at 11,000 AD for objects south of SFR.

Biosphere object	Object	Mire (mm/y)			
	Rock to Rego4	Rego4 to Rego3	Rego3 to Rego2	Rego2 to Rego1	Rego1 to surface
121_2	42	42	46	57	82
160	–10	–21	–31	–32	–60
121_1	66	53	51	51	63

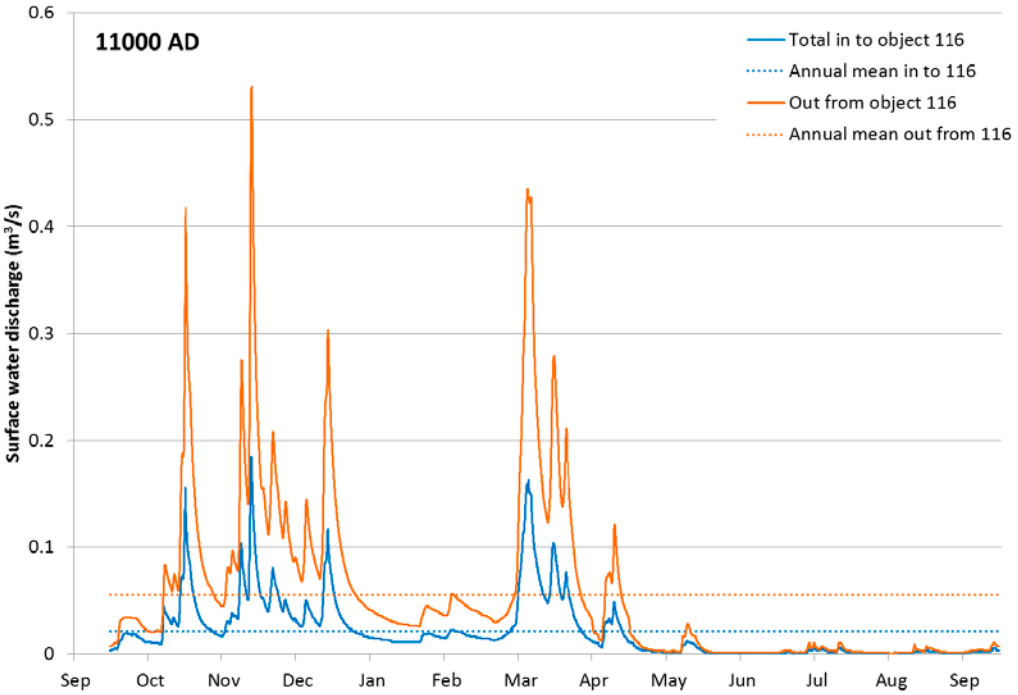

Figure 7-13. *MIKE 11-calculated stream discharges into (blue solid line) and out from (red solid line) biosphere object 116. Dotted lines represent corresponding annual averages.*

7.4 Water balances for other climate cases

7.4.1 Results for a wet and warm climate

Appendix 1 presents MIKE SHE-calculated water-balance components for biosphere objects at 5000 AD for a wet and warm climate. The wet and warm climate has significantly more precipitation (c 1,500 mm per year) than the normal year (less than 600 mm/y). Moreover, the MIKE SHE-calculated annual average ET in 5000 AD land areas is high (c 1,140 mm per year), with R being approximately 150% higher than the normal-year R (c 450 mm/year).

Figure 7-14 shows MIKE 11-calculated 5000 AD time series of stream discharges into and out from biosphere object 116 for a wet and warm climate. For comparison, the figure also shows the corresponding stream discharge out from the object for the normal year (cf Figure 7-12). As for the normal year, outflow fluctuations are smaller than fluctuations of the inflow, which illustrates the flow-dampening effect of the lake. Moreover, discharge peaks during autumn are of the same magnitudes for the wet and warm climate and the normal year, whereas discharge peaks during spring are approximately three times larger for the wet and warm climate.

Table 7-15 presents net vertical groundwater fluxes for biosphere objects north of SFR. Comparison with the corresponding results for the normal year (Table 7-10) shows that the wet and warm climate is associated with larger net vertical groundwater fluxes to the surface in mire areas, whereas fluxes in the regolith are less affected.

7.4.2 Results for periglacial conditions with permafrost

Water balances for periglacial conditions with permafrost are obtained from the MIKE SHE models developed by Bosson et al. (2010). Specifically, the modelling results presented here are based on the model setup developed for a case with a 100 m deep layer of permafrost, and water balances are extracted for all taliks that Bosson et al. (2010) identified as groundwater-discharge taliks. Moreover, separate water balances are extracted for two taliks (Appendix 1), chosen to represent areas with DarcyTools-calculated discharge locations for periglacial conditions with permafrost (cf Section 2.3.2). One of the chosen taliks is at the location of biosphere object 157_1 (i.e. discharge locations north of SFR), whereas the other is talik object 114 of Bosson et al. (2010), coinciding with discharge-location areas at the north-eastern DarcyTools model boundary (Figure 7-15). As the dynamic regolith depth and stratigraphy model used in the SR-PSU project slightly differs from that of SR-Site (cf Section 2.2.2), there are some differences in water-balance area extents between Bosson et al. (2010) and the present modelling (Figure 7-15). For further details on the permafrost-model setup in MIKE SHE, see Bosson et al. (2010).

Table 7-16 presents the results of the permafrost water balances in terms on net vertical groundwater fluxes for all discharge taliks, biosphere object 157_1 and the talik object of Bosson et al. (2010), whereas Figure 7-16 shows the MIKE SHE-calculated contribution to the stream discharge from talik object 114. In the permafrost case (Table 7-16), the net vertical groundwater flux from rock to regolith in biosphere object 157_1 is three times the corresponding flux at 11,000 AD for a temperate climate (normal year, Table 7-13). Moreover, the flux from regolith to the surface is more than ten times larger in the permafrost case. As expected, groundwater and overland water flow contribute to stream discharge only during thaw and the relatively short active period when the uppermost part of the regolith is unfrozen.

Table 7-15. Net vertical groundwater fluxes (mm/y) at 5000 AD for biosphere objects north of SFR.

Biosphere object	Object	Mire				Lake			
	Rock to Rego4	Rego4 to Rego3	Rego3 to Rego2	Rego2 to Rego1	Rego1 to surface	Rego4 to Rego3	Rego3 to Rego2	Rego2 to Rego1	Rego1 to surface
157_2	113	114	121	134	433	–	–	–	–
159	33	42	52	59	423	3	6	14	29
157_1	10	17	26	39	14	–1	0	2	26
116	7	7	11	15	4	0	–2	–1	49

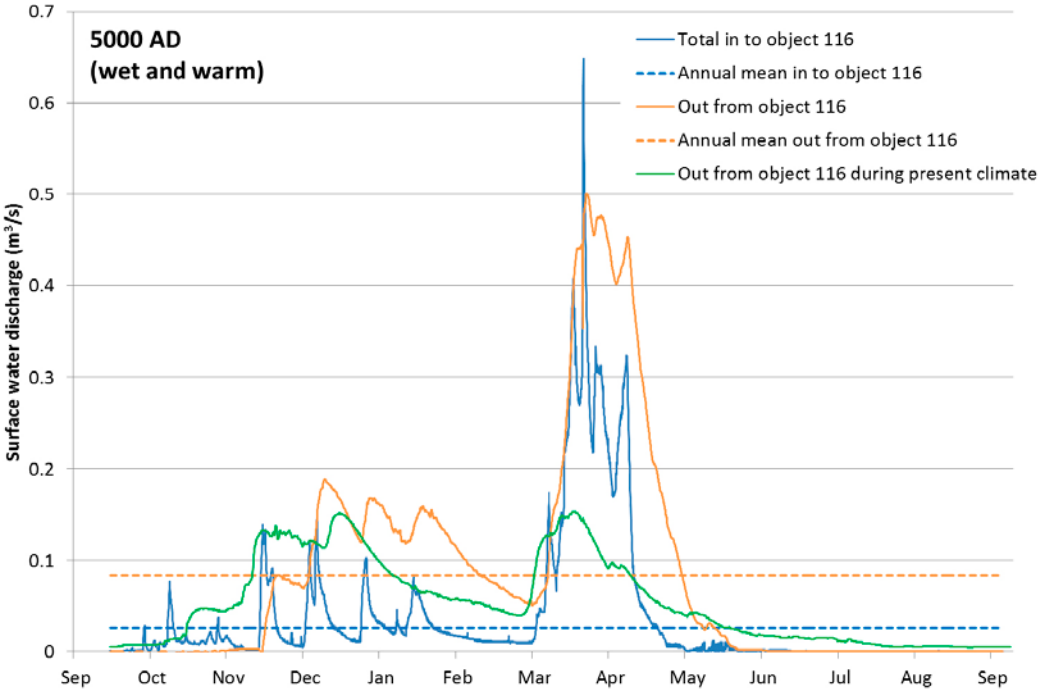

Figure 7-14. *MIKE 11-calculated stream discharges into (blue solid line) and out from (red solid line) biosphere object 116 for a wet and warm climate at 5000 AD. Dotted lines represent corresponding annual averages. For comparison, the figure also shows the corresponding stream discharge out from the object for the normal year (green solid line).*

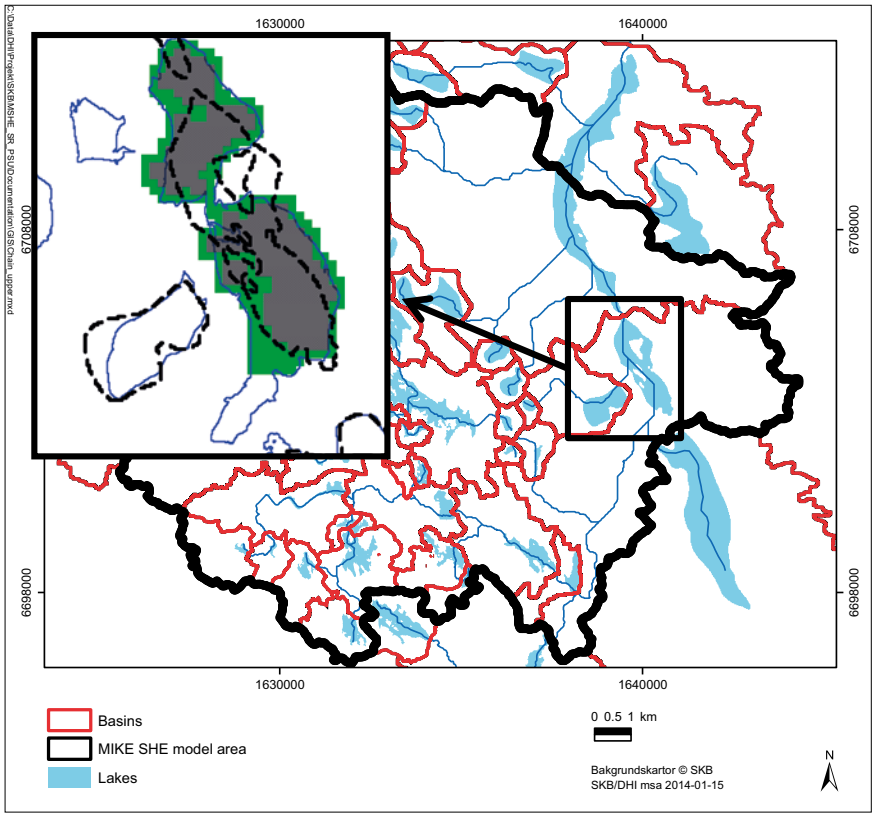

Figure 7-15. *Location of talik object 114 of Bosson et al. (2010) and associated water-balance areas in the present study and in Bosson et al. (2010), respectively. Specifically, the dotted black line is an extension of talik object 114 in the present water balance, whereas the blue line is the corresponding extent used in Bosson et al. (2010). The grey area is the talik defined by Bosson et al. (2010), and the green area is defined as mire for purposes of permafrost simulations.*

Table 7-16. Net vertical groundwater fluxes (mm/y) for all groundwater-discharge taliks, biosphere object 157_1 and talik object 114.

Water-balance area	Object	Mire		Lake	
	Rock to Rego2	Rego2 to Rego1	Rego1 to surface	Rego2 to Rego1	Rego1 to surface
All discharge taliks	8	–	–	9	371
Biosphere object 157_1	31	–	–	31	375
Talik object 114	3	0	–3	4	7

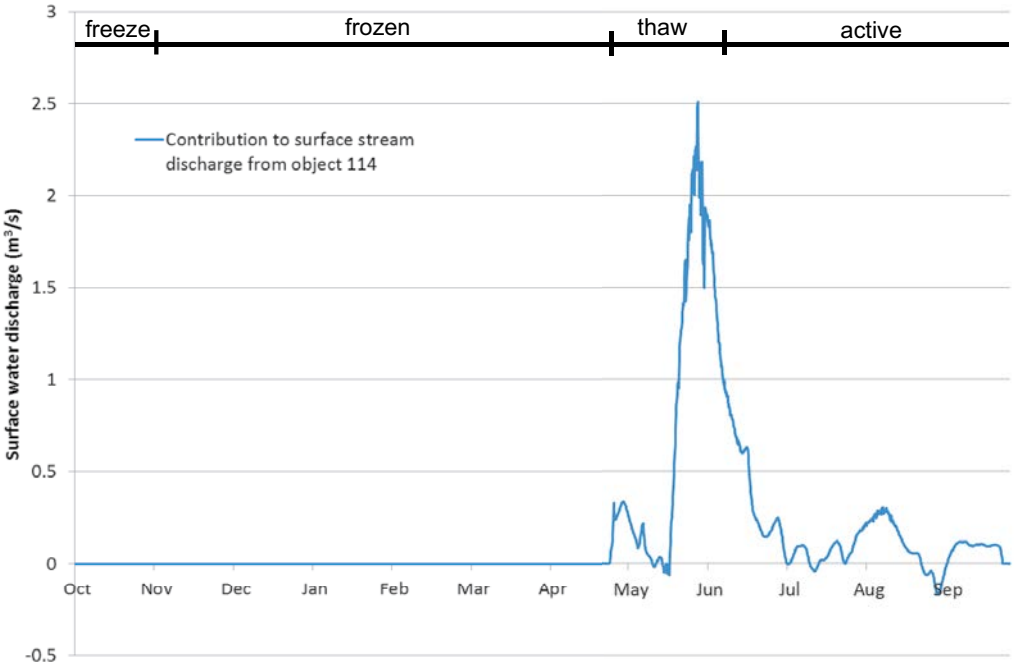

Figure 7-16. *MIKE SHE-calculated contribution to the stream discharge from talik object 114.*

7.5 Extended hydrological analyses of biosphere object 157_2

7.5.1 Water balances of biosphere object 157_2 subareas

In order to study the influence of object delineations, biosphere object 157_2 was divided into subareas for which water balances were extracted and delivered to the radionuclide-transport model. The study was done using the MIKE SHE 5000 AD local model setup to obtain water balances for different, partly coinciding subareas of biosphere object 157_2. Figure 7-17 shows the geographical extent of biosphere object 157_2 and the extents of the analysed subareas. Specifically, the first analysed subarea includes that with upward hydraulic gradients in the regolith, in the upper part of the rock and at c –60 m elevation in the rock (upper left in Figure 7-17). Gradient directions were calculated as the hydraulic-head difference between two adjacent layers, based on annual average hydraulic heads. The second subarea is with a shallow depth (less than 0.25 m) to the groundwater table (upper right), calculated as the annual average depth to the phreatic surface. The third subarea includes potential arable land (lower left), and the fourth analysis (lower right in Figure 7-17) concerns subareas with high discharge-location density at the interface between rock and regolith in the DarcyTools particle-tracking calculations (cf Section 2.3.1). This subarea was delineated based on results of particle releases at the six times 2000, 2500, 3000, 3500, 5000, and 9000 AD, using the base case model BASE_CASE1_DFN_R85 (Odén et al. 2014).

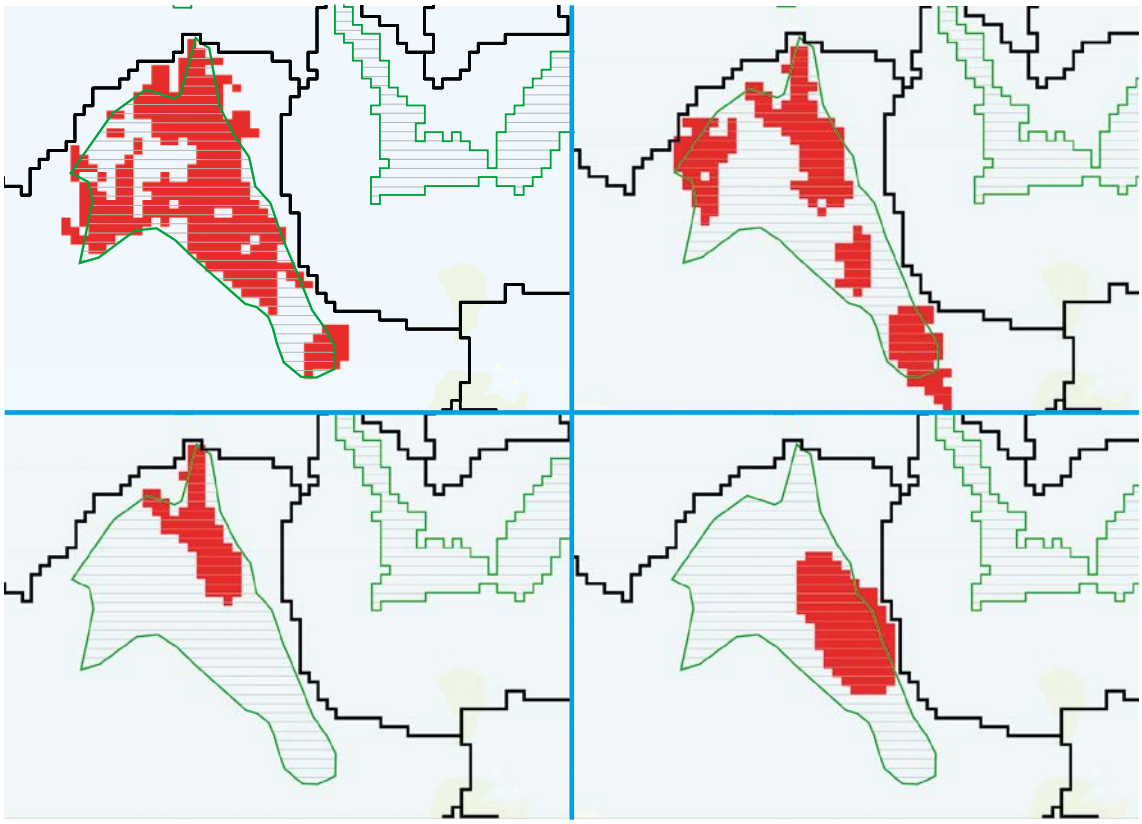

Figure 7-17. *Analysed subareas of biosphere 157_2. Upper left: Subareas with upward hydraulic gradients. Upper right: Subareas with shallow depth to the groundwater table. Bottom left: Subareas with future arable land. Bottom right: Subareas with high discharge-location density at the interface between rock and regolith.*

Table 7-17 exemplifies MIKE SHE-modelling results in terms of net vertical groundwater fluxes (for further results, see Appendix 1). As expected, the largest net vertical groundwater fluxes from rock to regolith are obtained for subareas with upward hydraulic gradients and high discharge-location density. The smallest net flux is obtained for arable land, which is characterised by thick layers of low-permeable regolith. In subareas with shallow depth to the groundwater table, net vertical groundwater fluxes are similar to those obtained for the entire biosphere object. For this subarea, it is also noted that the net flux between the two uppermost layers is significantly larger than for the other analysed subareas, which indicates that water from other parts of the object are directed to this specific subarea.

Table 7-17. Net vertical groundwater fluxes (mm/y) at 5000 AD for different subareas of biosphere object 157_2.

Biosphere object	Object		Mire			
	Area (m^2)	Rock to Rego4	Rego4 to Rego3	Rego3 to Rego2	Rego2 to Rego1	Rego1 to surface
Entire object	167,600	101	102	108	117	208
Upward gradients	132,400	141	142	152	187	264
Shallow gw. table	84,000	98	98	102	104	883
Discharge locations (DT)	47,200	134	136	147	174	596
Arable land	29,200	63	64	68	87	260

7.5.2 Influence of surface-water flow characteristics between biosphere objects 157_2 and 157_1

As mentioned in Section 6.2.3, neither the stream network by Brydsten and Strömgren (2013) nor the MIKE 11 stream network include a stream between biosphere object 157_2 to 157_1. This implies that MIKE SHE transfers surface water from object 157_2 to object 157_1 as overland water. The MIKE SHE 5000 AD model setup for the normal year was used to test an alternative representation of surface-water flow in this area. Specifically, in the MIKE 11 stream network at 5000 AD a stream was added between these two objects (Figure 7-18). The objective of this sensitivity case is to analyse the potential influence of the surface-water flow representation on the water balance of object 157_2.

The results from this sensitivity case show that stream-discharge between objects 157_2 and 157_1 only has minor effects on the water-balance components of biosphere object 157_2 (Appendix 1). Hence, regarding surface-water flow in the area between biosphere objects 157_2 and 157_1, it can be concluded that this area is likely to be rejected as water supply due to practical and water-quality reasons (Section 6.2.3), and that surface-water flow characteristics in this area only have small effects on the water balance of biosphere object 157_2.

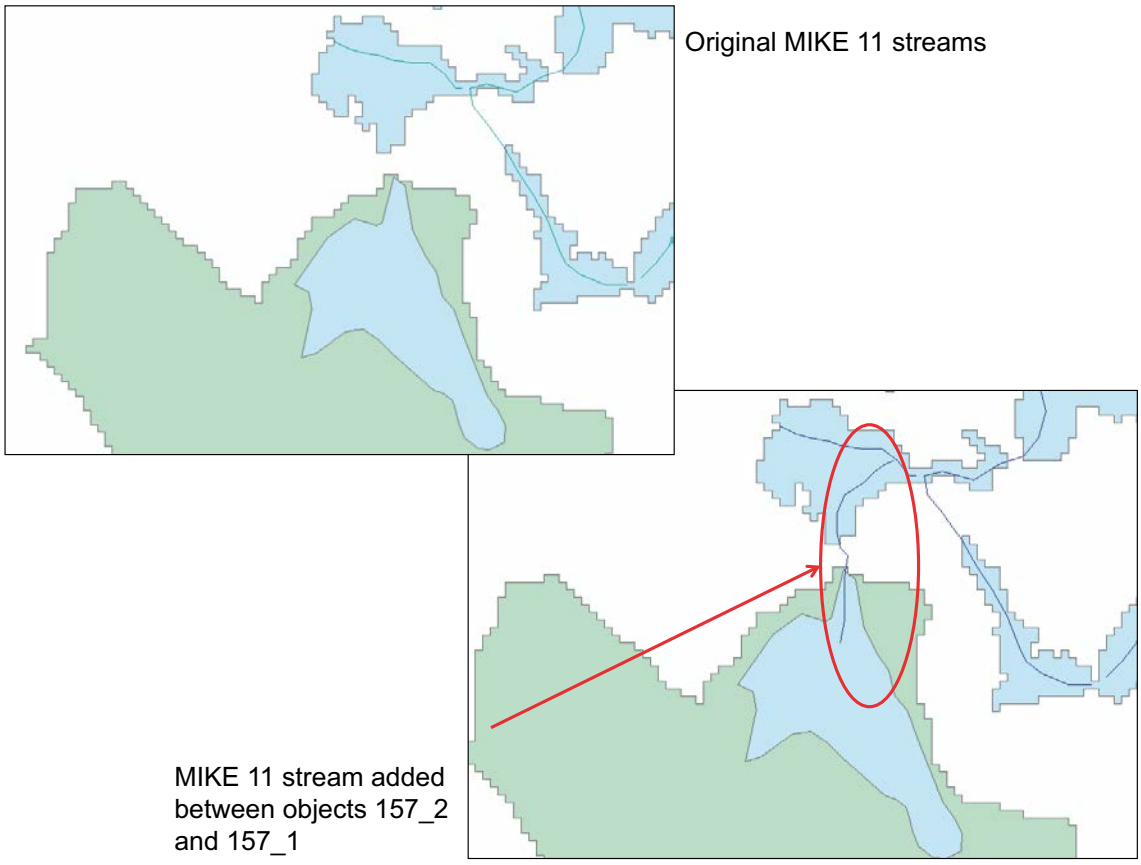

Figure 7-18. *Stream added between biosphere objects 157_2 and 157_1 in the MIKE 11 stream network.*

7.6 Transformation of water-balance components to radionuclide-transport model parameters

As described previously, fluxes obtained from the water-balance tool in MIKE SHE are mapped to relevant compartments of the radionuclide transport model (Figure 7-2). Upward and downward vertical fluxes across regolith layer boundaries are estimated under the assumption that fluxes across calculation layer boundaries, at which MIKE SHE calculates fluxes, change linearly with depth in each MIKE SHE calculation layer. For each biosphere object and time, the calculation of across-boundary fluxes is based on the average regolith thickness for the aquatic (lake) and the terrestrial (mire) part, respectively, for associated times in the dynamic regolith depth and stratigraphy model (Brydsten and Strömgren 2013). Hence, for each biosphere object upward and downward fluxes are calculated to obtain corresponding net fluxes at each regolith-layer boundary at the times 3000, 5000 and 11,000 AD. Using biosphere object 157_1 as an example (Figure 7-19), estimated fluxes across regolith layer boundaries are well balanced (upper right in the figure) and therefore appear to be reasonable.

Moreover, during transition from submerged to terrestrial conditions, biosphere objects are partitioned into lake and mire areas, in the present study represented by the time 5000 AD. In order to calculate vertical groundwater fluxes for each part, i.e. flow per unit area lake or mire, the corresponding flux (mm/y) for the entire object is scaled according to relative sizes of lake and mire areas (bottom left in Figure 7-19). In total, parameters representing 27 inter-compartment water fluxes (bottom right in Figure 7-19) are derived based on delivered results from the water-balance tool in MIKE SHE, and implemented in the radionuclide-transport modelling for the future times described above.

So called RTR (relative transfer rates) have been calculated to assess whether horizontal fluxes between regolith compartments, below the uppermost layers, for simplicity can be excluded in calculations of radionuclide transport in the regolith. Table 7-18 shows RTR for MIKE SHE calculation layers, based on the delivered MIKE SHE water balances and layer thicknesses. TR (transfer rate) is defined as groundwater flux (volumetric flow divided by cross-sectional area) divided by porosity-scaled distance (distance times porosity), whereas RTR is the ratio between TR in the vertical and horizontal directions. RTR for a certain layer is calculated using the upward flux from the lower layer boundary and the average horizontal flux from either the outer boundary towards the lake (Table 7-18, part A) or the flux out of the object (part B). Horizontal radial extents are approximated using sizes of mires areas and the total sizes of biosphere objects, assuming either a centrally located lake and circular geometries (part A) or no lake (part B).

Except for the uppermost calculation layers (i.e. surface water in lakes and overland water in terrestrial areas), according to MIKE SHE particle-tracking simulations vertical advective travel times in the regolith are typically 2–3 orders of magnitude shorter than horizontal travel times. Consequently, groundwater TR and the corresponding transfer rate of groundwater-carried radionuclides, is dominated by vertical groundwater flow (Table 7-18, part A). Therefore, the analysis shows that horizontal fluxes between regolith compartments below the uppermost layers can for simplicity be excluded in calculations of radionuclide transport in the regolith.

The exclusion of downwards and outgoing horizontal groundwater fluxes is cautious in a safety assessment perspective, because it implies that groundwater-carried export of radionuclides from biosphere objects is excluded from the analysis. However, it is less cautious in terms of horizontal fluxes, as the vertical groundwater transfer rates in those groundwater-discharge areas that receive the largest part of radionuclides are 3–4 orders of magnitude larger than horizontal transfer rates (Table 7-18, part B). Moreover, exclusion of downwards fluxes from the deepest regolith layer (RegoLow) is obviously consistent with the conceptual model of groundwater-carried transport of radionuclides from the geosphere to the biosphere (Saetre et al. 2013b).

As mentioned above, parameters representing 27 inter-compartment water fluxes are calculated and delivered to the radionuclide-transport modelling for the future times described above, using the water-balance tool in MIKE SHE. Table 7-19 lists these parameters, which are divided into the four categories marine, limnic and terrestrial systems and surface-water flows. The parameter names follow inter-compartment fluxes. For instance, the *q_low_gl_sea* parameter is the water flux (*q_*) from the RegoLow (*low_*) to the RegoGL (*gl_*) for the marine period (*sea*).

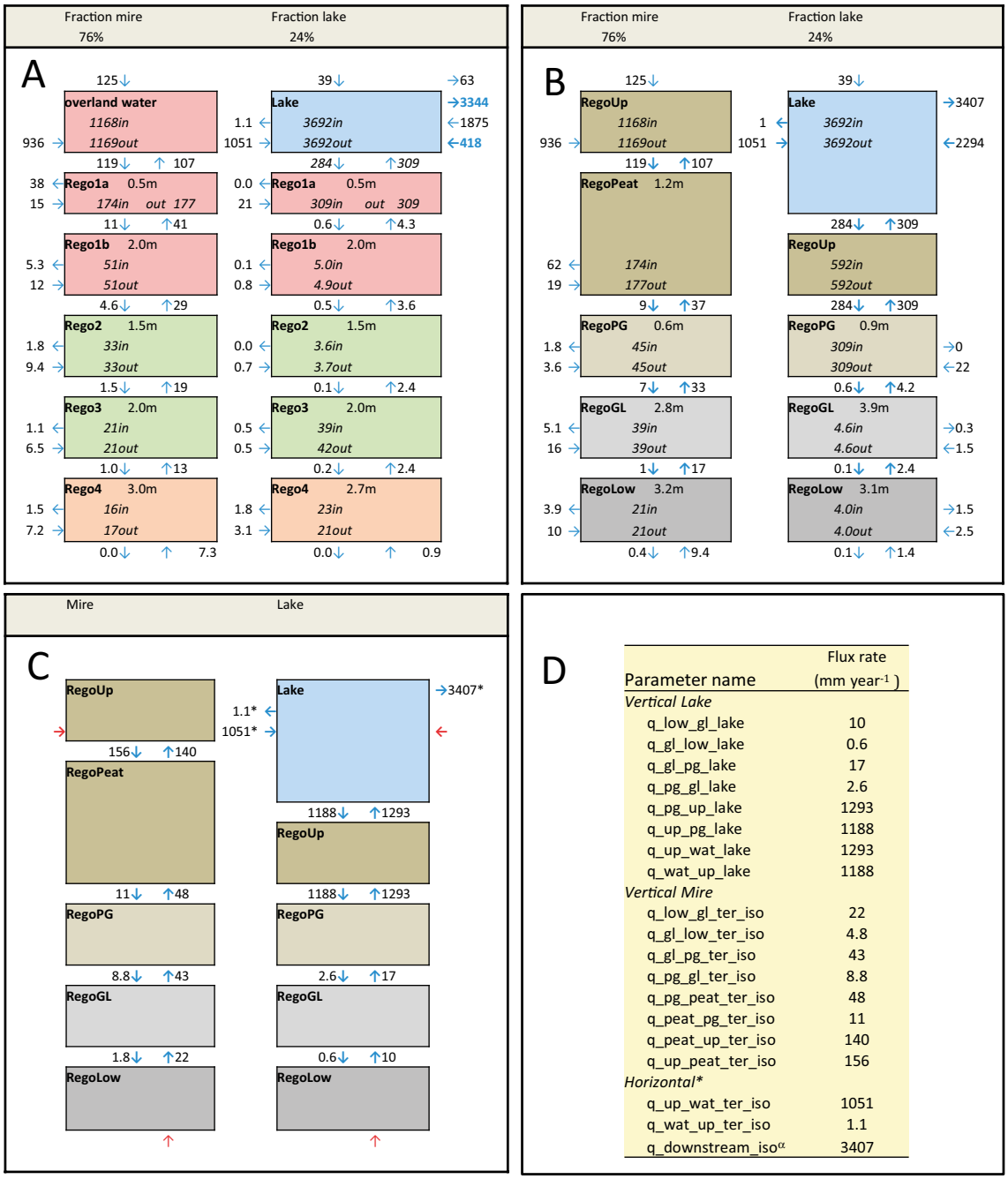

Parameter name	Flux rate (mm year^{-1})
Vertical Lake	
q_low_gl_lake	10
q_gl_low_lake	0.6
q_gl_pg_lake	17
q_pg_gl_lake	2.6
q_pg_up_lake	1293
q_up_pg_lake	1188
q_up_wat_lake	1293
q_wat_up_lake	1188
Vertical Mire	
q_low_gl_ter_iso	22
q_gl_low_ter_iso	4.8
q_gl_pg_ter_iso	43
q_pg_gl_ter_iso	8.8
q_pg_peat_ter_iso	48
q_peat_pg_ter_iso	11
q_peat_up_ter_iso	140
q_up_peat_ter_iso	156
*Horizontal**	
q_up_wat_ter_iso	1051
q_wat_up_ter_iso	1.1
q_downstream_iso$^{\alpha}$	3407

Figure 7-19. *Calculation of water fluxes (mm/y) across regolith layer boundaries. A) MIKE SHE-calculated water-balance components for biosphere object 157_1 at 5000 AD. B) Estimated across-layer fluxes. C) Fluxes delivered to the radionuclide transport modelling, scaled according to relative sizes of lake and mire areas. Red arrows represent potential release pathways for radionuclides (surface water from object 157_2 or groundwater discharge from the rock). D) Parameter names and associated inter-compartment water fluxes delivered to the radionuclide transport modelling (cf Table 7-19). used in the radionuclide model. *Horizontal surface-water fluxes retain original units (fluxes are scaled per unit object area).*

Table 7-18. Relative transfer rate (RTR) of groundwater for MIKE SHE calculation layers. A) RTR for mire areas of lake-mire complexes in the early terrestrial period (5000 AD). B) RTR for biosphere object 157_2 for the submerged period (3000 AD), and early and late terrestrial periods (5000 and 11,000 AD).

A (5000 AD)		Relative transfer rate, $TR_{vertical}/TR_{horizontal}$ ($year^{-1}/year^{-1}$)			
Object	Horizontal extent (m)	Rego1a (0.5 m)	Rego1b (2 m)	Rego2 (1.5 m)	Rego3 (2 m)
116	170	$4.4 \cdot 10^2$	$1.7 \cdot 10^2$	$3.1 \cdot 10^2$	$3.0 \cdot 10^2$
121_1	140	$5.3 \cdot 10^2$	$7.3 \cdot 10^2$	$1.1 \cdot 10^3$	$6.9 \cdot 10^2$
157_1	90	$4.1 \cdot 10^2$	$2.1 \cdot 10^2$	$2.3 \cdot 10^2$	$1.7 \cdot 10^2$
159	130	$2.3 \cdot 10^2$	$1.8 \cdot 10^2$	$2.4 \cdot 10^2$	$2.4 \cdot 10^2$
160	160	$1.2 \cdot 10^3$	$2.1 \cdot 10^2$	$3.2 \cdot 10^2$	$4.1 \cdot 10^2$
B (biosphere object 157_2)					
Period					
Submerged	230	N.A.	N.A.	$1.7 \cdot 10^4$	$6.2 \cdot 10^3$
Early terrestrial	230	$6.4 \cdot 10^3$	$2.3 \cdot 10^3$	$1.0 \cdot 10^4$	$2.2 \cdot 10^4$
Late terrestrial	230	$6.6 \cdot 10^3$	$3.6 \cdot 10^3$	$1.6 \cdot 10^4$	$2.5 \cdot 10^4$

Table 7-19. List of parameters representing inter-compartment water fluxes in marine, limnic and terrestrial systems, water fluxes between terrestrial and limnic compartments (q_up_wat_ter, q_wat_up_ter) and fluxes out from biosphere objects (q_downstream).

Marine (sea)	Limnic (lakes)	Terrestrial	Surface
q_low_gl_sea	q_low_gl_lake	q_low_gl_ter	q_up_wat_ter
q_gl_low_sea	q_gl_low_lake	q_gl_low_ter	q_wat_up_ter
q_gl_pg_sea	q_gl_pg_lake	q_gl_pg_ter	q_downstream
q_pg_gl_sea	q_pg_gl_lake	q_pg_gl_ter	
q_pg_up_sea	q_pg_up_lake	q_pg_peat_ter	
q_up_pg_sea	q_up_pg_lake	q_peat_pg_ter	
q_up_wat_sea	q_up_wat_lake	q_peat_up_ter	
q_wat_up_sea	q_wat_up_lake	q_up_peat_ter	

The blue arrows in Figure 7-2 are represented by the parameters in the second (limnic), third (terrestrial) and fourth (surface) columns of Table 7-19. The parameter names for the vertical fluxes follow the same system as for the marine phase. The only difference between marine and limnic parameter names is the suffix, *sea* vs. *lake*. For terrestrial systems, there is a difference in the layer description above the RegoPG compared to aquatic systems. Specifically, terrestrial systems has a peat compartment between the RegoGL and the RegoUp compartments, whereas aquatic systems have a surface-water compartment above the RegoUp compartment.

The parameter names for terrestrial systems are given in the same way as for marine and limnic systems, with the suffix *ter*. The surface-water parameters describe fluxes between limnic and terrestrial systems (*q_up_wat_ter* and *q_wat_up_ter*) as well as fluxes going out from the biosphere object (*q_downstream*). For biosphere objects that are transformed to mires subsequent to emergence (no lake), i.e. objects 121_2 and 157_2, the only vertical fluxes considered are those in the terrestrial part (left side of Figure 7-2), with parameter names according to the third column of Table 7-19. For these objects also the surface-water flux parameter *q_downstream* (fourth column) is used for describing the outflow to downstream objects.

For the time 11,000 AD, vertical fluxes in terrestrial systems (left side of Figure 7-2) are delivered to the radionuclide-transport modelling, with parameter names according to the third column of Table 7-19. At this time, in the radionuclide-transport modelling a stream remains in biosphere objects with a former lake (objects 116, 121_2, 157_1, 159 and 160). For these objects, also the surface-water flux parameters in the fourth column of Table 7-19 are delivered. The parameters *q_up_wat_ter* and *q_wat_up_ter* then represent surface-water fluxes between the terrestrial system and the stream. Also in this case, the *q_downstream* parameter represents the water flux exiting the biosphere object.

8 Summary and conclusions

8.1 Modelling and results for present conditions

Quality check and calibration of the regional MIKE SHE model were performed by comparing modelling results with monitoring data on groundwater levels in regolith and rock, surface-water levels and stream discharges. As part of this process, some adjustments were made of the initial MIKE SHE model setup, including increase of the hydraulic conductivity of gyttja/clay gyttja and increase of the hydraulic conductivity of glacial clay below some of the lakes.

The present MIKE SHE model setup underestimates surface-water levels and stream discharges, and they are also lower than those of the SDM-Site and SR-Site model setups (Bosson et al. 2008, 2010). In particular, the model-calculated accumulated stream discharge downstream of Lake Eckarfjärden is c 80% of the measured accumulated discharge, whereas the corresponding result was 87% in SDM-site and 112% in SR-Site. Part of this stream-discharge deficit is propagated to the inlet to Lake Bolundsfjärden, which is located downstream of Lake Eckarfjärden. Lake Eckarfjärden is located close to the upstream boundary of the MIKE SHE regional model area, i.e. relatively far from SFR. It is therefore judged that the stream-discharge deficit at Lake Eckarfjärden has minor or no effects for the hydrological conditions at SFR and downstream areas in the modelling of future conditions (Section 8.2).

In terms of groundwater levels in regolith, the averages of MAE (mean absolute error) and ME (mean error), respectively, of all considered groundwater-monitoring wells in regolith are similar to the those of SR-Site. However, there are some differences between model setups for individual wells. For instance, due to differences in the local topography, as described by the DEM, the MAE for groundwater-monitoring well SFM0036 is twice that of SR-Site. Specifically, in the present model setup the ground-surface elevation at SFM0036 is c 0.4 m lower than that of SR-Site. Both model setups include subsurface drainage at 0.5 m below ground, acting as a drainage for the groundwater level in regolith. The model-calculated groundwater level in SFM0036 is above the drainage level during two periods, associated with high sea levels in January, 2005 and January, 2007. The averages of MAE and ME, respectively, of all considered percussion boreholes in rock are lower (closer to zero) in the present model setup than that of Bosson et al. (2010), and model-calculated gradients between rock and regolith match drill-site observations.

In summary, it is judged that the present-day MIKE SHE model setup is able to reproduce monitoring data with sufficient accuracy, as a basis for models of future conditions. However, as indicated above there are some issues that may have to be investigated further prior to use in other model applications, in particular the stream-discharge deficit at Lake Eckarfjärden.

8.2 Modelling and results for future conditions

MIKE SHE models representing future conditions were set up for times 3000, 5000, and 11,000 AD. At 3000 AD, the coastline is located immediately downstream of SFR. 5000 AD represents an intermediate stage, with co-existing lakes and mires within the regional MIKE SHE model area, whereas at 11,000 AD all former lakes within the MIKE SHE regional model area are infilled. For each time, a regional model was set up to provide initial and boundary conditions to a local model that includes delineated biosphere objects, i.e. areas that may be affected by released radionuclides from SFR.

Modelling results show that when the shoreline is located some distance downstream from a certain land area, landscape development has larger, but still not dramatic, effects on the water balance compared to shoreline displacement. Permafrost influences the spatial distribution of groundwater recharge and discharge areas, and also the water exchange and flow paths between unfrozen layers below and above the permafrost.

Delineations of biosphere objects are inputs to the MIKE SHE modelling, as they define areas for extractions of water-balance and water-flow components required for modelling of radionuclide transport in the biosphere. Seven biosphere objects are delineated, based on DarcyTools particle-tracking

simulations and also other types of information related to landscape development. In the DarcyTools modelling, most particles released from SFR 1 discharge at the interface between rock and regolith in biosphere object 157_2, which is located within a low-lying area north of SFR 1, in the vicinity of the junction between two steeply dipping deformation zones. Discharge locations for particles released from SFR 3 are located north of the SFR facility but also southeast of SFR 3, which likely is due to the influence of the SFR pier on groundwater flow in the vicinity of SFR.

At 3000 AD, all biosphere objects are submerged and net vertical groundwater fluxes are generally small. At 5000 AD, all objects are emerged and there are large differences between objects in terms of net fluxes from rock to regolith. The largest net flux is noted for biosphere object 157_2. At 11,000 AD, all objects are transformed to mires. Figure 8-1 summarises net vertical fluxes (mm/y, positive for upward fluxes) at the times 3000, 5000 and 11,000 AD for the seven biosphere objects, between rock and regolith (left figure) and between the two calculation layers in regolith directly above rock (right figure). The largest net-flux increase between rock and regolith occurs 3000–5000 AD, i.e. during transition from submerged to emerged conditions. During the period 5000–11,000 AD, there are different net-flux changes for different biosphere objects. For instance, there is a net-flux decrease for object 160 and to a lesser exent also for object 121_1.

Although less pronounced compared to the period 3000–5000 AD, net fluxes increase between 5000 and 11,000 AD for the other five biosphere objects. In particular, net fluxes are largest for biosphere object 157_2 (more than 100 mm/y) at 5000 and 11,000 AD. Similar to the water-balance results (see above), the results show relatively small effects of shoreline displacement when the shoreline is located some distance downstream of objects.

Figure 8-2 shows the topography (upper figures) and MIKE SHE-calculated annual average vertical hydraulic-head differences in the regolith at biosphere object 160 at the times 3000, 5000 and 11,000 AD. At 3000 AD, when the object is submerged but close to the shoreline, there are weak upward hydraulic-head gradients in the regolith of object 160, and the annual average net vertical flux from the rock to the regolith is 1.4 mm (Figure 8-1). At 5000 AD, there is a lake surrounded by mire in the object and the shoreline is far away, whereas at 11,000 AD the lake is infilled. According to Figure 8-2, landscape development and associated topographic changes change the patterns of areas with upward and downward hydraulic-head gradients at the object. On an annual basis, there are downward hydraulic-head gradients in the regolith below almost the whole of biosphere object 160 at 11,000 AD (upward-downward hydraulic-head patterns change during the year).

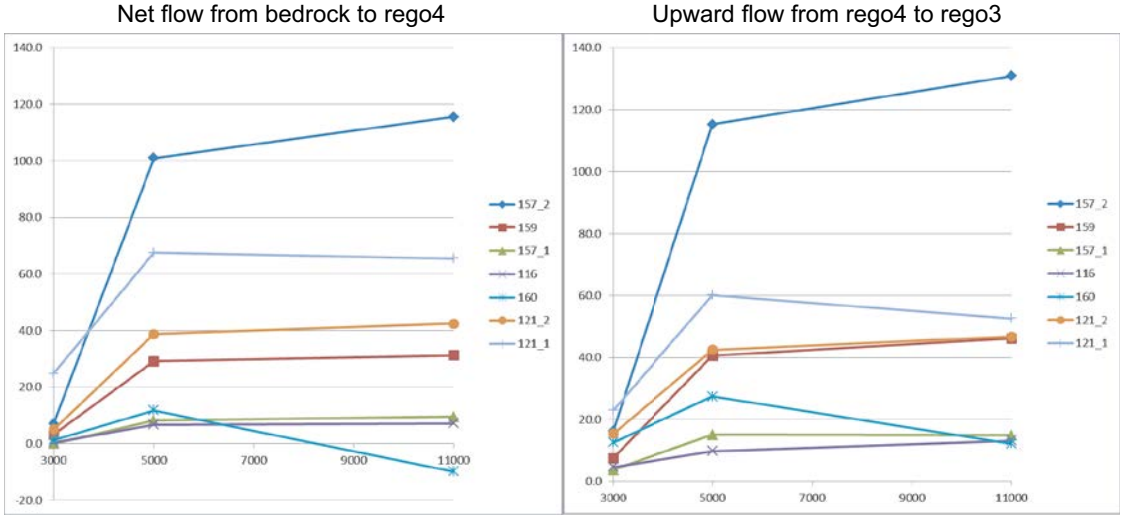

Figure 8-1. *Net vertical fluxes (mm/y, positive for upward fluxes) between MIKE SHE calculation layers below biosphere objects at 3000, 5000 and 11,000 AD. The left figure shows net fluxes between rock and regolith, whereas the right figure shows net fluxes between the two calculation layers in regolith directly above rock.*

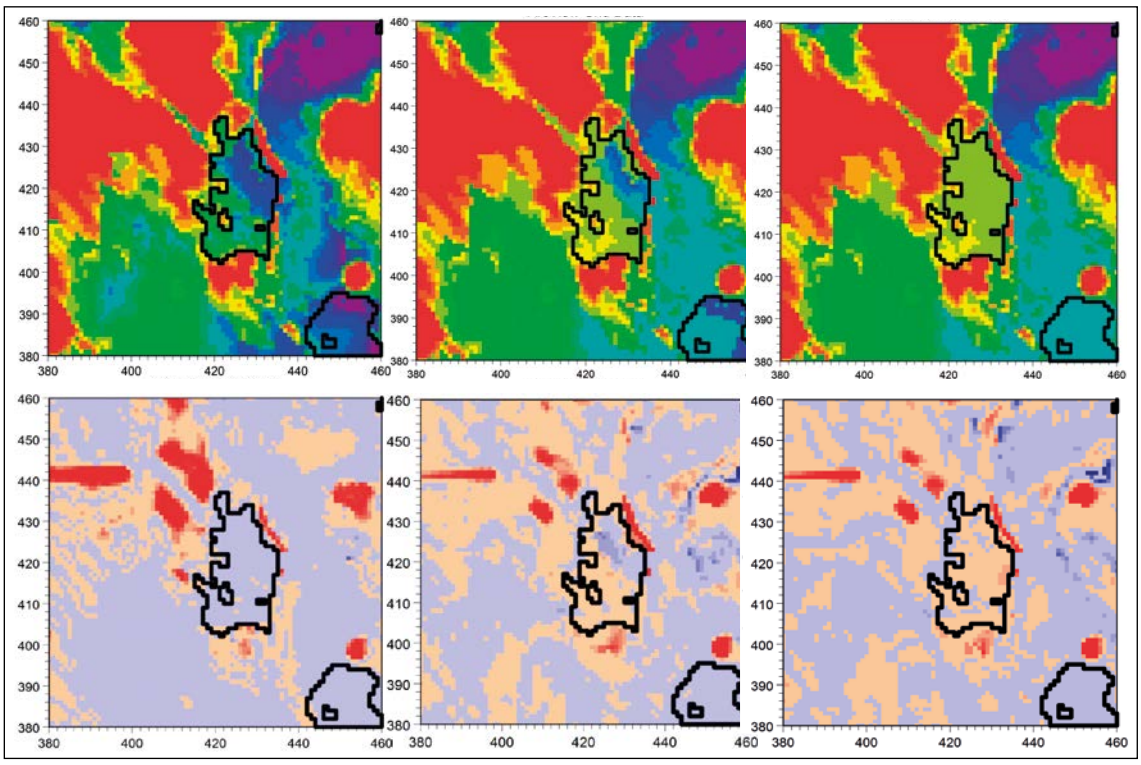

Figure 8-2. *Topography (upper figures) and MIKE SHE-calculated annual average vertical hydraulic-head differences in regolith (lower figures) at biosphere object 160 at the times 3000, 5000, and 11,000 AD. In the upper figures, red colours represent higher-elevated areas and blue colours represent lower-lying areas. In the lower figures, red colours represents areas with downward hydraulic-head gradients, whereas blue colours represent areas with upward hydraulic-head gradients.*

A sensitivity analysis was performed to investigate effects of different subarea divisions of biosphere object 157_2. Figure 8-3 shows MIKE SHE-calculated upward vertical fluxes (mm/y, left figure) and flows (m^3/y, right figure) as function of depth for the sensitivity cases. These include subareas with upward hydraulic-head gradients in rock and regolith, subareas with shallow groundwater table (less than 0.25 m below ground), potential arable land, and subareas with high discharge-location density from DarcyTools calculations (the originally delineated area is denoted Basecase in the figure).

As expected, the largest upward fluxes (left figure) from rock to regolith are obtained for subareas with upward hydraulic hydraulic-head gradients and high discharge-location density. As the latter subarea is small, there is less upward flow (flux times the size of the area) in this subarea compared to the entire object. The vertical flux in subareas with shallow groundwater table is similar as that for the entire object, whereas upward flow (right figure) close to the ground surface is significantly larger than for the other analysed subareas. This indicates that groundwater from other parts of the object are directed to these subareas. The smallest upward flux and flow are obtained for potential arable land, characterised by thick layers of low-permeable regolith.

Agriculture is a main food contributor for future, self-sufficient agricultural communities in the Forsmark landscape. The proportion of potential arable land will likely increase in the future as the broad and presently submerged Öregrundsgrepen valley is uplifted, and parts of the resulting shallow wetlands can probably be relatively easily drained and cultivated. The report presents conceptual description of water flow in agricultural land and parameterisations of percolation and groundwater uptake, i.e. downward and upward groundwater flow in the regoUp compartment that represents a biologically active layer above the groundwater table. Drainage depth and drainage-induced subsidence are also described, whereas some hydrological effects of drainage are not taken into account in the SR-PSU project.

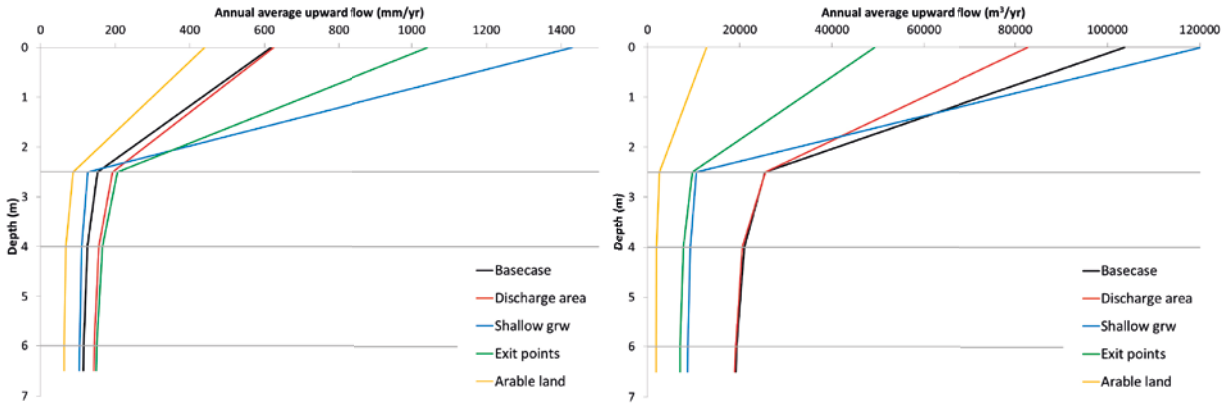

Figure 8-3. *MIKE SHE-calculated upward fluxes (mm/y, left) and flows (m^3/y, right) as function of depth for different subareas of biosphere object 157_2.*

The report describes future water uses and supplies for future, self-sufficient communities in the Forsmark landscape, and it presents results of conceptual and quantitative modelling of radionuclide transport to wells in regolith and wells drilled in rock. Based on these descriptions and results, the report provides approaches for identification of a representative of the most exposed group and for calculation of associated radiological exposure for the community types hunter-gatherers, infield-ouland farmers, modern farmers, and garden-plot households.

References

SKB's (Svensk Kärnbränslehantering AB) publications can be found at www.skb.se/publications. References to SKB's unpublished documents are listed separately at the end of the reference list. Unpublished documents will be submitted upon request to document@skb.se.

Agerstrand T, 1968. Ground water draft from earth layers. In Ground water problems: Proceedings of the International Symposium, Stockholm, October 1966. Oxford: Pergamon Press, 181–195.

Alinder S, 1984. Alternativa bevattningsformer: 1. Bevattningsramp. Rapport 141, Institutionen för markvetenskap, Sveriges Lantbruksuniversitet, Uppsala. (In Swedish.)

Alinder S, 1986. Alternativa bevattningsformer: 2. Reglering av grundvattennivån. Rapport 150, Institutionen för markvetenskap, Sveriges Lantbruksuniversitet, Uppsala. (In Swedish.)

Andersson C, 2009. Järnåldersboplatser och historiska byar: En studie av agrara bebyggelsemönster i mälarbygder under 1500 år. Bachelor thesis. Södertörn University. (In Swedish, with abstract in English.)

Andersson E (ed), 2010. The limnic ecosystems at Forsmark and Laxemar-Simpevarp. SR-Site Biosphere. SKB TR-10-02, Svensk Kärnbränslehantering AB.

Andersson M P, Woessner W W, 1992. Applied groundwater modeling: simulation of flow and advective transport. San Diego, CA: Academic Press.

Antoine J M, Magliola C, Counzy F, Darret G, Marechi J P, 1986. Estimation of the share of each water source for adults in France. Water intake provided to French adults. Annals of Nutrition & Metabolism 30, 407–414.

Aquilonius K (ed), 2010. The marine ecosystems at Forsmark and Laxemar-Simpevarp. SR-Site Biosphere. SKB TR-10-03, Svensk Kärnbränslehantering AB.

Armstrong B, 1985. Bevattning: en global översikt. Uppsala: Sveriges Lantbruksuniversitet. (Meddelande 85:7, Institutionen för markvetenskap, Avdelningen för lantbrukets hydroteknik) (In Swedish.)

Atlas Copco, 2012. Blasthole drilling in open pit mining. 3rd ed. Garland, TX: Atlas Copco Drilling Solutions LLC.

Avila R, Bergström U, 2006. Methodology for calculation of doses to man and implementation in Pandora. SKB R-06-68, Svensk Kärnbränslehantering AB.

Axelsson C-L, Byström J, Eriksson Å, Holmén J, Haitjema H M, 1991. Hydraulic evaluation of the groundwater conditions at Finnsjön. The effects on dilution in a domestic well. SKB TR 91-54, Svensk Kärnbränslehantering AB.

Ayars J E, Christen E W, Soppe R W, Meyer W S, 2006. The resource potential of in situ shallow ground water use in irrigated agriculture – a review. Irrigation Science 24, 147–160.

Beheim E, 2006. The effect of peat land drainage and afforestation on runoff dynamics: consequences on floods in the Glomma River. In Krecek J, Haigh M (eds). Environmental role of wetlands in headwaters. Dordrecht: Springer. (NATO Science Series IV: Earth and Environmental Sciences 63), 59–75.

Bjerketorp A, Johnson L, 1986. Kalhuggningens och skogsdikningens inflytande på vattendragens flöden: en kortfattad kunskapsöversikt. Avdelningsmedd. 86:2, Institutionen för markvetenskap, Sveriges Lantbruksuniversitet, Uppsala. (In Swedish.)

Bosson E, Gustafsson L-G, Sassner M, 2008. Numerical modelling of surface hydrology and near-surface hydrogeology at Forsmark. Site descriptive modelling, SDM-Site Forsmark. SKB R-08-09, Svensk Kärnbränslehantering AB.

Bosson E, Sassner, Sabel U, Gustafsson L-G, 2010. Modelling of present and future hydrology and solute transport at Forsmark. SR-Site Biosphere. SKB R-10-02, Svensk Kärnbränslehantering AB.

Bosson E, Sabel U, Gustafsson L-G, Sassner M, Destouni G, 2012. Influences of shifts in climate, landscape, and permafrost on terrestrial hydrology. Journal of Geophysical Research 117, D05120. doi:10.1029/2011JD016429

Bosson E, Selroos J-O, Stigsson M, Gustafsson L-G, Destouni G, 2013. Exchange and pathways of deep and shallow groundwater in different climate and permafrost conditions using the Forsmark site, Sweden, as an example catchment. Hydrogeology Journal 21, 225–237.

Bowman I, 1911. Well-drilling methods. Water-Supply Paper 257, U.S. Geological Survey.

Bradbury K R, Rotschild E R, 1985. A computerized technique for estimating the hydraulic conductivity of aquifers from specific capacity data. Groundwater 23, 240–246.

Brydsten L, Strömgren M, 2004. Forsmark site investigation. Measurements of brook graients and lake thresholds. SKB P-04-141, Svensk Kärnbränslehantering AB.

Brydsten L, Strömgren M, 2013. Landscape development in the Forsmark area from the past into the future (8500 BC – 40000 AD). SKB R-13-27, Svensk Kärnbränslehantering AB.

Carlie A (ed), 2005. Skånska spår – arkeologi längs Västkustbanan. In Järnålder vid Öresund. Band 1, Specialstudier och syntes. Lund: Riksantikvarieämbetet UV-Syd. (In Swedish.)

Carlsson A, Christiansson R, 2007. Construction experiences from underground works at Forsmark. Compilation report. SKB R-07-10, Svensk Kärnbränslehantering AB.

Chahar B R, Vadodaria G P, 2008. Drainage of ponded surface by an array of ditches. Journal of Irrigation and Drainage Engineering 134, 815–823.

Cooke R A, Badiger S, García A M, 2001. Drainage equations for random and irregular tile drainage systems. Agricultural Water Management 48, 207–224.

Curtis P, Markström I, Petersson J, Triumf C-A, Isaksson H, Mattsson H, 2011. Site investigation SFR. Bedrock geology. SKB R-10-49, Svensk Kärnbränslehantering AB.

Dahlgren L, 1974. Grundvattentäkter för bevattning. Stenciltryck 84, Institutionen för markvetenskap, Avdelningen för lantbrukets hydroteknik, Sveriges Lantbruksuniversitet, Uppsala. (In Swedish.)

DHI Software, 2010. MOUSE Pipe Flow – Reference manual. DHI Water & Environment, Hørsholm, Denmark.

DHI Software, 2012. MIKE SHE: user manual. DHI Water & Environment, Hørsholm, Denmark.

Elhammer A, Sandkvist Å, 2005. Forsmark site investigation. Detailed marine geological survey of the sea bottom outside Forsmark. SKB P-03-101, Svensk Kärnbränslehantering AB.

Engqvist P, Olsson T, 1974. Försök att ur återhämtningskurvor beräkna moränbrunnars kapacitet. Preliminär rapport. Vannet i Norden 4, 21–34. (In Swedish.)

Engqvist P, Olsson T, Svensson T, 1978. Pumping and recovery tests in wells sunk in till. In Proceedings of Nordic Hydrological Conference and Second Nordic IHP meeting, Hanasaari, Finland, 31 July – 3 August 1978, 134–142.

Ershow A G, Cantor K P, 1989. Total water and tapwater intake in the United States: population-based estimates of quantities and sources. Bethesda, MD: Life Sciences Research Office, Federation of American Societies for Experimental Biology.

Feddes R A, 1971. Water, heat and crop growth. PhD thesis. Wageningen University, the Netherlands. (Mededelingen Landbouwhogeschool Wageningen 71-12)

Follin S, 2008. Bedrock hydrogeology Forsmark. Site descriptive modelling, SDM-Site Forsmark. SKB R-08-95, Svensk Kärnbränslehantering AB.

Frampton A, Painter S, Lyon S W, Destouni G, 2011. Non-isothermal, three-phase simulations of near-surface flows in a model permafrost system under seasonal variability and climate change. Journal of Hydrology 403, 352–359.

Frampton A, Painter S L, Destouni G, 2013. Permafrost degradation and subsurface-flow changes caused by surface warming trends. Hydrogeology Journal 21, 271–280.

French H M, 2007. The periglacial environment. 3rd ed. Chichester: John Wiley & Sons Ltd.

Galili E, Weinstein-Evron M, Hershkovitz I, Gopher A, Kislev M, Lernau O, Kolska-Horwitz L, Lernau H, 1993. Atlit-Yam: a prehistoric site on the sea floor off the Israeli coast. Journal of Field Archaeology 20, 133–157.

Ge S, McKenzie J, Voss C, Wu Q, 2011. Exchange of groundwater and surface-water mediated by permafrost response to seasonal and long term air temperature variation. Geophysical Research Letters 38, L14402. doi:10.1029/2011GL047911

Gentzschein B, Levén J, Follin S, 2007. A comparison between well yield data from the site investigation in Forsmark and domestic wells in northern Uppland. SKB P-06-53, Svensk Kärnbränslehantering AB.

Gillham R W, 1984. The capillary fringe and its effect on water-table response. Journal of Hydrology 67, 307–324.

Gleick P H, 1996. Basic water requirements for human activities: meeting basic needs. Water International 21, 83–92.

Graham D N, Butts M B, 2005. Flexible, integrated watershed modelling with MIKE SHE. In Singh V P, Frevert D K (eds). Watershed models. Boca Raton, FL: CRC Press, 245–272.

Grenier, C, Régnier D, Mouche E, Benabderrahmane H, Costard F, Davy, P, 2013. Impact of permafrost development on groundwater flow patterns: a numerical study considering freezing cycles on a two-dimensional vertical cut through a generic river-plain system. Hydrogeology Journal 21, 257–270.

Grip H, Rodhe A, 1994. Vattnets väg från regn till bäck. 3rd ed. Uppsala: Hallgren & Fallgren. (In Swedish.)

Grolander S, 2013. Biosphere parameters used in radionuclide transport modelling and dose calculations in SR-PSU. SKB R-13-18, Svensk Kärnbränslehantering AB.

Gustafsson Y, 1955. Några historiska notiser om dikning. Grundförbättring 8, 73–101. (In Swedish.)

Hallgren G, 1955. Forskning och teknisk utveckling på bevattningens område – en översikt. Grundförbättring 8, 190–222.

Hartikainen J, Kouhia R, Wallroth T, 2010. Permafrost simulations at Forsmark using a numerical 2D thermo-hydro-chemical model. SKB TR-09-17, Svensk Kärnbränslehantering AB.

Hedenström A, Sohlenius G, 2008. Description of the regolith at Forsmark. Site descriptive modelling, SDM-Site. SKB R-08-04, Svensk Kärnbränslehantering AB.

Hedenström A, Sohlenius G, Strömgren M, Brydsten L, Nyman H, 2008. Depth and stratigraphy of regolith at Forsmark. Site descriptive modelling, SDM-Site Forsmark. SKB R-08-07, Svensk Kärnbränslehantering AB.

Hoekstra A Y, Chapagain A K, 2007. Water footprint of nations: water use by people as a function of their consumption pattern. Water Resources Management 21, 35–48.

Holden J, Evans M G, Burt T P, Horton M, 2006. Impact of land drainage on peatland hydrology. Journal of Environmental Quality 35, 1764–1778.

Holmén J G, 2005. SFR-1. Inverse modelling of inflow to tunnels and propagation of estimated uncertainties to predictive stages. SKB R-05-74, Svensk Kärnbränslehantering AB.

Holmén J, 2007. SFR inverse modelling Part 2. Uncertainty factors of predicted flow in deposition tunnels and uncertainty in distribution of flow paths from deposition tunnels. SKB R-07-61, Svensk Kärnbränslehantering AB.

Holmén J G, Stigsson M, 2001a. Details of predicted flow in deposition tunnels at SFR, Forsmark. SKB R-01-21, Svensk Kärnbränslehantering AB.

Holmén J G, Stigsson M, 2001b. Future hydrogeological conditions at SFR. SKB R-01-02, Svensk Kärnbränslehantering AB.

Hult A, 2011. Gamla tiders brunnsgrävning. Borrsvängen 1, 14–16. (In Swedish.)

Huntley D, Nommensen R, Steffey D, 1992. The use of specific capacity to assess transmissivity in fractured-rock aquifers. Groundwater 30, 396–402.

Håkansson A, Kreuger J, 1986. Kemisk vattenkvalitet vid bevattning. Vägledning för bedömning av kemisk vattenkvalitet vid bevattning. Rapport 149, Institutionen för markvetenskap, Sveriges Lantbruksuniversitet, Uppsala. (In Swedish.)

ICRP, 1975. Report of the Task group on reference man: a report. Oxford: Pergamon. (ICRP Publication 23)

ICRP, 2002. Basic anatomical and physiological data for use in radiological protection: reference values. Oxford: Pergamon. (ICRP Publication 89; Annals of ICRP 32 (3–4))

Johansson P-O, 2008. Description of surface hydrology and near-surface hydrogeology at Forsmark. Site descriptive modelling, SDM-Site Forsmark. SKB R-08-08, Svensk Kärnbränslehantering AB.

Johansson P-O, Öhman J, 2008. Presentation of meteorological, hydrological and hydrogeological monitoring data from Forsmark. Site descriptive modelling, SDM-Site Forsmark. SKB R-08-10, Svensk Kärnbränslehantering AB.

Johansson W, 1973/74. Metod för beräkning av vatteninnehåll och vattenomsättning i odlad jord med ledning av meteorologiska data. Grundförbättring 26, 57–153. (In Swedish.)

Johansson W, Klingspor P, 1977. Bevattningen inom lantbruket 1976: bevattnad areal, vattenåtgång och vattentäkter. Stenciltryck 100, Institutionen för markvetenskap, Avdelningen för lantbrukets hydroteknik, Lantbrukshögskolan, Uppsala. (In Swedish.)

Jonsson E, 1977. Bevattning med förorenat vatten: hygieniska risker för människor och djur: en litteraturstudie. Stenciltryck 107, Institutionen för markvetenskap, Avdelningen för lantbrukets hydroteknik, Sveriges Lantbruksuniversitet, Uppsala. (In Swedish.)

Jordbruksverket, 1999. Vatten till husdjur. Jönköping: Jordbruksverket. (Jordbruksinformation 13) (In Swedish.)

Joyce S, Simpson T, Hartley L, Applegate D, Hoek J, Jackson P, Swan D, Marsic N, Follin S, 2010. Groundwater flow modelling of periods with temperate climate conditions – Forsmark. SKB R-09-20, Svensk Kärnbränslehantering AB.

Juhlin-Dannfeldt H (ed), 1923. Lantmannens uppslagsbok. Stockholm: Norstedt. (In Swedish.)

Kane, D L, Yoshikawa K, McNamara J P, 2013. Regional groundwater flow in an area mapped as continuous permafrost, NE Alaska (USA). Hydrogeology Journal 21, 41–52.

Kao C, Bouarfa S, Zimmer D, 2001. Steady state analysis of unsaturated flow above a shallow water-table aquifer drained by ditches. Journal of Hydrology 250, 122–133.

Karlsson A, Eriksson C, Borell Lövstedt C, Liungman O, Engqvist A, 2010. High-resolution hydrodynamic modelling of the marine environment at Forsmark between 6500 BC and 9000 AD. SKB R-10-09, Svensk Kärnbränslehantering AB.

Kasimir-Klemedtsson Å, Klemedtsson L, Berglund K, Martikainen P, Silvola J, Oenema O, 1997. Greenhouse gas emission from farmed organic soils: a review. Soil Use and Management 13, 245–250.

Kattilakoski E, Suolanen V 2000. Groundwater flow analysis and dose rate estimates from releases to wells at a coastal site. STUK-YTO-TR 169, Radiation and Nuclear Safety Authority, Finland.

Kautsky U (ed), 2001. The biosphere today and tomorrow in the SFR area. SKB R-01-27, Svensk Kärnbränslehantering AB.

Kjellström E, Strandberg G, Brandefelt J, Näslund J-O, Smith B, Wolfarth B, 2009. Climate conditions in Sweden in a 100,000-year time perspective. SKB TR-09-04, Svensk Kärnbränslehantering AB.

Kohler A, Abbaspour K C, Fritsch M, Schulin R, 2001. Functional relationship to describe drains with entrance resistance. Journal of Irrigation and Drainage Engineering 127, 355–362.

Kuhn O, 2004. Ancient Chinese drilling. CSEG Recorder 2004, 39–43.

Larsson-McCann S, Karlsson A, Nord M, Sjögren J, Johansson L, Ivarsson M, Kindell S, 2002. Meteorological, hydrological and oceanographical information and data for the site investigation program in the communities of Östhammar and Tierp in the northern part of Uppland. SKB TR-02-02, Svensk Kärnbränslehantering AB.

Lindgren M, Pettersson M, Karlsson S, Moreno L, 2001. Project SAFE. Radionuclide release and dose from the SFR repository. SKB R-01-18, Svensk Kärnbränslehantering AB.

Logsdon S D, Hernandez-Ramirez G, Hatfield J L, Sauer T J, Prueger J H, Schilling K E, 2009. Soil water and shallow groundwater relations in an agricultural hillslope. Soil Science Society of America Journal 73, 1461–1468.

Lundin L, 1994. Impacts of forest drainage on flow regime. Uppsala: Swedish University of Agricultural Sciences. (Studia Forestalia Suecica 192)

Löfgren A (ed), 2008. The terrestrial ecosystems at Forsmark and Laxemar-Simpevarp. Site descriptive modelling, SDM-Site. SKB R-08-01, Svensk Kärnbränslehantering AB.

Löfgren A (ed), 2010. The terrestrial ecosystems at Forsmark and Laxemar-Simpevarp. SR-Site Biosphere. SKB TR-10-01, Svensk Kärnbränslehantering AB.

McDonald M K, Pomeroy J W, Pietroniro A, 2010. On the importance of sublimation to an alpine snow mass balance in the Canadian Rocky Mountains. Hydrology and Earth System Sciences 14, 1401–1415.

Meier P M, Carrera J, Sánchez-Vila X, 1999. A numerical study on the relationsship between transmissivity and specific capacity in heterogeneous aquifers. Groundwater 37, 611–617.

Mueller L, Behrendt A, Schalitz G, Schindler U, 2005. Above ground biomass and water use efficiency of crops at shallow water tables in a temperate climate. Agricultural Water Management 75, 117–136.

Mårtensson E, Gustafsson L-G, 2010. Hydrological and hydrogeological effects of an open repository in Forsmark. Final MIKE SHE flow modelling results for the Environmental Impact Assessment. SKB R-10-18, Svensk Kärnbränslehantering AB.

Mårtensson E, Gustafsson L-G, Werner K, 2010. Hydrological and hydrogeological effects of a deep-rock repository for spent nuclear fuel in Sweden: application of a new coupling routine between MIKE SHE and MOUSE. Paper presented at the International MIKE by DHI 2010 Conference, Copenhagen, 6–8 September 2010.

National Academy of Sciences, 1977. Drinking water and health. Washington, DC: National Academy Press.

Nilsson A-C, Borgiel M, 2005. Forsmark site investigation. Sampling and analysis of near surface groundwater. Results from sampling of shallow soil monitoring wells, BAT pipes, a natural spring and private wells, May 2003 – April 2005. SKB P-05-171, Svensk Kärnbränslehantering AB.

Nilsson A-C, Tullborg E-L, Smellie J, Gimeno M J, Gómez J B, Auqué L F, Sandström B, Pedersen K, 2011. SFR site investigation. Bedrock hydrogeochemistry. SKB R-11-06, Svensk Kärnbränslehantering AB.

Nordén S, Avila R, de la Cruz I, Stenberg K, Grolander S, 2010. Element-specific and constant parameters used for dose calculations in SR-Site. SKB TR-10-07, Svensk Kärnbränslehantering AB.

Nyberg J, Elhammer A, Sohlenius G, Kjellin B, Nordgren P, 2011. Results from marine geological investigations outside Forsmark. SKB P-11-39, Svensk Kärnbränslehantering AB.

Odén M, Follin S, Öhman J, Vidstrand P, 2014. SR-PSU Bedrock hydrogeology. Groundwater flow modelling methodology, set up and results. SKB R-13-25, Svensk Kärnbränslehantering AB.

Persson K M, 2011. Om drivkrafter bakom några sjösänkningar i Sverige – exempel från Näsbyholmssjön (Skåne) och Hjälmaren (Närke-Södermanland-Västmanland). Vatten 67, 101–111. (In Swedish, with abstract in English).

Persson K M, Larsson, 2011. Synpunkter på vattenförsörjning i nordisk forntid, med exempel från Uppåkra. Vatten 67, 31–38. (In Swedish, with abstract in English).

Pousette J, Müllern C-F, Engqvist P., Knutsson G, 1981. Hydrogeologisk karta över Kalmar län med beskrivning och bilagor. Uppsala: SGU. (Sveriges geologiska undersökning Ser. Ah 1)

Quinton W L, Carey S K, 2008. Towards an energy-based runoff generation theory for tundra landscapes. Hydrological Processes 22, 4649–4653.

Razack M, Huntley D, 1991. Assessing transmissivity from specific capacity in a large and heterogeneous alluvial aquifer. Groundwater 29, 856–861.

Reba M L, Pomeroy J, Marks D, Link T E, 2011. Estimating surface sublimation losses from snowpacks in a mountain catchment using eddy covariance and turbulent transfer calculations. Hydrological Processes 26, 3699–3711.

Ritzema H P (ed), 1994. Drainage principles and applications. 2nd ed. Wageningen: International Institute for Land Reclamation and Improvement.

Saetre P, Valentin J, Lagerås P, Avila R, Kautsky U, 2013a. Land use and food intake of future inhabitants: outlining a representative individual of the most exposed group for dose assessment. Ambio 42, 488–496.

Saetre P, Ekström P-A, Nordén S, Keesmann S, 2013b. The biosphere model for radionuclide transport and dose assessment in SR-PSU. SKB R-13-46, Svensk Kärnbränslehantering AB.

Schlotzhauer S M, Price J S, 1999. Soil water flow dynamics in a managed cutover peat field, Quebec: field and laboratory investigations. Water Resources Research 35, 3675–3683.

Schnell J-B, 1966. Vatten och fornfynd: bebyggelsehistoriska studier på Västergötlands kambrosilur-område. Lic. thesis. Institutionen för Nordisk och jämförande fornkunskap, Göteborgs universitet. (In Swedish.)

Schyman J, 2009. Den gotländska vikingatida bebyggelsens rumsliga placering i landskapet – en empirisk detaljstudie av Hemse socken. Bachelor thesis. Gotland University. (In Swedish, with abstract in English.)

Seuna P, 1981. Long-term influence of forestry drainage on the hydrology of an open bog in Finland. Publication of the Water Research Institute 43, 3–14.

SGU, 2008. Att borra brunn för energi och vatten – en vägledning: normförfarande vid utförande av vatten- och energibrunnar: Normbrunn -07. Uppsala: Sveriges geologiska undersökning. (In Swedish.)

Singh R, Kundu D K, Tripathi V K, 2006. Contribution of upward flux from shallow ground water table to crop water use in major soil groups of Orissa. Journal of Agricultural Physics 6, 1–6.

SKB, 1999. Deep repository for spent nuclear fuel. SR-97 – Post-closure safety. SKB TR-99-06, Svensk Kärnbränslehantering AB.

SKB, 2000. Förstudie Östhammar. Slutrapport. Svensk Kärnbränslehantering AB.

SKB, 2006. Long-term safety for KBS-3 repositories at Forsmark and Laxemar – a first evaluation. Main report of the SR-Can project. SKB TR-06-09, Svensk Kärnbränslehantering AB.

SKB, 2008a. Safety analysis SFR 1. Long-term safety. SKB R-08-130, Svensk Kärnbränslehantering AB.

SKB, 2008b. Site description of Forsmark at completion of the site investigation phase. SDM-Site Forsmark. SKB TR-08-05, Svensk Kärnbränslehantering AB.

SKB, 2008c. Geovetenskapligt undersökningsprogram för utbyggnad av SFR. SKB R-08-67, Svensk Kärnbränslehantering AB. (In Swedish.)

SKB, 2011. Long-term safety for the final repository for spent nuclear fuel at Forsmark. Main report of the SR-Site project. SKB TR-11-01, Svensk Kärnbränslehantering AB.

SKB, 2013. Site description of the SFR area at Forsmark at completion of the site investigation phase. SDM-PSU Forsmark. SKB TR-11-04, Svensk Kärnbränslehantering AB.

SKB, 2014a. Biosphere synthesis report for the safety assessment SR-PSU. SKB TR-14-06, Svensk Kärnbränslehantering AB.

SKB, 2014b. Climate and climate related issues for the safety assessment SR-PSU. SKB TR-13-05, Svensk Kärnbränslehantering AB.

SKB, 2014c. FEP report for the safety assessment SR-PSU, SKB TR-14-07, Svensk Kärnbränslehantering AB.

SKB, 2014d. Handling of future human actions in the safety assessment SR-PSU. SKB TR-14-08, Svensk Kärnbränslehantering AB.

SKB, 2014e. Radionuclide transport and dose calculations for the safety assessment SR-PSU. SKB TR-14-09, Svensk Kärnbränlsehantering AB.

SKB, 2014f. Safety analysis for SFR. Long-term safety. Main report for the safety assessment SR-PSU. SKB TR-14-01, Svensk Kärnbränslehantering AB.

Sohlenius G, Hedenström A, 2009. Platsundersökning Forsmark. Stratigrafiska undersökningar i våtmarksobjekt. SKB P-09-18, Svensk Kärnbränslehantering AB. (In Swedish, with abstract in English).

Sohlenius G, Strömgren M, Hartz F, 2013a. Depth and stratigraphy of regolith at Forsmark. SR-PSU Biosphere. SKB R-13-22, Svensk Kärnbränslehantering AB.

Sohlenius G, Schoning K, Baumgartner A, 2013b. Development, carbon balance and agricultural use of peatlands – overview and examples from Uppland Sweden. SKB TR-13-20, Svensk Kärnbränslehantering AB.

Stephens M B, Fox A, La Pointe P, Simeonov A, Isaksson H, Hermanson J, Öhman J, 2007. Geology Forsmark. Site descriptive modelling, Forsmark stage 2.2. SKB R-07-45, Svensk Kärnbränslehantering AB.

Strack O D L, 1989. Groundwater mechanics. Englewood Cliffs, NJ: Prentice-Hall.

Strömgren M, Brydsten L, 2013. Digital elevation model of Forsmark. Site descriptive modelling. SR-PSU Biosphere. SKB R-12-03, Svensk Kärnbränslehantering AB.

Svenskt Vatten, 2005. Fakta om vatten och avlopp. Stockholm: Svenskt Vatten AB. (In Swedish.)

Svensson U, Kuylenstierna H-O, Ferry M, 2010. DarcyTools version 3.4 – Concepts, methods and equations. SKB R-07-38, Svensk Kärnbränslehantering AB.

Tegel W, Elburg R, Hakelberg D, Stäuble H, Ulf Büntgen, 2012. Early Neolithic water wells reveal the world's oldest wood architecture. PLoS ONE 7: e51374. doi:10.1371/journal.pone.0051374

Thunvik R, 1983. Calculation of fluxes through a repository caused by a local well. SKBF/KBS TR 83-50, Svensk Kärnbränsleförsörjning AB.

Tröjbom M, Söderbäck B, Johansson P-O, 2007. Hydrochemistry in surface water and shallow groundwater. Site descriptive modelling, SDM-Site Forsmark. SKB R-07-55, Svensk Kärnbränslehantering AB.

US Army, 2008. Water planning guide. Potable water consumption planning factors by environmental region and command level. Force Development Directorate, United States Army Combined Arms Command, Fort Lee, VA.

US EPA, 2000. Methodology for deriving ambient water quality criteria for the protection of human health. EPA822-B-00-004, U.S. Environmental Protection Agency, Washington, DC.

US EPA, 2011. Exposure factors handbook. EPA/600/R-09/052F, U.S. Environmental Protection Agency, Washington, DC.

Verry E S, 1997. Hydrological processes of natural, northern forested wetlands. In Trettin C C, Jurgensen M F, Grigal D F, Gale M R, Jeglum J K (eds). Northern forested wetlands: ecology and management. Boca Raton, FL: Lewis, 61–70.

Werner K, Lundholm L, Johansson P-O, 2009. Platsundersökning Forsmark. Installation av grundvattenrör och pegelrör i våtmarker och sjön Tjärnpussen. SKB P-09-17, Svensk Kärnbränslehantering AB. (In Swedish, with abstract in English).

Werner K, Hamrén U, Collinder P, 2010. Vattenverksamhet i Forsmark (del I). Bortledande av grundvatten från slutförvarsanläggningen för använt kärnbränsle. SKB R-10-14, Svensk Kärnbränslehantering AB. (In Swedish, with summary in English).

Werner K, Norville J, Öhman J, 2013. Meteorological, hydrological and hydrogeological monitoring data from Forsmark – compilation and analysis for the SR-PSU project. SR-PSU Biosphere. SKB R-13-20, Svensk Kärnbränslehantering AB.

Westrell T, Andersson Y, Stenström T A, 2006. Drinking water consumption patterns in Sweden. Journal of Water and Health 4, 511–522.

White D, Hinzman L, Alessa L, Cassano J, Chambers M, Falkner K, Francis J, Gutowski B, Holland D, Holmes R M, Huntington H, Kane D, Kliskey A, Lee C, McClelland J, Peterson B, Straneo F, Steele M, Woodgate R, Yang D, Yoshikawa K, Zhang T, 2007. The Arctic freshwater system: changes and impacts. Journal of Geophysical Research 112, G04S54. doi:10.1029/2006JG000353

WHO, 2003a. Chloride in drinking-water. Background document for development of WHO guidelines for drinking-water quality. Geneva: World Health Organization.

WHO, 2003b. Iron in drinking-water. Background document for development of WHO guidelines for drinking-water quality. Geneva: World Health Organization.

WHO, 2004. Sulfate in drinking-water. Background document for development of WHO guidelines for drinking-water quality. Geneva: World Health Organization.

WHO, 2011. Guidelines for drinking-water quality. 4th ed. Geneva: World Health Organization.

Widgren M, 1979. A simulation model of farming systems and land use in Sweden during the early Iron Age, c. 500 B.C.–A.D. 550. Journal of Historical Geography 5, 21–32.

Öhman J, 2010. Site investigation SFR. Hydrogeologic modelling of SFR v 0.1. Influence of the ridge on the flow fields for different target volumes. SKB R-09-43, Svensk Kärnbränslehantering AB.

Öhman J, Follin S, 2010a. Site investigation SFR. Hydrogeological modelling of SFR. Data review and parameterisation of model version 0.1. SKB P-09-49, Svensk Kärnbränslehantering AB.

Öhman J, Follin S, 2010b. Site investigation SFR. Hydrogeological modelling of SFR, model version 0.2. SKB R-10-03, Svensk Kärnbränslehantering AB.

Öhman J, Vidstrand P, 2014. SR-PSU Bedrock hydrogeology. TD12 – Water-supply wells in rock. SKB P-14-05, Svensk Kärnbränslehantering AB.

Öhman J, Bockgård N, Follin S, 2012. Bedrock hydrogeology. Site investigation SFR. SKB R-11-03, Svensk Kärnbränslehantering AB.

Öhman J, Follin S, Odén M, 2013. Bedrock hydrogeology – Groundwater flow modelling. Site investigation SFR. SKB R-11-10, Svensk Kärnbränslehantering AB.

Öhman J, Follin S, Odén M, 2014. SR-PSU Hydrogeological modelling. TD11 – Temperate climate conditions. SKB P-14-04, Svensk Kärnbränslehantering AB.

Unpublished documents

SKBdoc id, version	Title	Issuer, year
1346469 ver 1.0	Hydrogeologisk utredning rörande befintligt SFR och planerad utbyggnad. (In Swedish.)	SKB, 2014
1350092 ver 1.0	Plats för slutförvaring av kortlivat rivningsfavfall. (In Swedish.)	SKB, 2013

Appendix 1

MIKE SHE modelling results for future conditions at Forsmark

Water balances for the MIKE SHE local model area

Water balance PSU, local model area, 3000AD_land3000rev, PRESENT climate ("normal year")

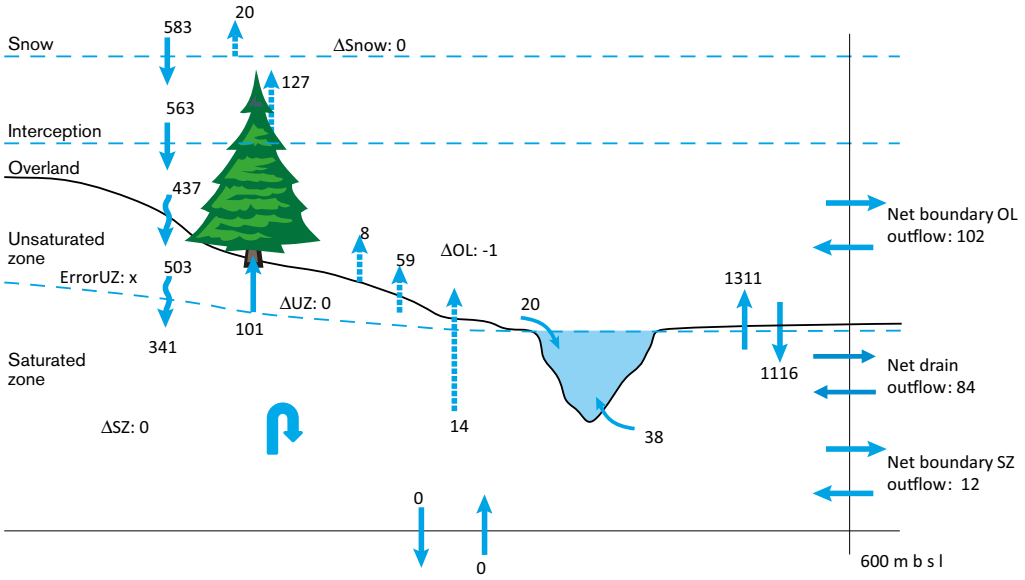

Figure A1-1. Water balance (mm/y) for land areas at 3000 AD (normal year).

Water balance PSU, local 5000AD_land3000, PRESENT climate ("normal year")

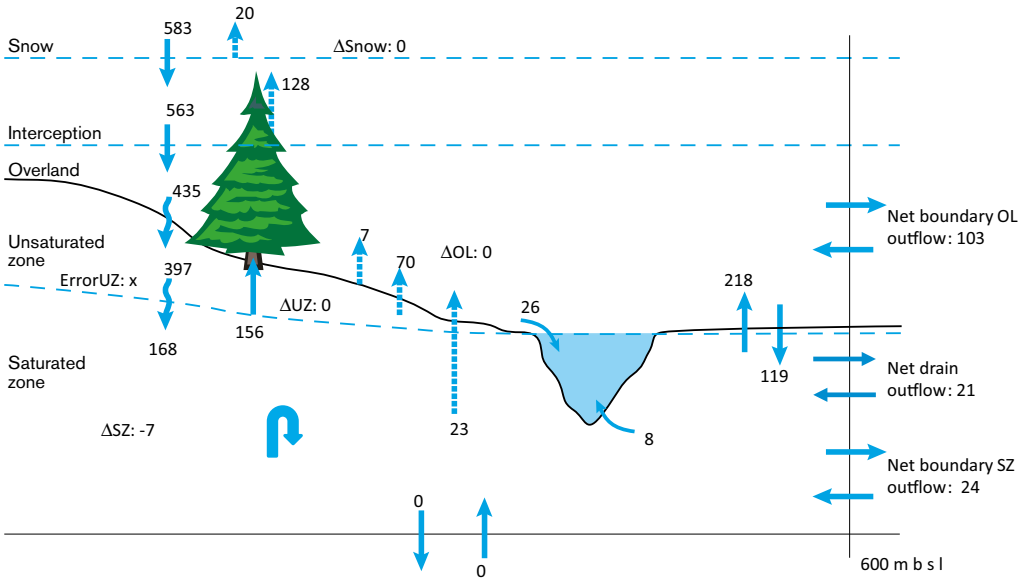

Figure A1-2. Water balance (mm/y) at 5000 AD, for areas constituting land at 3000 AD (normal year).

Water balance PSU, local 11000AD_land3000, PRESENT climate ("normal year")

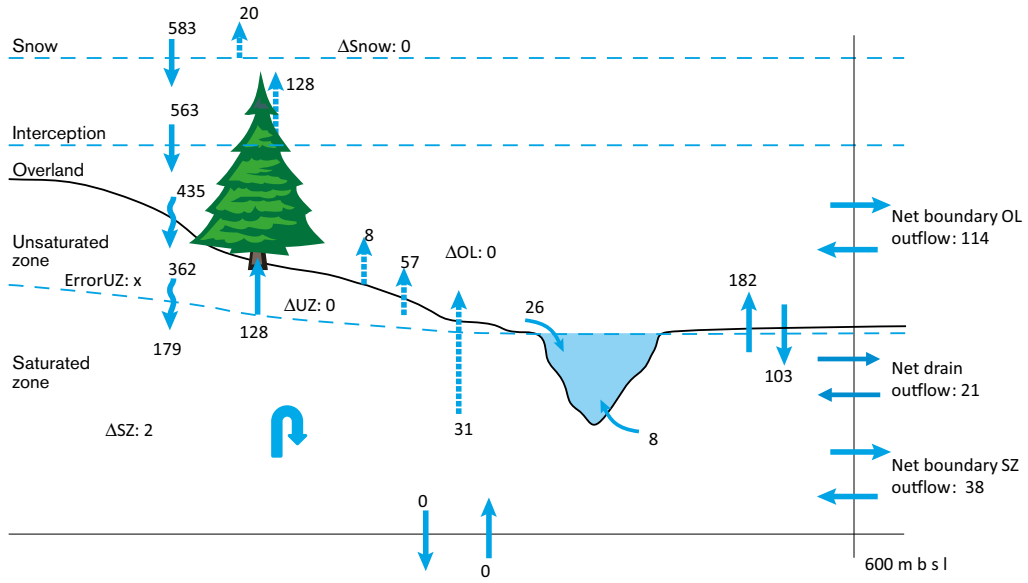

Figure A1-3. *Water balance (mm/y) at 11,000 AD, for areas constituting land at 3000 AD (normal year).*

Water balance PSU, 5000AD, model area, PRESENT climate ("normal year")

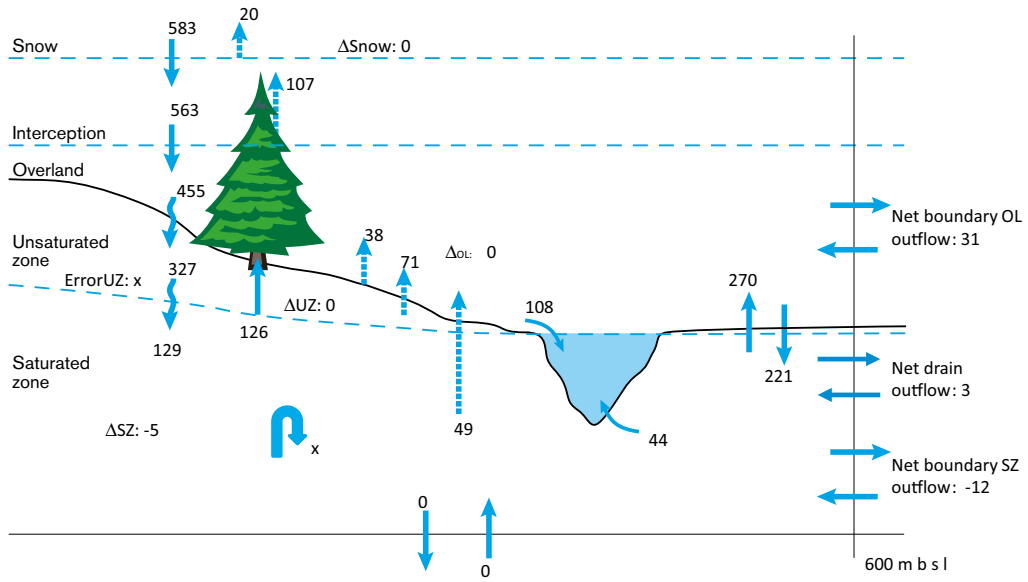

Figure A1-4. *Water balance (mm/y) for land areas at 5000 AD (normal year).*

Water balance PSU, 11000AD, model area, PRESENT climate ("normal year")

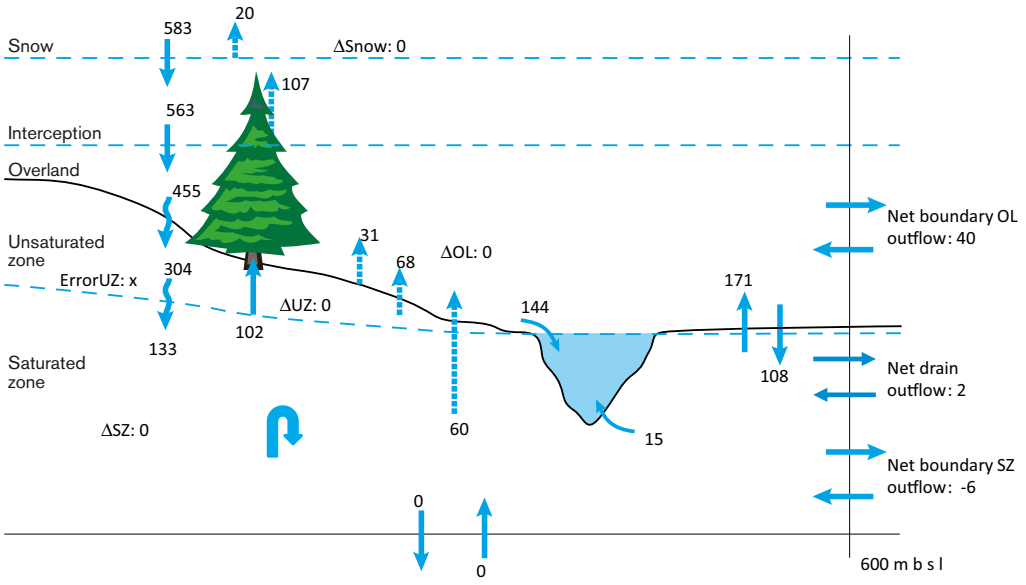

Figure A1-5. *Water balance (mm/y) at 11,000 AD, for areas constituting land at 5000 AD (normal year).*

Water balance PSU, local 5000AD, model area, WET and WARM climate (3rd year)

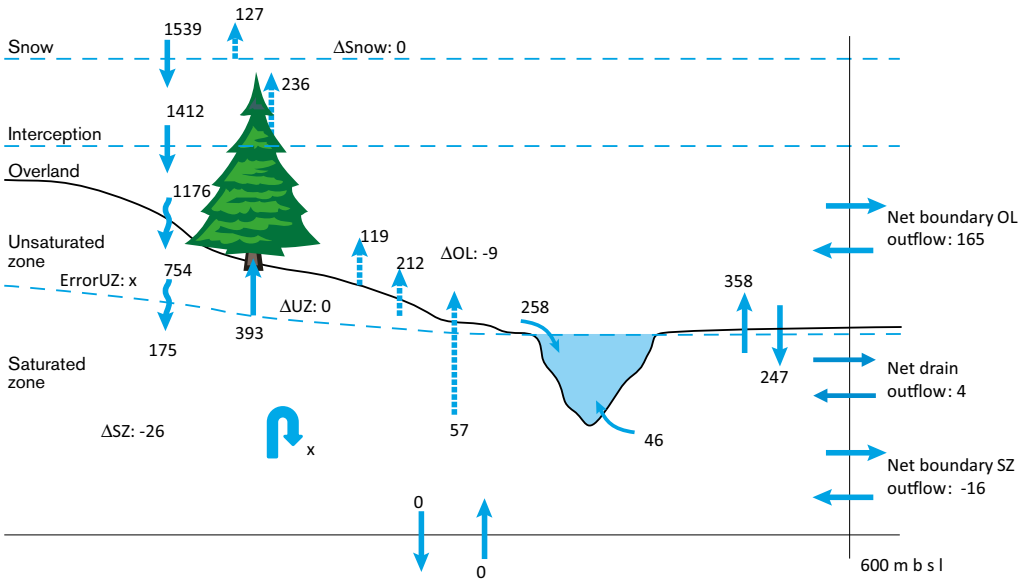

Figure A1-6. *Water balance (mm/y) for land areas at 5000 AD (wet and warm climate).*

Depth of overland water, depth to the groundwater table and vertical hydraulic-head differences in rock – normal year (3000 AD)

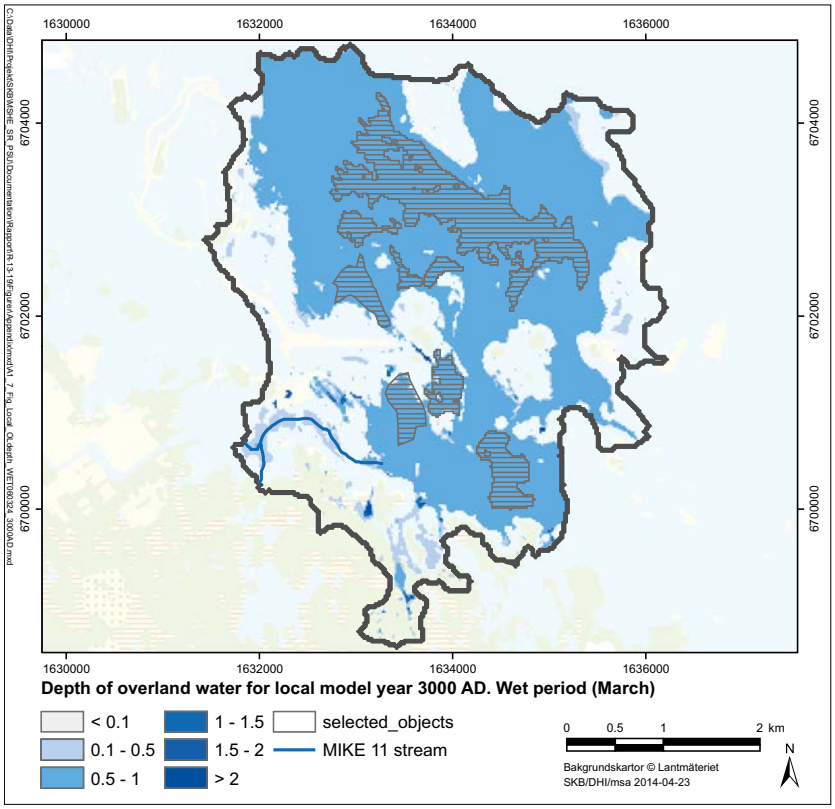

Figure A1-7. *Depth of overland water (m) during a wet period (March) at 3000 AD (normal year).*

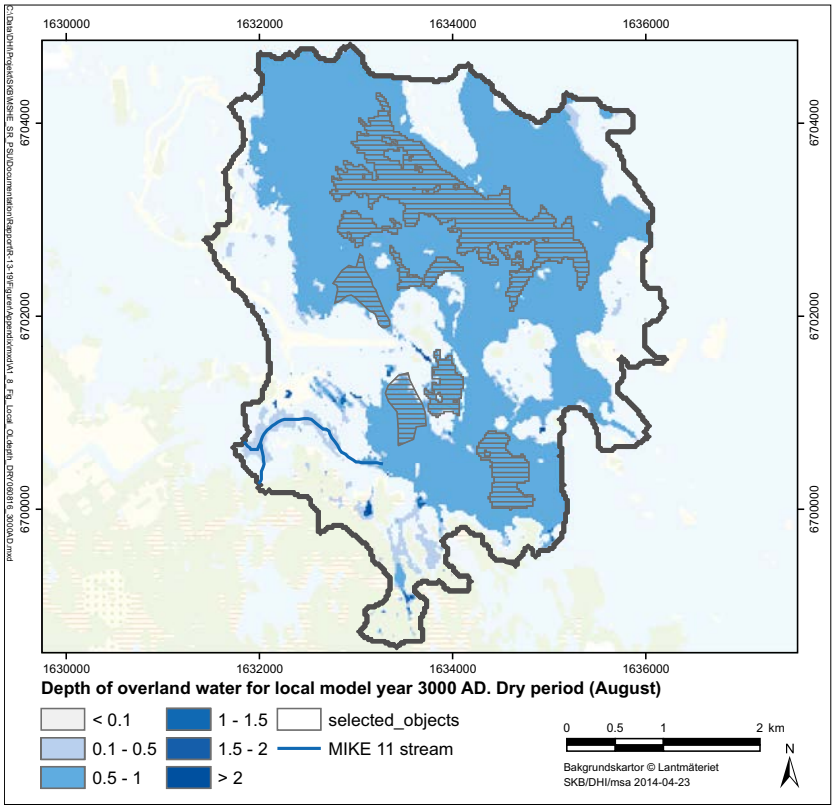

Figure A1-8. *Depth of overland water (m) during a dry period (August) at 3000 AD (normal year).*

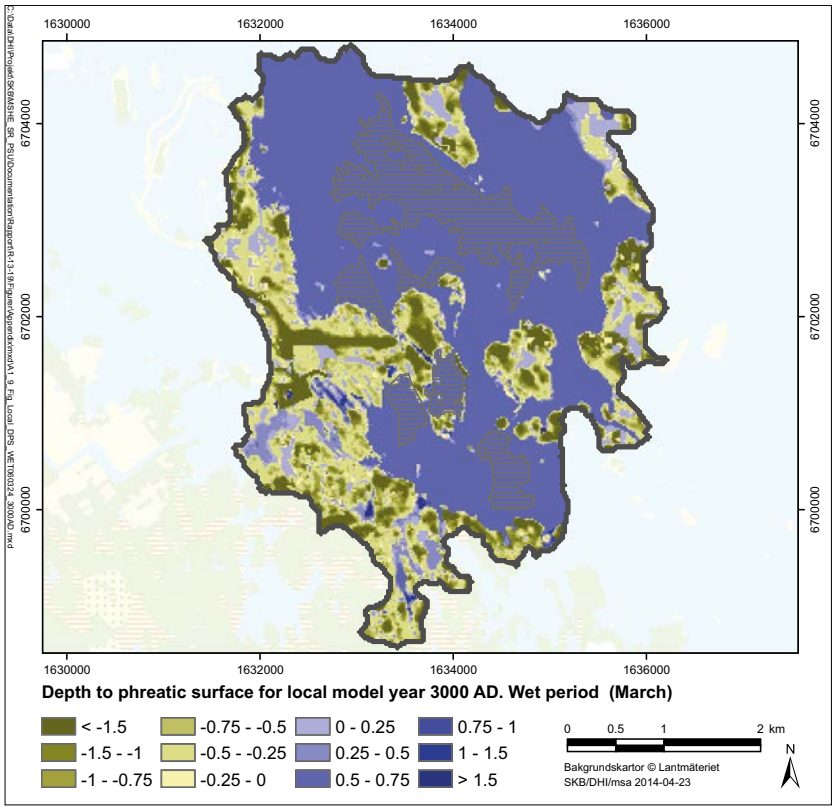

Figure A1-9. *Depth to the groundwater table (mbgs) during a wet period (March) at 3000 AD (normal year).*

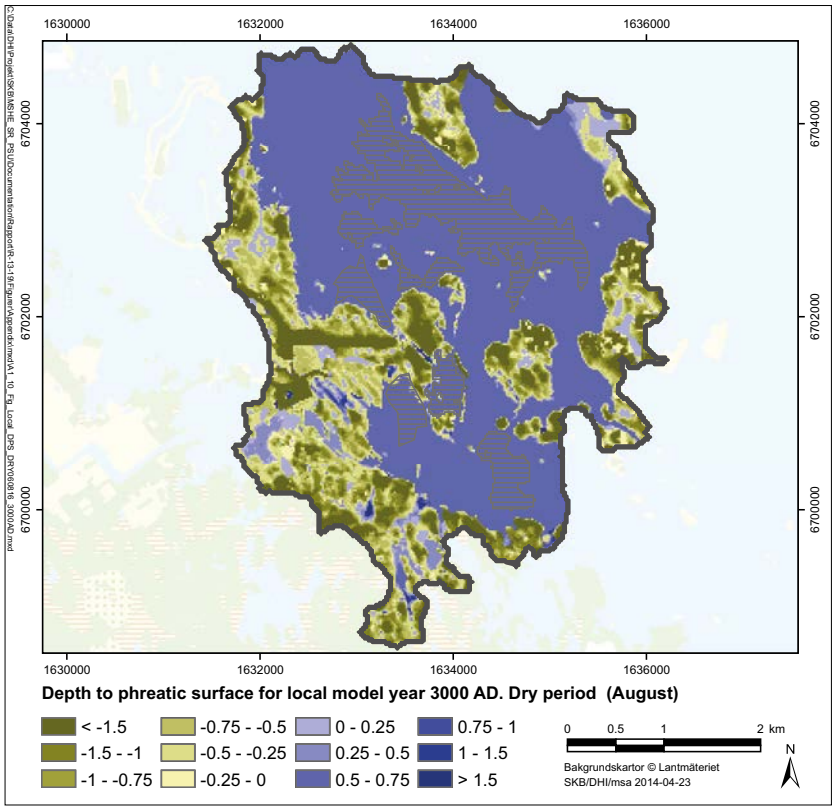

Figure A1-10. *Depth to the groundwater table (mbgs) during a dry period (August) at 3000 AD (normal year).*

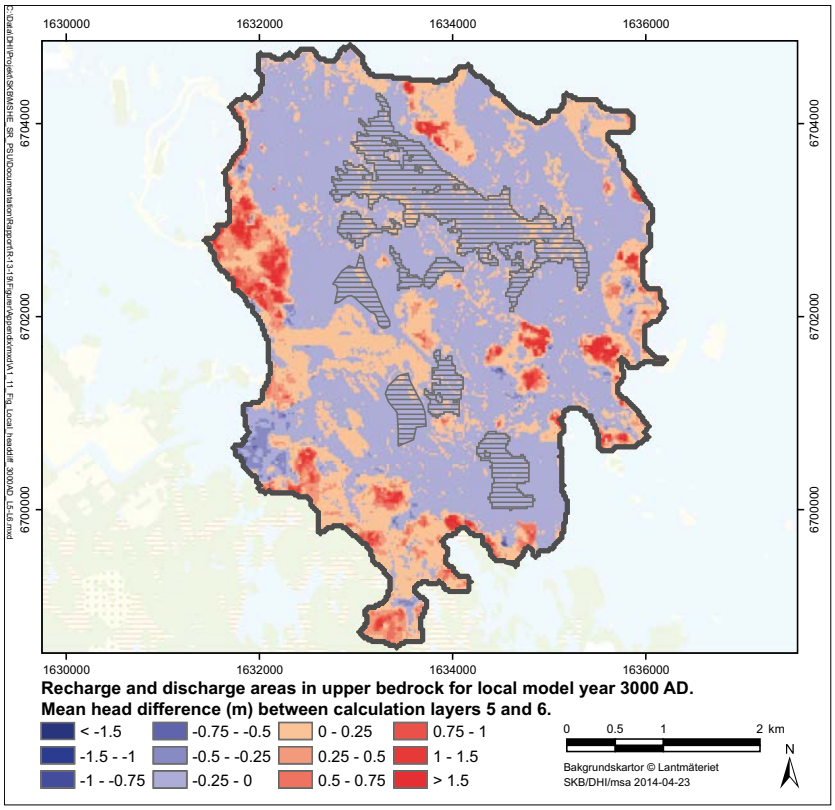

Figure A1-11. *Annual average hydraulic-head differences (m) in the rock (c –20 m elevation) at 3000 AD (normal year). Blue colours represent areas with upward gradients and red colours represent areas with downward gradients.*

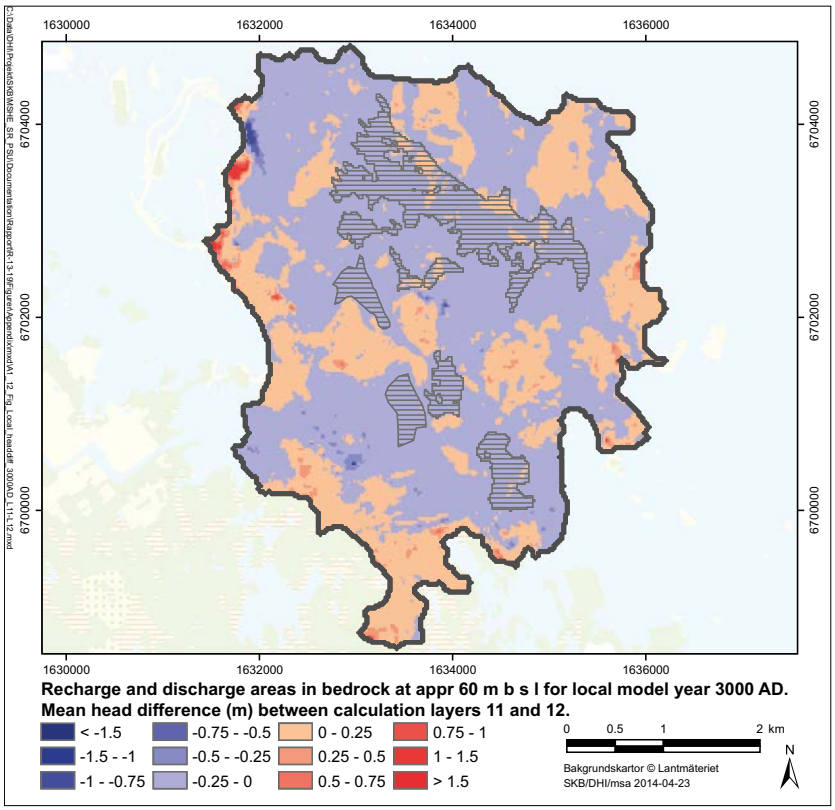

Figure A1-12. *Annual average hydraulic-head differences (m) in the rock (c –60 m elevation) at 3000 AD (normal year). Blue colours represent areas with upward gradients and red colours represent areas with downward gradients.*

Depth of overland water, depth to the groundwater table and vertical hydraulic-head differences – normal year (5000 AD)

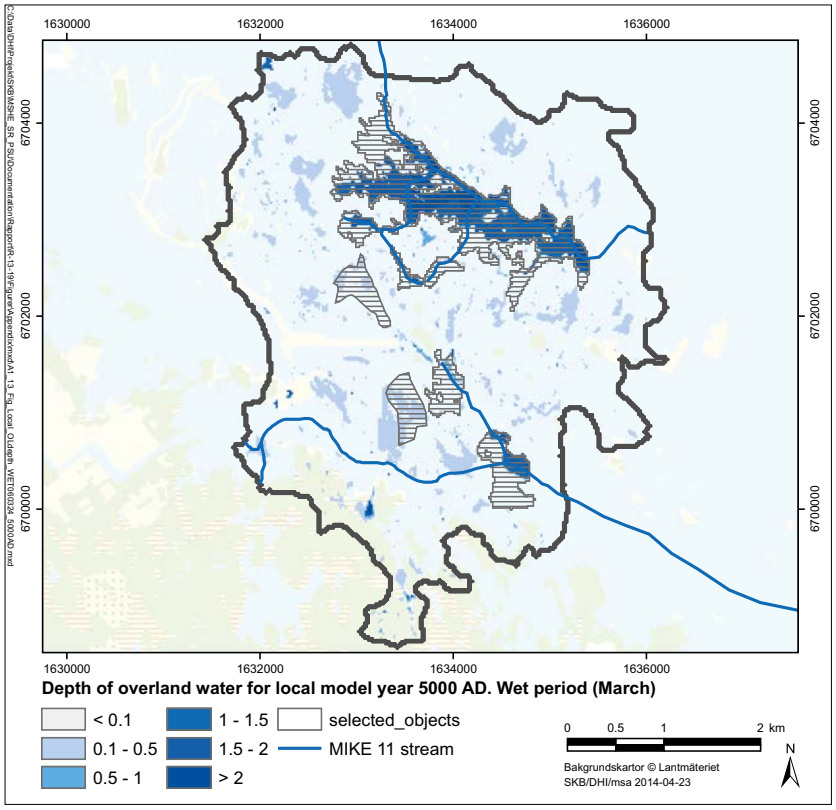

Figure A1-13. *Depth of overland water (m) during a wet period (March) at 5000 AD (normal year).*

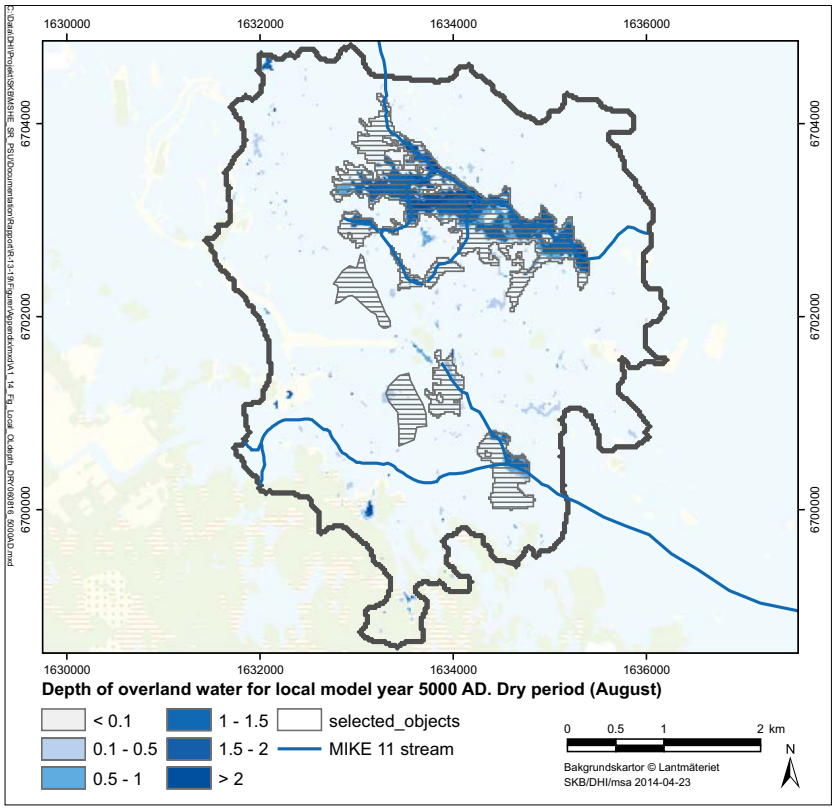

Figure A1-14. *Depth of overland water (m) during a dry period (August) at 5000 AD (normal year).*

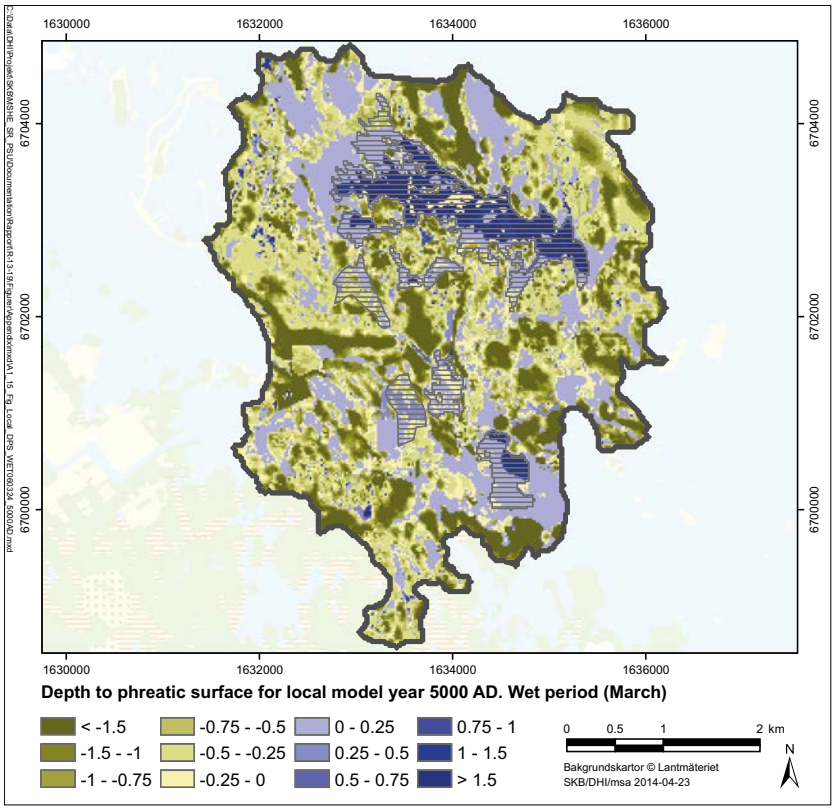

Figure A1-15. *Depth to the groundwater table (mbgs) during a wet period (March) at 5000 AD (normal year).*

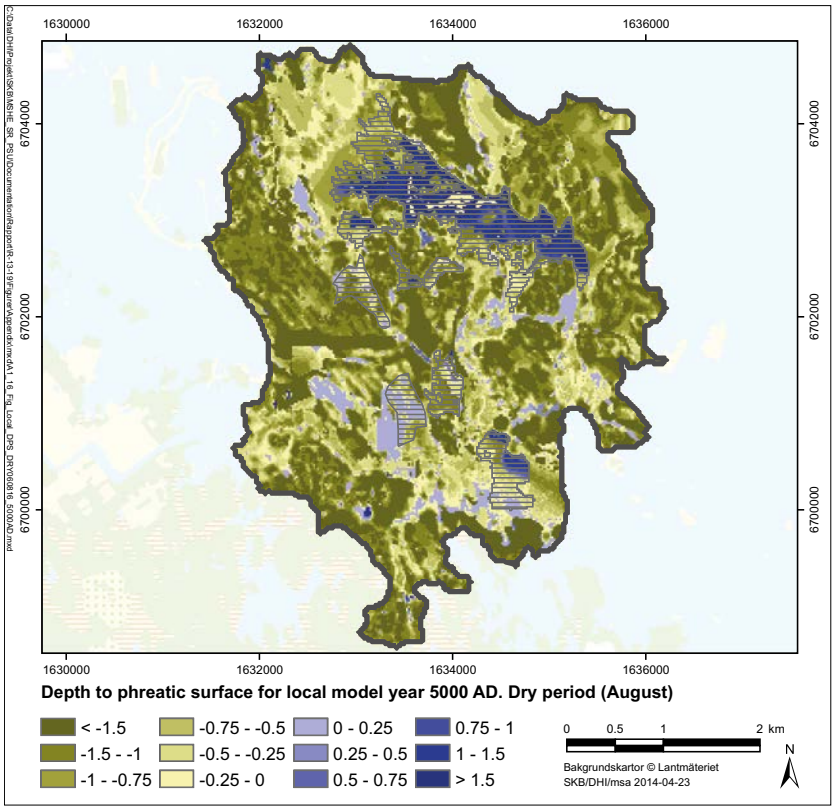

Figure A1-16. *Depth to the groundwater table (mbgs) during a dry period (August) at 5000 AD (normal year).*

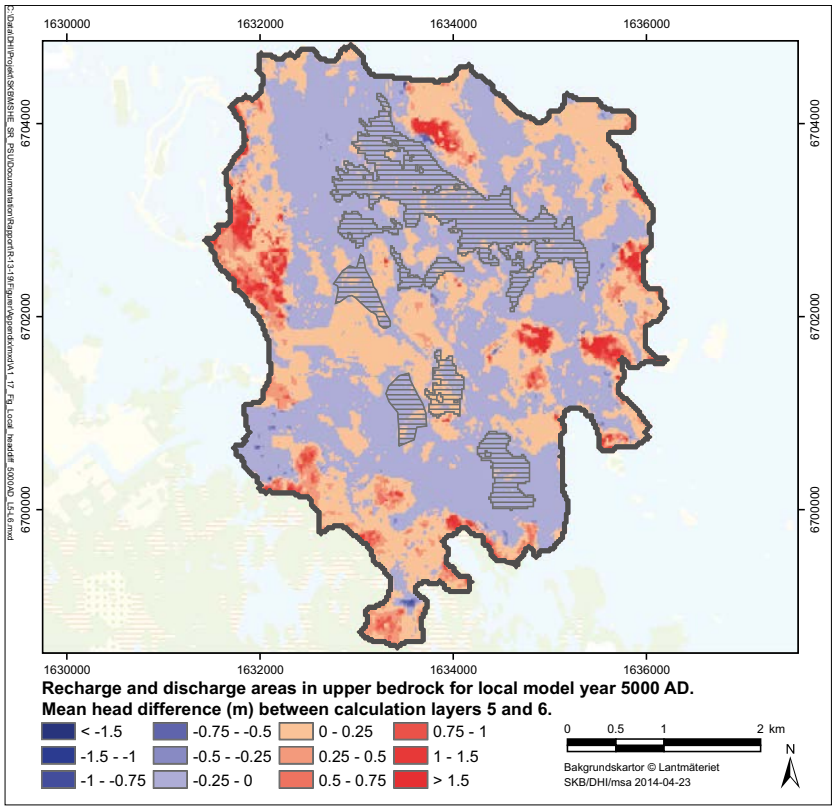

Figure A1-17. *Annual average hydraulic-head differences (m) in the rock (c –20 m elevation) at 5000 AD (normal year). Blue colours represent areas with upward gradients and red colours represent areas with downward gradients.*

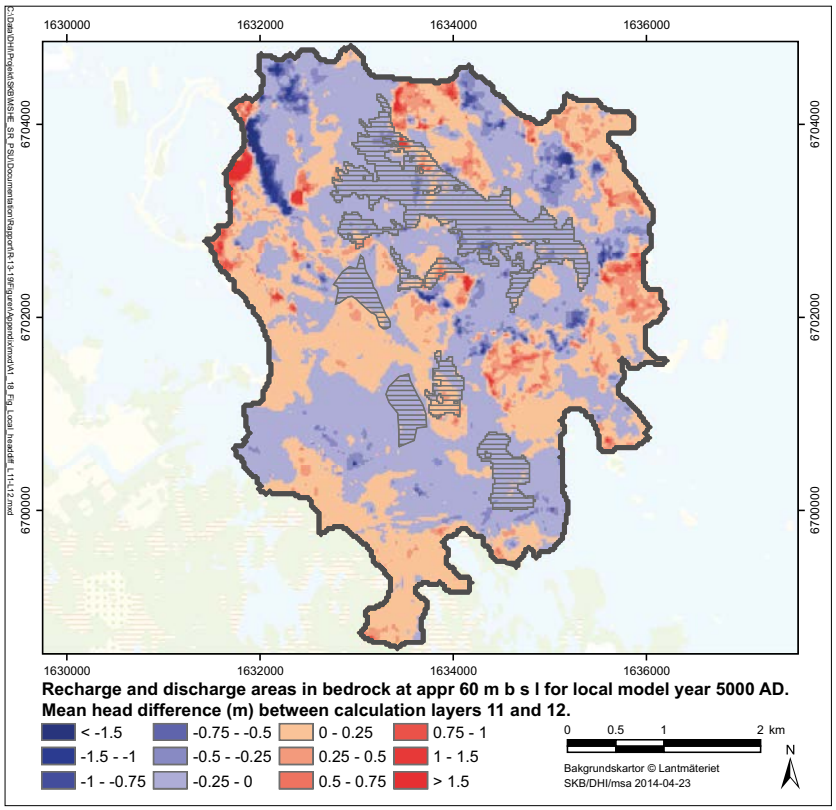

Figure A1-18. *Annual average hydraulic-head differences (m) in the rock (c –60 m elevation) at 5000 AD (normal year). Blue colours represent areas with upward gradients and red colours represent areas with downward gradients.*

Depth of overland water, depth to the groundwater table and vertical hydraulic-head differences in rock – normal year (11,000 AD)

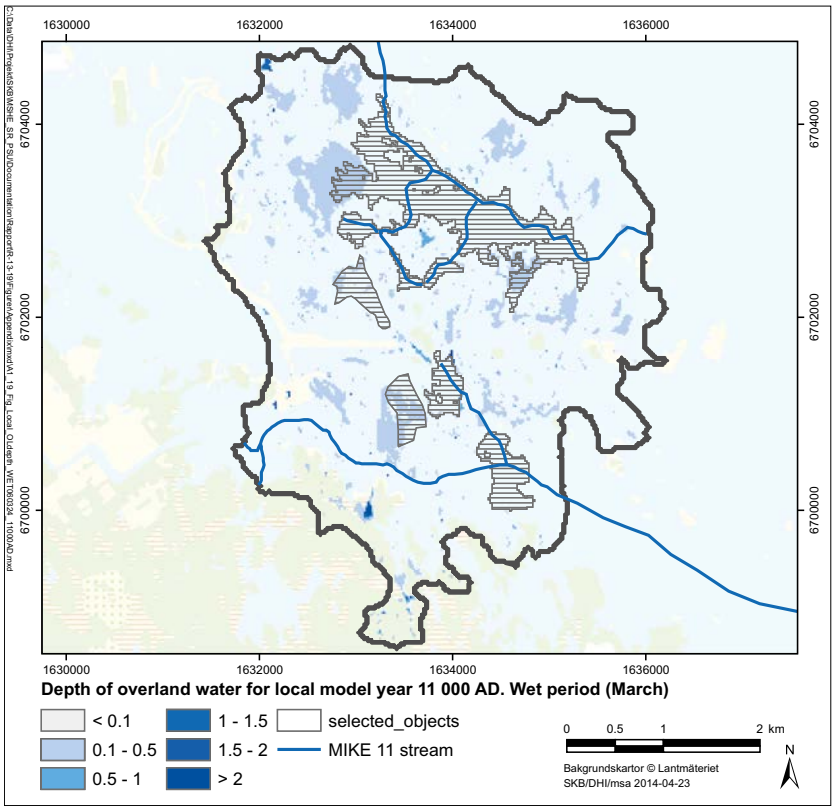

Figure A1-19. *Depth of overland water (m) during a wet period (March) at 11,000 AD (normal year).*

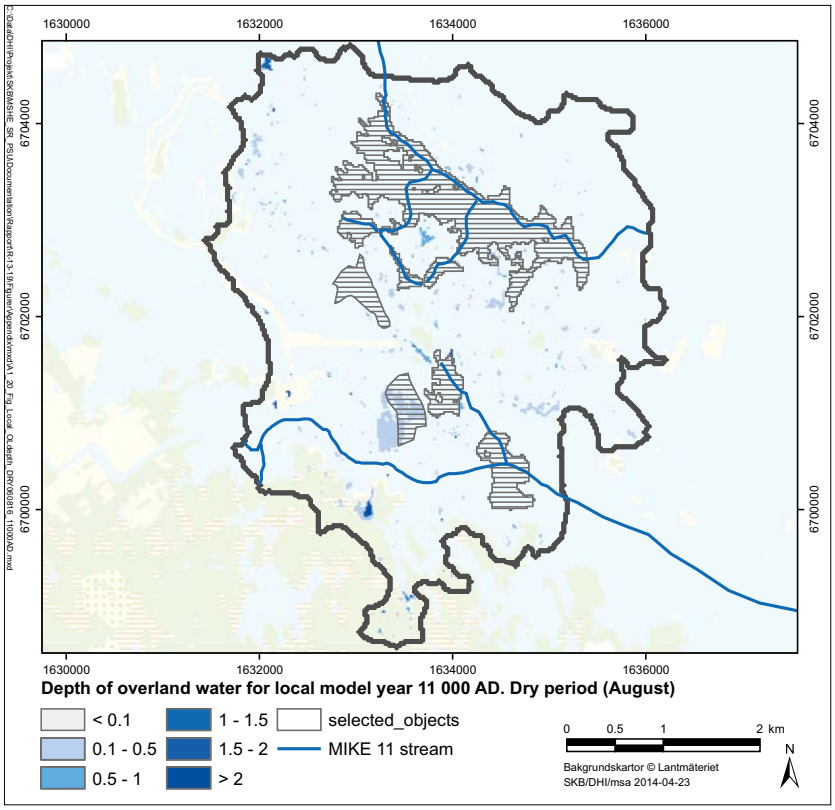

Figure A1-20. *Depth of overland water (m) during a dry period (August) at 11,000 AD (normal year).*

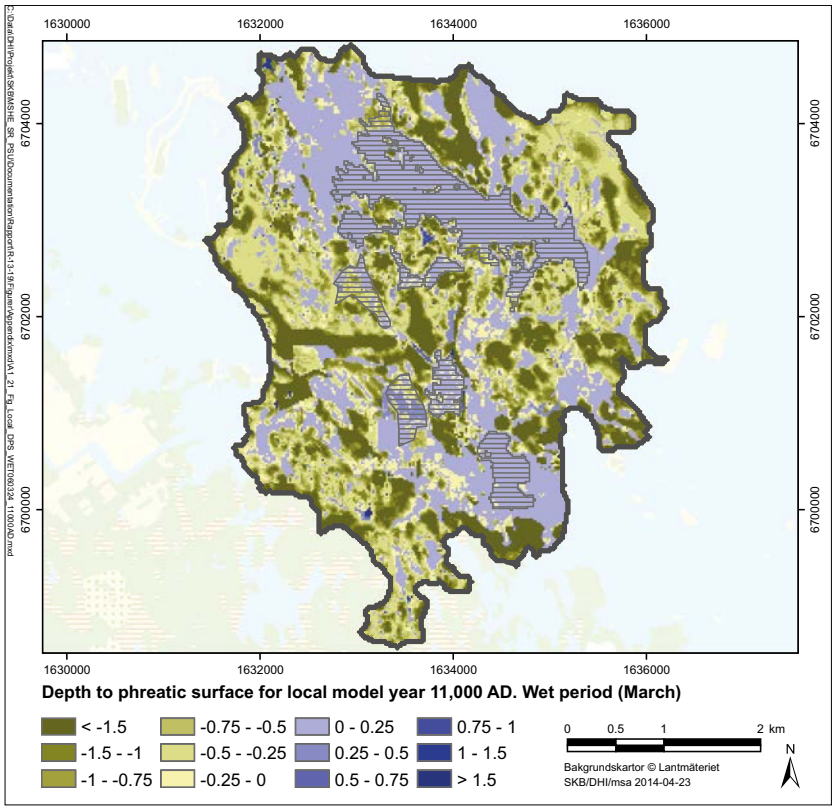

Figure A1-21. *Depth to the groundwater table (mbgs) during a wet period (March) at 11,000 AD (normal year).*

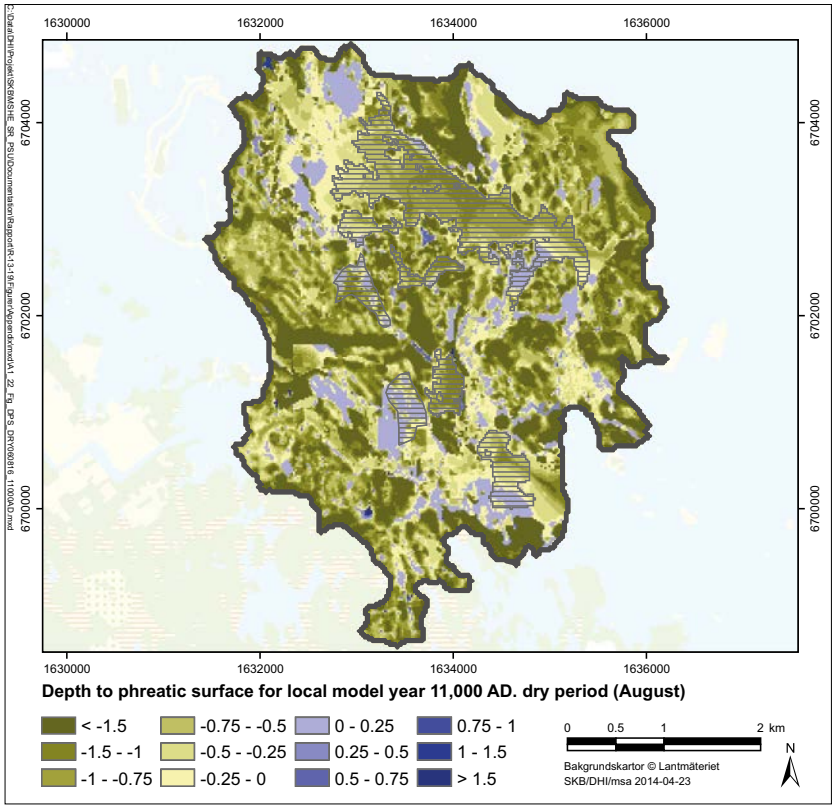

Figure A1-22. *Depth to the groundwater table (mbgs) during a dry period (August) at 11,000 AD (normal year).*

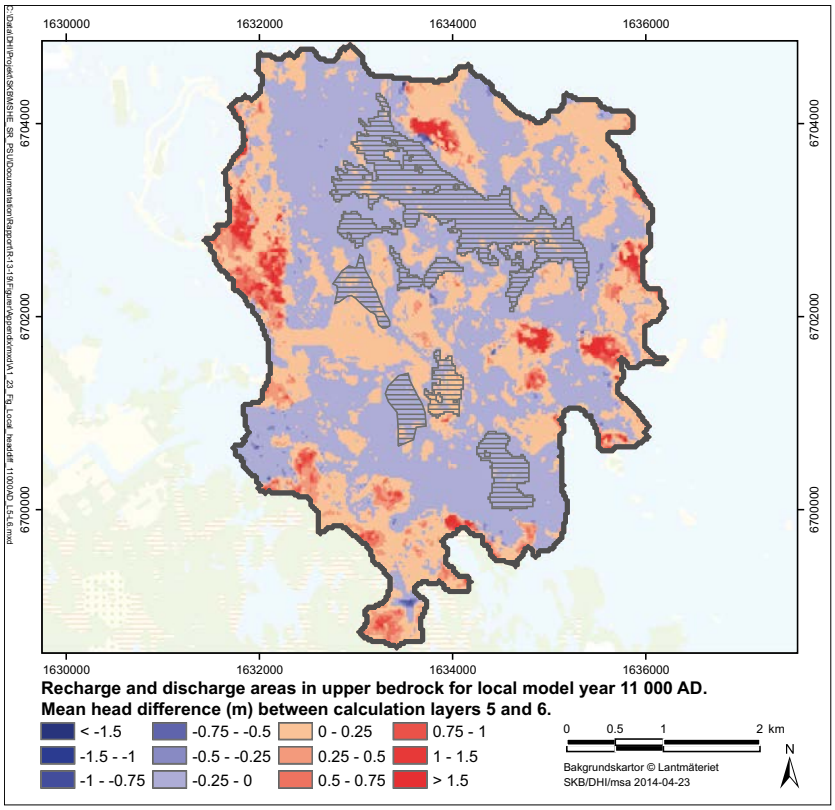

Figure A1-23. *Annual average hydraulic-head differences (m) in the rock (c –20 m elevation) at 11,000 AD (normal year). Blue colours represent areas with upward gradients and red colours represent areas with downward gradients.*

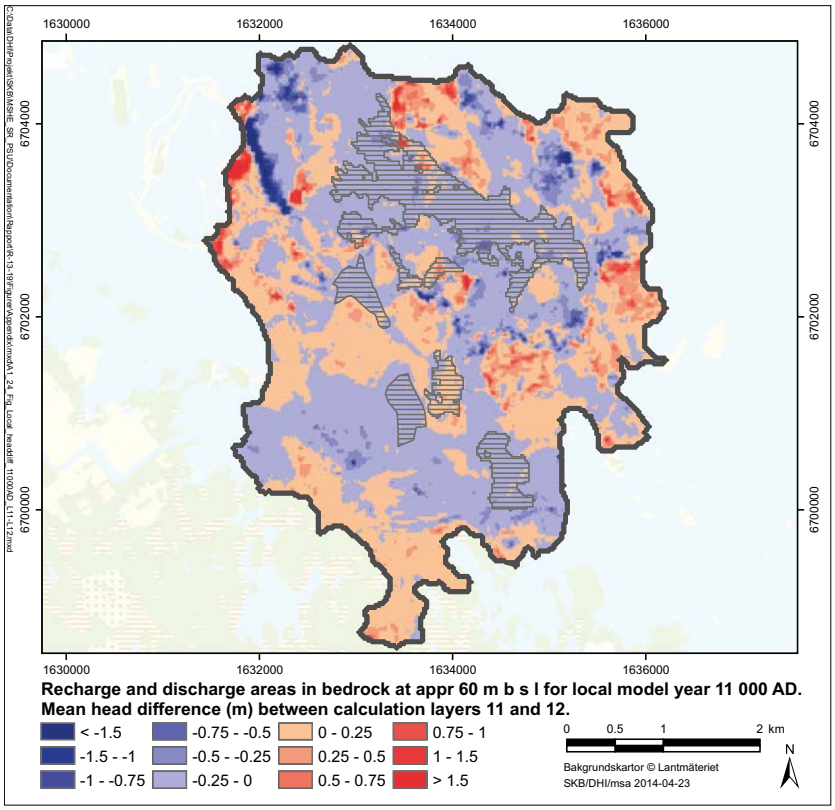

Figure A1-24. *Annual average hydraulic-head differences (m) in the rock (c –60 m elevation) at 11,000 AD (normal year). Blue colours represent areas with upward gradients and red colours represent areas with downward gradients.*

Depth of overland water, depth to the groundwater table and vertical hydraulic-head differences in rock – wet and warm climate (5000 AD)

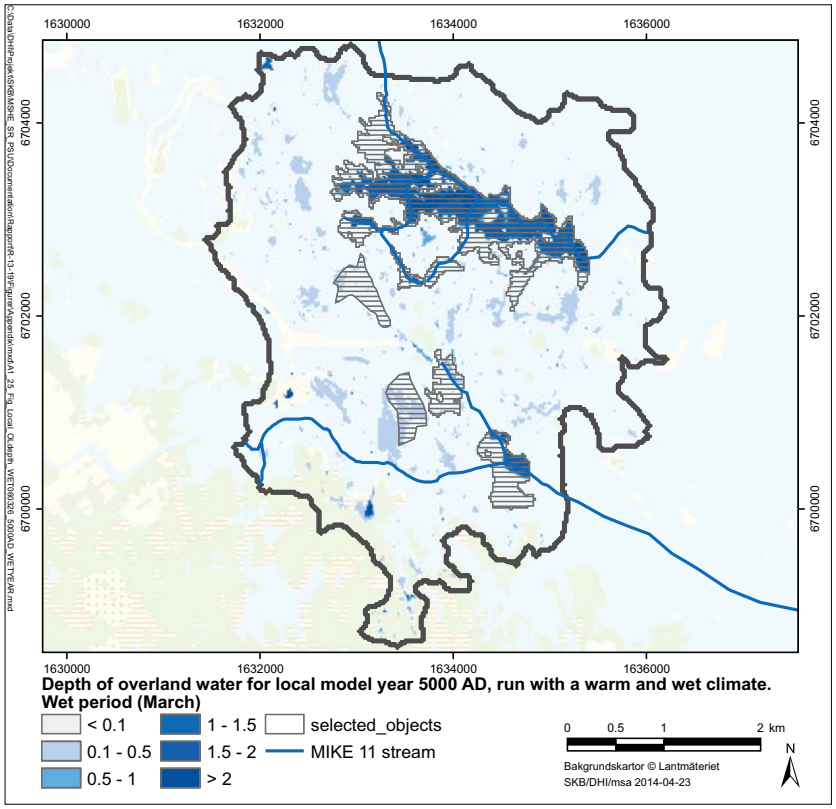

Figure A1-25. Depth of overland water (m) during a wet period (March) at 5000 AD (wet and warm climate).

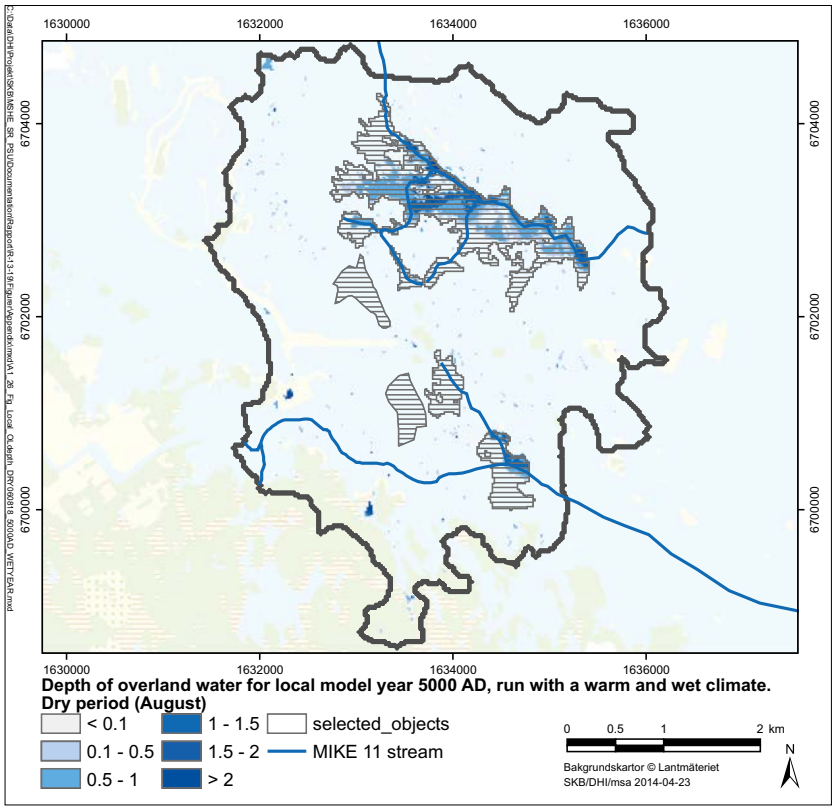

Figure A1-26. Depth of overland water (m) during a dry period (August) at 5000 AD (wet and warm climate).

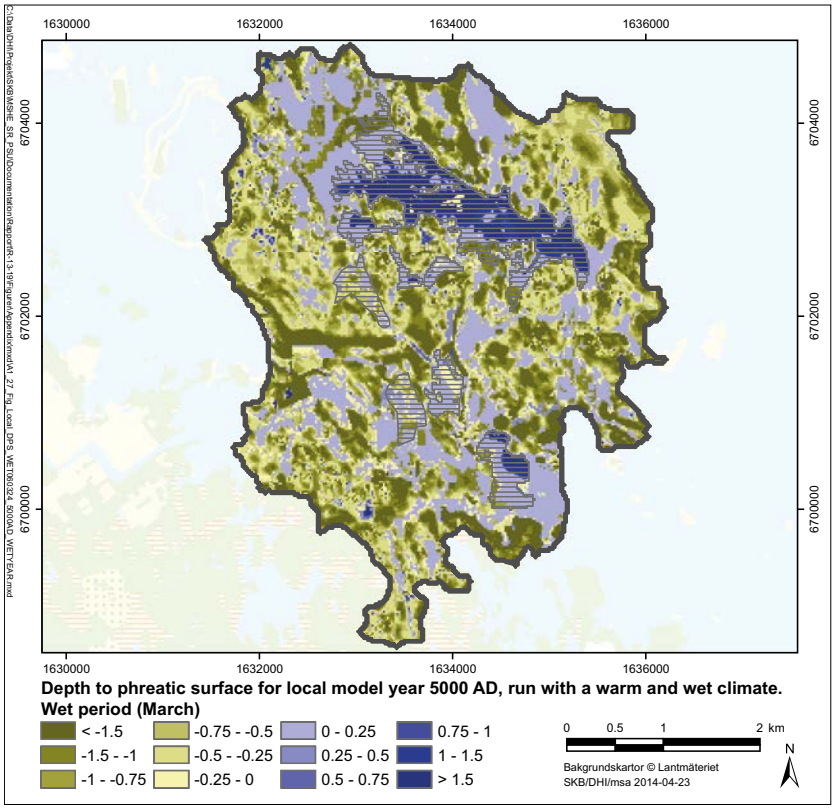

Figure A1-27. *Depth to the groundwater table (mbgs) during a wet period (March) at 5000 AD (wet and warm climate).*

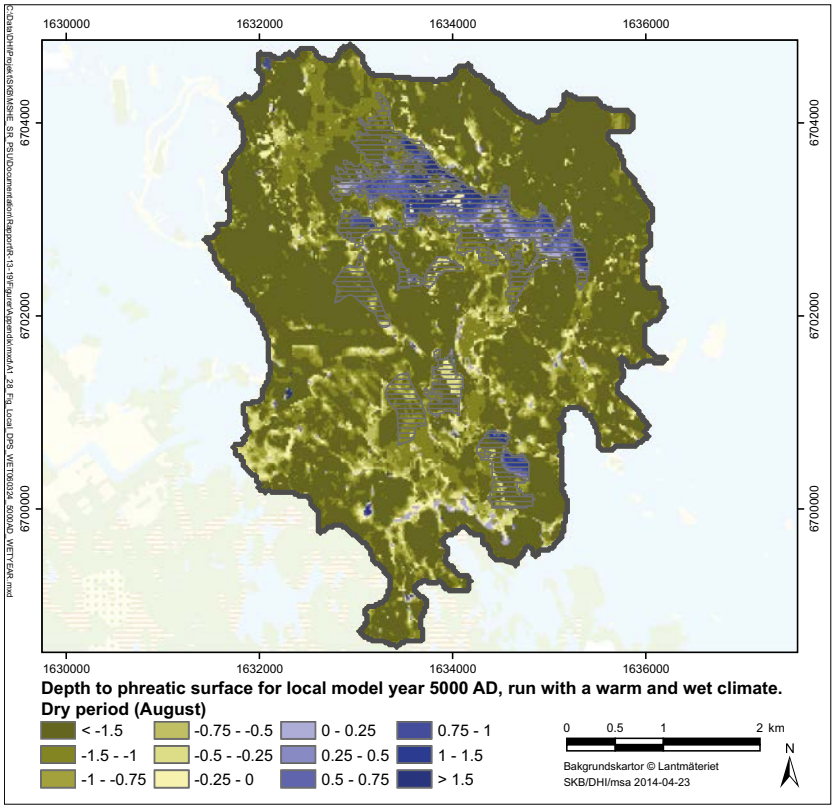

Figure A1-28. *Depth to the groundwater table (mbgs) during a dry period (August) at 5000 AD (wet and warm climate).*

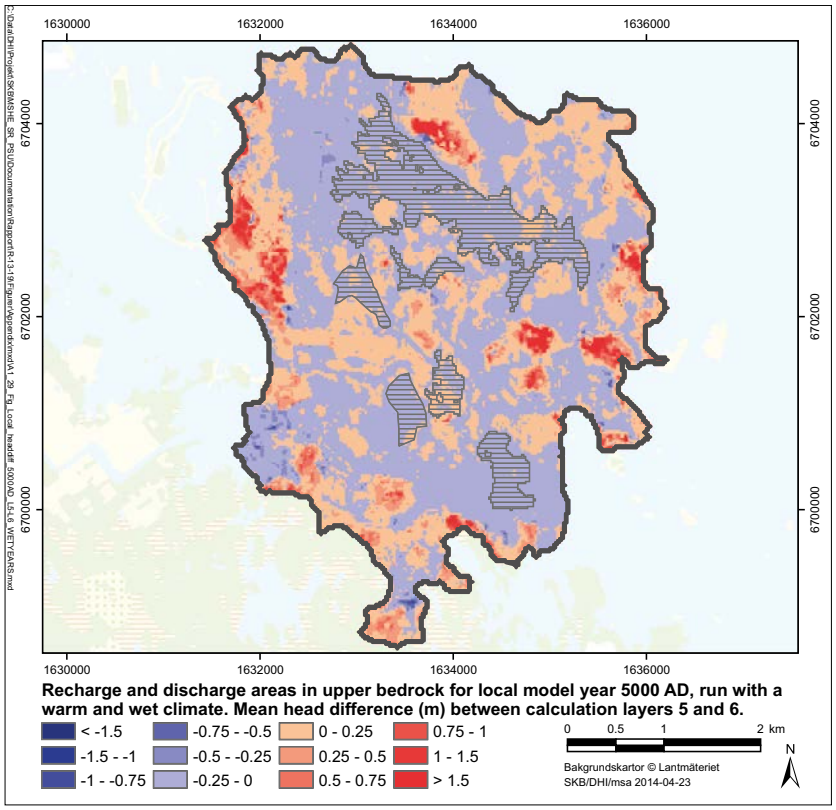

Figure A1-29. *Annual average hydraulic-head differences (m) in the rock (c –20 m elevation) at 5000 AD (wet and warm climate). Blue colours represent areas with upward gradients and red colours represent areas with downward gradients.*

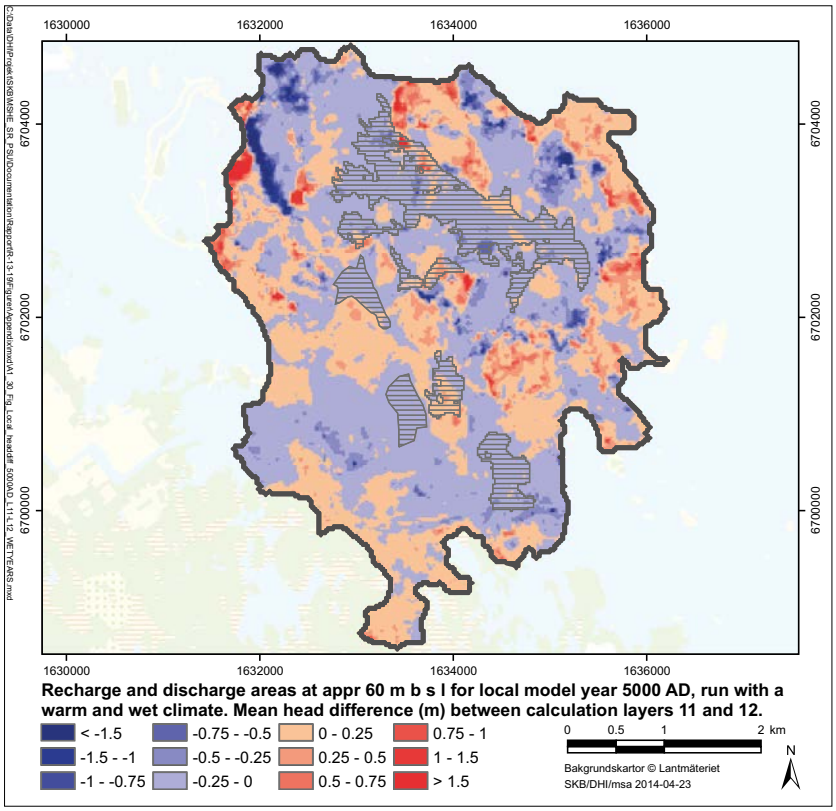

Figure A1-30. *Annual average hydraulic-head differences (m) in the rock (c –60 m elevation) at 11,000 AD (wet and warm climate). Blue colours represent areas with upward gradients and red colours represent areas with downward gradients.*

Water balances for biosphere objects – normal year (3000 AD)

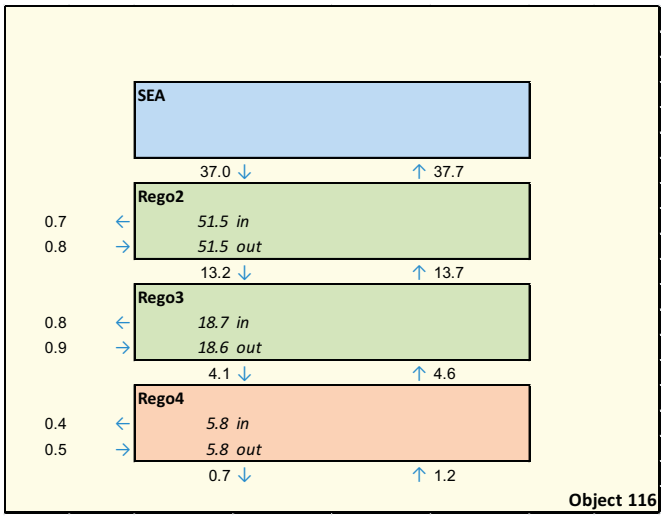

Figure A1-31. *Water balance for biosphere object 116 at 3000 AD (normal year).*

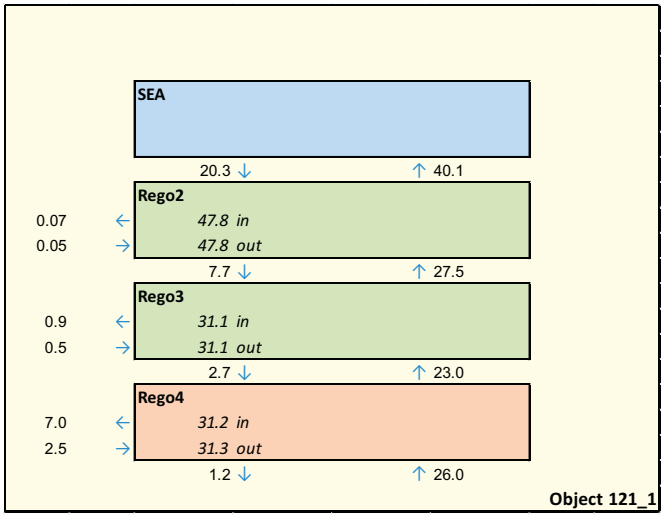

Figure A1-32. *Water balance for biosphere object 121_1 at 3000 AD (normal year).*

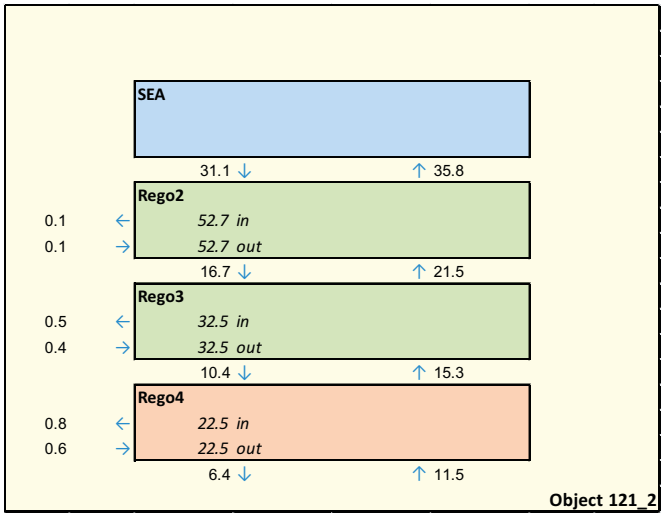

Figure A1-33. *Water balance for biosphere object 121_2 at 3000 AD (normal year).*

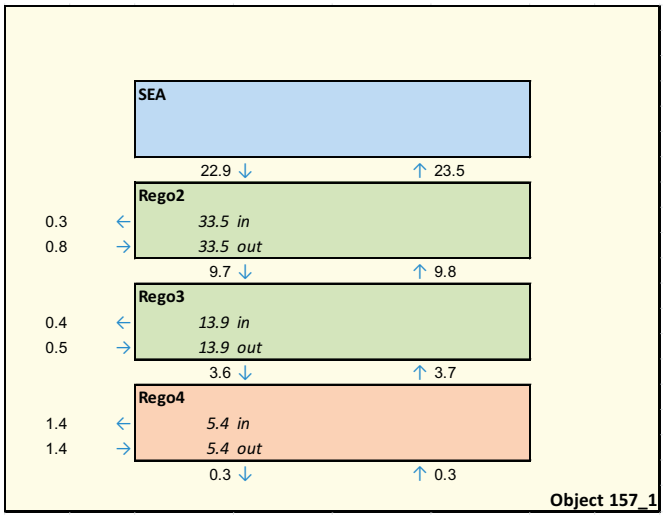

Figure A1-34. *Water balance for biosphere object 157_1 at 3000 AD (normal year).*

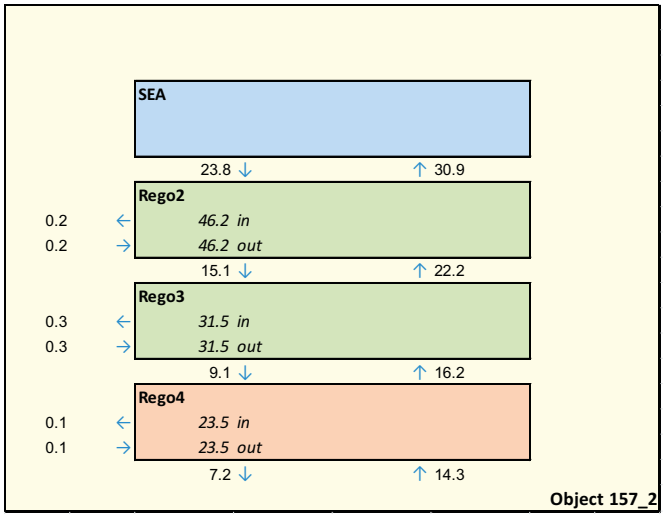

Figure A1-35. *Water balance for biosphere object 157_2 at 3000 AD (normal year).*

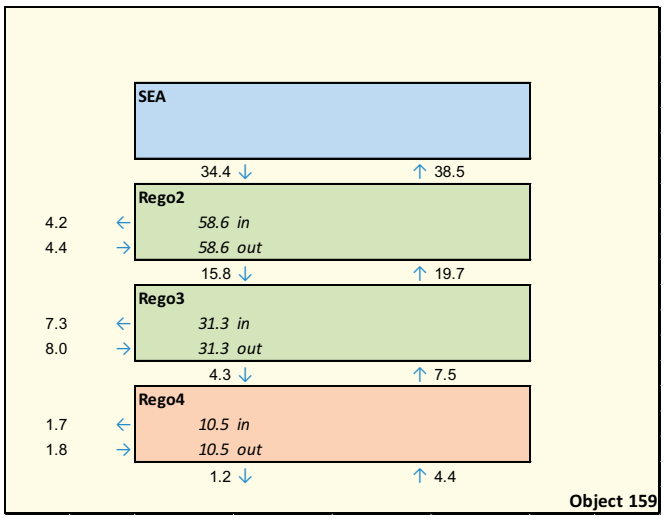

Figure A1-36. *Water balance for biosphere object 159 at 3000 AD (normal year).*

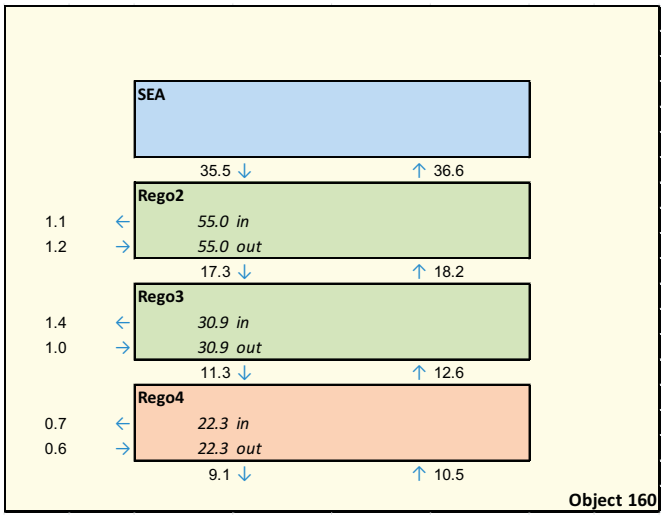

Figure A1-37. *Water balance for biosphere object 160 at 3000 AD (normal year).*

Water balances for biosphere objects – normal year (5000 AD)

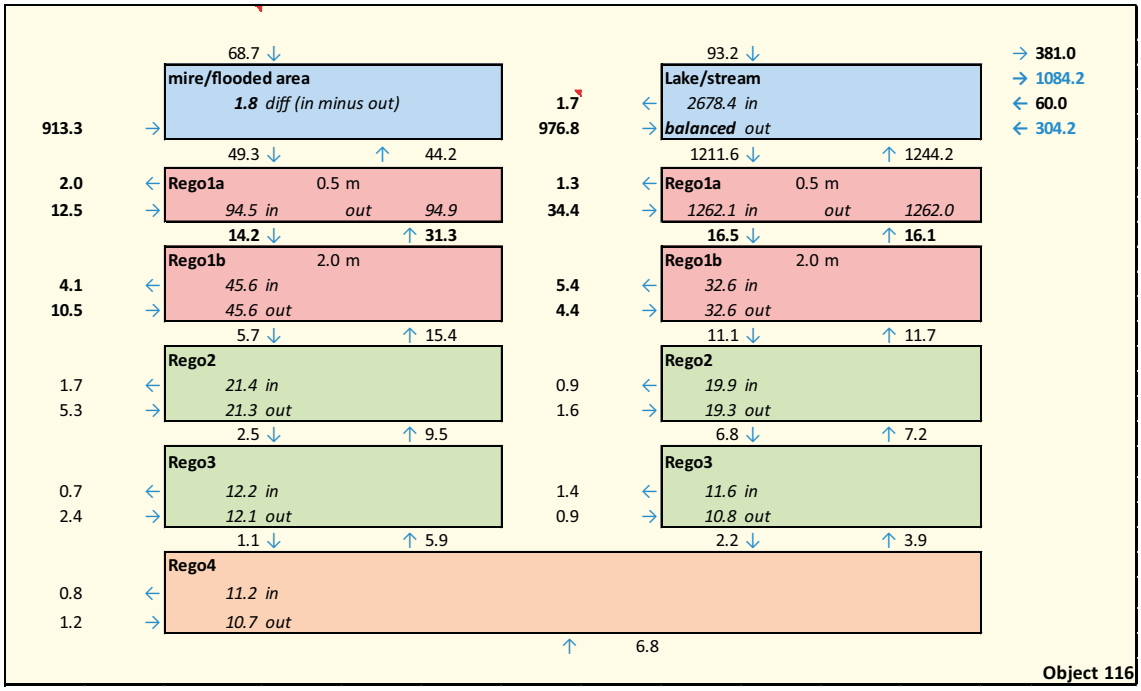

Figure A1-38. *Water balance for biosphere object 116 at 5000 AD (normal year).*

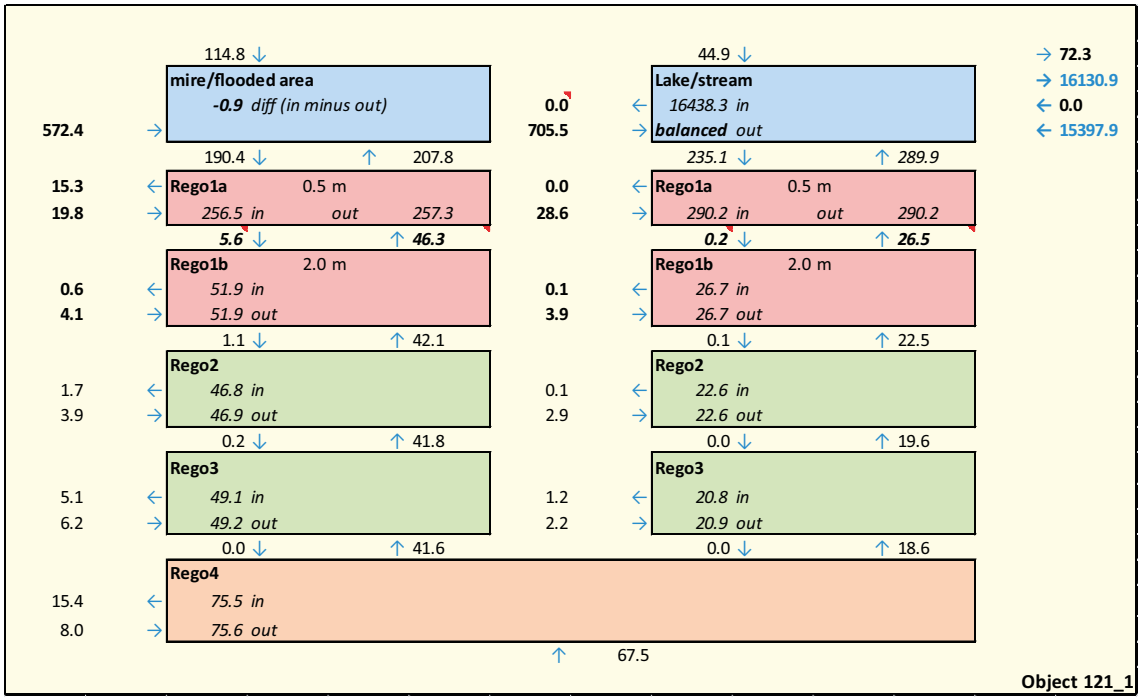

Figure A1-39. *Water balance for biosphere object 121_1 at 5000 AD (normal year).*

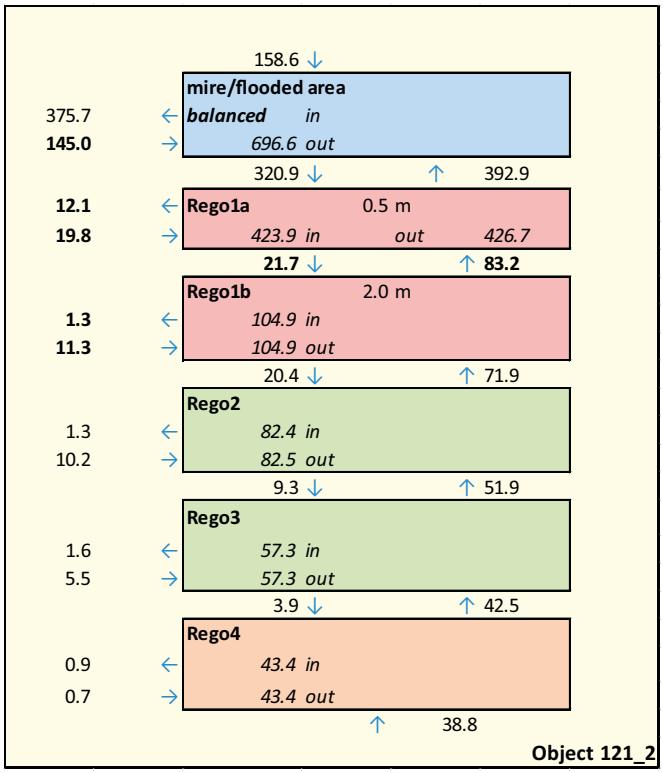

Figure A1-40. *Water balance for biosphere object 121_2 at 5000 AD (normal year).*

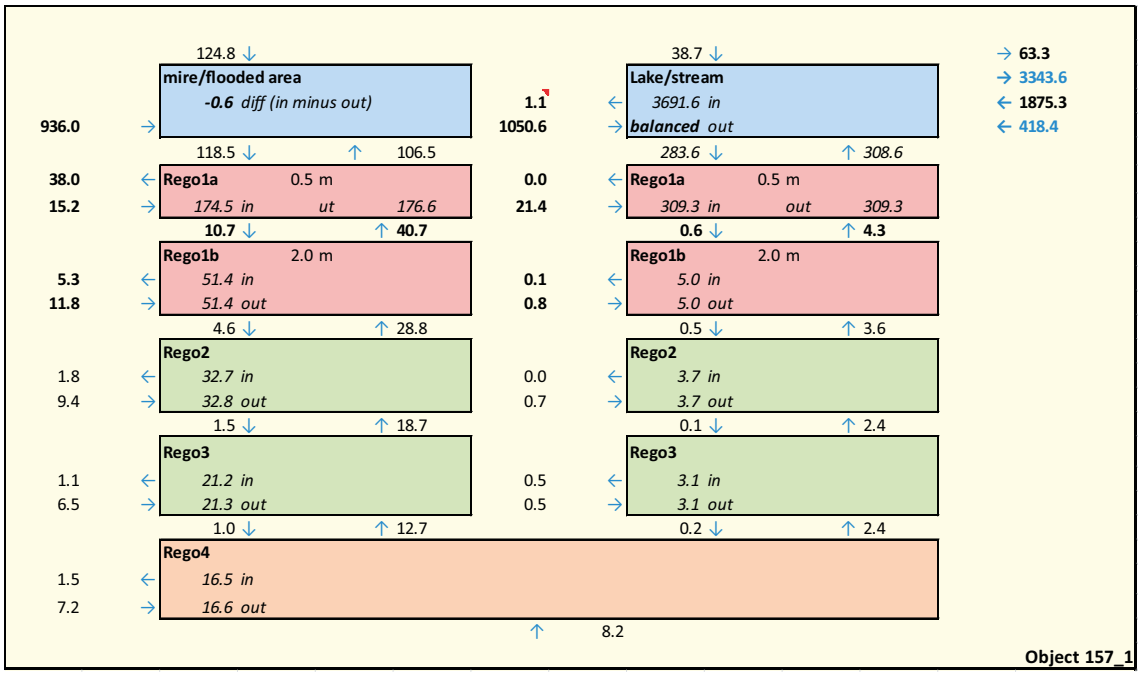

Figure A1-41. *Water balance for biosphere object 157_1 at 5000 AD (normal year).*

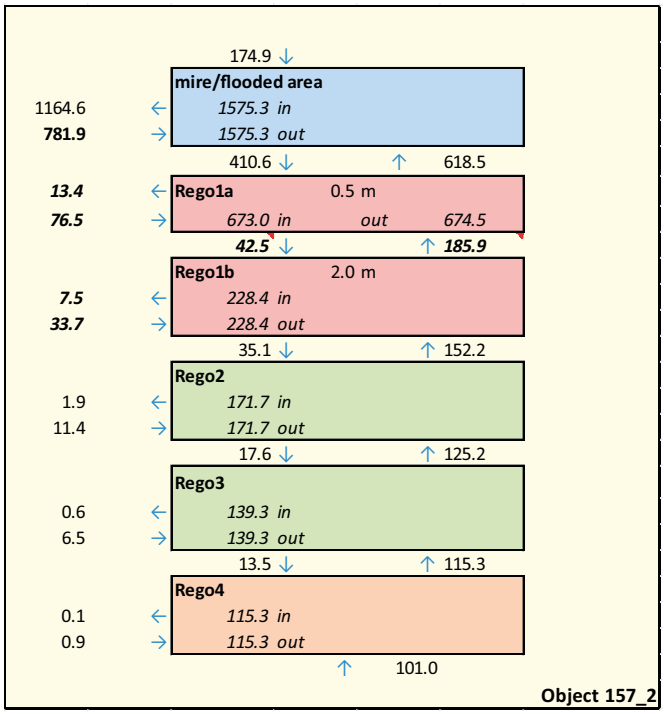

Figure A1-42. *Water balance for biosphere object 157_2 at 5000 AD (normal year).*

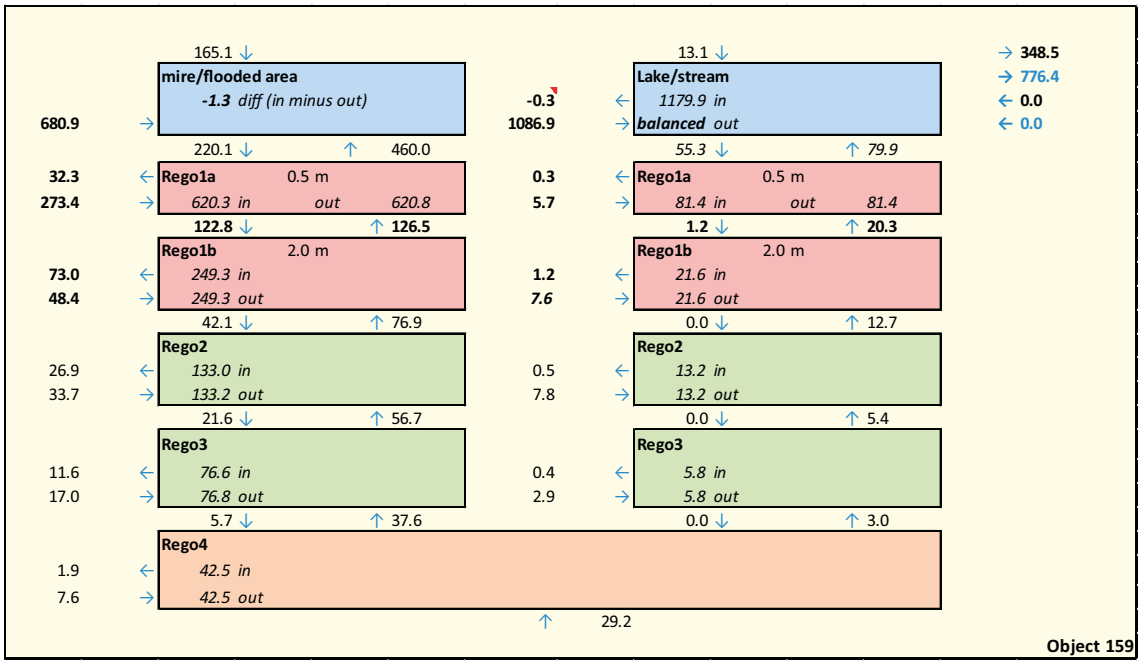

Figure A1-43. *Water balance for biosphere object 159 at 5000 AD (normal year).*

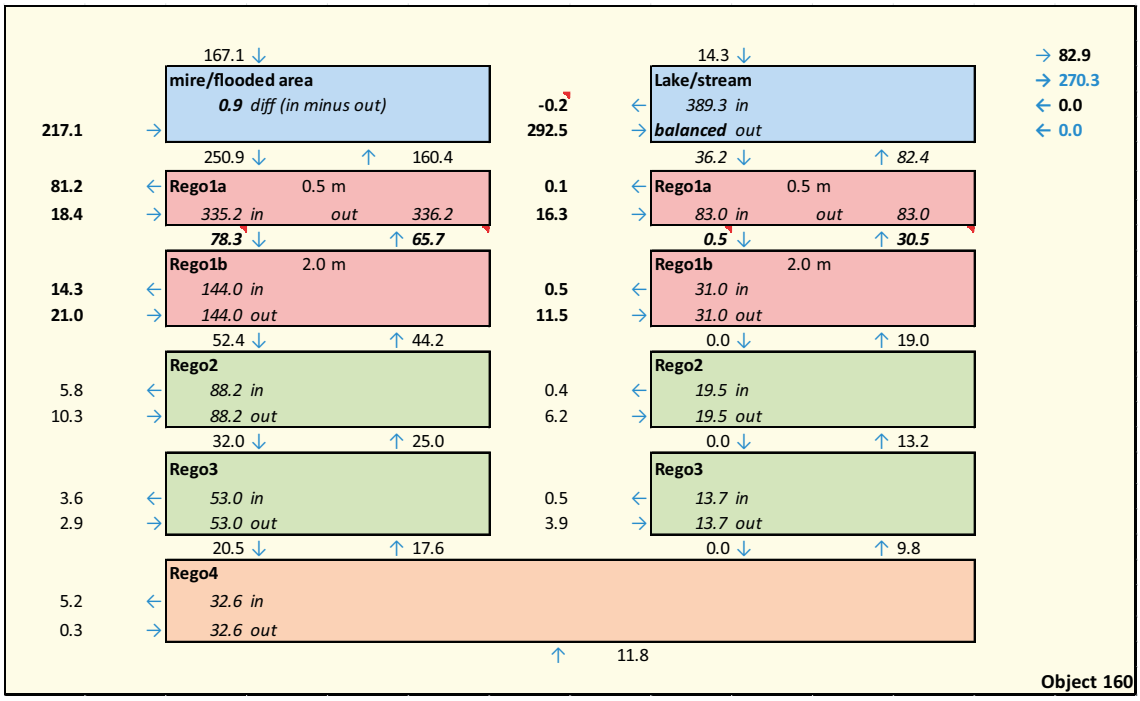

Figure A1-44. *Water balance for biosphere object 160 at 5000 AD (normal year).*

Water balances for biosphere objects – normal year (11,000 AD)

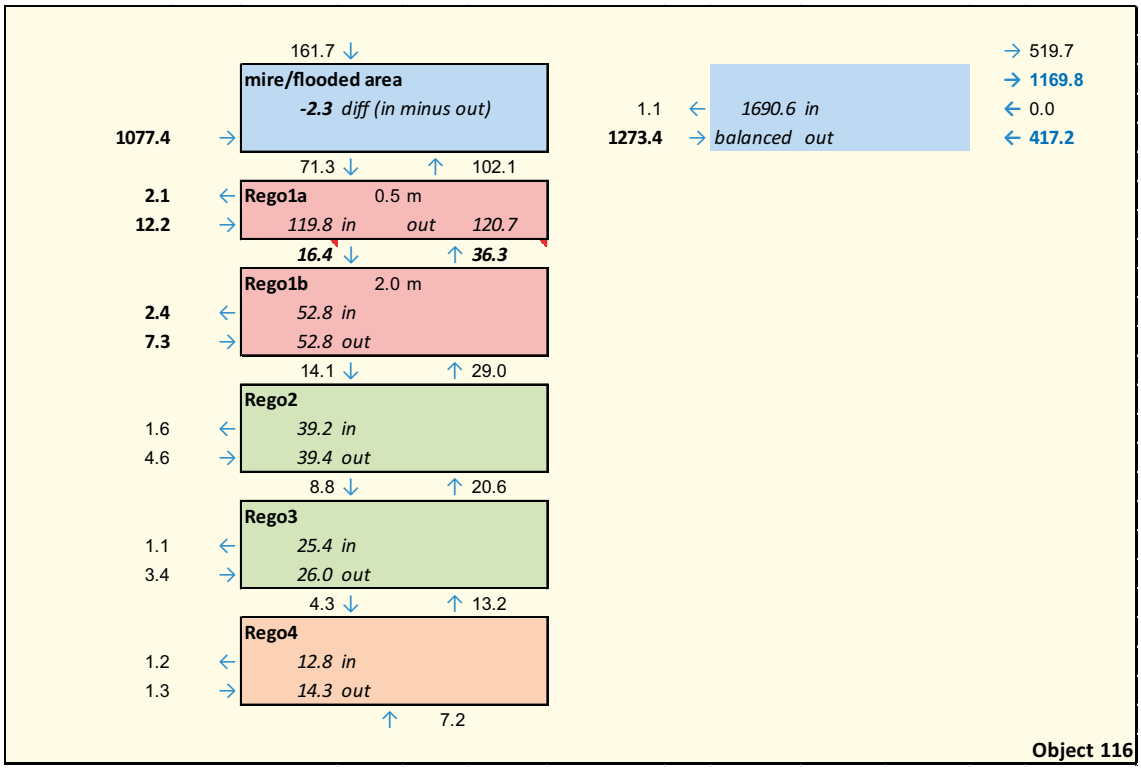

Figure A1-45. *Water balance for biosphere object 116 at 11,000 AD (normal year).*

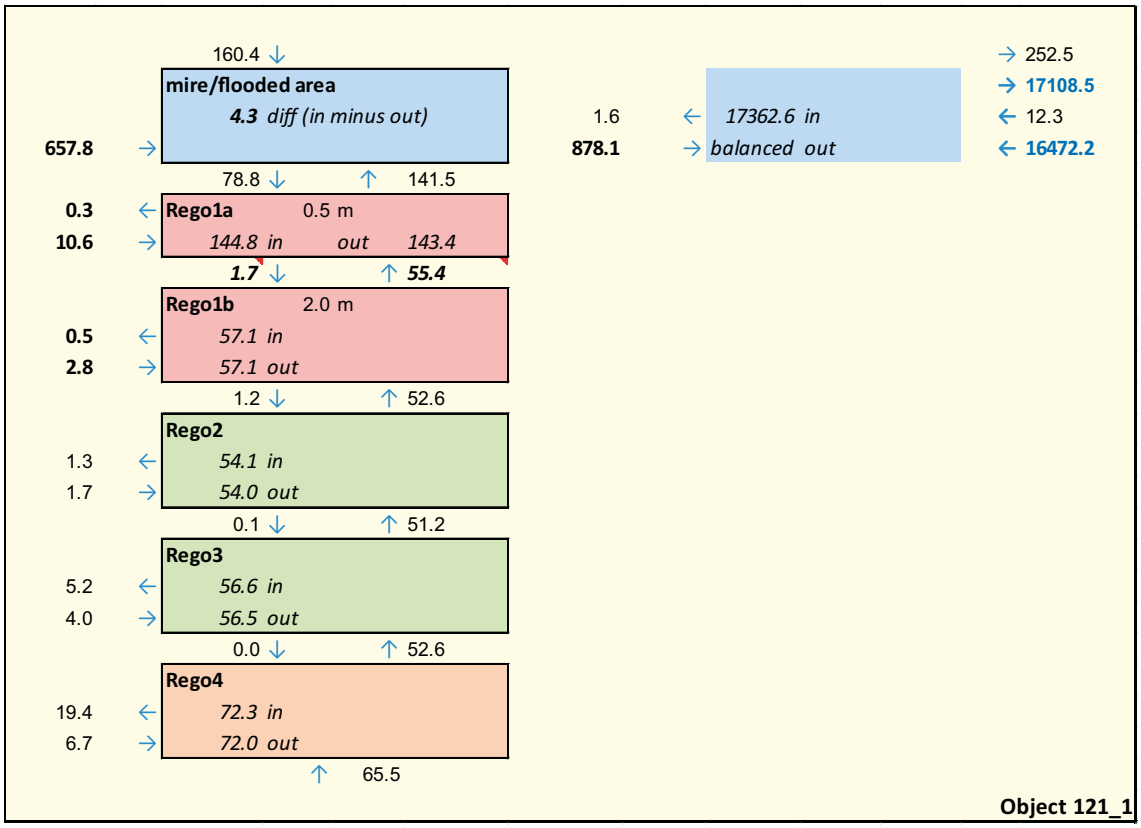

Figure A1-46. *Water balance for biosphere object 121_1 at 11,000 AD (normal year).*

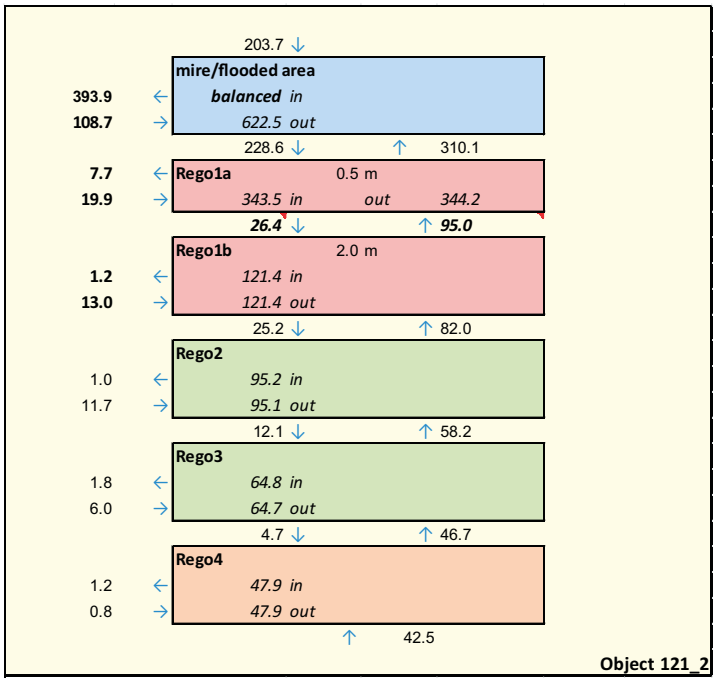

Figure A1-47. *Water balance for biosphere object 121_2 at 11,000 AD (normal year).*

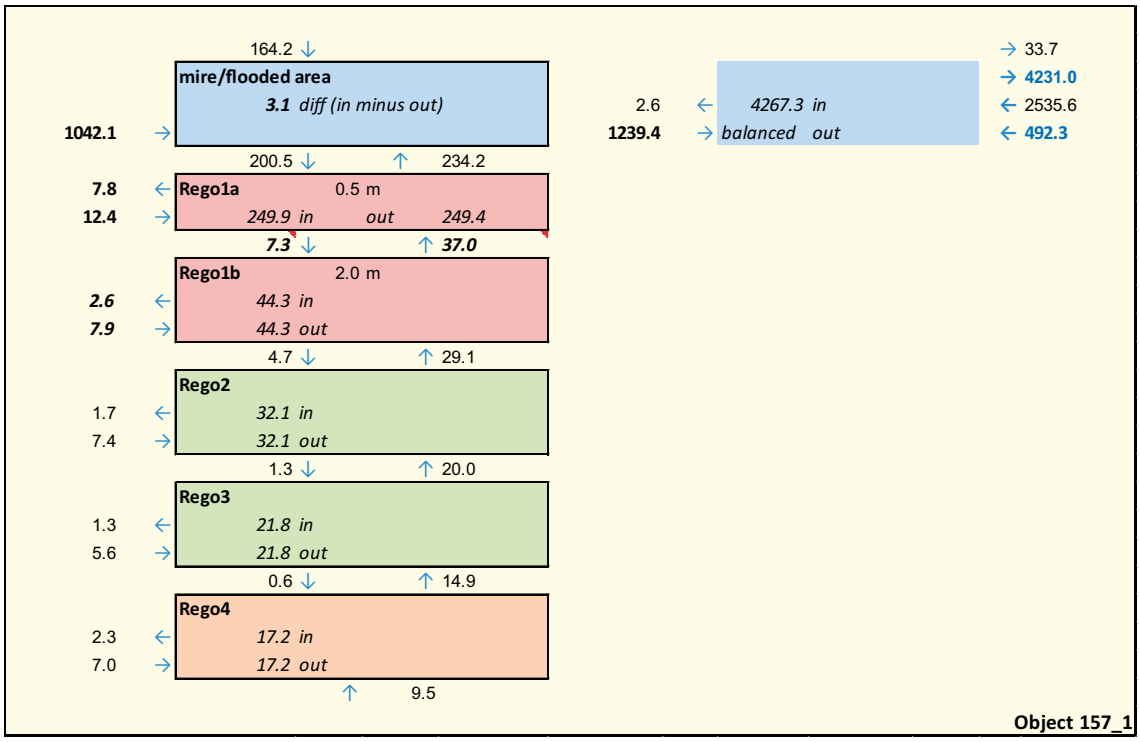

Figure A1-48. *Water balance for biosphere object 157_1 at 11,000 AD (normal year).*

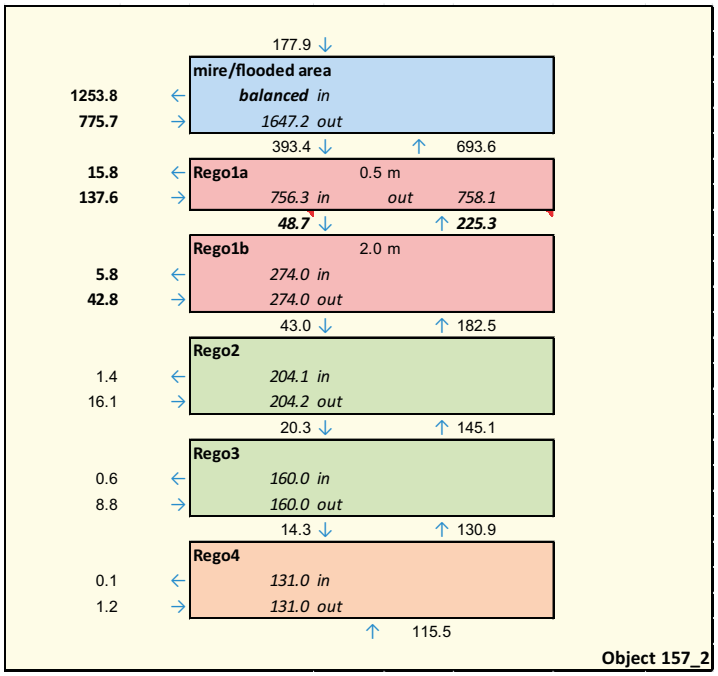

Figure A1-49. *Water balance for biosphere object 157_2 at 11,000 AD (normal year).*

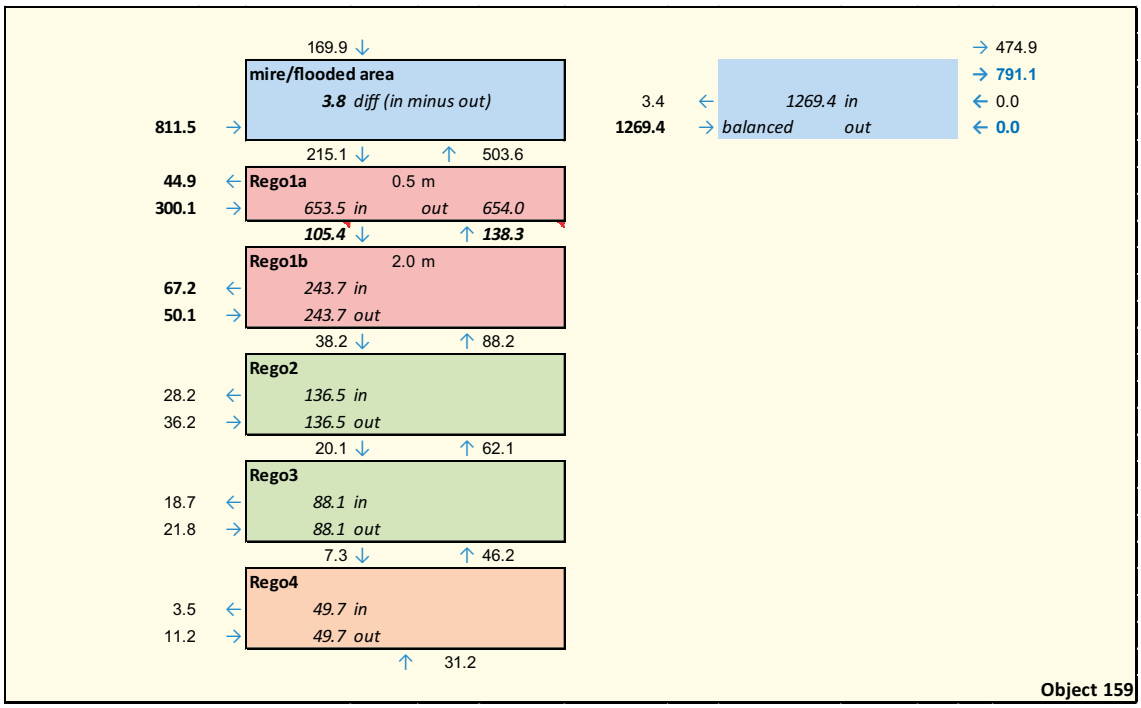

Figure A1-50. *Water balance for biosphere object 159 at 11,000 AD (normal year).*

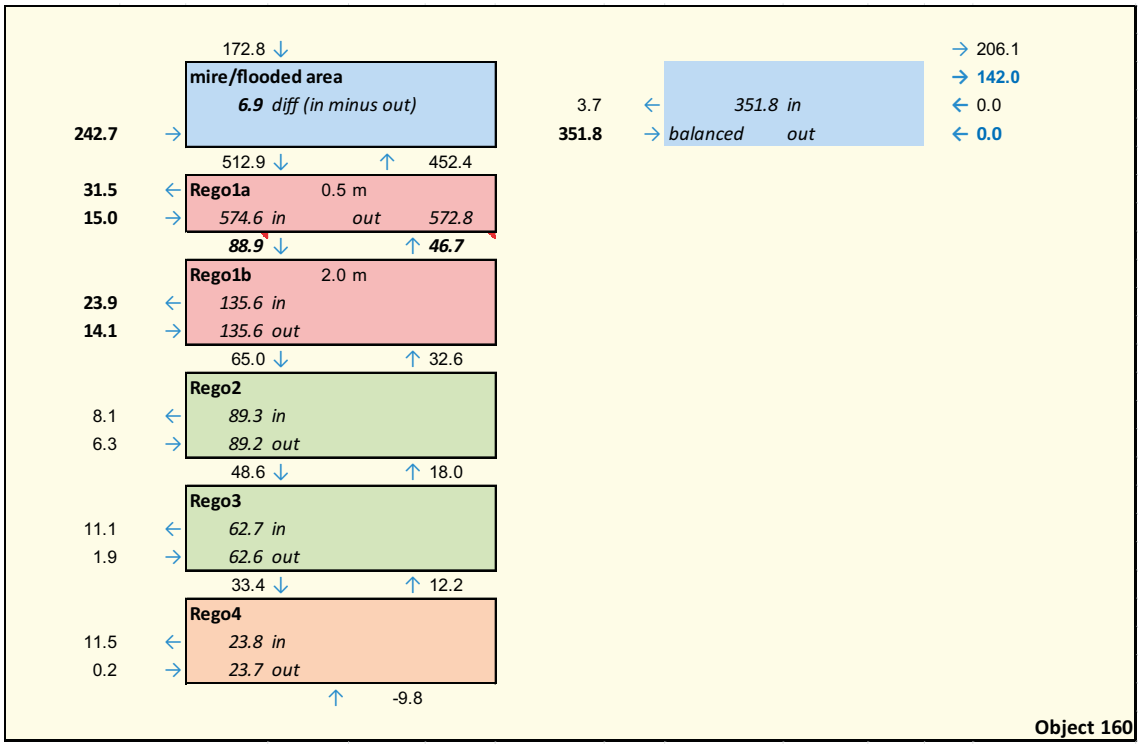

Figure A1-51. *Water balance for biosphere object 160 at 11,000 AD (normal year).*

Water balances for subareas of biosphere object 157_2 (normal year)

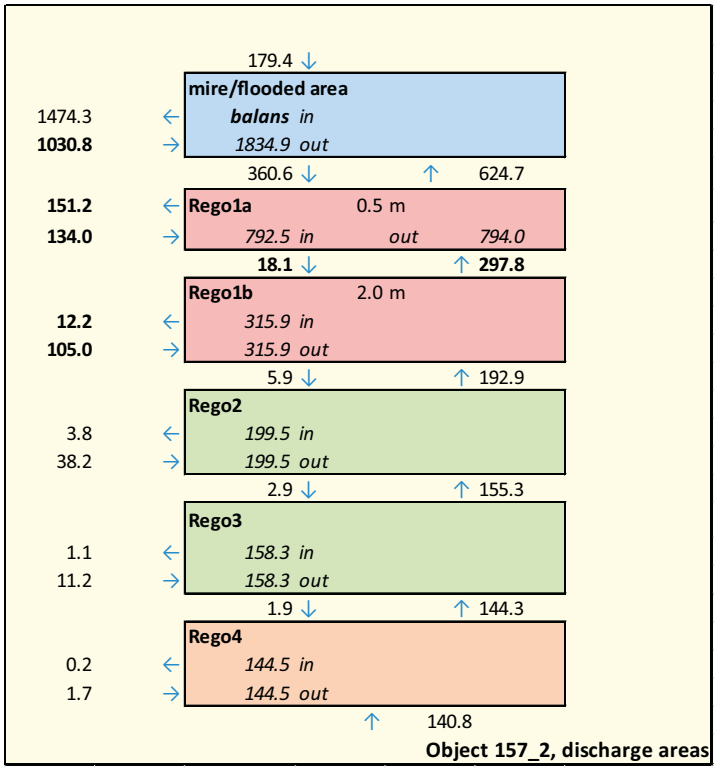

Figure A1-52. *Water balance for subareas with upward hydraulic gradients in regolith, in the upper part of rock and in the rock at –60 m elevation (5000 AD, normal year).*

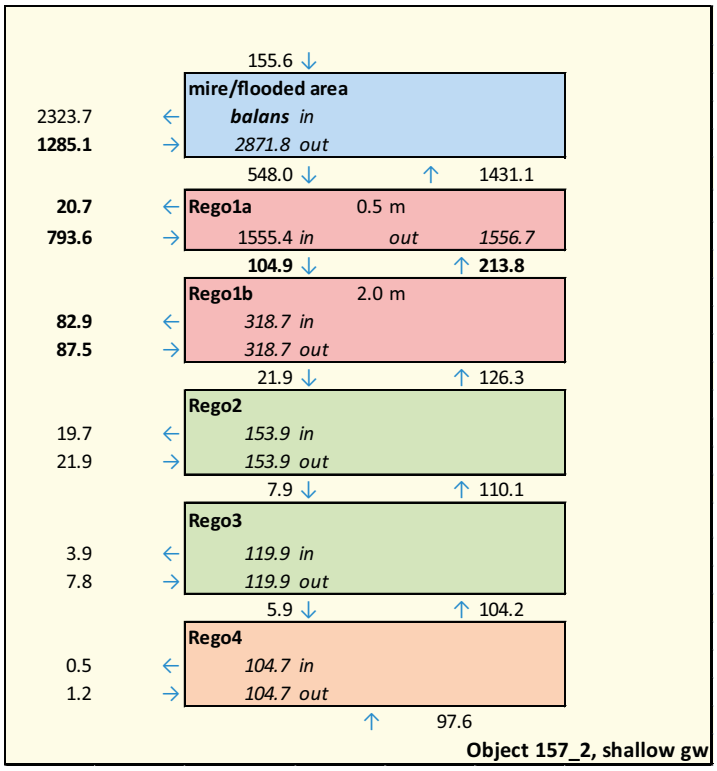

Figure A1-53. *Water balance for subareas with shallow (less than 0.25 mbgs) depth to the groundwater table (5000 AD, normal year).*

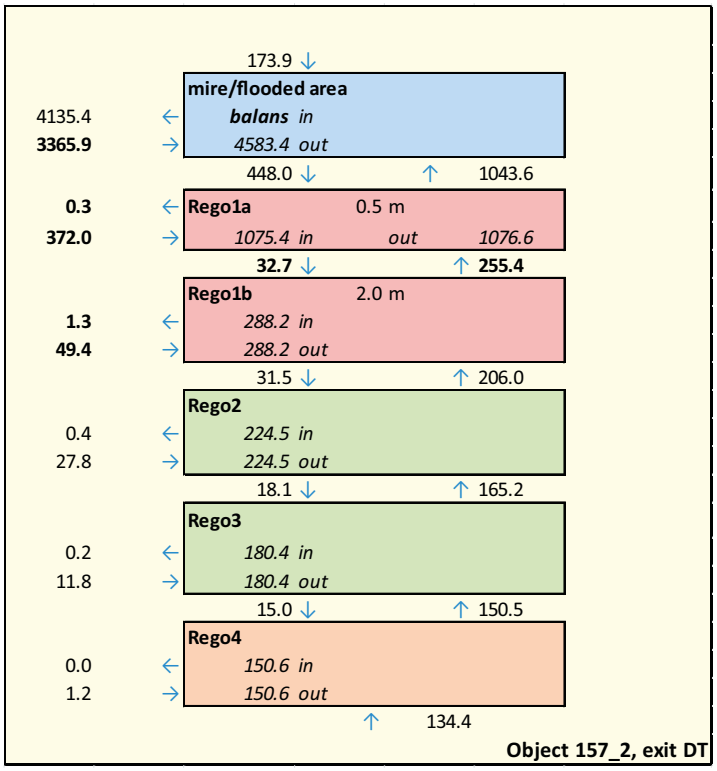

Figure A1-54. *Water balance for subareas with high discharge-location density (DarcyTools particle tracking) at the interface between rock and regolith (5000 AD, normal year).*

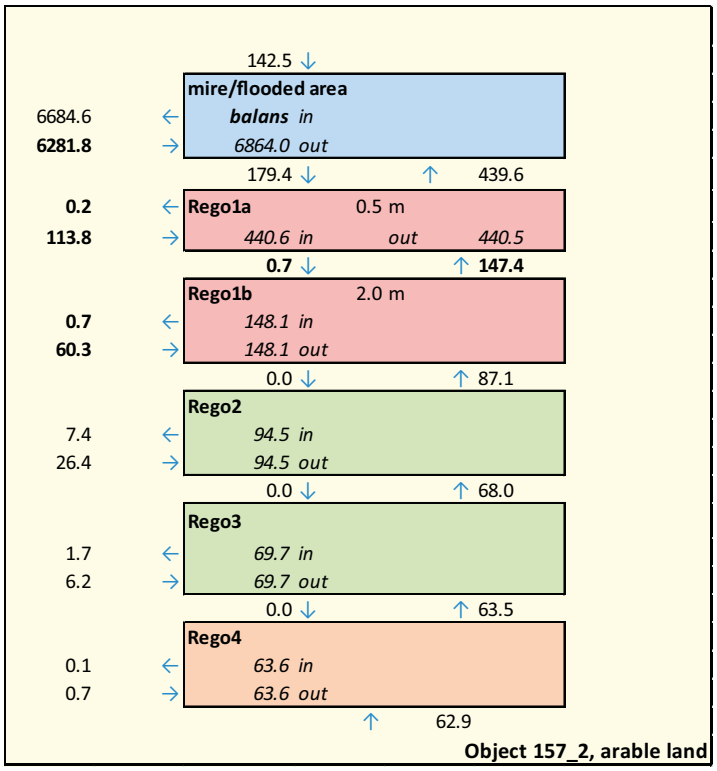

Figure A1-55. *Water balance for subareas with potential arable land (5000 AD, normal year).*

Water balance for biosphere object 157_2 – stream between objects 157_2 and 157_1 (normal year)

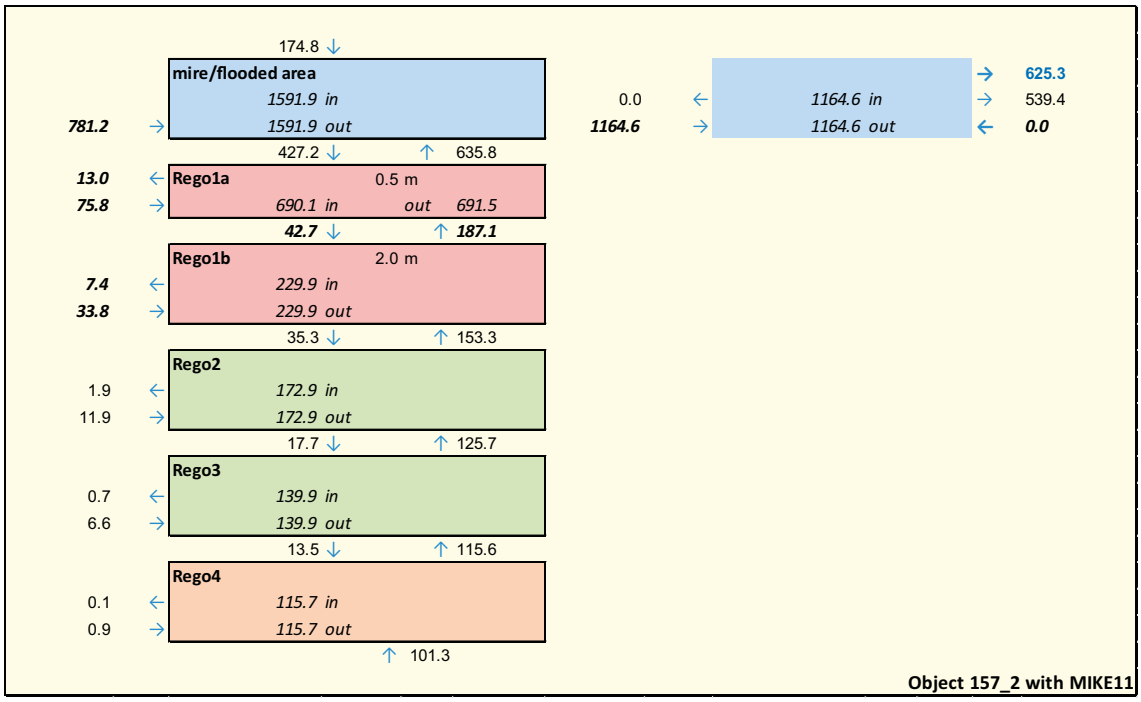

Figure A1-56. Water balance for biosphere object 157_2 at 5000 AD (normal year), with a stream between objects 157_2 and 157_1.

Water balances for biosphere objects – wet and warm climate

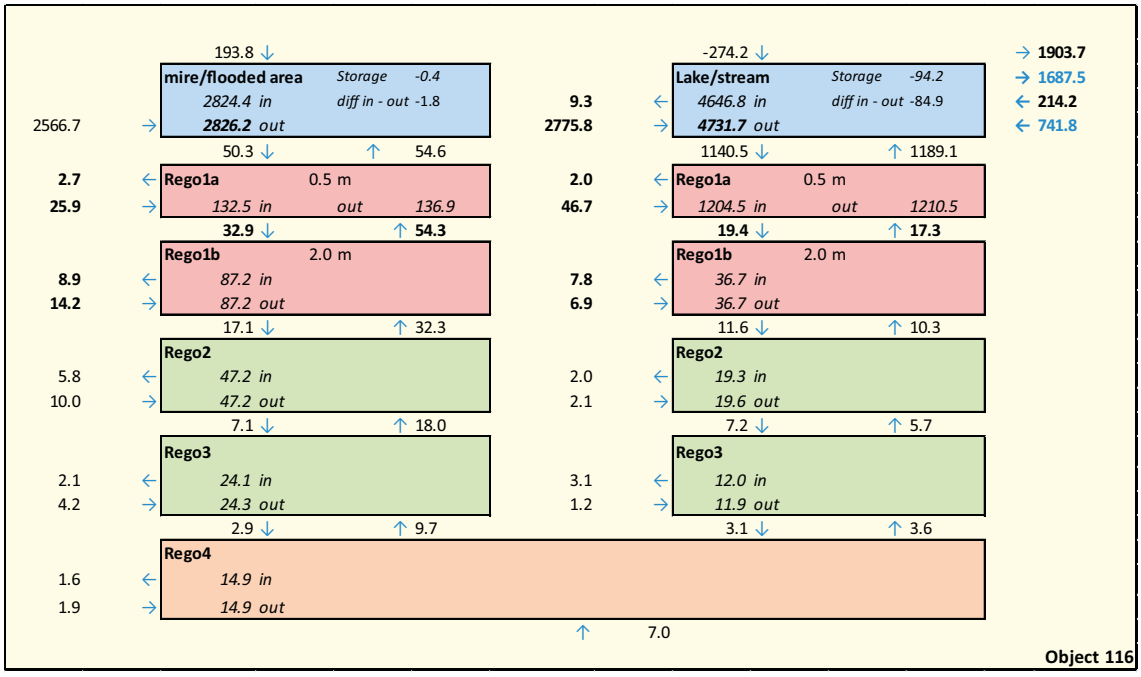

Figure A1-57. Water balance for biosphere object 116 at 5000 AD (wet and warm climate).

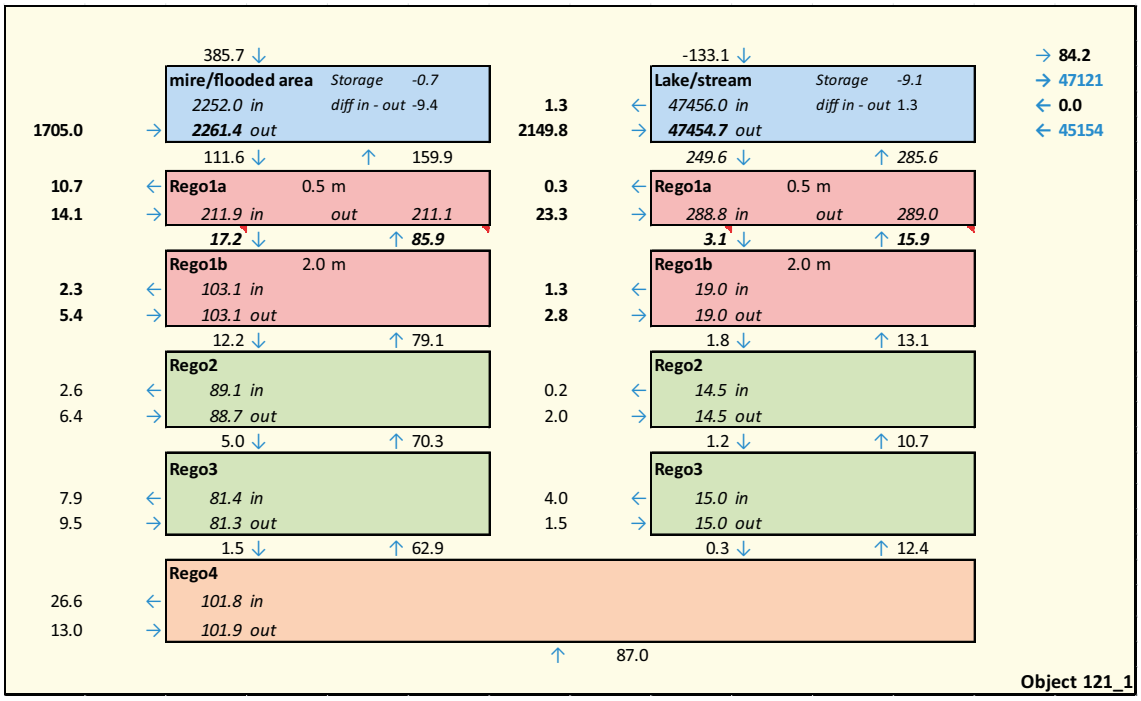

Figure A1-58. *Water balance for biosphere object 121_1 at 5000 AD (wet and warm climate).*

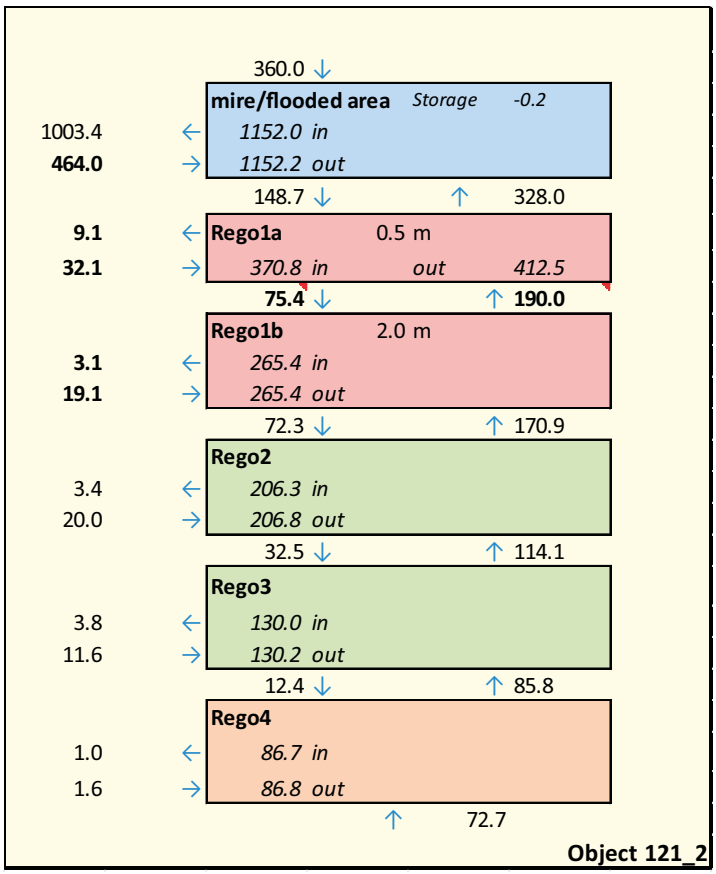

Figure A1-59. *Water balance for biosphere object 121_2 at 5000 AD (wet and warm climate).*

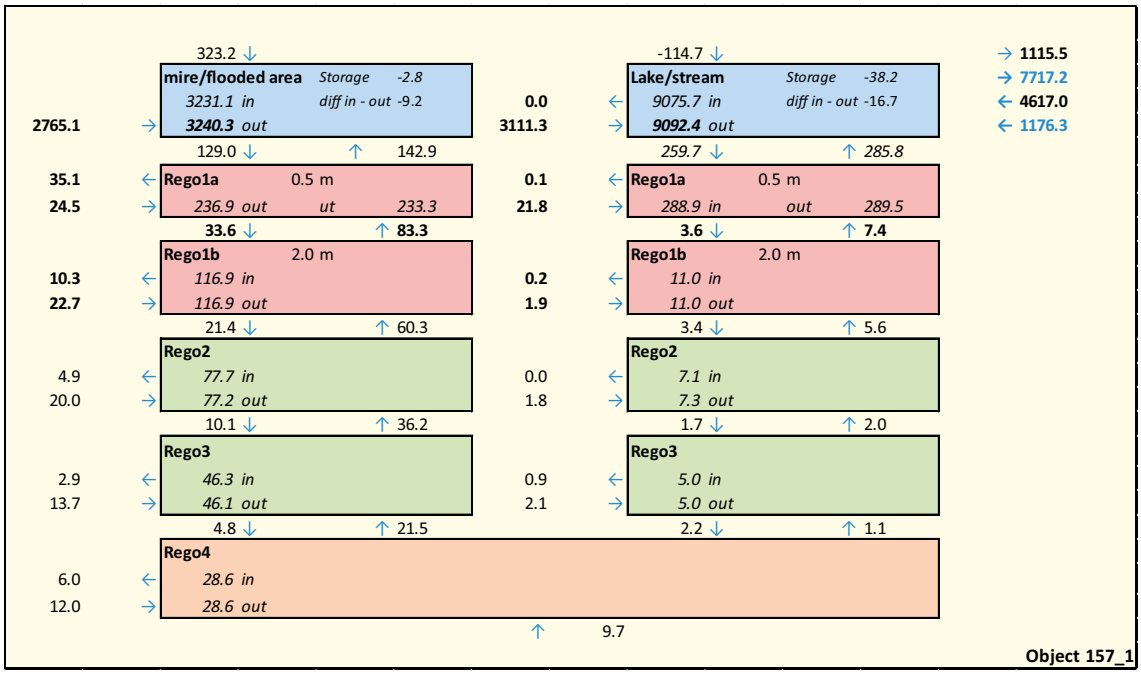

Figure A1-60. *Water balance for biosphere object 157_1 at 5000 AD (wet and warm climate).*

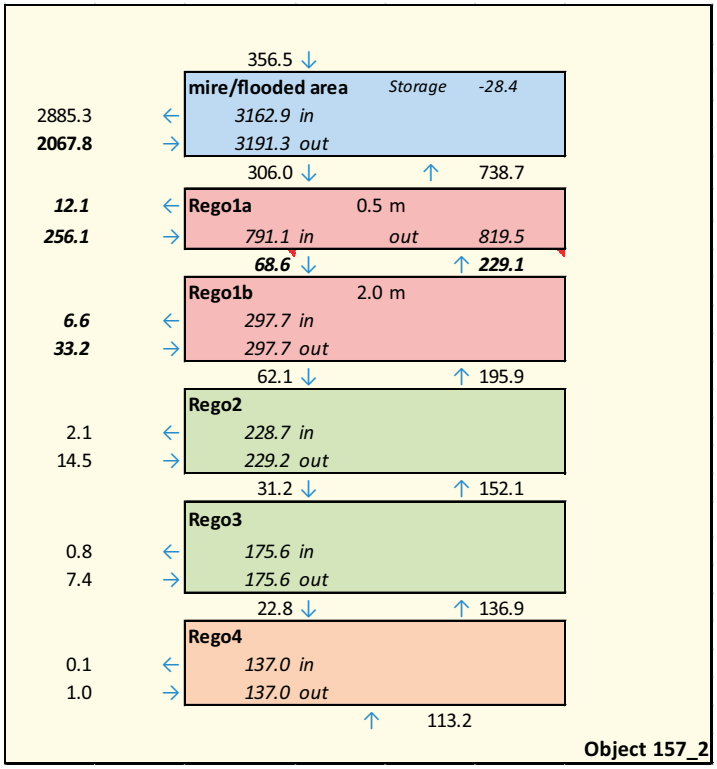

Figure A1-61. *Water balance for biosphere object 157_2 at 5000 AD (wet and warm climate).*

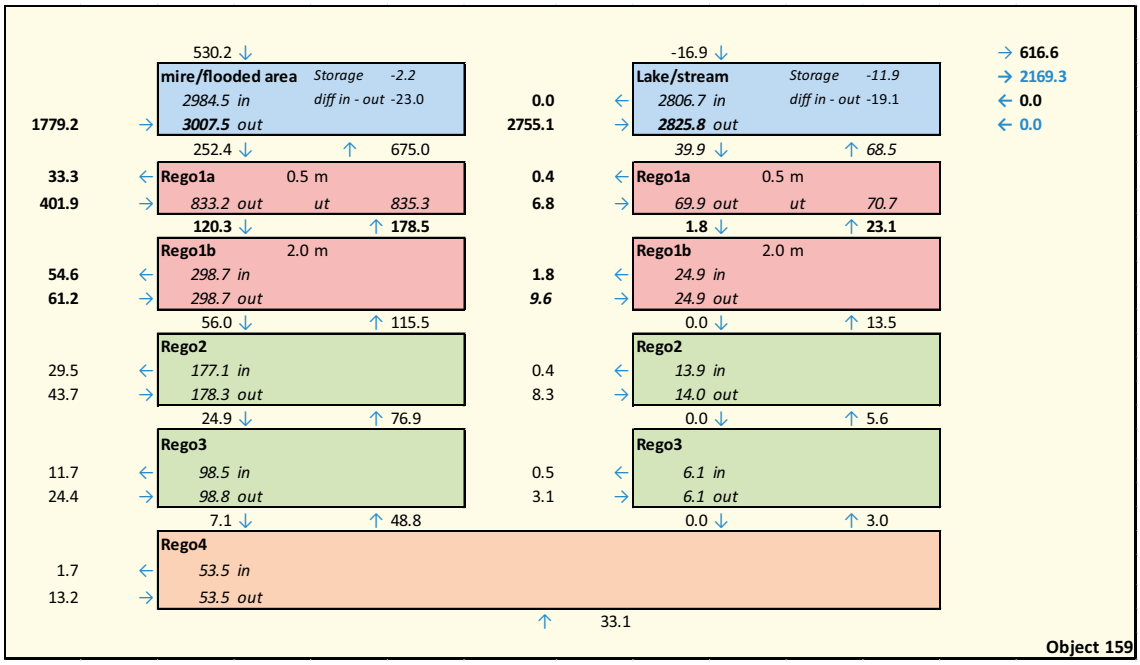

Figure A1-62. *Water balance for biosphere object 159 at 5000 AD (wet and warm climate).*

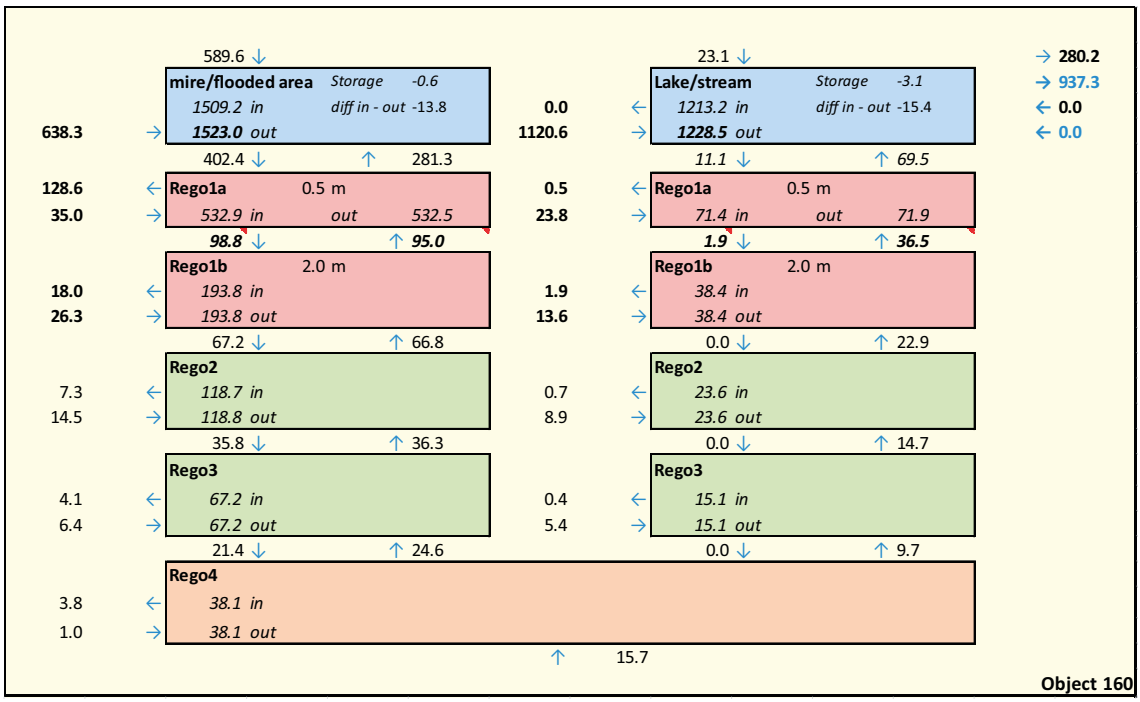

Figure A1-63. *Water balance for biosphere object 160 at 5000 AD (wet and warm climate).*

Water balances for periglacial conditions with 100 m permafrost (cf Bosson et al. 2010)

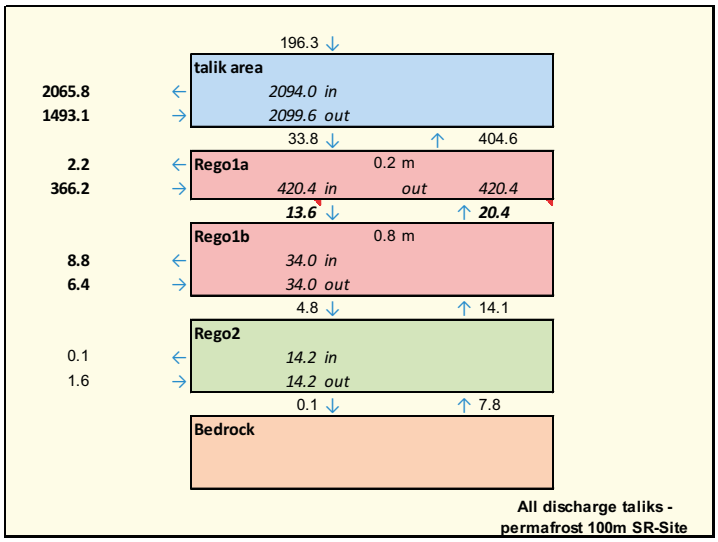

Figure A1-64. Water balance for all discharge taliks.

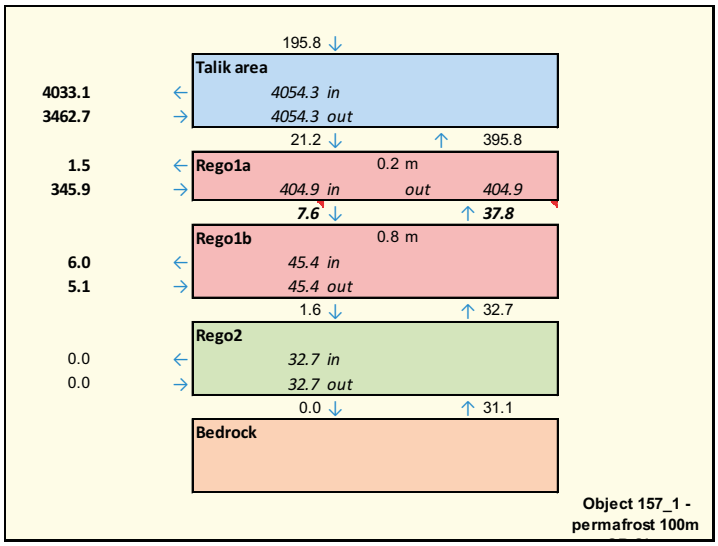

Figure A1-65. Water balance for a discharge talik at the location of biosphere object 157_1.

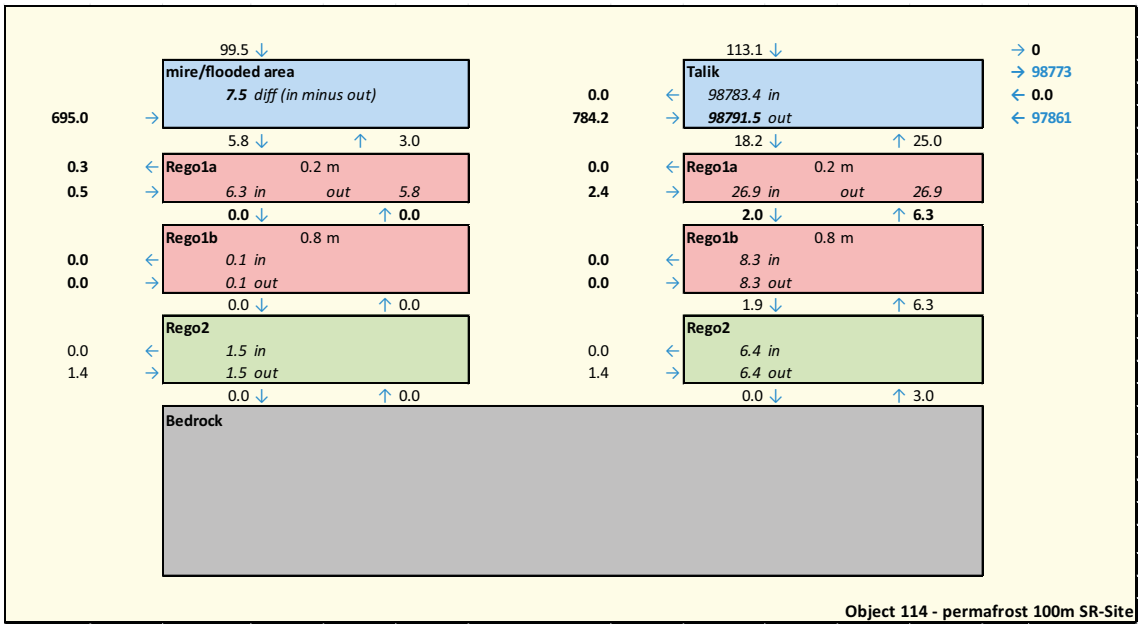

Figure A1-66. *Water balance for a discharge talik at the SR-Site biosphere object 114.*

Regolith-layer thicknesses for water-balance calculations

Table A1-1. Regolith-layer thicknesses 3000 AD water balances (normal year).

	Thickness rego-layer (m)											
	Object 157_2			Object 159			Object 157_1			Object 116		
Layer name	Mean	Min	Max	Mean	Min	Max	Mean	Min	Max	Mean	Min	Max
Peat / organic	-	-	-	-	-	-	-	-	-	-	-	-
Post-glacial lacustrine	-	-	-	-	-	-	-	-	-	-	-	-
Post-glacial marine	0.27	0.20	0.37	0.33	0.20	0.37	0.37	0.37	0.37	0.31	0.20	0.54
Glacial clay	0.17	0.00	2.68	0.45	0.00	2.78	3.13	0.00	6.45	2.04	0.00	10.11
Fill	-	-	-	-	-	-	-	-	-	-	-	-
Glaciofluvium	-	-	-	0.11	0.00	3.49	-	-	-	0.08	0.00	5.10
Till	2.44	0.36	6.17	2.55	0.00	6.14	3.10	0.00	6.57	2.97	0.00	10.47
Total	2.88			3.44			6.60			5.40		

	Thickness rego-layer (m)								
	Object 121_2			Object 160			Object 121_1		
Layer name	Mean	Min	Max	Mean	Min	Max	Mean	Min	Max
Peat / organic	-	-	-	-	-	-	-	-	-
Post-glacial lacustrine	-	-	-	-	-	-	-	-	-
Post-glacial marine	0.54	0.54	0.54	0.37	0.12	0.54	0.54	0.54	0.54
Glacial clay	0.84	0.00	3.62	0.90	0.00	5.34	3.99	0.00	9.23
Fill	-	-	-	-	-	-	-	-	-
Glaciofluvium	-	-	-	0.01	0.00	0.61	-	-	-
Till	3.93	0.88	6.47	2.27	0.00	6.08	6.34	1.53	12.44
Total	5.31			3.55			10.87		

Table A1-2. Regolith-layer thicknesses for 5000 AD water balances (normal year).

	Thickness rego-layer (m)					
	Object157_2					
	Lake area			Mire area		
Layer name	Mean	Min	Max	Mean	Min	Max
Peat / organic	-	-	-	0.17	0.00	1.76
Post-glacial lacustrine	-	-	-	-	-	-
Post-glacial marine	-	-	-	0.31	0.20	0.44
Glacial clay	-	-	-	0.17	0.00	2.68
Fill	-	-	-	-	-	-
Glaciofluvium	-	-	-	-	-	-
Till	-	-	-	2.40	0.36	6.17
Total	0.00			3.06		
	Object 159					
	Lake area			Mire area		
Layer name	Mean	Min	Max	Mean	Min	Max
Peat / organic	0.00	0.00	0.00	1.11	0.00	2.11
Post-glacial lacustrine	0.51	0.51	0.51	0.14	0.00	0.51
Post-glacial marine	0.46	0.44	0.50	0.43	0.27	0.50
Glacial clay	0.15	0.00	0.93	0.46	0.00	2.78
Fill	-	-	-	-	-	-
Glaciofluvium	-	-	-	0.11	0.00	3.49
Till	2.47	0.11	4.35	2.60	0.00	7.19
Total	3.59			4.85		
	Object 157_1					
	Lake area			Mire area		
Layer name	Mean	Min	Max	Mean	Min	Max
Peat / organic	0.06	0.04	0.10	1.20	0.00	3.26
Post-glacial lacustrine	0.33	0.10	0.53	0.10	0.00	0.53
Post-glacial marine	0.50	0.50	0.50	0.50	0.33	0.50
Glacial clay	3.93	0.00	5.81	2.80	0.00	6.45
Fill	-	-	-	-	-	-
Glaciofluvium	-	-	-	-	-	-
Till	3.08	0.95	4.47	3.22	0.00	9.88
Total	7.90			7.82		
	Object 116					
	Lake area			Mire area		
Layer name	Mean	Min	Max	Mean	Min	Max
Peat / organic	0.36	0.02	0.65	0.79	0.00	4.40
Post-glacial lacustrine	0.19	0.05	0.42	0.02	0.00	0.05
Post-glacial marine	0.48	0.20	0.74	0.45	0.20	0.74
Glacial clay	1.83	0.00	9.78	2.12	0.00	10.11
Fill	-	-	-	-	-	-
Glaciofluvium	0.11	0.00	5.10	0.04	0.00	3.39
Till	2.88	0.00	8.64	3.07	0.00	10.47
Total	5.85			6.49		

Table A1-2. Regolith-layer thicknesses, cont'd.

Thickness rego-layer (m)						
	Object 121_2					
	Lake area			Mire area		
Layer name	Mean	Min	Max	Mean	Min	Max
Peat / organic	-	-	-	0.21	0.00	1.59
Post-glacial lacustrine	-	-	-	-	-	-
Post-glacial marine	-	-	-	0.52	0.29	0.54
Glacial clay	-	-	-	0.62	0.00	3.62
Fill	-	-	-	-	-	-
Glaciofluvium	-	-	-	-	-	-
Till	-	-	-	3.90	0.00	
Total	0.00			5.25		
	Object 160					
	Lake area			Mire area		
Layer name	Mean	Min	Max	Mean	Min	Max
Peat / organic	0.00	0.00	0.01	0.97	0.00	3.31
Post-glacial lacustrine	1.13	1.13	1.13	0.41	0.00	1.13
Post-glacial marine	0.33	0.29	0.37	0.37	0.12	0.54
Glacial clay	1.11	0.00	3.46	0.56	0.00	5.34
Fill	-	-	-	-	-	-
Glaciofluvium	0.02	0.00	0.61	0.04	0.00	4.84
Till	2.55	1.68	4.26	2.27	0.00	6.66
Total	5.14			4.62		
	Object 121_1					
	Lake area			Mire area		
Layer name	Mean	Min	Max	Mean	Min	Max
Peat / organic	0.18	0.09	0.22	0.68	0.00	3.24
Post-glacial lacustrine	0.50	0.17	1.78	0.06	0.00	1.67
Post-glacial marine	0.61	0.54	0.61	0.61	0.54	0.61
Glacial clay	3.57	0.00	8.54	4.05	0.00	9.23
Fill	-	-	-	-	-	-
Glaciofluvium	-	-	-	-	-	-
Till	6.19	2.15	10.79	6.41	1.53	12.44
Total	11.05			11.81		

Table A1-3. Regolith-layer thicknesses for 11,000 AD water balances (normal year).

	Thickness rego-layer (m)											
	Object 157_2			Object 159			Object 157_1			Object 116		
Layer name	Mean	Min	Max	Mean	Min	Max	Mean	Min	Max	Mean	Min	Max
Peat / organic	0.17	0.00	1.76	1.39	0.00	2.11	1.43	0.00	2.26	1.29	0.00	4.40
Post-glacial lacustrine	-	-	-	0.23	0.00	1.58	0.18	0.00	1.11	0.52	0.00	3.41
Post-glacial marine	0.31	0.20	0.44	0.43	0.27	0.50	0.50	0.50	0.50	0.47	0.20	0.74
Glacial clay	0.17	0.00	2.68	0.44	0.00	2.78	3.13	0.00	6.45	2.04	0.00	10.11
Fill	-	-	-	-	-	-	-	-	-	-	-	-
Glaciofluvium	-	-	-	0.10	0.00	3.49	-	-	-	0.08	0.00	5.10
Till	2.40	0.36	6.17	2.59	0.00	7.19	3.10	0.00	6.57	2.97	0.00	10.47
Total	3.05			5.18			8.34			7.37		

	Thickness rego-layer (m)								
	Object 121_2			Object 160			Object 121_1		
Layer name	Mean	Min	Max	Mean	Min	Max	Mean	Min	Max
Peat / organic	0.21	0.00	1.59	1.46	0.00	3.31	0.93	0.00	3.24
Post-glacial lacustrine	-	-	-	0.71	0.00	2.80	0.24	0.00	2.12
Post-glacial marine	0.52	0.29	0.54	0.36	0.12	0.54	0.61	0.54	0.61
Glacial clay	0.62	0.00	3.62	0.61	0.00	5.34	3.98	0.00	9.23
Fill	-	-	-	-	-	-	-	-	-
Glaciofluvium	-	-	-	0.04	0.00	4.84	-	-	-
Till	3.90	0.00	6.57	2.29	0.00	6.66	6.34	1.53	12.44
Total	5.25			5.47			12.10		

Table A1-4. Regolith-layer thicknesses for periglacial-climate water balances with 100 m permafrost.

	Thickness rego-layer (m) (from SR-Site, see Bosson et al 2010)											
	All discharge taliks			Talik object 157_1			Talik object 114					
							Talik area			Mire area		
Layer name	Mean	Min	Max	Mean	Min	Max	Mean	Min	Max	Mean	Min	Max
Lake sediments	0.65	1.53	0.00	0.00	0.00	0.00	1.12	1.34	0.00	0.60	1.34	0.00
Marine sediments	1.89	3.63	0.00	0.00	0.00	0.00	3.08	3.63	0.87	2.71	3.63	0.00
Z1a_10000	0.60	0.60	0.00	0.60	0.60	0.60	0.60	0.60	0.60	0.59	0.60	0.00
Z4a	2.14	4.38	0.00	0.00	0.00	0.00	3.60	4.38	0.27	2.74	4.38	0.00
Z4b	2.97	20.25	0.00	0.68	4.52	0.00	3.81	20.25	0.00	2.73	8.88	0.00
Z5	5.20	9.20	0.00	4.19	6.94	2.02	5.26	9.02	0.00	5.13	7.20	0.00
Z6	0.60	0.60	0.59	0.60	0.60	0.60	0.60	0.60	0.60	0.60	0.60	0.59
Total	14.05			6.07			18.07			15.10		

Table A1-5. Regolith-layer thicknesses for water balances for object 157_2 subareas.

	Thickness rego-layer (m), sensitivity cases for object 157_2											
	Discharge areas			Shallow gw-level			Exit points			Arable land		
Layer name	Mean	Min	Max	Mean	Min	Max	Mean	Min	Max	Mean	Min	Max
Peat / organic	0.17	0.00	1.76	0.40	0.00	1.76	0.23	0.00	1.76	0.58	0.00	1.76
Post-glacial marine	0.33	0.20	0.50	0.36	0.20	0.44	0.31	0.12	0.44	0.41	0.37	0.44
Glacial clay	0.23	0.00	2.68	0.35	0.00	2.68	0.11	0.00	1.74	1.04	0.00	2.68
Till	2.23	0.34	4.30	1.89	0.65	3.28	2.66	1.59	5.85	1.82	0.34	2.55
Total	2.96			3.00			3.31			3.85		

Appendix 2

Chemistry data from private wells in northern Uppland (chloride, iron and sulphate)

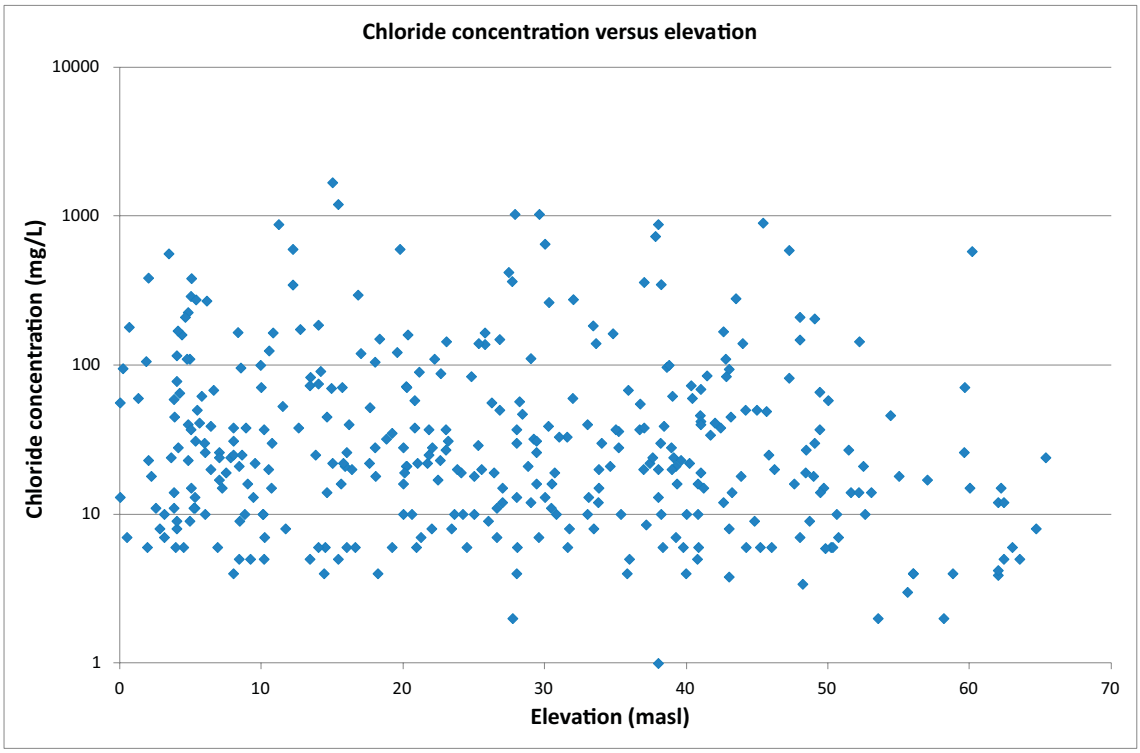

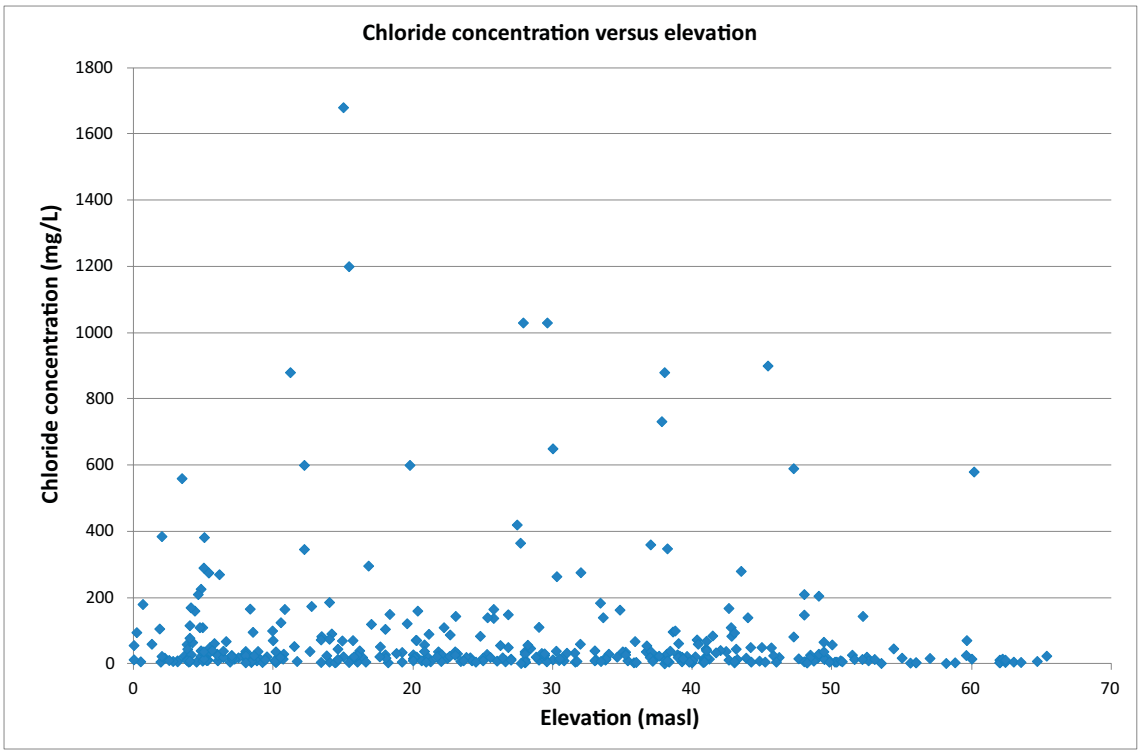

Figure A2-1. *Chloride concentration (mg/L) in private wells in northern Uppland, plotted as function of ground-surface elevation. Upper plot: Logarihmic concentrations scale. Lower plot: Linear concentration scale.*

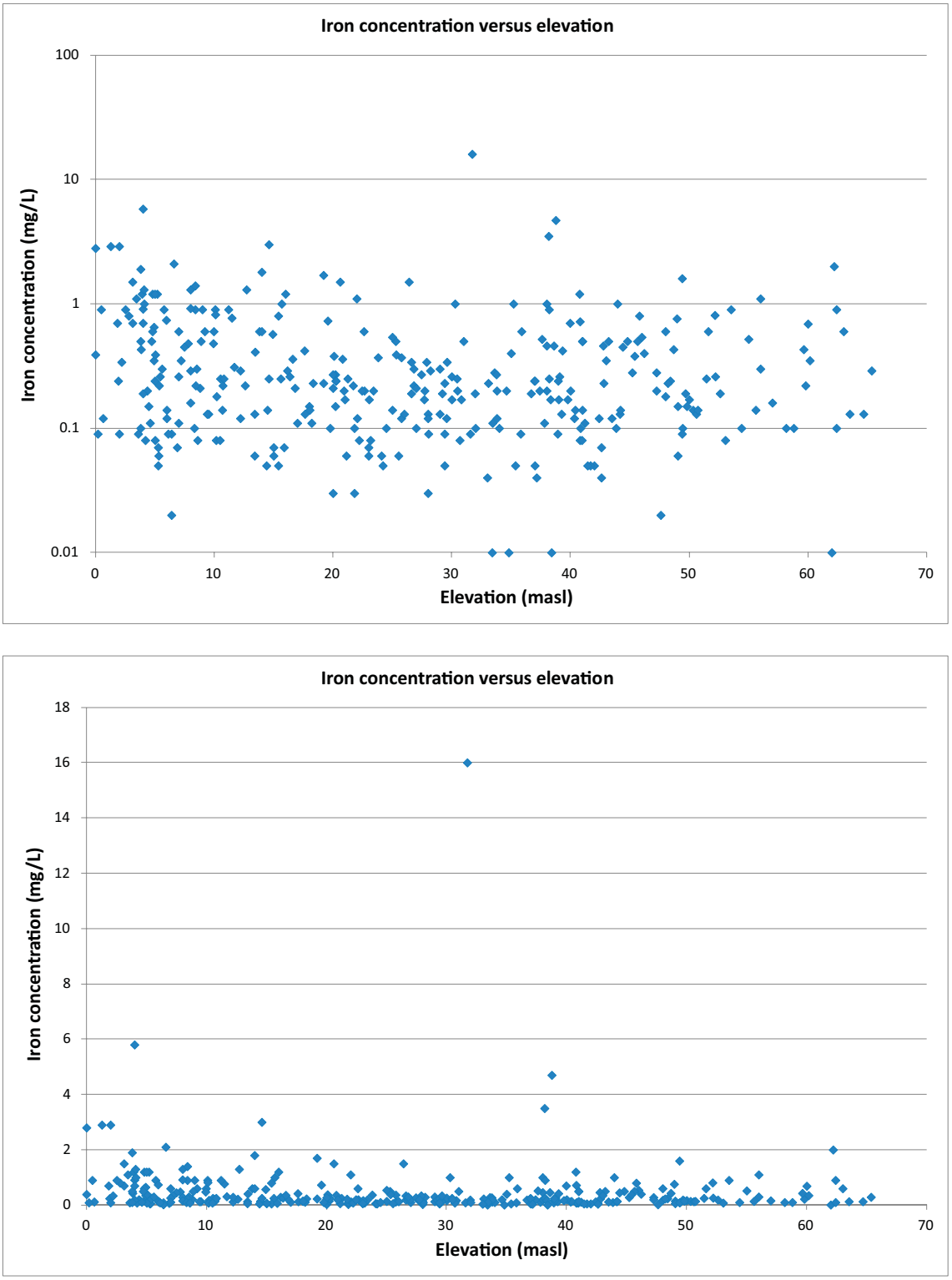

Figure A2-2. *Iron concentration (mg/L) in private wells in northern Uppland, plotted as function of ground-surface elevation. Upper plot: Logarihmic concentrations scale. Lower plot: Linear concentration scale.*

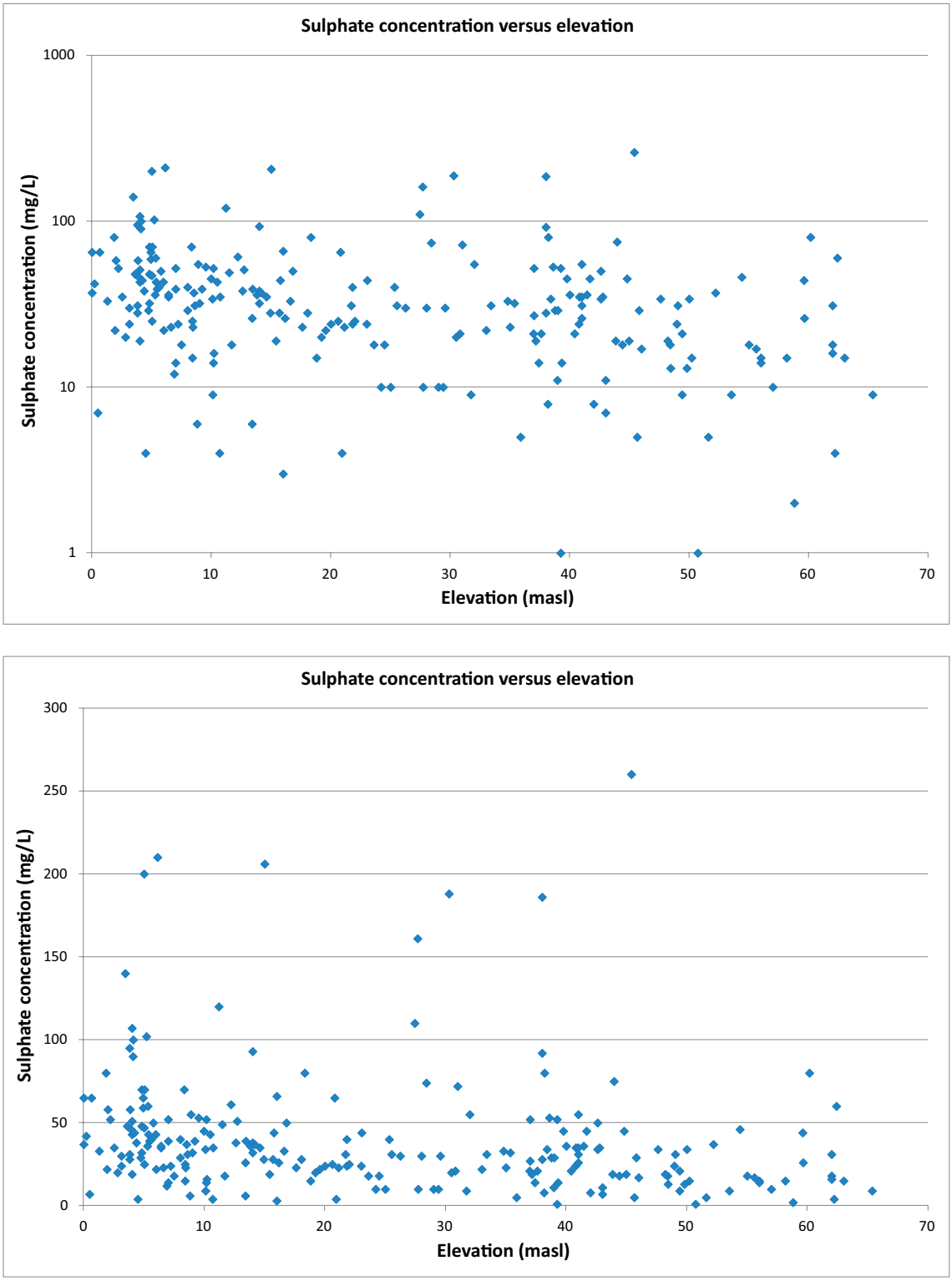

Figure A2-3. *Sulphate concentration (mg/L) in private wells in northern Uppland, plotted as function of ground-surface elevation. Upper plot: Logarihmic concentrations scale. Lower plot: Linear concentration scale.*

Appendix 3

Analysis of wells drilled in rock

Results of flow modelling and particle tracking (Section 6.4.4)

Table A3-1. Results of forward particle tracking in terms of particle-capture ratios. Q_{well} = 700 L/d. The first column shows well id and associated biosphere object.

SFR 1						
Well id (ass. b. obj.)	**1BTF**	**2BTF**	**1BLA**	**1BMA**	**Silo**	
11 (157_2)	$2.00 \cdot 10^{-5}$	$1.00 \cdot 10^{-5}$	0	0	$9.00 \cdot 10^{-5}$	
SFR 3						
Well id	**2BLA**	**3BLA**	**4BLA**	**5BLA**	**2BMA**	**1BRT**
3 (157_1)	0	$4.00 \cdot 10^{-5}$	$3.00 \cdot 10^{-5}$	$2.00 \cdot 10^{-5}$	$2.00 \cdot 10^{-5}$	$2.00 \cdot 10^{-5}$
5 (157_2 or 159)	0	$1.00 \cdot 10^{-5}$	$2.00 \cdot 10^{-5}$	$2.10 \cdot 10^{-4}$	$9.1 \cdot 10^{-4}$	0
11 (157_2)	$1.19 \cdot 10^{-3}$	$1.72 \cdot 10^{-3}$	$1.01 \cdot 10^{-3}$	$5.60 \cdot 10^{-4}$	$4.3 \cdot 10^{-4}$	$8.70 \cdot 10^{-4}$

Wells drilled in the well interaction area downstream of SFR (Section 6.4.5)

Table A3-2. Results of SFR 1 forward particle tracking in terms of particle-capture ratios. Q_{well} = 700 L/d.

Well id	1BTF	2BTF	1BLA	1BMA	Silo	Average (per well)
21	0	0	0	0	0	0
22	0	0	0	0	0	0
23	$5.43 \cdot 10^{-2}$	$1.43 \cdot 10^{-2}$	$4.78 \cdot 10^{-3}$	$1.51 \cdot 10^{-4}$	$1.71 \cdot 10^{-1}$	$4.88 \cdot 10^{-2}$
24	0	$3.02 \cdot 10^{-4}$	$8.54 \cdot 10^{-3}$	$4.92 \cdot 10^{-2}$	0	$1.94 \cdot 10^{-2}$
25	$4.81 \cdot 10^{-2}$	$5.77 \cdot 10^{-2}$	$6.18 \cdot 10^{-2}$	$4.65 \cdot 10^{-2}$	$1.01 \cdot 10^{-1}$	$6.30 \cdot 10^{-2}$
26	$1.99 \cdot 10^{-2}$	$2.29 \cdot 10^{-2}$	$2.42 \cdot 10^{-2}$	$1.81 \cdot 10^{-2}$	$5.36 \cdot 10^{-2}$	$2.77 \cdot 10^{-2}$
27	$7.28 \cdot 10^{-3}$	$8.40 \cdot 10^{-5}$	0	0	$6.64 \cdot 10^{-2}$	$2.46 \cdot 10^{-2}$
28	0	0	$6.30 \cdot 10^{-5}$	$1.06 \cdot 10^{-3}$	0	$5.60 \cdot 10^{-4}$
29	$2.30 \cdot 10^{-1}$	$3.18 \cdot 10^{-1}$	$3.13 \cdot 10^{-1}$	$1.67 \cdot 10^{-1}$	$1.43 \cdot 10^{-2}$	$2.08 \cdot 10^{-1}$
Average (per disp. room)	$\mathbf{7.19 \cdot 10^{-2}}$	$\mathbf{6.89 \cdot 10^{-2}}$	$\mathbf{6.87 \cdot 10^{-2}}$	$\mathbf{4.70 \cdot 10^{-2}}$	$\mathbf{8.12 \cdot 10^{-2}}$	

Table A3-3. Results of SFR 3 forward particle tracking in terms of particle-capture ratios. Q_{well} = 700 L/d.

Well id	2BLA	3BLA	4BLA	5BLA	2BMA	1BRT	Average (per well)
21	$9.00 \cdot 10^{-6}$	$2.36 \cdot 10^{-4}$	$9.05 \cdot 10^{-4}$	$1.21 \cdot 10^{-2}$	$4.24 \cdot 10^{-2}$	$4.00 \cdot 10^{-6}$	$9.29 \cdot 10^{-3}$
22	$1.04 \cdot 10^{-2}$	$1.36 \cdot 10^{-2}$	$1.96 \cdot 10^{-2}$	$2.14 \cdot 10^{-2}$	$1.28 \cdot 10^{-2}$	$1.02 \cdot 10^{-3}$	$1.31 \cdot 10^{-2}$
23	$1.15 \cdot 10^{-1}$	$9.83 \cdot 10^{-2}$	$6.29 \cdot 10^{-2}$	$3.78 \cdot 10^{-2}$	$3.34 \cdot 10^{-2}$	$1.22 \cdot 10^{-1}$	$7.82 \cdot 10^{-2}$
24	0	0	0	0	0	$1.00 \cdot 10^{-6}$	$1.67 \cdot 10^{-7}$
25	$9.34 \cdot 10^{-2}$	$4.42 \cdot 10^{-2}$	$2.46 \cdot 10^{-2}$	$1.85 \cdot 10^{-2}$	$1.99 \cdot 10^{-2}$	$1.30 \cdot 10^{-1}$	$5.51 \cdot 10^{-2}$
26	$6.24 \cdot 10^{-2}$	$3.15 \cdot 10^{-2}$	$2.00 \cdot 10^{-2}$	$1.63 \cdot 10^{-2}$	$1.87 \cdot 10^{-2}$	$8.48 \cdot 10^{-2}$	$3.90 \cdot 10^{-2}$
27	$6.48 \cdot 10^{-2}$	$4.52 \cdot 10^{-2}$	$4.41 \cdot 10^{-2}$	$3.88 \cdot 10^{-2}$	$2.09 \cdot 10^{-2}$	$3.36 \cdot 10^{-2}$	$4.12 \cdot 10^{-2}$
28	0	0	0	0	0	0	0
29	$1.69 \cdot 10^{-2}$	$4.20 \cdot 10^{-3}$	$1.10 \cdot 10^{-3}$	$4.30 \cdot 10^{-4}$	$3.6 \cdot 10^{-4}$	$5.57 \cdot 10^{-2}$	$1.31 \cdot 10^{-2}$
Average (per. disp. room)	$\mathbf{5.18 \cdot 10^{-2}}$	$\mathbf{3.39 \cdot 10^{-2}}$	$\mathbf{2.47 \cdot 10^{-2}}$	$\mathbf{2.08 \cdot 10^{-2}}$	$\mathbf{2.12 \cdot 10^{-2}}$	$\mathbf{5.34 \cdot 10^{-2}}$	

Influence of well discharge (Section 6.4.6)

Table A3-4. Influence of well discharge on particle capture, illustrated by results of forward particle tracking in terms of particle-capture ratios for well 29.

SFR 1 Q_{well} (L/d)	1BTF	2BTF	1BLA	1BMA	Silo	
700	$2.30 \cdot 10^{-1}$	$3.18 \cdot 10^{-1}$	$3.13 \cdot 10^{-1}$	$1.67 \cdot 10^{-1}$	$1.43 \cdot 10^{-2}$	
1,000	$2.92 \cdot 10^{-1}$	$4.01 \cdot 10^{-1}$	$3.96 \cdot 10^{-1}$	$2.21 \cdot 10^{-1}$	$2.09 \cdot 10^{-2}$	
1,400	$3.68 \cdot 10^{-1}$	$4.96 \cdot 10^{-1}$	$4.89 \cdot 10^{-1}$	$2.89 \cdot 10^{-1}$	$3.21 \cdot 10^{-2}$	
2,800	$5.65 \cdot 10^{-1}$	$7.30 \cdot 10^{-1}$	$7.20 \cdot 10^{-1}$	$4.99 \cdot 10^{-1}$	$9.29 \cdot 10^{-2}$	
SFR 3 Q_{well} (L/d)	**2BLA**	**3BLA**	**4BLA**	**5BLA**	**2BMA**	**1BRT**
700	$1.69 \cdot 10^{-2}$	$4.20 \cdot 10^{-3}$	$1.10 \cdot 10^{-3}$	$4.30 \cdot 10^{-4}$	$3.60 \cdot 10^{-4}$	$5.57 \cdot 10^{-2}$
1,000	$2.29 \cdot 10^{-2}$	$6.00 \cdot 10^{-3}$	$1.70 \cdot 10^{-3}$	$8.00 \cdot 10^{-4}$	$6.00 \cdot 10^{-4}$	$7.36 \cdot 10^{-2}$
1,400	$3.28 \cdot 10^{-2}$	$8.60 \cdot 10^{-3}$	$2.70 \cdot 10^{-3}$	$1.30 \cdot 10^{-3}$	$7.00 \cdot 10^{-4}$	$9{,}89 \cdot 10^{-2}$
2,800	$7.59 \cdot 10^{-2}$	$2.40 \cdot 10^{-2}$	$8.70 \cdot 10^{-3}$	$3.90 \cdot 10^{-3}$	$3.00 \cdot 10^{-3}$	$1.92 \cdot 10^{-1}$

Table A3-5. Results of forward particle tracking in terms of well-discharge and particle-capture ratios for well 29.

SFR 1 Q_{well} (L/d)	Well-discharge ratio	Particle-capture ratio					
		1BTF	2BTF	1BLA	1BMA	Silo	
700	1	1	1	1	1	1	
1,000	1.43	1.27	1.26	1.27	1.32	1.46	
1,400	2	1.60	1.56	1.56	1.73	2.24	
2,800	4	2.45	2.29	2.30	2.99	6.50	
SFR 3		**2BLA**	**3BLA**	**4BLA**	**5BLA**	**2BMA**	**1BRT**
700	1	1	1	1	1	1	1
1,000	1.43	1.36	1.43	1.55	1.86	1.67	1.32
1,400	2	1.94	2.04	2.45	3.02	1.94	1.78
2,800	4	4.49	5.71	7.91	9.07	8.33	3.45